

AN EXPERIMENTAL STUDY TO INVESTIGATE THE POSSIBILITY OF
USING MACRO-SYNTHETIC FIBERS IN PRECAST TUNNEL SEGMENTS

A THESIS SUBMITTED TO
THE GRADUATE SCHOOL OF NATURAL AND APPLIED SCIENCES
OF
MIDDLE EAST TECHNICAL UNIVERSITY

BY

OĞUZ TENGİLİMOĞLU

IN PARTIAL FULFILLMENT OF THE REQUIREMENTS
FOR
THE DEGREE OF MASTER OF SCIENCE
IN
CIVIL ENGINEERING

FEBRUARY 2019

Approval of the thesis:

**AN EXPERIMENTAL STUDY TO INVESTIGATE THE POSSIBILITY OF
USING MACRO-SYNTHETIC FIBERS IN PRECAST TUNNEL SEGMENTS**

submitted by **OĞUZ TENGİLİMOĞLU** in partial fulfillment of the requirements for
the degree of **Master of Science in Civil Engineering Department, Middle East
Technical University** by,

Prof. Dr. Halil Kalıpçılar
Dean, Graduate School of **Natural and Applied Sciences**

Prof. Dr. Ahmet Türer
Head of Department, **Civil Engineering**

Prof. Dr. Uğurhan Akyüz
Supervisor, **Civil Engineering, METU**

Examining Committee Members:

Prof. Dr. Erdem Canbay
Civil Engineering, METU

Prof. Dr. Uğurhan Akyüz
Civil Engineering, METU

Prof. Dr. İsmail Özgür Yaman
Civil Engineering, METU

Assoc. Prof. Dr. Burcu Burak Bakır
Civil Engineering, METU

Assist. Prof. Dr. Alper Aldemir
Civil Engineering, Hacettepe University

Date: 18.02.2019

I hereby declare that all information in this document has been obtained and presented in accordance with academic rules and ethical conduct. I also declare that, as required by these rules and conduct, I have fully cited and referenced all material and results that are not original to this work.

Name, Surname: Oğuz Tengilimođlu

Signature:

ABSTRACT

AN EXPERIMENTAL STUDY TO INVESTIGATE THE POSSIBILITY OF USING MACRO-SYNTHETIC FIBERS IN PRECAST TUNNEL SEGMENTS

Tengilimođlu, Ođuz
Master of Science, Civil Engineering
Supervisor: Prof. Dr. Uđurhan Akyüz

February 2019, 175 pages

With the development of tunnel construction techniques, segmental tunnel linings have begun to play a crucial role in preserving ground surfaces and solving traffic problems in metropolitan areas. In parallel with growing interest in precast tunnel lining, engineers are in the search of solutions that improve precast production efficiency and obtain higher structural performance. Nonetheless, the number of studies related to precast tunnel segments in Turkey is quite limited. Fibers have used as reinforcements in many projects due to significant advantages and nowadays, there is a general interest in the field of civil engineering on macro-synthetic fibers to use in precast tunnel segmental lining. However, it is a controversial issue on whether it is proper or not, compared to the commonly used conventional rebars. Within this framework, experimental studies on full-scale segments of Mecidiyeköy - Mahmutbey metro line project in İstanbul were performed to investigate the possibility of using polypropylene fiber reinforcements with or without using rebars in precast tunnel segments. In these experiments, for reliability and usability of glass fiber reinforced polymer rebars instead of conventional rebars were also investigated. Flexural test was carried out in order to compare the flexural bearing capacity of tunnel segments, also point load test was developed with the purpose of observing the real effect of thrust forces on precast tunnel segments.

Keywords: Precast tunnel segments, Macro-synthetic fibers, Glass fiber reinforced polymer rebars, Full scale tests

ÖZ

MAKRO SENTETİK LİFLERİN PREKAST TÜNEL SEGMANLARINDA KULLANILABİLİRLİĞİNİN DENEYSEL YÖNTEM İLE ARAŞTIRILMASI

Tengilimoğlu, Oğuz
Yüksek Lisans, İnşaat Mühendisliği
Tez Danışmanı: Prof. Dr. Uğurhan Akyüz

Şubat 2019, 175 sayfa

Tünel yapım tekniklerinin gelişmesi ile birlikte segmental tünel kaplamaları, metropol alanlardaki yer yüzeyinin korunmasında ve trafik sorunlarının çözümünde önemli bir rol oynamaya başlamıştır. Prekast tünel kaplamasına olan ilginin artmasıyla birlikte, mühendisler prekast üretim verimliliğini artıran ve daha yüksek yapısal performans sağlayan çözümler arayışındadırlar. Buna karşın, Türkiye'de prekast tünel segmentaları ile ilgili çalışmaların sayısı oldukça sınırlıdır. Lifler önemli avantajları nedeniyle birçok projede donatı olarak kullanılmıştır; günümüzde ise, inşaat mühendisliği alanında makro sentetik fiberlerin prekast tünel segmental kaplamalarında kullanılması noktasında genel bir ilgi vardır. Ancak, yaygın olarak kullanılan geleneksel donatılar ile karşılaştırıldığında, fiberlerin uygun olup olmadığı tartışmalı bir konudur. Bu çerçevede, polipropilen fiberlerin prekast tünel segmentalarının içerisinde donatı ile birlikte veya tek başlarına kullanılması olasılığını araştırmak amacıyla İstanbul'daki Mecidiyeköy-Mahmutbey metro hattı projesinin tam ölçekli segmentaları üzerinde deneysel çalışmalar yapılmıştır. Bu deneylerde, ayrıca cam elyaf takviyeli polimer donatıların geleneksel donatılar yerine kullanılabilirliği araştırılmıştır. Eğilme testi, tünel segmentalarının eğilme altındaki taşıma kapasitesini karşılaştırmak, noktasal basınç testi ise prekast tünel segmentalarının itme kuvvetli altındaki gerçek etkisini gözlemlemek amacıyla gerçekleştirilmiştir.

Anahtar Kelimeler: Prekast tünel segmanları, Makro-sentetik lifler, Cam elyaf takviyeli polimer donatılar, Tam ölçekli testler

To my beloved family for their love, endless support, encouragement & sacrifices.

ACKNOWLEDGMENTS

This thesis is a product of a collaborative work supported by many people in their own ways. First of all, I would like to express my deepest gratitude to my thesis advisor Prof. Dr Uğurhan Akyüz of the Civil Engineering department at Middle East Technical University. The door to Prof. Akyüz office was always open whenever I ran into a trouble spot or had a question about my research or writing. He consistently allowed this dissertation to be my own work but steered me in right direction whenever he thought I needed it.

I would like to acknowledge the Forta Ferro Company for the financial support of the experimental process. I am also very thankful to Selçuk Mert, Serhat Aydın and Burak Sönmez for spending their time. I am deeply grateful for their generous support.

I would like to acknowledge the Yuksel Project International for significant contribution of my thesis. In particular, their experiences in the field of underground structure and railways systems in Turkey has taught me a lot.

I must express my gratitude to Dr. Tuğçe Akbaş and Atak Mühendislik for their endless support during the design and manufacturing process of the test apparatus.

I would like to acknowledge the Gülermak-Nurol Joint Venture for their valuable technical support on this project

I am also very grateful for the help of the technician staffs of the laboratory, Barış Esen, Osman Keskin, Murat Demirel and Salim Azak for all fun and hard moments we experienced during the experimental campaign.

I would like to thank Dr. Burhan Aleessa Alam for his endless support during material tests.

Finally, I must express my very profound gratitude to my parents and to my girlfriend for providing me with unfailing support and continuous encouragement throughout my years of study and through the process of researching and writing this thesis. This accomplishment would not have been possible without them. Thank you.

TABLE OF CONTENTS

ABSTRACT.....	v
ÖZ	vii
ACKNOWLEDGMENTS	x
TABLE OF CONTENTS.....	xi
LIST OF TABLES	xv
LIST OF FIGURES	xvii
LIST OF ABBREVIATIONS	xxiii
1. INTRODUCTION	1
1.1. Background	1
1.2. Aim and Scope	4
1.3. Thesis Overview.....	4
2. LITERATURE REVIEW	5
2.1. Literature Study on Fiber Reinforced Concrete	5
2.1.1. General.....	5
2.1.2. Fiber Types and Classification	7
2.1.2.1. Synthetic Fibers.....	9
2.1.3. Polypropylene Fiber Reinforced Concrete (PFRC)	9
2.1.3.1. Post-cracking Behavior of PFRC	10
2.1.4. Precast Tunnel Segments Reinforced by Fibers	14
2.1.5. Experimental and Numerical Studies on FRC Precast Tunnel Segments	18
2.2. Literature Study on Fiber Reinforced Polymer Bars.....	22

2.2.1. General	22
2.2.2. Types and Classification of FRP Reinforcing Bars.....	23
2.2.2.1. Glass Fiber Reinforced Polymer Rebars.....	25
2.2.3. Precast Tunnel Segments Reinforced by GFRP Rebars.....	26
2.2.4. Experimental Studies on Precast Tunnel Segments Reinforced by Glass Fiber Reinforced Polymer Bars	27
3. OVERVIEW OF TBM TUNNELING TECHNIQUE.....	29
3.1. Brief History of Mechanized Shield Tunneling.....	29
3.1.1. Operating Principle of Tunnel Boring Machines	32
3.1.2. Types of Tunnel Boring Machines	36
3.1.2.1. Rock Tunneling Machines.....	37
3.1.2.2. Soft Ground Tunneling Machines	40
3.2. Segmental Tunnel Linings	43
3.2.1. Precast Concrete Segments	44
3.2.1.1. Joint Details	46
3.2.1.1.1. Longitudinal Joints.....	46
3.2.1.1.2. Circumferential (or Ring) Joints	49
3.2.1.2. Waterproofing System	50
4. TEST SPECIMENS AND MATERIALS	53
4.1. Test Specimens	58
4.1.1. Specimen Geometry	58
4.1.2. Reinforcement Details.....	62
4.1.2.1. Type A - RC Sample.....	63
4.1.2.2. Type B - RC+PFRC Sample.....	65

4.1.2.3. Type C - GFRP + PFRC Sample	67
4.1.2.4. Type D - PFRC Sample	69
4.2. Material Properties	70
4.2.1. Concrete Properties.....	70
4.2.2. Reinforcements Properties.....	83
4.2.2.1. Conventional Steel Rebars	83
4.2.2.2. Polypropylene Fibers	83
4.2.2.3. Glass Fiber Reinforced Polymer Rebars	84
5. FULL-SCALE EXPERIMENTAL TESTS	85
5.1. Flexural Test.....	85
5.1.1. Test Set-up and Instrumentation of Flexural Test	86
5.1.2. Experimental Results of Flexural TestAdd text here.....	92
5.1.3. Creep tests.....	104
5.1.3.1. Cyclic Loading for PFRC specimen	105
5.1.3.2. Cycling Loading for GFRP+ PFRC specimen.....	108
5.2. Point Load Test	110
5.2.1. Test Set-up and Instrumentation of Point Load Test	111
5.2.2. Experimental Results of Point Load Test	120
6. CONCLUSIONS	133
6.1. Summary	133
6.2. Conclusion.....	133
6.3. Future studies	135
A. THE DESIGN VALUES OF MECİDİYEKÖY-MAHMUTBEY METRO PROJECT.....	147

B. FULL-SCALE TEST RESULTS 161

LIST OF TABLES

TABLES

Table 2.1. Physical properties of fibers (Löfgren, 2005)	8
Table 2.2. Tunnels lined by FRC precast tunnel segments (ITA report n.16, 2016) .	16
Table 2.3. Previous experimental studies on FRC tunnel segments, adopted from Gong et al. (2017)	20
Table 2.4. Previous numerical and analytical studies on FRC tunnel segments, adopted from Gong et al. (2017).....	21
Table 2.5. General mechanical and physical properties of FRP, adopted from ACI 440.1R-15 (2015)	24
Table 2.6. Previous experimental and numerical studies on tunnel segments reinforced by glass fiber reinforced polymer rebars.....	28
Table 3.1. Ranges for the dimensions of segmental linings, from Thewes (2008) (as cited in Çimentepe, 2010)	45
Table 4.1. General geological description between Yenimahalle and Mahmutbey stations	55
Table 4.2. Segmental lining ring – general features.....	58
Table 4.3. Segment designations, concrete and reinforcement details	62
Table 4.4. Concrete mix designs of specimens	72
Table 4.5. The cubic compressive strength at 90 days.....	73
Table 4.6. The cylindrical compressive strength at 7 days	73
Table 4.7. The cylindrical compressive strength at 28 days	73
Table 4.8. Residual tensile strengths of test specimens and compressive strength of concrete	82
Table 4.9. Polypropylene fiber properties.....	83
Table 4.10. Properties of Glass Fiber Reinforced Polymer Rebars.	84
Table 5.1. Force corresponding to 2 mm vertical deflection	93
Table 5.2. First cracking width vs. corresponding loads, moments and deflection ...	97

Table 5.3. Load and the corresponding moment at allowable SLS crack width limit (0.3 mm).	98
Table 5.4. Maximum load and the corresponding crack width and moment	99
Table 5.5. Features of TBM.....	112
Table A.1. Storage configuration detail.....	149
Table A.2. Forces action on the storage systems.....	149
Table A.3. Calculations' results and design values of storage phase	149
Table A.4. Transportation configuration detail	150
Table A.5. Forces action on the transportation phases	151
Table A.6. Calculations' results and design values of transportation phase	151
Table A.7. Design values of production and transient load cases	151
Table A.8. Critical sections were considered in the TBM tunnel segmental lining	155
Table A.9. Design values of full section segments- Combination A and B	158
Table A.10. Design values of full section segments- Combination C.....	158
Table A.11. Design forces on radial joint segments – Combination A&B	159
Table A.12. Design forces on radial joints – Combination C.....	160

LIST OF FIGURES

FIGURES

Figure 2.1. Examples of fibers’ cross sectional geometries (Löfgren, 2005)	7
Figure 2.2. Examples of fibers’ typical geometries (Löfgren, 2005).....	8
Figure 2.3. Softening and hardening behavior of PRC in axial tension (fib Model Code 2010, 2012)	11
Figure 2.4. Softening and hardening behavior differences at the point of the structural level, from (fib Model Code 2010, 2012)	12
Figure 2.5. Difference in tensile behavior for cement-based materials (Löfgren, 2005)	13
Figure 2.6. Types of FRP (ACI 440.1R-15, 2015)	24
Figure 3.1. “Teredo Navalis”, working on the excavation and the lining (Guglielmetti, 2007)	30
Figure 3.2. Brunel’s shield tunnel excavation under River Thames in London (Guglielmetti et al., 2007)	31
Figure 3.3. Tunnel boring machine and segmental tunnel lining (Arnau & Molins, 2015)	32
Figure 3.4. System groups of a Tunnel Boring Machine (Maidl et al., 2008)	33
Figure 3.5. Working stages of TBM tunneling, from Wittke (2007) (as cited in Çimentepe, 2010)	34
Figure 3.6. Shield tail with grouting of the ground-lining gap (Möller, 2006).....	36
Figure 3.7. Classification of Tunnel Boring Machine (TBM) (Çimentepe, 2010)	37
Figure 3.8. Rock tunneling machines: a) Unshielded TBM, b) Single shielded TBM, c) Double shielded TBM, from Wittke (2007) (as cited in Çimentepe, 2010)	39
Figure 3.9. Regulation of support pressure, source: https://www.herrenknecht.com/en/products/core-products/tunnelling/epb-shield.html	41

Figure 3.10. Shield tunneling with a) natural support, b) mechanical support, c) compressed air support, d) slurry support, e) earth pressure balance support (Maidl et al., 1996)	42
Figure 3.11. The advance of mechanized shield tunneling method (Tiberti et al., 2018)	43
Figure 3.12. Lining definitions (Hurt & Hart, 2011).....	44
Figure 3.13. Segment types (Guglielmetti et al., 2007).....	46
Figure 3.14. Longitudinal joints with a) two flat surfaces, b) two convex surfaces, c) convex-concave surfaces (Maidl et al., 2008)	47
Figure 3.15. Longitudinal joints with a) straight bolt, b) curved bolt, c) inclined bolt, from AFTES 1999 (as cited in Fabozzi, 2017).....	48
Figure 3.16. Detailing of precast tunnel segment	48
Figure 3.17. a) Joints with dowels, from AFTES (1999) (as cited in Fabozzi, 2017), b) joints with pin and socket system (Maidl et al., 2008)	50
Figure 3.18. Tunnel segments with kaubit used as a packing material (Luttikhokt, 2007).....	50
Figure 4.1. Longitudinal profile corresponding to the Line 1 tube of metro project, taken from related project report prepared by Yuksel Project International	53
Figure 4.2. Geological profile between Yenimahalle and Mahmutbey stations.....	54
Figure 4.3. Segmental lining ring geometry (units mm)	57
Figure 4.4. 3D view of the segmental lining	57
Figure 4.5. 4.5 Segment C	59
Figure 4.6. 3D view of segment C	59
Figure 4.7. Outer view (units mm & not to scale).....	60
Figure 4.8. Inner view (units mm & not to scale).....	60
Figure 4.9. Section A-A (units mm & not to scale).....	61
Figure 4.10. Section B-B (units mm & not to scale)	61
Figure 4.11. Central deployment (units mm & not to scale)	62
Figure 4.12. Reinforcement details of RC segments	63
Figure 4.13. Reinforcement details of RC segments (units mm, not to scale)	64

Figure 4.14. Reinforcement details of RC + PFRC segments	65
Figure 4.15. Reinforcement details of RC + PFRC segments (units mm, not to scale)	66
Figure 4.16. Reinforcement details of GFRP + PFRC segments.....	67
Figure 4.17. Reinforcement details of GFRP + PFRC segments (units mm, not to scale)	69
Figure 4.18. Reinforcement details of PFRC segments	70
Figure 4.19. Examples of cracked samples after the test	74
Figure 4.20. Dimensions of 3-point bending test on a notched beam (EN 14651, 2005)	74
Figure 4.21. Test specimen and experimental set-up.....	75
Figure 4.22. Example of load versus CMOD diagram (EN 14651, 2005).....	76
Figure 4.23. Experimental results of bending tests in terms of load versus vertical deflection.....	77
Figure 4.24. Nominal stress vs. CMOD curve	77
Figure 4.25. Simplified stress-strain relationships (fib Model Code 2010, 2012).....	78
Figure 4.26. Enter the Figure Caption here.....	84
Figure 5.1. Test set-up and flexural loading system	87
Figure 5.2. Side description of test set-up.....	88
Figure 5.3. Instrumentation details of flexural test (units mm, not to scale).	89
Figure 5.4. Vertical and horizontal LVDTs	90
Figure 5.5. Left side of the flexural test set-up	90
Figure 5.6. Broken strain gauge and vertical LVDTs	90
Figure 5.7. Right side and bottom view of the flexural test.....	91
Figure 5.8. View of located 2 LVDTs instead of strain gauges.....	91
Figure 5.9. Load versus time graph of flexural tests.....	92
Figure 5.10. Load versus mid-span displacement curves	93
Figure 5.11. Load versus mid-span displacement curves up to 2 mm	93
Figure 5.12. Load versus flexural crack width.....	95
Figure 5.13. Load versus flexural crack width up to 0.3 mm	96

Figure 5.14. Final crack pattern of specimens (bottom view)	102
Figure 5.15. Final crack pattern of specimens (side view)	104
Figure 5.16. Load versus time graph of D3 specimen	105
Figure 5.17. Load vs. mid-span displacement curve	106
Figure 5.18. Load vs. flexural crack width of D3 specimen.....	106
Figure 5.19. Load vs. horizontal displacement curve of D3 specimen-right.....	107
Figure 5.20. Load vs. horizontal displacement curve of D3 specimen-left.....	108
Figure 5.21. Load vs. time graph of C4 specimen.....	109
Figure 5.22. Load vs. mid-span deflection curve of C4 specimen	109
Figure 5.23. Final crack pattern of C4 specimen (right side)	110
Figure 5.24. Final crack pattern of C4 specimen (left side)	110
Figure 5.25. Local tensile stresses due to applied high concentrated load (Bakhshi, 2015).....	111
Figure 5.26. TBM jack configurations (adopted from Meda, 2016)	112
Figure 5.27. Point load testing system.....	114
Figure 5.28. Instrumentation details of point load test (units mm, not to scale).	115
Figure 5.29. Point load test set-up and loading systems.....	116
Figure 5.30. Outer surface of test specimen	116
Figure 5.31. Point load test set-up and instrumentation details (1)	117
Figure 5.32. Point load test set-up and instrumentation details (2)	118
Figure 5.33. Point load test set-up and instrumentation details (3)	119
Figure 5.34. Load vs. time graph of point load tests	120
Figure 5.35. Load vs. spalling cracking width (H1-I)	121
Figure 5.36. Load vs. spalling cracking width (H1-T)	121
Figure 5.37. Load vs. spalling cracking width (H2-I)	123
Figure 5.38. Load vs. spalling cracking width (H2-T)	123
Figure 5.39. Load vs. splitting cracking width (H3-I).....	124
Figure 5.40. Load vs. average of vertical displacement curve (V1-O and V3-I)	126
Figure 5.41. Load vs. average of vertical displacement curve (V2-O and V2-I)	126
Figure 5.42. Load vs. average of vertical displacement curve (V3-O and V1-I)	127

Figure 5.43. Crack pattern and crack depth of PFRC specimen	128
Figure 5.44. Crack pattern and crack depth of RC + PFRC specimen	129
Figure 5.45. Crack pattern and crack depth of RC specimen.....	130
Figure 5.46. Final view of GFRP + PFRC specimen.....	130
Figure 5.47. Horizontal strain values at the spalling and splitting region.....	131
Figure A.1. Statical scheme of the demoulding phases (units mm).....	147
Figure A.2. Storage configuration of entire ring segments (units mm)	148
Figure A.3. Static condition in the transporting phase (units mm)	150
Figure A.4. Load distribution for the partially loaded area (Eurocode-2)	152
Figure A.5. Static condition to evaluate the bursting effect in segments perpendicular plane	153
Figure A.6. Empirical method and FEA method for the evaluation of splitting.....	153
Figure A.7. Finite Element Analysis model and results of segment C	154
Figure A.8. Section 1 geometry	156
Figure A.9. Section 2 geometry	156
Figure A.10. Section 3 geometry	157
Figure A.11. Section 4 geometry	157
Figure A.12. Section 5 geometry	157
Figure B.1 Load versus vertical displacement curves obtained by left LVDT	161
Figure B.2. Load versus vertical displacement curves obtained by right LVDT.....	161
Figure B.3. Load versus vertical displacement curves obtained by average of 4 LVDTs.	162
Figure B.4. Load versus flexural crack width graph measured by left LVDT.....	162
Figure B.5. Load versus flexural crack width graph measured by left LVDT, up to 0.3 mm.	163
Figure B.6. Load versus flexural crack width graph measured by right LVDT.	163
Figure B.7. Load versus flexural crack width graph measured by right LVDT, up to 0.3 mm.	164
Figure B.8. Load versus flexural crack opening width curves obtained average of 2 LVDTs, around the SLS limit.	164

Figure B.9. Load versus flexural crack width curves measured from the left strain gauge.....	165
Figure B.10. Load versus flexural crack width curves measured from the right strain gauge.....	165
Figure B.11. Load versus flexural crack width curves measured by left LVDT located at the strain gauge position.	166
Figure B.12. Load versus flexural crack width curves measured by right LVDT located at the strain gauge position.	166
Figure B.13. Load versus horizontal displacement curves obtained from left LVDT	167
Figure B.14. Load versus horizontal displacement curves obtained from right LVDT	167
Figure B.15. Load versus vertical displacement curve obtained from left LVDT ..	168
Figure B.16. Load versus vertical displacement curve obtained from right LVDT	168
Figure B.17. Load versus flexural crack width curve measured by left LVDT	169
Figure B.18. Load versus flexural crack width curve measured by right LVDT	169
Figure B.19. Load versus flexural crack width curves measured by left LVDT located at the strain gauge position.	170
Figure B.20. Load versus flexural crack width curves measured by right LVDT located at the strain gauge position.	170
Figure B.21. Cracking width versus vertical displacement curve	171
Figure B.22. Load versus vertical displacement curve obtained from left LVDT ..	171
Figure B.23. Load versus vertical displacement curve obtained from right LVDT	172
Figure B.24. Load versus vertical displacement curves (V1-I).....	172
Figure B.25. Load versus vertical displacement curves (V2-I).....	173
Figure B.26. Load versus vertical displacement curves (V3-I).....	173
Figure B.27. Load versus vertical displacement curves (V1-O)	174
Figure B.28. Load versus vertical displacement curves (V2-O)	174
Figure B.29. Load versus vertical displacement curves (V3-O)	175

LIST OF ABBREVIATIONS

ABBREVIATIONS

ACI	American Concrete Institute
AFRP	Aramid Fiber Reinforced Polymer
AFTES	French Tunnelling and Underground Engineering Association
CEN	European Committee for Standardization
CFRC	Conventional Fiber Reinforced Concrete
CFRP	Carbon Fiber Reinforced Polymer
CMOD	Crack Mouth Opening Displacement
CNR	The National Research Council of Italy
DafStb	German Committee for Reinforced Concrete
DAUB	German Committee for Underground Construction
EN	European Standards
EPB	Earth Pressure Balance
FIB	International Federation for Structural Concrete
FRC	Fiber Reinforced Concrete
FRHPC	Fiber Reinforced High Performance Concrete
FRP	Fiber Reinforced Polymer
GFRP	Glass Fiber Reinforced Polymer
HFRC	Hybrid Fiber Reinforced Concrete
HPC	High Performance Concrete
HPFRC	High Performance Fiber Reinforced Concrete
ISO	International Organization for Standardization
ITA	International Tunneling and Underground Space Association
JSCE	Japan Society of Civil Engineers
LOP	Limit of Proportionality
LVDT	Linear Variable Differential Transformers

MSF	Macro Synthetic Fiber
NATM	New Austrian Tunneling Method
PC	Plain Concrete
PFRC	Polypropylene Fiber Reinforced Concrete
PP	Polypropylene
RC	Reinforced Concrete
RILEM	International Union of Laboratory and Experts in Construction Materials, Systems and Structures
RMR	Rock Mass Rating
SCFRC	Self-Compacting Fiber Reinforced Concrete
SFRC	Steel Fiber Reinforced Concrete
SG	Strain Gauge
SLS	Serviceability Limit State
TBM	Tunnel Boring Machine
UHPRC	Ultra High Performance Fiber Reinforced Concrete
ULS	Ultimate Limit State
2D	Two Dimensional
3D	Three Dimensional

CHAPTER 1

INTRODUCTION

1.1. Background

In today's world, due to the increasing traffic extensively in metropolitan areas and need to preserving ground surfaces, there is a growing interest in tunnel lining (Conforti et al., 2017). In parallel with the developments of the tunnel construction techniques and adoption of more powerful Tunnel Boring Machines, using of precast tunnel segmental lining has increased in the last two decades. Precast tunnel segmental lining serves as both initial ground support and final lining in the modern tunnel which is constructed with Tunnel Boring Machines (Bakhshi and Nasri, 2015). In addition, it provides the required operational cross-sections for water supply, wastewater, gas pipeline power cable, railways etc. However, there are some drawbacks in terms of structural performance and manufacturing process. The curved shape of the precast tunnel segment causes using conventional reinforcement with complex detailing (Caratelli et al., 2011). This situation leads to the delay of the project period and it also increases the labour cost. In addition, using conventional reinforcing bars causes corrosion problems for precast tunnel segments especially, in harsh soil environment and damaged part of the tunnel. In order to prevent this effect, cathodic protection generally is used in tunnel lining. Nonetheless, this protection causes extra expense for the project. Consequently, the main subject is decreasing the construction time and the enhancement of the structural behavior of precast tunnel segments in terms of flexural bearing capacity, corrosion resistance and crack control. For these reasons, fiber reinforced concrete is commonly tried to be used for the construction of tunnel lining, due to possible reduction or disuse in conventional reinforcement. However, in this field limited studies have been carried out to investigate the structural behavior of tunnel segments reinforced by fibers.

Fibers were used for the first time in pavements and they allowed completely replacing the steel mesh reinforcements (Falkner et al., 1995). This practice revealed the possibility of using fibers instead of traditional reinforcements. After that, lots of applications have been developed especially, in pavements, shotcrete and precast industry (Di Carlo et al., 2016). Apart from that, according to recent data (Gong et al., 2017), various studies both experimental and numerical have been performed in order to investigate the fiber reinforced concrete in the last twenty years. A common result of these studies is that the use of fibers enhances the structural performance of concrete particularly, post-cracking tensile strength and durability of concrete. In addition, using fiber reinforced concrete for the precast tunnel segments leads to several benefits in terms of production efficiency, since fibers distributed uniformly in segments can be easily added during concrete mixing (Conforti et al., 2017).

In the last decade, totally more than 500 km length of the tunnel has started to construct in the different regions of Istanbul/Turkey, some of them have already finished (Istanbul Metropolitan Municipality, 2017). Basically, these applications are related to heavy rail transit systems, also known as metro. Additionally, when the tunnels which are constructed for the purpose of hydraulic conduits taken into consideration, tunnels length to be constructed is much longer than that. In Turkey, fiber reinforced concrete was introduced in tunnels during the application of shotcretes. However, the structural effect of fibers in concrete has not been taken into consideration exactly since there is no information or provisions on fiber reinforced concrete in Turkish Code at all. According to ITA report n.16 (2016), some countries have published guidelines on the structural design of fiber reinforced concrete (e.g.: RILEM, 2003; CNR DT 204, 2006; DAfStb, 2012). Moreover, fiber reinforced concrete has taken place recently in the fib Model Code 2010 (2012) and Eurocode 2 (CEN TC 250/SC2.WG1.TG2, 2016). Apart from that, the American Concrete Institute and the International Tunnelling Association published guidelines for fiber reinforced concrete segmental linings (ACI 544.7R-16, 2016; ITA report n.16, 2016). It should be noted that compared to the previous ones, these are not related to general fiber

reinforced concrete, but are specifically published for the tunnel segmental lining. Recent study (ITA report n.16, 2016) indicates that although steel fiber reinforced concrete has been commonly used in precast tunnel segments, significant research has been performed to enhance the structural performance of macro-synthetic fibers in the last decade. There is an increasing interest in the field of engineering on macro-synthetic fibers to obtain more durable precast tunnel segments due to its higher resistance to corrosion, compared to steel fibers (Conforti et al 2017). However, in a similar manner, limited experimental studies on macro-synthetic fibers (MSF) in precast tunnel segments have been conducted for the metro tunnels. More importantly, no research has ever been associated with MSF in tunnel segments in Turkey.

In addition to macro-synthetic fibers, for the reliability and usability of glass fiber reinforced polymer (GFRP) reinforcing bars in metro tunnel segments, there are not much experimental studies (Caratelli et al., 2016,2017; Spagnuolo et al., 2017). The experimental studies carried out by Caratelli et al., 2016,2017 demonstrated that using of glass fiber reinforced polymer rebars instead of conventional reinforcements in precast tunnel segments increases the corrosion resistance and allows many advantages in the sense of structural durability. Therefore, for the purpose of removing the cathodic protection in the tunnel and reducing project cost, macro-synthetic fibers and GFRP rebars can be used in precast tunnel segment together. However, due to the lack of special design rules for tunnel segments reinforced by macro-synthetic or GFRP reinforcing bars, they are usually designed by considering the national codes concerning the design of an FRC structure. Full-scale tests are one of the effective ways to investigate the mechanical and structural behavior of fiber reinforced concrete segments (ITA report n.16, 2016). Within this framework, to provide the possibility of using macro-synthetic fibers with or without rebars in precast tunnel segments and also to show the usability of glass fiber reinforced polymer (GFRP) reinforcing bars instead of conventional bars in precast tunnel segments, experimental programs on fifteen full-scale segments of Mecidiyeköy-Mahmutbey metro tunnel (İstanbul) were carried out.

The special motivation of this thesis is that it is the first study in the literature that has been performed by combining macro-synthetic fibers with glass fiber reinforced polymer rebars in tunnel segments and also the first experimental study on precast tunnel segments by using MSF in Turkey.

1.2. Aim and Scope

Showing the possibility of using macro-synthetic fibers with or without reinforcing bars in precast tunnel segments and investigating the usability of glass fiber reinforced polymer reinforcing bars as conventional rebar are possible by performing full-scale experimental tests on four different reinforcement solutions.

The main objective is to enhance the structural performance of precast tunnel segments and to reduce the construction time by using macro-synthetic (Polypropylene) fibers in precast tunnel segments. Additionally, using macro-synthetic fibers along with glass fiber reinforced polymer rebars in precast segments enables exclusion of the cathodic protection in tunnels. As a consequence, the total cost of metro projects will decrease at a certain extent.

1.3. Thesis Overview

This thesis consists of six chapters. Chapter 1 (Introduction) generally presents the background information about the main subject, the aim and scope of the research. Chapter 2 (Literature Review) describes the theoretical background of fibers and fiber reinforced polymers and gives a summary of previous studies. In Chapter 3 (Overview of TBM Tunneling Technique), a brief history of mechanized tunneling, principles and types of Tunnel Boring Machine and segmental tunnel lining are introduced. Chapter 4 (Test Specimens and Materials) briefly describes the general features of the Mecidiyeköy - Mahmutbey metro project, specimen types and their reinforcement details, characteristic of the materials used in the production of specimens. In Chapter 5 (Full-Scale Experimental Tests), experimental tests procedures and the results of experiments are detailed. Chapter 6 (Conclusions) summarizes the thesis study and gives the recommendations for further studies.

CHAPTER 2

LITERATURE REVIEW

2.1. Literature Study on Fiber Reinforced Concrete

2.1.1. General

Fiber reinforced concrete (FRC) is a composite material that comprised of a cementitious matrix containing relatively short, discrete, discontinuous fibers of various shapes and sizes (Abid and B. Franzen, 2011). In general, fibers are used in concrete mix for two main purposes. The first one is a non-structural purpose which is preventing the plastic cracks occurring in the early stage of concrete. On the other hand, the second one is the structural purpose, such as controlling the crack widths (Löfgren, 2005). However, structural performance of FRC is changed considerably with the types and quantity of fibers in the concrete matrix. After a long research, Jansson (2008, p.31) emphasized that “when adding fibers to concrete, in order to choose the most suitable fiber, it is important to identify the type of effect the Fibers are expected to provide”. Today man-made fibers are produced from synthetics, steel, glass and natural fibers such as, jute, cellulose and bamboo used in fiber reinforced concrete. Steel fibers are probably the most investigated and widely used in the 20th century. However, there is no doubt that using synthetic fibers in concrete, such as polypropylene, polyester and polyethene, are growing gradually in the 21st century due to several advantages compared to steel fibers.

Plain concrete that is also known as unreinforced concrete, has brittle behavior that shows high compressive strength but low tensile capacity. For this reason, concrete requires reinforcement in most of the applications. It is the most preferred method to use ordinary continuous reinforcing bars in the tensile and shear zones for increasing the load carrying capacity of concrete (Abid and B. Franzen, 2011). Fibers are short

materials that spread randomly in the concrete mix, as well as they are discontinuous. Therefore, the use of low quantity fibers in concrete cannot increase the tensile strength of concrete remarkably since they are dispersed. In general, fiber dosages used in concrete for crack control correspond to a volume fraction (V_f) below 1 percent. Nevertheless, the tensile strength can be increased when a higher volumetric ratio of fibers is used in concrete. Using high amount of fiber in order to get any substantial increase in tensile strength leads to uneconomical solutions or workability problems. For this reason, fibers are generally used in members that require less amount of tensile reinforcement. However, fibers are significantly effective in term of controlling cracks due to random distribution of fibers in the concrete mix. This is because the fibers tend to bridge the cracks after the initial crack occurred. In this way, they control the development of cracks and prevent increasing crack widths. ITA report n.16 (2016) emphasizes that even if the content of fiber is low, the addition of fibers in concrete considerably increases the post-cracking tensile behavior, also known as toughness, and ductility of the concrete. Moreover, the number of fiber in the concrete matrix affects the post cracking tensile strength of structure significantly. Since at a given fiber content, the number of micro fibers in concrete is higher compared to macro fibers, and this situation leads to increasing the chance of fibers crossing the cracks. Apart from that, fibers can also be thought of as an alternative solution in a thin and complex structure where ordinary reinforcement cannot fit (Abid and B. Franzen, 2011). Nedrelid (2015, p.3) stated that in his research “The enhanced post-cracking tensile behavior and improved crack control of concrete may lead to significant improvements in the behavior of the resulting structural members, both at the serviceability limit state (SLS) and at the ultimate limit state (ULS)”. As a consequence, using fibers in concrete for structural applications makes it possible for reducing conventional reinforcements. Even sometimes, they lead to eliminate all traditional reinforcements in structure, such as in pavements.

2.1.2. Fiber Types and Classification

According to Naaman (2003) fibers used in concrete can be classified by considering different criteria. These are summarized below;

- 1) Fibers can be classified based on the origins: Natural organic, natural inorganic and man-made (e.g. synthetic, polymer, carbon, glass, steel).
- 2) Fibers are characterized on the basis of their physical or chemical properties such as surface roughness, density, reactivity or non-reactivity with the cementitious matrix, flammability.
- 3) Classification of fibers is also based their mechanical properties: like ductility, elastic modulus, tensile strength, elongation at failure, stiffness, surface adhesion, specific gravity etc.
- 4) Fibers can also be classified according to their geometric properties such as length, diameter, cross sectional shape, surface deformation. As it is seen in Figure 2.1 fibers can be produced in any cross-section (e.g. circular, square, rectangular, triangular, flat, diamond, polygonal and substantially polygonal shape).

Different cross-sectional geometries of fibers and typical fibers' geometries are shown in Figure 2.1 and Figure 2.2, respectively.

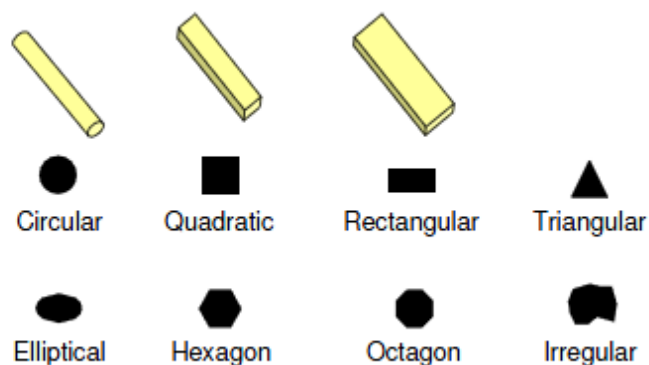


Figure 2.1. Examples of fibers' cross sectional geometries (Löfgren, 2005)

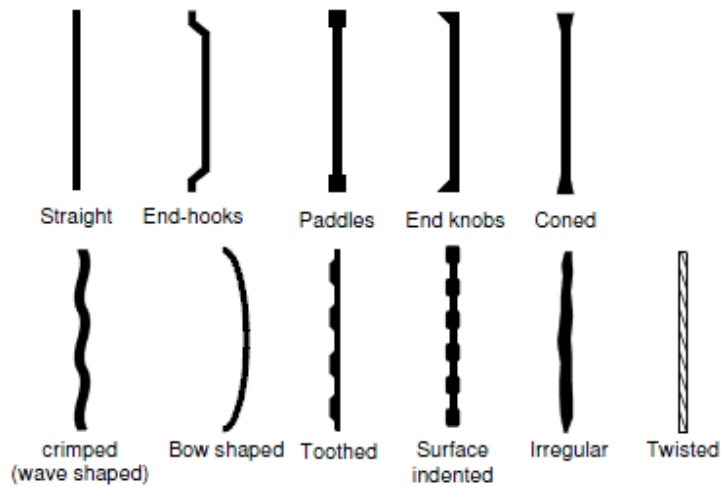


Figure 2.2. Examples of fibers' typical geometries (Löfgren, 2005)

Table 2.1 summarizes typical physical properties of fibers commonly used. According to this table, fibers are categorized basically as synthetic, steel, glass, and natural fiber materials.

Table 2.1. Physical properties of fibers (Löfgren, 2005)

Type of Fibre	Diameter [μm]	Specific gravity [g/cm^3]	Tensile strength [MPa]	Elastic modulus [GPa]	Ultimate elongation [%]
Metallic					
Steel	5-1 000	7.85	200-2 600	195-210	0.5-5
Glass					
E glass	8-15	2.54	2 000-4 000	72	3.0-4.8
AR glass	8-20	2.70	1 500-3 700	80	2.5-3.6
Synthetic					
Acrylic (PAN)	5-17	1.18	200-1 000	14.6-19.6	7.5-50.0
Aramid (e.g. Kevlar)	10-12	1.4-1.5	2 000-3 500	62-130	2.0-4.6
Carbon (low modulus)	7-18	1.6-1.7	800-1 100	38-43	2.1-2.5
Carbon (high modulus)	7-18	1.7-1.9	1 500-4 000	200-800	1.3-1.8
Nylon (polyamide)	20-25	1.16	965	5.17	20.0
Polyester (e.g. PET)	10-8	1.34-1.39	280-1 200	10-18	10-50
Polyethylene (PE)	25-1 000	0.96	80-600	5.0	12-100
Polyethylene (HPPE)	-	0.97	1000-4 000	80-150	2.9-4.1
Polypropylene (PP)	10-200	0.90-0.91	310-760	3.5-4.9	6-15.0
Polyvinyl acetate (PVA)	3-8	1.2-2.5	800-3 600	20-80	4-12
Natural - organic					
Cellulose (wood)	15-125	1.50	300-2 000	10-50	20
Coconut	100-400	1.12-1.15	120-200	19-25	10-25
Bamboo	50-400	1.50	200-440	33-40	-
Jute	100-200	1.02-1.04	250-350	25-32	1.5-1.9
Natural - inorganic					
Asbestos	0.02-25	2.55	200-1 800	164	2-3
Wollastonite	25-40	2.87-3.09	2 700-4 100	303-530	-

2.1.2.1. Synthetic Fibers

Jansson (2008, p.35) described synthetic fibers in his research as “man-made fibers resulting from research and development in the petrochemical and textile industries”. With the development of the chemical technology, synthetic fibers have been increasingly used in the last decades for the reinforcement in cementitious materials. Many commercially available fibers in the constructions field have been formulated and manufactured specifically in order to use as a reinforcement in mortars and concrete. Fibers derived from polymers are generally used in synthetic fiber reinforced concretes. As it is seen in Table 2-1 most common types of fibers used in concrete matrices include polypropylene, polyethylene, carbon, nylon, and polyester. Some of the listed fibers in Table 2-1 are produced and sold in many commercial applications. Therefore, they have been subject of extensive research especially, polypropylene. While for the others, a limited number of researches are available in the literature. It should be noted that the properties of synthetic fibers show a huge variety with regard to tensile strength and modulus of elasticity (see Table 2-1).

2.1.3. Polypropylene Fiber Reinforced Concrete (PFRC)

Polypropylene (PP) fibers are made from homopolymer polypropylene resin in various shapes and sizes with different properties (Bentur and Mindess, 2007). The main benefits of polypropylene fibers are high alkali resistance, high melting point and low cost. In addition to advantages, however, there are many drawbacks of PP fibers, such as poor bond properties with the matrix, sensitivity to sunlight and oxygen. Also, they have a lower modulus of elasticity, which changes to from 1 to 8 GPa, compared to many fibers. Nonetheless, polypropylene fibers that have a relatively high modulus of elasticity have been developed in the last decade for the purpose of reinforcement in concrete.

According to studies that conducted by Bentur and Mindess (2007), polypropylene fibers can be used for different purposes to strengthen cementitious composites. For example, fibers that have a discrete and small component may be used as a primary

reinforcement in concrete if the fiber volume content is higher than 5 per cent. This volume content is relatively higher compared to common application and the material is referred to as High Performance Fiber Reinforced Concrete (HPFRC). However, it is not easy to produce such a compound by simply mixing the fibers and the concrete matrix. Instead of using small and discrete fibers, continuous fiber mats can be used in the concrete matrix by hand lay-up of layer method or industrial mechanized processes to obtain high performance. Another application of fibers in the concrete is as secondary reinforcement purpose, for instance, to decrease the plastic shrinkage effect. The volume content of polypropylene fibers is generally below 1 % and they have a low modulus. Moreover, this low volume content in concrete is not an effective solution for hardened concrete because of having low cracking control. Apart from that, according to Jansson (2008), polypropylene fibers can be used in concrete as fire protection. He also summarized the behavior of polypropylene fibers under the fire as “the fibers melt, leaving empty channels that provide an escape route for the steam produced during the fire, thus preventing spalling of the reinforcement cover” from Bentur and Mindess (2007).

2.1.3.1. Post-cracking Behavior of PFRC

The behavior of fiber reinforced concrete (FRC) shows variety with the fiber content, type and matrix composition. In other words, obtaining the desired behavior of FRC depends on many parameters. However, there are two types of mechanical behavior that fiber reinforced concrete show under axial tension. The first one is post cracking softening behavior that the deformations localize in one crack and no other crack is observed. After the first crack, strength of the structure decreases, and this situation prevents further cracks. The second one is post crack hardening behavior that multiple crack formation before reaching the peak value. This is also known as strain hardening, strength increases before the failure of the structure. Softening and hardening behaviors under the axial tension are shown in Figure 2.3.

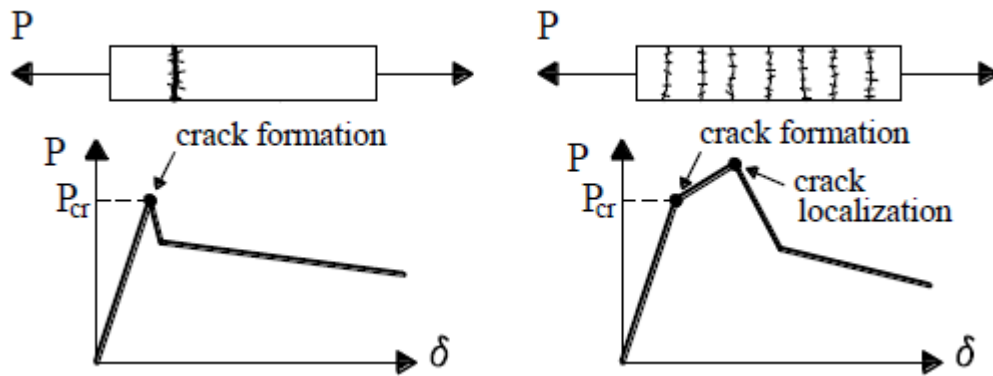


Figure 2.3. Softening and hardening behavior of PRC in axial tension (fib Model Code 2010, 2012)

In general, uniaxial test is made to directly evaluate the post cracking tensile behavior of fiber reinforced concrete. However, uniaxial tensile testing is not suggested by fib Model Code 2010, (2012) for standard testing of new mixtures because interpretation and performing of tensile tests are quite difficult. Another reason explained in the code is that fiber orientation that depends on manufacturing method affect the results significantly. Since the specimens used in the tests are normally small, the number of fibers in the governing plane, where the cracking occurs, are small, as well. Therefore, bending tests, such as EN 14651, are usually advised by design recommendations in order to analyze the flexural response of cementitious composites after cracking (ITAtch report n.7, 2016).

In addition, it should be considered that behavior of FRC shows huge differences between the test methods. Fib Model Code 2010, (2012, p.220) touches an important point before the determination of fiber reinforced concrete behavior and this is explained as follows “Softening behavior in tension can correspond to hardening behavior in bending. Even a bending softening material can result in a hardening behavior of a suitable structure”. This condition is clearly represented in Figure 2.4. The lines in this figure represent the possible results of test.

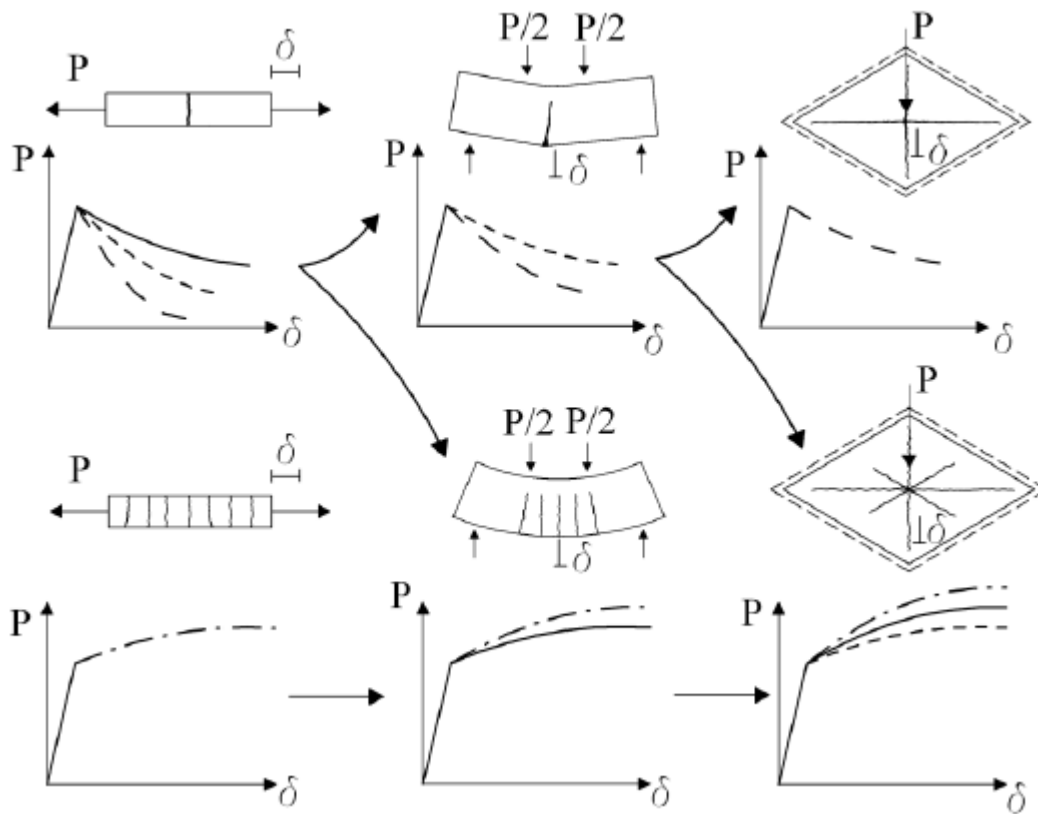


Figure 2.4. Softening and hardening behavior differences at the point of the structural level, from (fib Model Code 2010, 2012)

Nowadays, majority of the fiber reinforced concrete used in projects shows a post cracking softening behavior. Nonetheless, some fiber reinforced concrete especially, in high fiber content shows a hardening behavior under tension. As previously mentioned, these are called as high performance fiber reinforced concrete (HPFRC). Figure 2.5 illustrates schematically the post cracking behavior differences between plain concrete and two types of FRC.

To evaluate the behavior of polypropylene fiber reinforced concretes (PFRC), some experimental studies have been carried out in the literature (Cominoli et al., 2007; Jose et al., 2015). These comparison studies of polypropylene and steel fiber reinforced concrete, with contain normal fiber dosages, revealed that the majority of polypropylene FRC show softening behavior under bending. In contrast, steel fiber

reinforced concrete exhibited strain hardening behavior that increased load bearing capacity after cracking.

Another important point is that if fiber reinforcement is used in concrete for structural purposes without any conventional flexural reinforcement, they exhibit quasi-strain hardening (a post-cracking strength greater than the cracking strength) or pseudo-strain hardening (elastic-plastic response) behavior. For some kinds of structures such as thin elements subjected only to flexural loading, a material that having deflection hardening behavior would be proper (Jansson, 2008). However, according to Kanstad and Dössland (2004), strain/deflection-softening material is sufficient for walls, slabs on grounds, tunnel linings and structures, where extreme loading would not cause undesired consequences or where compressive stresses are present.

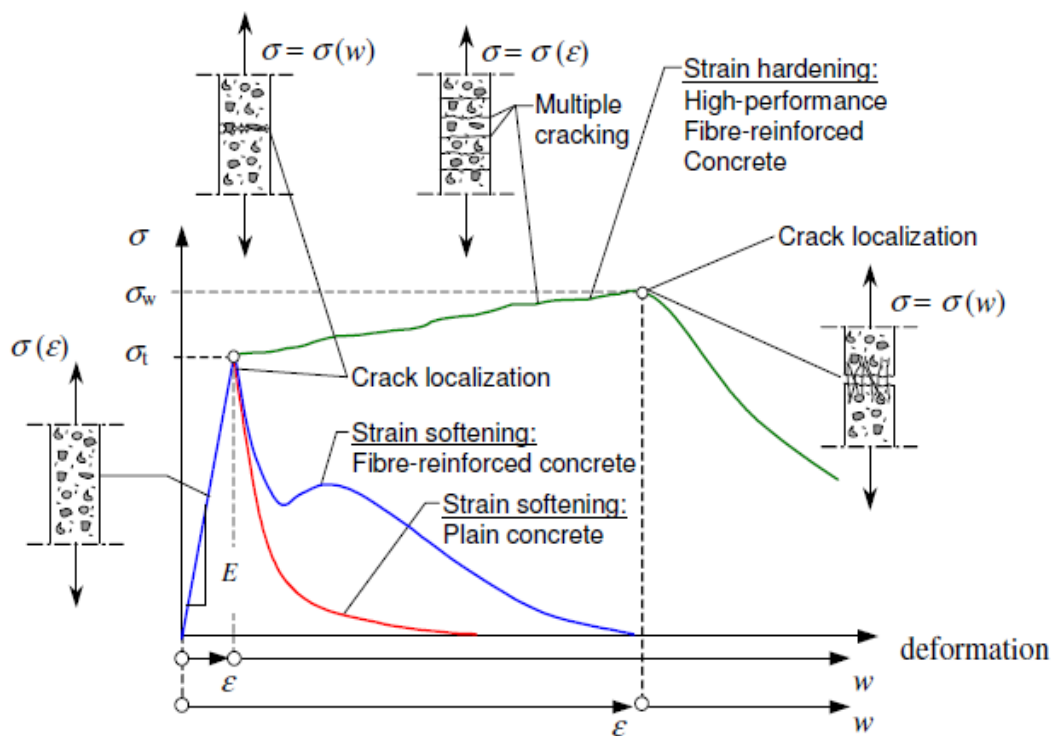


Figure 2.5. Difference in tensile behavior for cement-based materials (Löfgren, 2005)

2.1.4. Precast Tunnel Segments Reinforced by Fibers

Research on fiber reinforced concrete (FRC) started in the 1960s. Since then, extensive researches have been done to get a deeper understanding of fibers, especially steel fibers. Parallel to the success achieved in the researches, FRC has been used in a different application for structural purposes (Liao, 2015). As previously mentioned, fibers that randomly distributed and discrete material are included in the concrete matrix like aggregates, and they enhance the mechanical behavior of concrete. They allow not only to improve structural performance of concrete but also, in most of the applications economical solutions are obtained. Since fibers are easily added in concrete matrix, labour and manufacturing cost decrease. In addition to this, they provide opportunities for saving the time of project due to easy workability of fibers. For these reasons, nowadays, one of the most common uses of FRCs is precast segments of tunnels.

Precast concrete segments have been used in tunnels with the invention of the shield tunnelling technique. Today's most of tunnels are constructed with the help of Tunnel Boring Machines (TBM), which allows safer excavation for long tunnels especially in weak rock or soft soil. These precast concrete segments are generally reinforced with conventional reinforcing bars to resist the tensile forces both at SLS and ULS. However, the possibility of a totally or partially replacement of the traditional reinforcement with FRC has been investigated extensively in the past decades. Since 1980s fiber reinforced concretes have been involved in projects as innovative material for the construction of tunnel segments. One of the main reasons for this is that FRC provides elimination of time, which needed for the preparation of rebars, before the casting the tunnel segments. Another important reason for using fibers in the concrete segment is structural responsibilities. Except in the case of asymmetric loading situation, tunnels are mainly subjected to compression during the service stage. Therefore, fibers may be used alone as a reinforcement in order for resisting of tensile stresses that arise in the transient stages and avoiding brittle failure. However, FRCs have to satisfy the minimum ductility requirements established in recommendations

and codes (Liao, 2015). Apart from that, using only traditional reinforcement in precast tunnel segments may not be enough to prevent formation of cracks during the transient phase (demoulding, storage, transportation and handling). Spalling and splitting stresses that occurred during the construction phase cause visible cracks on the segments. These cracks affect concrete durability particularly, in aggressive soil conditions such as high level of water table. Since fibers have advantages in terms of cracking control due to the enhancement of post cracking tensile strength of concrete, nowadays, there is a growing interest on fibers.

Some researchers conducted a literature search on tunnels made by fiber reinforced concrete precast tunnel segments. These are; de la Fuente et al., (2012) covers the period from 1993 to 2010; Liao et al., (2015) cover the period from 1982 to 2014; Gong et al., (2017) covers the period from 1999 to 2015. However, the most comprehensive study related to FRC precast segment is included in the ITA report n.16, (2016) report. In this report, totally, 73 case histories take place from 1982 to 2016 and also covers under construction tunnel. These tunnels constructed with FRC are presented in Table 2-2. It is revealed that FRC precast tunnel segments have been used for different purposes, i.e. gas pipeline, water supply, waste water, subway, and railway. According to this report, the first precast fiber reinforced tunnel segments have been used for the construction of Metrosud in 1982. However, the first synthetic fibers have been used in precast tunnel segments in 2009; Harefield Gas Tunnel and Malaga Rail Tunnel. In addition, nowadays, hybrid solutions that the combination of conventional rebars and fiber reinforcement are investigated extensively for using in the precast tunnel segments. The data reported in Table2-2 indicated that the tunnel linings reinforced with only fiber reinforcement are nearly 71%, and for the remaining 29% with a hybrid solution. Moreover, steel fiber is the main type of fiber used in the cases reported in Table- 2.2, with a content that ranges from 25 kg/m³ to 60 kg/m³. Nonetheless, synthetic fibers content used in the tunnels are 5 kg/m³ and 7 kg/m³. Detailed information on real case studies of FRC tunnels can be found in ITA report

n.16, (2016) “Twenty Years of FRC Tunnel Segments Practice: Lesson Learnt and Proposed Design Principles”.

Table 2.2. Tunnels lined by FRC precast tunnel segments (ITA report n.16, 2016)

TUNNEL NAME	YEAR	COUNTRY	FUNCTION	DI (M)	H (M)	D/H (-)	TYPE OF FRC	FIBRE CONTENT (KG/m ³)	FIBRE VOLUME FRACTION (%)	REBAR ⁹ USED
Metrosud	1982	Italy	Subway	5.8	0.30	19.3	SFRC	N.A.	N.A.	No
Fanaco	1989	Italy	Water Supply	3.0	0.20	15.0	SFRC	N.A.	N.A.	No
Heathrow Baggage Handling	1993	England	Service	4.5	0.15	30.0	SFRC	30	0.38%	No
Heathrow Express	1994	England	Railway	5.7	0.22	25.9	SFRC	30	0.38%	No
Napoli metro	1996	Italy	Subway	5.8	0.30	19.3	SFRC	40	0.51%	No
Lesotho Highlands	1996	South Africa	Water Supply	4.5	0.30	15.0	SFRC	50	0.64%	No
Hachinger	1998	Germany	Water Supply	2.2	0.18	12.2	SFRC	N.A.	N.A.	No
2nd Heinenoord	1999	Netherlands	Road	7.6	0.35	21.7	SFRC	N.A.	N.A.	No
Jubilee Line	1999	England	Subway	4.5	0.20	22.3	SFRC	30	0.38%	No
Trasvases Mariabí (La Esperanza)	2001	Ecuador	Water Supply	3.5	0.20	17.5	SFRC	30	0.38%	No
Essen	2001	Germany	Subway	7.3	0.35	20.9	SFRC	N.A.	N.A.	No
Sorenberg	2002	Switzerland	Gas Pipeline	3.8	0.25	15.2	SFRC	40	0.51%	No
Canal de Navarra	2003	Spain	Water Supply	5.4	0.25	21.6	N.A.	N.A.	N.A.	No
Oberberg tunnel	2003	Switzerland	Railway	10.8	0.30	36.0	N.A.	N.A.	N.A.	No
Oberberg-TBM	2003	Switzerland	Railway	11.4	0.40	28.5	SFRC	30	0.38%	Yes
Oberberg-Shield	2003	Switzerland	Railway	11.4	0.40	28.5	SFRC	60	0.76%	No
Barcelona Metro Lín 9 - Can Zam Stretch	2003	Spain	Subway	10.9	0.35	31.1	SFRC	60	0.76%	No
Channel Tunnel Rail Link (CTRL)	2004	England	Railway	7.2	0.35	20.4	SFRC	30	0.38%	No
Heathrow Express Extension (HexEx)	2005	England	Railway	5.7	0.22	25.9	SFRC	30	0.38%	No
Metropolitan Expressway Central Circular Shinjuku Route tunnel	2005	Japan	Road	10.9	0.45	24.2	SFRC	63	0.80%	Yes
San Vicente	2006	USA	Water Supply	3.2	0.18	17.8	SFRC	30	0.38%	No
Heathrow- SWOT	2006	England	Water Supply	2.9	0.20	14.5	SFRC	30	0.38%	No
Barcelona Metro Line 9 - Stretch I	2006	Spain	Subway	8.4	0.32	26.3	SFRC	30 and 25	0.38% and 0.32%	Yes
Lötschberg	2007	Switzerland	Temporary pilot	4.5	0.22	20.5	SFRC	N.A.	N.A.	No
Beacon Hill Tunnels	2007	USA	Road	6.7	0.30	22.3	N.A.	N.A.	N.A.	No
Hofoldingner Stollen	2007	Germany	Water Supply	2.9	0.18	16.1	SFRC	40	0.51%	No
Madrid Metro	2007	Spain	Subway	8.4	0.30	28.0	SFRC	25	0.32%	Yes
Gold Coast Desalination Plant	2008	Australia	Water Supply	3.4	0.20	17.0	SFRC	35	0.45%	No
Big Walnut Sewer	2008	USA	Waste Water	3.7	0.23	16.1	SFRC	35	0.45%	Yes
Heathrow - PiccEx	2008	England	Subway	4.5	0.15	30.0	SFRC	30	0.38%	No
Heathrow Express Ext. Tunnel to T5	2008	England	Railway	5.7	0.22	25.9	SFRC	30	0.38%	No
Hobson Bay	2009	New Zealand	Waste Water	3.7	0.25	14.8	SFRC	40	0.51%	No
Sao Paulo Metro Line 4	2009	Brazil	Subway	8.4	0.35	24.0	SFRC	35	0.45%	No
Copenhagen District Heating Tunnel	2009	Denmark	Water Supply	4.2	0.30	14.0	SFRC	35	0.45%	No
Docklands Light Railway (DLR) Extension	2009	England	Railway	5.3	0.25	21.2	SFRC	N.A.	N.A.	No
Harefield Gas Tunnel	2009	England	Gas Pipeline	2.6	0.18	14.4	SynFRC	7	0.78%	No

Continuing part of Table 2-2 (ITA report n.16, 2016)

TUNNEL NAME	YEAR	COUNTRY	FUNCTION	DI (M)	H (M)	DI/H (-)	TYPE OF FRC	FIBER CONTENT (KG/M ³)	FIBER VOLUME FRACTION (%)	REBARS USED
Malaga Rail Tunnel	2009	Spain	Railway	8.4	0.32	26.3	SynFRC	5	0.56%	Yes
Fontsaneta-Thiniat Interconnection	2010	Spain	Water Supply	5.2	0.20	26.0	SFRC	25	0.32%	Yes
Clem Jones - Clem 7	2010	Australia	Road	11.2	0.40	28.0	SFRC	37	0.47%	Yes
Ems-Dollard Crossing	2010	Germany-Netherlands	Gas Pipeline	3.0	0.25	12.0	N.A.¹	N.A.¹	N.A.¹	No
City West Cable Tunnel (CWCT)	2010	Australia	Power Cable	2.5	0.20	12.5	N.A.¹	N.A.¹	N.A.¹	No
Adelaide Desalination Plant	2010	Australia	Water Supply	2.8	0.20	14.0	SFRC	35	0.45%	No
FGC Terrassa	2010	Spain	Railway	6.0	0.30	20.0	SFRC	25	0.32%	Yes
Kelo Iine	2010	Japan	Railway	6.7	0.30	22.3	SFRC	63	0.80%	Yes
Brightwater East	2011	USA	Waste Water	5.1	0.26	19.6	SFRC	35	0.45%	No
Brightwater Central	2011	USA	Waste Water	4.7	0.33	14.2	SFRC	40	0.51%	No
Brightwater West	2011	USA	Waste Water	3.7	0.26	14.2	SFRC	35	0.45%	No
East side CSO	2011	USA	Waste Water	6.7	0.36	18.6	SFRC	32	0.40%	No
Izumi-Otsu	2011	Japan	Water Supply	1.8	0.13	14.4	SFRC	32	0.40%	Yes
Metropolitan Expressway	2011	Japan	Road	13.4	0.45	29.8	SFRC	47	0.60%	Yes
Victorian Desalination Plant	2011	Australia	Water Supply	4.0	0.23	17.4	N.A.¹	N.A.¹	N.A.¹	No
Monte Lirio	2012	Panama	Water Supply	3.2	0.25	12.8	SFRC	40	0.51%	No
Pando	2012	Panama	Water Supply	3.0	0.25	12.0	SFRC	40	0.51%	No
Airport Link	2012	Australia	Road	11.4	0.40	28.4	SFRC	35	0.45%	No†
Midosuji Utility	2012	Japan	Utility	5.1	0.15	33.8	SFRC	32	0.40%	Yes
Sagami Line	2012	Japan	Road	11.8	0.50	23.6	SFRC	47	0.60%	Yes
El Alto	2013	Panama	Water Supply	5.8	0.35	16.6	SFRC	40	0.51%	No
Asada Trunk Line	2013	Japan	Sewage	4.6	0.20	22.8	SFRC	25	0.32%	Yes
Koishikawa Kasen	2013	Japan	Railway	6.7	0.30	22.3	SFRC	47	0.60%	Yes
Oi-Ariake Cable	2013	Japan	Power Cable	4.0	0.20	20	SFRC	32	0.40%	Yes
Wehrhahn	2014	Germany	Subway	8.3	0.30	27.7	SFRC	30	0.38%	No
STEP Abu Dhabi Lot T-02	2014	UAE	Waste Water	6.3	0.28	22.5	SFRC	30	0.38%	Yes
San Francisco Central Subway	2014	USA	Railway	5.4	0.28	19.3	SFRC	30	0.38%	Yes
Legacy Way	2015	Australia	Road	11.3	0.35	32.3	SFRC	40	0.51%	No†
Metropolitan Expressway	2015	Japan	Road	12.3	0.40	30.8	SFRC	47	0.60%	Yes
Abu Hamour	2016	Qatar	Water Drainage	3.7	0.25	14.8	SFRC	40	0.51%	No
Doha Metro Red North Line	2016	Qatar	Subway	6.17	0.30	20.6	SFRC	40	0.51%	No
Abatemarco	-	Italy	Water Supply	3.5	0.20	17.5	SFRC	40	0.51%	No
Public Sewage	-	Japan	Sewage	5.6	0.18	32.0	SFRC	43	0.55%	Yes
Lee Tunnel Sewer	U.C.*	England	Waste Water	7.2	0.35	20.6	N.A.¹	N.A.¹	N.A.¹	No
Downtown Line 3	U.C.*	Singapore	Subway	5.8	0.28	21.1	SFRC	40	0.51%	No
Thomson Line	U.C.*	Singapore	Subway	5.8	0.28	21.1	SFRC	40	0.51%	No
Crossrail	U.C.*	England	Railway	6.2	0.30	20.7	SFRC	30-40	0.38% and 0.51%	No

2.1.5. Experimental and Numerical Studies on FRC Precast Tunnel Segments

Up to the present, there have been several experimental and numerical studies carried out to investigate the mechanical and structural behavior of fiber reinforced concrete tunnel segments. Some of the researchers collected the studies related to FRC tunnel segments from the scientific literature (Liao, (2015); Gong et al.,(2017)). The survey of experimental and numerical research on scaled or full-scale precast tunnel segments are tabulated in Table 2-3 and Table 2-4. Some of these studies were performed in order to improve the design of FRC precast segments under concentrated loads arisen by TBMs during the installation of segments. Some of these studies carried out using real tunnels segments (e.g. Saronno-Malpensa Railway (Plizzari and Tiberti 2007), Brennero Base Tunnel (Caratelli et al. 2011), Barcelona Metro Line 9 (de la Fuente et al 2012), Prague Metro Line (Beno and Hilar 2013), and Monte Lirio Hydraulic Tunnel (Conforti et al. 2017)). The general inferences from these studies is that the presence of fibers in concrete mix enhances the concrete capacity against cracking due to the spalling and splitting stresses. Within this framework, comparison studies between fiber reinforced concrete and plain concrete or reinforced concrete were performed in order to obtain more detailed and accurate information. Since asymmetric loading situations, imperfection support conditions and eccentricity of the loading create significant stresses on the segments, these effects are considered comprehensively in the design part of tunnels. Experimentally, Meda et al. (2016) investigated how boundary conditions and asymmetric loading affect the structural behavior of tunnel segments. In addition to this, Beno and Hilar (2013) conducted an experiment upon the precast segments with the cantilevered configuration. Apart from that, Gong et al. (2017) made an experimental investigation of segmental joints effect on precast tunnel segments. The radial joint is the contact between segments of the same ring and allows the force transmission due to ground loads. If some irregularity occurs in the joints, extreme stresses arise in that region. Similar to TBM thrust forces, this effect leads to cracking on segments. In addition to axial loading test, bending or

flexural tests were performed by many researchers, to determine and analyse the bearing capacity and ductility of segments. In a similar manner to point load test, reference samples were used in order to investigate the capacities of tunnel segments. Moreover, de la Fuente et al. (2012) performed in situ loading test in the tunnel. As a result of these experiments, FRCs have been used in the construction of many tunnels (see Table 2-2). Moreover, under fire effect, the behavior of fibers has been the subject of debate. In order to evaluate the structural behavior of fiber reinforced concrete tunnel segments under fire, Yan et al. (2015, 2016) carried out experiments.

In the literature, some of the researchers performed numerical studies on precast tunnel segments, especially to investigate the TBM thrust effect. For this, 2D or 3D finite element models were used and made calibrations comparing with the previous experimental results. However, in order to analyze concrete behavior, 3D finite element models with local approaches such as smeared cracking has been extensively used by researchers (e.g. Plizzari and Tiberti, (2007); de la Fuente et al., (2012); Meda et al., (2016)). The most common software packages applied for this purpose are DIANA, ATENA, FLAC and ABAQUS. Apart from evaluating the structural behavior of segments, numerical studies also performed in order to optimize the amount of fibers and design check. Since performing full scale test is difficult and expensive, some researches like Di Carlo et al. (2016) tried to develop analytical formulations for the design of FRC tunnel segments.

As it is seen in Table 2-3 and Table 2-4, most studies focus on elements with steel fiber reinforced concrete due to several advantages. However, it should be noted that synthetic fibers such as polypropylene are very new material compared to steel. With the development of chemical technologies, nowadays, man-made fibers are extensively produced. Although the number of studies on synthetic fibers is yet limited, it is increasing substantially (Yan et al., (2015); Yan et al., (2016); Conforti et al., (2017)). The fiber dosage used in the experiments ranges from 10 to 120 kg/m³ (all types of fibers) and concrete class ranges from normal concrete (C35 grade) to high performance concrete (C150).

Table 2.3. Previous experimental studies on FRC tunnel segments, adopted from Gong et al. (2017)

Type of test	Numerical simulation	Material	Dimension (mm) Length x Width x Thickness	Concrete Class	Conventional reinforcement (kg/m ³)	Fiber dosage (kg/m ³)	Objective	References
Full-scale bending and point load	-	PC SFRC SFRC	2359 x 1400 x 350	C60	Unknown - -	- 30 40	Load bearing capacity of segments	Poh et al. (2009)*
Full-scale bending and point load	-	RC SFRC	3640 x 1500 x 200	C50	- -	None 40	Structural behavior of segments	Caratelli et al. (2011)
Full-scale bending in situ loading	-	SFRC	Unknown x 1800 x 350	C50	-	60	Structural response under real work condition	Molins and Armau (2011)
Bending on symmetric inclination beam	-	HPC FRHPC FRHPC	1100 x 150 x 150	C60	Unknown Unknown Unknown	None 25 50	Mechanical behavior of segments	Ding et al. (2011)*
Full-scale bending and point load	-	SFRC	1840 x 1200 x 250	C35/45	-	40	Ductile behavior of segments	Caratelli et al. (2012)
1/3-scale vertical and horizontal loading	-	RC SFRC	1530 x 300 x 120	C55	Unknown -	None 63	Structural behavior of linings in fire	Yan et al. (2013)*
Full-scale bending and point load	2D (ATENA)	SFRC SFRC	Unknown x Unk. x Unk.	Unknown	- -	40 50	Structural behavior of segments	Beno and Hilar (2013)
Full-scale settlement and punching	-	RC SFRC	2120 x 1500 x 235	C60	Unknown -	None 120	Settlement and punching behavior of segments	Abbas et al. (2014)
Full-scale monotonic & cyclic bending and point load	-	RC SFRC	3180 x 1500 x 235	C60	Unknown -	None 120	Structural behavior of segments	Abbas et al. (2014b)*
Full-scale bending and point load	-	SFRC	1670 x 1200 x 250	Unknown	-	40	Load bearing capacity of segments	Meda and Rinaldi (2015)*
1/3-scale bending and point loading	-	UHPRC	1000 x 500 x 100	C150	Unknown - - -	None 30 60 90	Ultimate bearing capacity of segments	Nehdi et al. (2015)
1/3-scale flexural and axial loading	-	RC HFRC	1530 x 300 x 120	C70	Unknown -	None 78+2	Structural behavior of segments in fire	Yan et al. (2015)
1/3-scale flexural and axial loading	-	RC HFRC	1530 x 300 x 120	C70	Unknown -	None 78+2	Structural behavior of segments in fire	Yan et al. (2016)
Full-scale bending	-	CFRC SCDRC	5500 x 1200 x 300	C40	Unknown -	None 50	Ductile behavior of segments	Liao et al. (2016)
Full-scale biaxial loading	-	RC + SFRC RC + SFRC RC + SFRC	3167 x 1200 x 300	C50	Unknown Unknown Unknown	30 25 30	Mechanical behavior of segments	Meng et al. (2016)
Full-scale bending and point load	-	RC PFRC RC + PFRC	1810 x 1200 x 250	C40/50	114 None 52	None 10 10	Structural behavior of segments	Conforti et al. (2017)
Full-scale monotonic vertical and horizontal loading	-	RC SFRC	1200 x 1000 x 600	C60	164 -	None 80	Ultimate bearing capacity of segmental joints	Gong et al. (2017)

Table 2.4. Previous numerical and analytical studies on FRC tunnel segments, adopted from Gong et al. (2017)

Approach	Type of test	Numerical simulation	Material	Dimension (mm) Length x Width xThickness	Concrete Class	Conventional reinforcement (kg/m3)	Fiber dosage (kg/m3)	Objective	References
Numerical	None	2D & 3D (DIANA)	PC SFRC	Unknown x Unk. x Unk.	Unknown	Unknown -	None 40	Structural behavior of segments	Plizzari and Tiberti (2006)*
	None	3D (DIANA)	RC SFRC RC + SFRC	2700 x 1700 x 300	Unknown	82 - 55	None 30 30	Structural behavior of segments	Plizzari and Tiberti (2007)
	None	2D (FLAC)	SFRC	Unknown x 1500 x 300	C50/60	-	35	Design check	Kasper et al. (2008)*
	None	2D & 3D (DIANA)	SFRC	Unknown x 1800 x 350	C50	-	60	Comparison with experimental results	Arnua and Molins (2011)
	None	3D (DIANA)	RC	3000 x 1400 x 300	Unknown	Unknown	None	Comparison with experimental results	Cignitti et al. (2012)
	None	3D (FLAC)	SFRC	Unknown x 1400 x 300 Unknown x 1500 x 350	C50/60 C30/37	- -	25 25	Optimization of the amount of fibers	de la Fuente et al. (2016)
Analytical	None	None	SFRC	3500 x 2500 x 300	C40	-	None	Design procedure of segments	Di Carlo et al. (2016)
Experimental + Numerical	Full-scale bending	3D (ABAQUS)	SFRC	2438 x 1500 x 235	Unknown	-	57	Structural behavior of segments	Blazejowski (2012)*
	Full-scale point load	3D (DIANA)	RC	3000 x 1400 x 300	Unknown	Unknown	None	Structural behavior of segments	Meda et al. (2016)

* as cited in Gong et al., (2017)

Material abbreviations in Table 2-3 and Table 2-4;

PC: plain concrete, RC: reinforced concrete, SFRC: steel fiber reinforced concrete, PFRC: polypropylene fiber reinforced concrete; CFRC: conventional fiber reinforced concrete; SCFRC: self-compacting fiber reinforced concrete, UHPFRC: ultra-high fiber reinforced concrete, HPC: high performance concrete, FRHPC: fiber reinforced high performance concrete, HFRC: hybrid fiber reinforced concrete that consist of polypropylene and steel fibers.

2.2. Literature Study on Fiber Reinforced Polymer Bars

2.2.1. General

Fiber reinforced polymer (FRP) materials have been manufactured as an innovative solution for concrete structures. According to ACI 440.1R-15 (2015, p.3) design guideline report, fiber reinforced polymer (FRP) is defined as “composite materials made of fibers embedded in a polymeric resin”. Traditional steel reinforcing bars used most commonly in the construction field are very sensitive to aggressive environmental conditions, such as moisture, temperature differences, sulphate, and chlorides. These aggressive conditions cause corrosion of reinforcing steel bars in concrete due to reducing alkalinity of concrete. As a consequence of corrosion, the durability and serviceability of structures are decreasing significantly as the time passes. For these reasons, for structures exposed to aggressive conditions such as, underground structures, marina structures, and bridges, some precautions are taken in order to protect against corrosion. Designing higher concrete cover thickness in order to decrease external attack, cathodic protections in tunnels segments in order to preventing corrosion or using insulation materials to prevent sealing are some of the examples of precautions. However, these are also extra effort and cost for projects. Even, excessive corrosion causes high maintenance costs in some projects.

In addition to the non-corrosive characteristic, some FPR reinforcing bars are nonmagnetic and they do not conduct the electricity. This feature has a crucial role for some type of constructions, (e.g. airport runways, highway control point, electronics laboratories) in overcoming the problems of electromagnetic interference. Therefore, fiber reinforced polymer reinforcing bars are preferred in many projects due to its advantages in the aggressive environments and being electrically nonconductive reinforcement compared to conventional steel reinforcing bars.

The mechanical behavior of fiber reinforced polymer reinforcing bars is quite different from the behavior of traditional steel reinforcements. In contrast to steel reinforcements, FRP rebars do not show ductile behavior, they are very brittle. In fact,

FRP materials do not yield and they stay in elastic range until the failure. Furthermore, FRP materials have anisotropic structure and they exhibit different properties depending on their orientations. FRCs have significantly high tensile strength only in the direction of reinforcing fibers, in other words, longitudinal direction. This anisotropy also affects the shear strength and bond performance of FRP reinforcing bars (ACI 440.1R-15, 2015). For this reason, use of FRP reinforcing bars in concrete for structural purposes needs consideration of related specifications and guidelines, such as ACI 440.1R-15, (2015); fib Bulletin 40, (2007); CNR-DT 203, (2006).

2.2.2. Types and Classification of FRP Reinforcing Bars

Fiber reinforced polymer materials can be classified into three main categories based on the material used in the manufacturing process. These are polymeric fibers, carbon fibers, and inorganic fibers. Under the three main categories, there are many types of fiber reinforced polymer reinforcing bars are available in the markets. However, the most commonly used ones in the construction industry are;

- 1- Aramid fiber reinforced polymer (AFRP)
- 2- Carbon fiber reinforced polymer (CFRP)
- 3- Glass fiber reinforced polymer (GFRP)

Examples of fiber reinforced polymer reinforcing bars are shown in Figure 2.6. Moreover, general mechanical and material characteristic of FRP are tabulated in Table 2-5.



Figure 2.6. Types of FRP (ACI 440.1R-15, 2015)

Table 2.5. General mechanical and physical properties of FRP, adopted from ACI 440.1R-15 (2015)

		Steel	AFRP	CFRP	GFRP
Density (g/cm ³)		7.9	1.25 to 1.40	1.50 to 1.60	1.25 to 2.10
Coefficient of thermal expansion (x10 ⁻⁶ C)	Longitudinal direction	11.7	-6.0 to -2.0	-9.0 to 0.0	6.0 to 10.0
	Transverse direction	11.7	60.0 to 80.0	74.0 to 104.0	21.0 to 23.0
Nominal yield stress (MPa)		276 to 517	-	-	-
Tensile strength (MPa)		483 to 1600	1720 to 2540	600 to 3690	483 to 690
Elastic modulus (GPa)		200.0	41.0 to 125.0	120.0 to 580.0	35.0 to 51.0
Yield strain (%)		0.14 to 0.25	-	-	-
Rupture strain (%)		6.0 to 12.0	1.9 to 4.4	0.5 to 1.7	1.2 to 3.1

It should be noted that the material properties of FRP bars change the manufacturer to manufacturer because they are man-made materials and largely depends on the used materials quality.

2.2.2.1. Glass Fiber Reinforced Polymer Rebars

Glass fiber reinforced polymer reinforcing bars are most commonly used FRP rebar type all over the world. In civil engineering, the application of GFRP reinforcements in concrete structures has shown huge variety from bridge decks to rail plinths. The Headingley Bridge in Manitoba, The Floodway Bridge in Winnipeg, Gonda Building in Rochester and State Avenue in Kansas City are some of the examples that GFRP reinforcing bars were used for the structural purposes in concrete (ACI 440.1R-15, 2015). In Turkey, GFRP rebars are the widely used in temporary stations walls, where excavated by TBM. As previously mentioned, the main advantages of the GFRP reinforcing bars are the high tensile strength, lightweight and non-corrosive properties. Furthermore, compared to other types of FRP, GFRP materials do not conduct the electricity and they are non-magnetic (ACI 440.1R-15, 2015). Nevertheless, there are some drawbacks in terms of structural performance and there is a need for extra attention. Moreover, it should be noted that GFRP reinforcing bars are not suitable for all type of applications. Firstly, Almusallam et al.'s study (as cited in Caratelli et al., 2016) reveal that GFRP reinforcement has a static fatigue problem when exposed to high level long term tensile stresses. Secondly, since the GFRP material has anisotropic property, coefficient of thermal expansion differs in longitudinal and radial directions. This also affects the shear strength capacity of GFRP rebar which is lower than steel reinforcement. Thirdly, concrete structures reinforced with GFRP bars have low ductility since they show linear elastic behavior up to failure. Moreover, during design part of structure serviceability has to be controlled because of lower modulus of elasticity of GFRP bars. Fourthly, according to Yoo et al.'s study (as cited in Caratelli et al., 2016), GFRP reinforcing bars show a poor bond behavior with respect to the traditional steel reinforcement. Finally, the cost of GFRP reinforcing bars is quite expensive compared to steel reinforcement.

2.2.3. Precast Tunnel Segments Reinforced by GFRP Rebars

Today, most of the tunnels are mechanically excavated by tunnel boring machines (TBMs). As previously mentioned, the tunnel lining is composed of precast concrete elements placed by the TBM during the excavation process. The application of glass fiber reinforced polymer (GFRP) reinforcing bars instead of traditional reinforcement in the precast tunnel segments is very new and controversial issue. In the last two years, a limited number of studies were carried out in order to investigate the possibility of using GFRP rebars in the tunnel linings (Caratelli et al., (2016); Caratelli et al., (2017); Spangnuolo et al., (2017)). These researchers thought that GFRP rebars could be suitable solution for tunnel segments because of many reasons. Firstly, since GFRP rebars have non-corrosive property, they are able to overcome the durability problems of tunnels caused by the aggressive environments, such as waste water tunnels or hydraulics tunnels. Moreover, the use of this non-metallic reinforcing bars in precast tunnel segments allows less concrete cover thickness. This situation is significantly important for preventing possible cracks that occur during construction of tunnel or production and transient stages of tunnel segments, due to increasing of the bending capacity of segments. Furthermore, the use of GFRP rebars in tunnels reduce stray currents since they are non-conductive materials. This also provides exclusion cathodic protection which is essential in ordinary tunnels. Finally, GFRP reinforcing bars are convenient for tunnel sections to be demolished because of easy disposal. Cross passage or emergency exit sections are typical examples of such tunnel sections to be modified after the construction.

Although, GFRP rebars are used in many structural applications, there is only one example in the literature for the tunnel lining reinforced with GFRP reinforcing bars. This is the Milan Metro Rapid Transit Line planned to be completed in 2022. Within this framework, experimental studies are being performed to obtain optimized segments with the support of Horizon 2020 European Commission. (Source: <https://www.thecompositeshub-india.com/gfrp-rebar-for-tunnel-lining>)

From the manufacturing point of view, however, there are some difficulties to produce curvilinear bars. Since precast tunnel segments have a curvilinear shape, the reinforcement needs to be curvilinear. There are many experimental studies performed to determine the mechanical properties of straight GFRP reinforcing bars (Caratelli et al., 2017). However, identify of the behavior and properties of the curvilinear rebars are required for the design. Apart from that, the cost of glass fiber reinforced polymer rebars is much higher than traditional steel; but, the higher cost can be balanced when the maintenance and cathodic protection is considered.

2.2.4. Experimental Studies on Precast Tunnel Segments Reinforced by Glass Fiber Reinforced Polymer Bars

In the literature, there is a limited number of experimental studies carried out on full-scale precast tunnel segments with GFRP reinforcing bars. The first study was performed by Caratelli et al. (2016) to evaluate the performance of a segment under the effect of TBM thrust force. In addition to this, bending tests were conducted to determine the structural behavior of segments. For that, comparison studies were done by using reference samples that containing ordinary steel reinforcements. This study indicated that using GFRP rebars in tunnel segments can be possible. The next step was optimization study on the geometry of GFRP reinforcing bars in the concrete segment. In this context, four different reinforcing models were adapted for segments and results were compared with the reference specimen. In this study cost-benefit analysis was taken into consideration to enhance crack control (Caratelli et al., 2017). These researches show that GFRP rebars geometry significantly affect the structural behavior of precast segments. Compared to the previous study, using a curvilinear reinforcement with closed ring model increase the segment capacity to a huge extent. Previous studies on full-scale precast tunnel segments reinforced by GFRP reinforcing bars in the literature tabulated in Table 2-3.

Table 2.6. Previous experimental and numerical studies on tunnel segments reinforced by glass fiber reinforced polymer rebars

References	Approach	Type of test	Material	Dimension (mm)			Concrete grade	Reinforcement detail	Objective
				Length	Width	Thickness			
Caratelli et al. (2016)	Experimental	Full-scale point load	GFRP-RC	Unknown	Unknown	250	C40/50	13+13Ø14 longitudinal bars, 13+13Ø12 straight crossbars and 42Ø14 brackets hoops	Structural behavior of segment
Caratelli et al. (2016)	Experimental	Full-scale bending	RC GFRP-RC	4150	1483	400	C40/50	12Ø12 longitudinal bars in the inner and outer surface 14Ø12 bars in the inner and 12Ø12 in the outer surface	Ultimate bearing capacity of segments
Caratelli et al. (2017)	Experimental	Full-scale bending and point load	RC GFRP-RC GFRP-RC GFRP-RC	Unknown	1420	300	C50	12Ø12 bars in the inner and outer surface, Ø8 stirrups 12Ø12 closed-rings longitudinal, Ø8 closed-rings stirrups 9 Ø16 curvilinear bar in the inner and 8 Ø16 outer surface, 12 Ø8 lattice reinforcement, 14 Ø8 stirrups Mesh 140 x 140 mm Ø13 Ø8 respectively in the outer surface and 150 x 140 mm Ø13 Ø8 respectively in the inner surface 11Ø8 pins 9 Ø16 curvilinear bar in the inner and 8 Ø16 outer surface, 12 Ø8 lattice reinforcement, 14 Ø8 stirrups	Structural behavior of segments that consist of different types of reinforcement
Spangnuolo et al. (2017)	Experimental + Analytical	Full-scale bending	RC GFRP-RC	4500	1485	400	C40	12Ø12 longitudinal bars in the inner and outer surface, 32Ø14 stirrups 12Ø14 longitudinal bars in the inner and 12Ø12 outer surface, 32Ø14 stirrups	Ultimate bearing capacity of segments

Material abbreviations in Table 2-6; RC: reinforced concrete; GFRP-RC: glass fiber reinforced polymer reinforced concrete.

CHAPTER 3

OVERVIEW OF TBM TUNNELING TECHNIQUE

In general, there are two common criteria for the classification of tunnels. The first one is based on the function of tunnels such as railway tunnels, highway tunnels, metro tunnels, pedestrian tunnels and conveyance tunnels. The second one is to classify the tunnels according to the method of constructions technique like: New Austrian Tunneling Method (NATM), cut-and-cover, drill-and-blast push or pulling box and mechanized shield tunnelling. This chapter provides brief information on mechanized shield tunnelling, principles and types of Tunnel Boring Machines, and segmental tunnel linings.

3.1. Brief History of Mechanized Shield Tunneling

Mechanized shield tunnelling is a kind of excavation method that provides a temporary support structure for the tunnel during the excavation phase, while at the same time it allows the installations of the tunnel lining directly in the underground space, thanks to the use of Tunnel Boring Machine. With the help of sophisticated automation and control systems of TBMs, tunnels can be constructed in a wide range of geological environments, including difficult conditions, such as high groundwater pressure and soft soils.

In modern societies, especially in metropolitan areas that have soft soils or weak rocks, shield tunnelling has an important role in developing urban infrastructures, and it is the best suitable method of excavation since it has a less impact on the surrounding environments (Fabozzi, 2017).

For nearly 5000 years, people have thought about the construction of tunnels for different purposes. Tunnels have been dug to protect goods and persons or to provide secret access to prohibited places, extract natural resources or speed up transport (Maidl et al., 1996). Until the early 19th century, construction of tunnels in urban areas

was possible applying two different methods. These are the cut-and-cover method, and excavation of a tunnel by means of timber frames inside the advancing cavity and then lining immediately with masonry. These excavation methods have been successfully applied in both cohesive and non-cohesive grounds, also possible in grounds with limited seepage or fissure water, but it is not possible below the groundwater table (Guglielmetti et al., 2007). However, this situation changed in 1806 when Sir Marc Isambard Brunel invented the principle of shield tunnelling in London, and he patented his invention that is the shield excavating machine in 1818 (Maidl et al., 1996). The tunnel project under the Thames River in London finally enabled Brunel to put his ideas into practice. This was recorded as the first successful shield tunnelling attempt to excavate the soft ground underneath river the Thames Tunnel in London in 1825. According to Fabozzi (2017), “M.I. Brunel is said to have been inspired in his design by the shell of the shipworm *Teredo Navalis*, a mollusc whose efficiency at boring through submerged timber he observed while working in a shipyard (see Figure 3.1)”.



Figure 3.1. “Teredo Navalis”, working on the excavation and the lining (Guglielmetti, 2007)

The working principle of Brunel’s shield tunnel excavation was that pressing a rigid frame (shield) forward through a soft ground with jacks, thereby preventing the ground from collapsing and building the tunnel structure within the frames; the tunnel would move forward by repeating the jacking process and then building the support structure (Fabozzi, 2017). As it is seen in Figure 3.2 the shield of Thames Tunnel had a rectangular shape and comprised of 12 adjacent frames that each divided into 3

chambers. In each of these chambers one worker, thus totally 36 people could work simultaneously (Maidl et al., 1996).

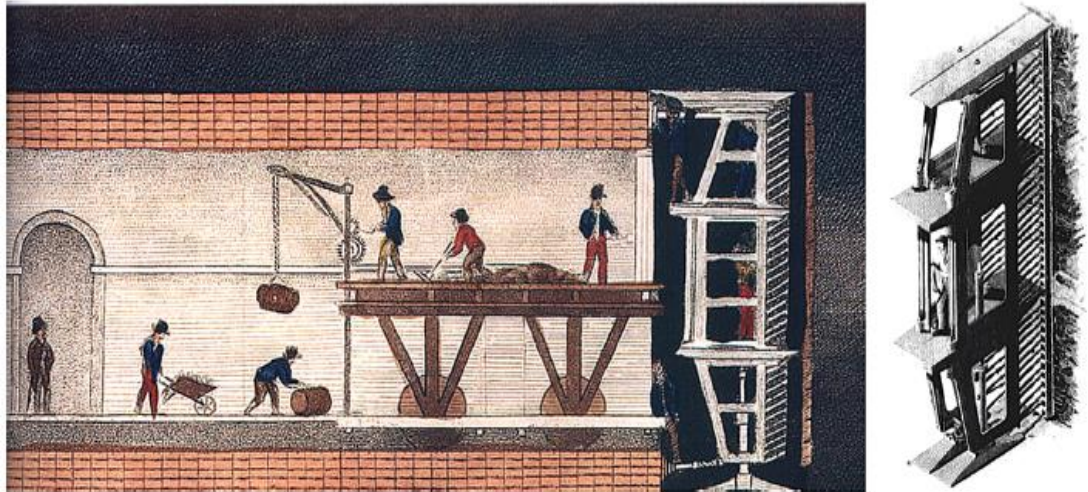


Figure 3.2. Brunel's shield tunnel excavation under River Thames in London (Guglielmetti et al., 2007)

In 1865, Peter Barlow of London patented a much simpler shield of a circular cross-section with a diameter of 2.5 m, with which James Henry Greathead drove a small bore tunnel under the River Thames at a modest cost in less than a year. At the same time, Alfred Ely Beach designed a circular cross-sectional shield that he used to drive a short experimental subway under Broadway in New York City. In the 1880s, Greathead successfully used compressed air behind his shield in order to prevent flooding during the installation of the lining in Woolwich Tunnel in London. The combination of shield and compressed air made it possible to build tunnels beneath large rivers. Modern tunneling shields (see Figure 3.3) are fundamentally the same as the Greathead design, which means strong steel cylinders are moved forward by hydraulic jacks (Britannica, 2011).

With the use of cylindrical steel shield, tunneling techniques have been steadily mechanized in the following years. In particular, with the development of urban tunneling in the second half of the twentieth century, considerable technological progress has been shown in this area. Meanwhile, the conditions surrounding the

construction of the tunnel have become increasingly complex and difficult. In recent years, tunneling technologies have been developed using sophisticated and multidisciplinary principles of engineering to deal with the various physical, environmental and social circumstances (ITA WG 14, 2000).

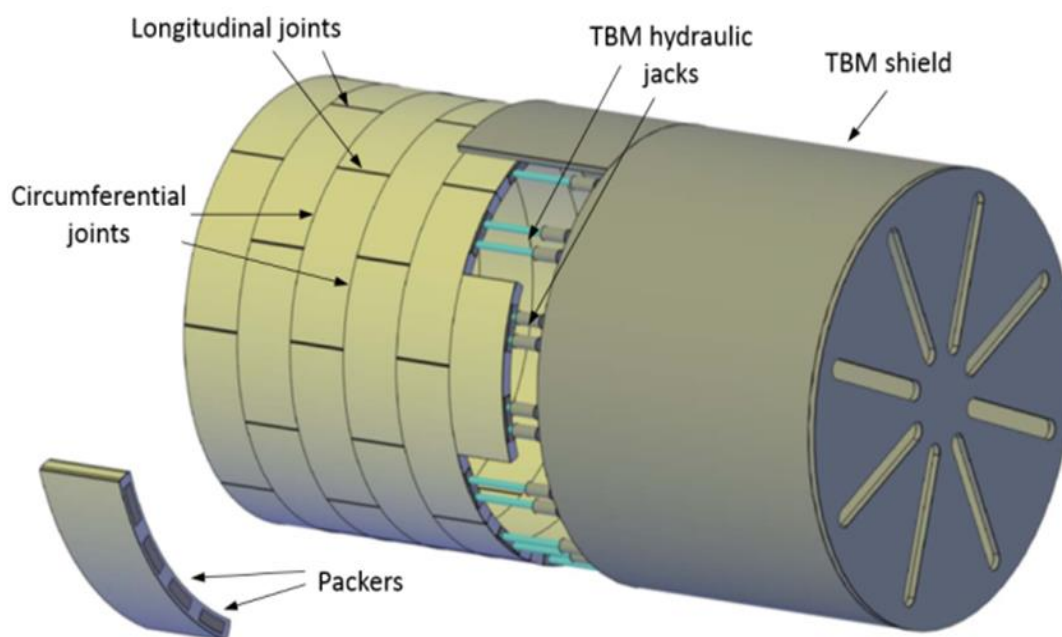


Figure 3.3. Tunnel boring machine and segmental tunnel lining (Arnau & Molins, 2015)

3.1.1. Operating Principle of Tunnel Boring Machines

In the scope of this thesis, general overview of the operation principle of TBMs is necessary for an understanding of full-scale experimental tests.

Maidl et al. (2008) described that the Tunnel Boring Machine (TBM) consists of four basic elements. These are cutter head, cutter head carrier with the cutter head drive motors, the machine frame, and clamping and driving equipments. Moreover, the necessary control and ancillary functions are connected to this basic construction on one or more trailers. As it is seen in Figure 3.4, the operating systems of TBM are divided into four groups. These are;

1. Boring system
2. Thrust and clamping system
3. Muck removal system
4. Support system

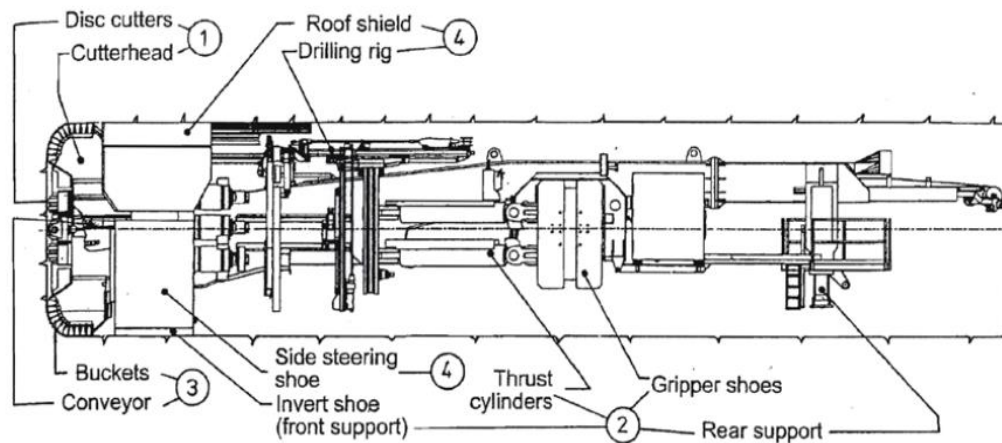


Figure 3.4. System groups of a Tunnel Boring Machine (Maidl et al., 2008)

(1) Boring Systems: The boring (excavation) systems of TBM are comprised of the cutter head and disc cutters that are mounted on a cutter head. It plays an important role in determining the performance of a TBM. Cutter disc is used to excavate rock or soft ground by the rotation of assembly of teeth or cutting wheels under pressure against the rock face. The range of application of these excavation machines depends on the surrounding ground type, therefore, selection of discs depends on the ground type and convenience of cutting (Maidl et al., 2008).

(2) Thrust and Clamping Systems: The thrust and clamping system is an element which affects the performance of a TBM. This system is responsible for the advance and the boring progress of tunnel. The cutter head with its drive unit is thrust forward with the required pressure by hydraulic cylinders which are illustrated in Figure 3.2a. The maximum stroke is governed by the length of the piston of the thrust cylinder. Today developed TBMs achieve a stroke value of up to 2.0 m (Maidl et al., 2008). However, during the excavation process of tunnel, pushing distance is generally

determined by the length of the tunnel segments. After boring tunnel length reached the one segments length, the hydraulic jacks are released to give space for a new ring to be built (see Figure 3.2b). Apart from that, the Gripper TBM, also known as open TBM, is the classic form of Tunnel Boring Machine and it is generally used in the hard rock area (Maidl et al., 2008). In these types of TBMs, in addition to hydraulic cylinders that provide forward movement, the gripper shoes are pushed against the sidewall. The stability of forward moving is provided by the friction between the grippers and the side walls. Moreover, the front shoe, side-steering shoe, supporting invert shoe, and rear support hold the TBM off the invert (Hemphill, 2013).

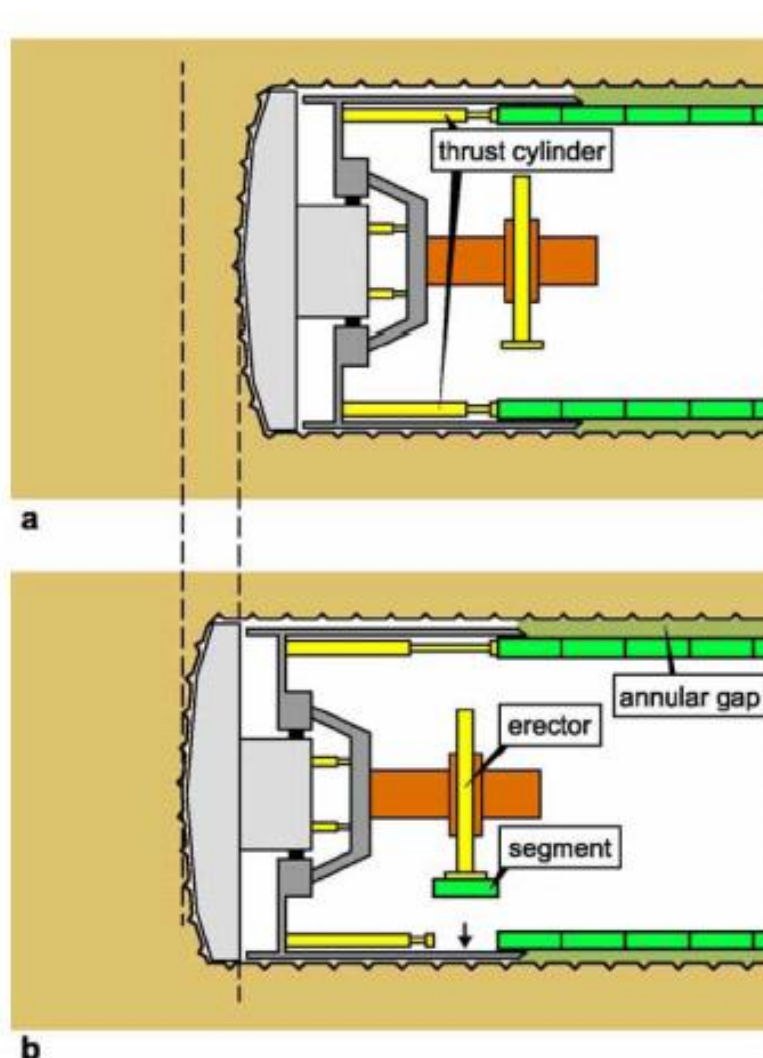


Figure 3.5. Working stages of TBM tunneling, from Wittke (2007) (as cited in Çimentepe, 2010)

(3) Muck Removal Systems: The muck removal system is one of the important operation parts of TBM since it has a significant role in obtaining efficient tunnel boring. This system consists of two stages. The first stage is the removal of the muck (soil) from the bottom of the cutter head and the second is transportation of these soil to the ventilation or working shaft. Firstly, the muck is collected at the face by cutter buckets and delivered to the conveyor down transfer chutes. Then, the muck is transported from the completed tunnel section to the access shafts or to the tunnel portals (Çimentepe, 2010).

(4) Support Systems: The support systems of Tunnel Boring Machines change according to their type and ground conditions. Today, many support methods like bolts, piles injection or even freezing can be used the over or in front of the cutter head for stabilization of the ground that it provides further driving with the TBM. In mechanized shield tunnelling, the shield of TBM provides a temporary support to the rock around the shield. The shield casing begins directly behind the circumferential discs and also encloses the area where the support elements are installed. Reinforced concrete segments, which are mostly used for the support, are installed singly by the erector and form an immediate support. A shield TBM can be equipped with compressed air, hydraulic (slurry) or earth pressure support, and then it can be used under water table. As it is seen in Figure 3.2b, segmental lining elements are erected with a hydraulically-operated erector arm and segments are installed inside the tail of the shield. Figure 3.2a shows that the shield tail, which is the rearmost part of the shield, overlaps the last segment and protects the soil from being deformed or falling into the excavated tunnel (Maidl et al., 2008). Additionally, the grouting process is applied inside the annular gap to prevent any possible loosening of the ground. In this way, a connection between ground and lining is provided. Moreover, to prevent flowing of grout into the shield, sealing is installed between the shield tail and segmental ring. During the movement of TBM, this sealing is sliding over the linings and advance with the tunnel (Möller, 2006). This process is illustrated in Figure 3.3.

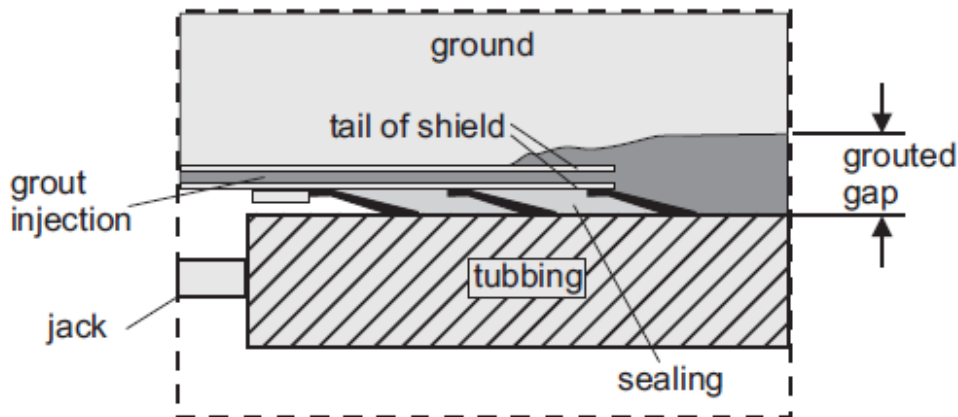


Figure 3.6. Shield tail with grouting of the ground-lining gap (Möller, 2006)

3.1.2. Types of Tunnel Boring Machines

Today, various types of machine are used for the mechanised tunneling in both rock and soft ground. However, the problem is that there is no acceptable definition and criteria for the classification of tunnelling machines. The leading national tunneling associations such as German Committee for Underground Construction (DAUB), French Tunneling and Underground Engineering Association (AFTES) and Japan Society of Civil Engineers (JSCE) have their own classification system based on different criteria for tunneling machines. Nonetheless, full-face excavation type of Tunnel Boring Machines is universally adapted for all the classification systems (Çimentepe, 2010). Therefore, this study focus on only full-face excavations type of Tunnel Boring Machines.

Moreover, in this study, the tunnelling machines are classified according to ITA report, (2000) published by International Tunneling Association (ITA) Working Group 14 “Mechanized Excavation”. TBMs are categorised according to both the type of ground that a machine operates in and the support system of the machine. Figure 3.4 shows the overview of the Tunnel Boring Machine with full-face excavation.

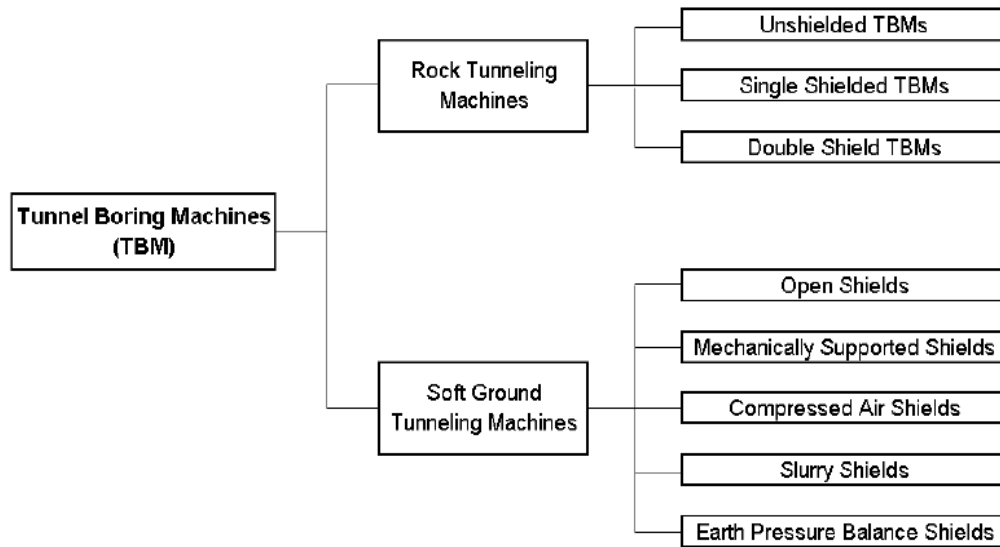


Figure 3.7. Classification of Tunnel Boring Machine (TBM) (Çimentepe, 2010)

3.1.2.1. Rock Tunneling Machines

- Unshielded Tunnel Boring Machines

The unshielded TBMs are generally used in rocks with good or very good class levels. During the excavation process, similar to conventional method primary support systems are used such as shotcrete, rock bolts, and steel arches. As it is seen in Figure 3.5a, the cutter head is pushed forward by means of hydraulic cylinders, which are supported by the gripper shoes that are pushed against the sidewall. In these types of TBMs, the stability of moving forward is provided by the friction between the grippers and the side walls. In this way, the thrust forces are not transferred to the tunnel lining.

The working cycle of these machines consists of four steps and these are: 1) gripping to stabilize the machine; 2) excavating for a length equivalent to the effective stroke of the hydraulic jacks; 3) regripping; 4) new excavation (Çimentepe, 2010).

- **Single Shield Tunnel Boring Machines**

The single shielded TBMs are generally used in rocks whose characteristics vary from moderate to poor. The excavation and muck transportation procedure are the same with unshielded machines. However, as it is seen in Figure 3.5b, forward movement of the machine is provided by hydraulic jacks that directly lean against the existing tunnel lining. In these types of TBMs, the shield is used to temporarily support the tunnel and protect the machine. The tunnel lining is installed under the projection of the shield tail and they provide the permanent support of the tunnel (Maidl et al., 2008).

The working cycle of single shielded TBMs consists of four steps and these are: 1) excavating for a length equivalent to the effective stroke of the hydraulic jacks; 2) retraction of the jacks; 3) assembling of tunnel linings by using precast segments 4) new excavation (ITA WG 14, 2000).

- **Double Shield Tunnel Boring Machines**

The double shield or telescopic shield TBMs are generally used in rocks whose characteristics vary from excellent to poor. They are very practical machines, in particular for the ground conditions that show a variety along the tunnel route (mixed rock conditions). In contrast to single shielded TBMs, double shield TBMs provide continuous work cycle due to their double thrust system. As it is seen in Figure 3.5, this machine consists of both the hydraulic jacks and a series of grippers that are installed in the front part of the shield. Therefore, the forward movement of this machine can be achieved in both two ways. The advance of the machine can be performed by hydraulic jacks that directly lean against the existing tunnel lining. Moreover, even without installing the tunnel linings, the cutter head can be pushed forward by means of hydraulic cylinders, which are supported by the gripper shoes that are pushed against the sidewall (Maidl et al., (2008); Çimentepe, (2010)). However, according to Maidl et al. (2008), these machines are not economical because of high prices and high maintenance costs

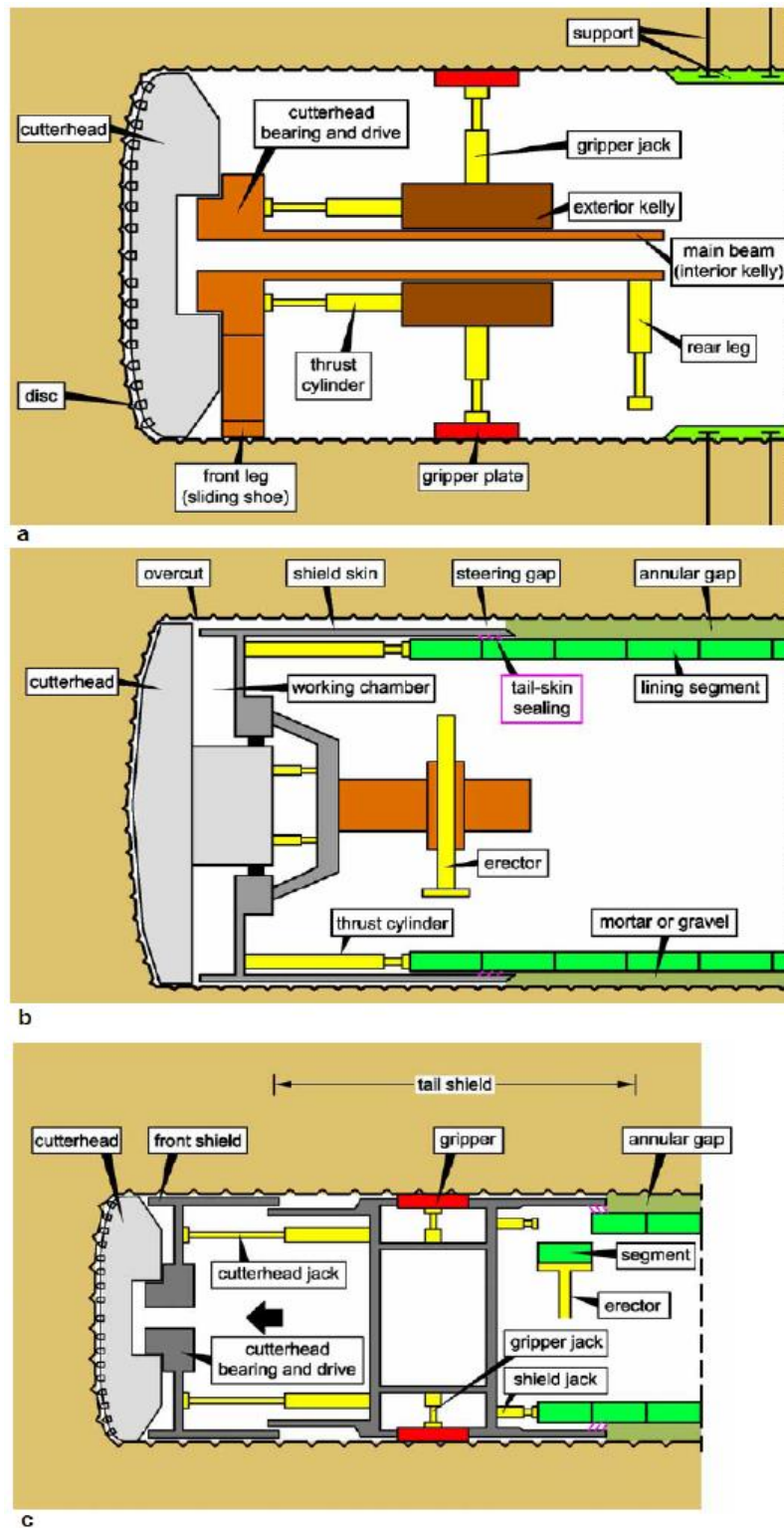


Figure 3.8. Rock tunneling machines: a) Unshielded TBM, b) Single shielded TBM, c) Double shielded TBM, from Wittke (2007) (as cited in Çimentepe, 2010)

3.1.2.2. Soft Ground Tunneling Machines

- Naturally Supported

Naturally supported also known as open shield TBMs are generally used for rock masses whose characteristics vary from poor to very bad. In these types of TBMs, there is no pressure regulation system at the tunnel face to take precaution for groundwater. Therefore, they are used in ground conditions where the groundwater does not exist, or the groundwater table lowered beforehand. As shown in Figure 3.7a, the soil at the tunnel face is given its natural inclinations by using the cutter head equipped with tools or roadheader, and the loosened soil is transported by means of conveyor belts or scraper chains. (Maidl et al., (1996); ITA WG 14, (2000)).

- Mechanically Supported

Mechanically supported TBMs are used for soft rocks and cohesive or partially cohesive ground. Similar to open shield TBMs, this method is suitable for levels above the groundwater table or absence of groundwater. The cutter head of these TBMs plays a critical role in providing pressure to support the face during the excavation. As it is seen in Figure 3.7b, steel support plates are installed in between the free spaces of the cutting arms, to slide along the cutting face while rotating the boring machine. The debris is extracted through adjustable openings or buckets and conveyed to the mucking system (ITA WG 14, (2000); Möller, (2006)).

- Compressed Air Supported

Compressed air supported TBMs are used for grounds that have medium-low permeability in the presence of groundwater, in order to avoid water influx. Compressed air supports the tunnel face by balancing the hydrostatic pressure of the ground. The debris of excavation is extracted from the pressurized excavation chamber using a ball valve-type rotary hopper and then conveyed to the mucking system of TBM (ITA WG 14, (2000); Möller, (2006)). The typical working principle of these TBMs is shown in Figure 3.7c.

- **Slurry Supported**

Slurry supported TBMs are most commonly preferred for soft soils having limited self-supporting capacity. In other words, they are generally used for excavation in ground that consists of sand and gravels with silts under the groundwater table. The stabilization of tunnel face are provided by applying pressurized bentonite or clay and water mix (slurry). The soil is mixed into the slurry during the operation and at the end, the soil is removed from the slurry in a separation plant (see Figure 3.7d). The separation plant is generally located on the ground. A chamber with air pressure is connected to the slurry in order to control the slurry pressure. (ITA WG 14, (2000); Möller, (2006); Çimentepe, (2010)).

- **Earth Pressure Balance (EPB) Supported**

The earth pressure balance supported TBMs are the most commonly used TBM types in soft grounds. These TBMs are mainly used in soft ground that has limited or no self-supporting capacity in the presence of groundwater. That is, typical application ground condition of EPB TBMs is silts or clays with sand. Additionally, excavation of rocks is possible by using disc cutters. As it is seen in Figure 3.7e, face support is provided by the excavated material which is kept under pressure inside the excavation chamber by the thrust jacks. As shown in Figure 3.6, excavation debris are removed from the excavation chamber by a screw conveyor which enables the pressure control by variation of its rotation speed (ITA WG 14, (2000); Möller, (2006)).

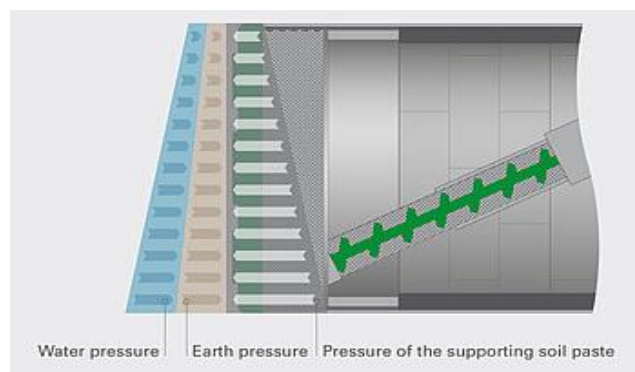


Figure 3.9. Regulation of support pressure, source: <https://www.herrenknecht.com/en/products/core-products/tunnelling/epb-shield.html>

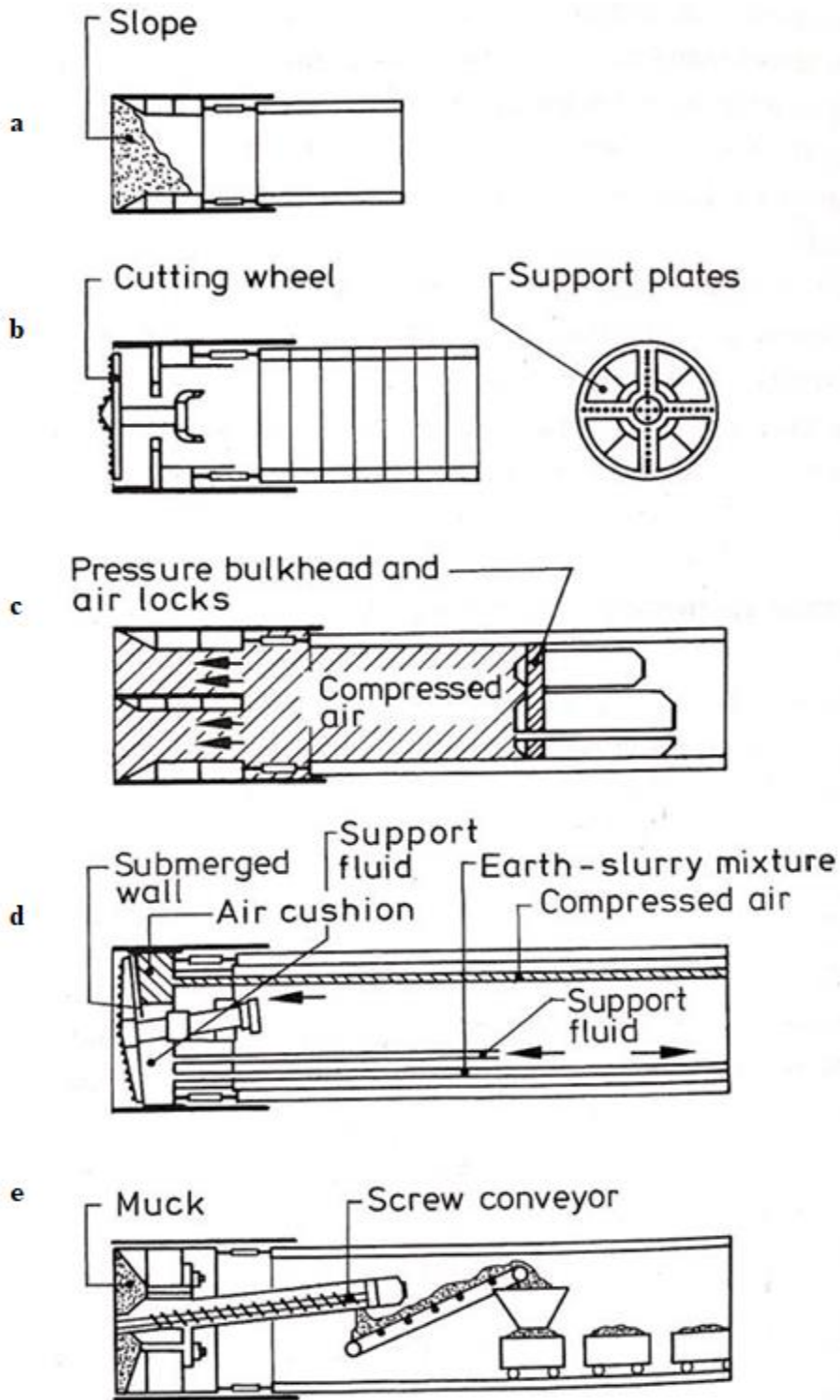


Figure 3.10. Shield tunneling with a) natural support, b) mechanical support, c) compressed air support, d) slurry support, e) earth pressure balance support (Maidl et al., 1996)

3.2. Segmental Tunnel Linings

The lining installed with mechanized tunnelling can be single or double layered constructions, however, in this scope of thesis, only single layered tunnelling is handled. Tunnel linings are structural elements that provide a secure operational cross-section for different demands by resisting several effects such as, the surrounding ground and water pressures. Additionally, they provide immediate initial ground support required during the construction stage in both soft grounds and broken rocks and also they serve as watertight final support. (Hurt and Hart, 2011). However, they have to fulfil the requirements of stability, durability and serviceability during the entire working lifetime. Within this framework, different lining types such as pipe linings, in-situ lining and segmental lining are used for tunnel linings. With the development of the mechanized tunnelling technology and improvement of tunnelling construction techniques, the segmental lining method has become the most commonly used tunnel linings. Segmental linings may consist of cast iron segments, structural steel (welded) segments, reinforced concrete segments or fiber reinforced concrete segments. Selection of the type of segments depends on conditions of project and availability of materials (Maidl et al., 1996; 2008). Today, the precast concrete segments are the most commonly used in the segmental lining constructed by Tunnel Boring Machines (TBMs). As previously mentioned, placements of the segments in the shield tail and excavation of ground are carried out simultaneously by means of Tunnel Boring Machine (see Figure 3.9).

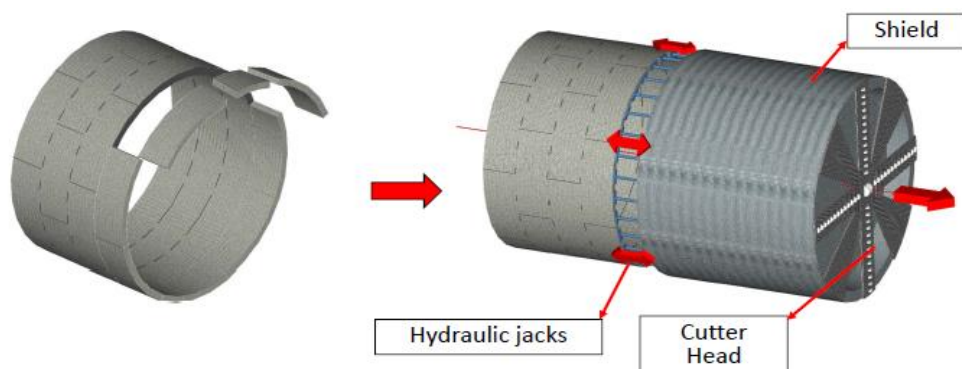


Figure 3.11. The advance of mechanized shield tunneling method (Tiberti et al., 2018)

3.2.1. Precast Concrete Segments

Segments are prefabricated concrete elements that are built together to form a ring and serves as the tunnel lining. Precast concrete segments are manufactured at a segment manufacturing yard and then when they reached desired durability, they are transported to the place where they will be positioned. As it is seen in Figure 3.9, rings are composed of several numbers of segments, which are installed within the protection of the tail shield of TBM with the help of erector. In general, circular cross-sections are preferred for construction of tunnelling. The internal radius of the tunnel is determined by the requirements regarding purpose of usage. In other words, the design layout of lining depends on the requirements for tunnel use. On the other hand, the dimensions of the lining are determined from loadings, which are mainly surrounding ground and water pressure. The special characteristic of the segmental linings is high number of joints due to construction technique. These are divided into two categories; longitudinal (or radial) joints between the segments located in the same ring, and circumferential (or ring) joints between the rings (Maidl et al., 1996; 2008). The general components of segmental lining are shown in Figure 3.10

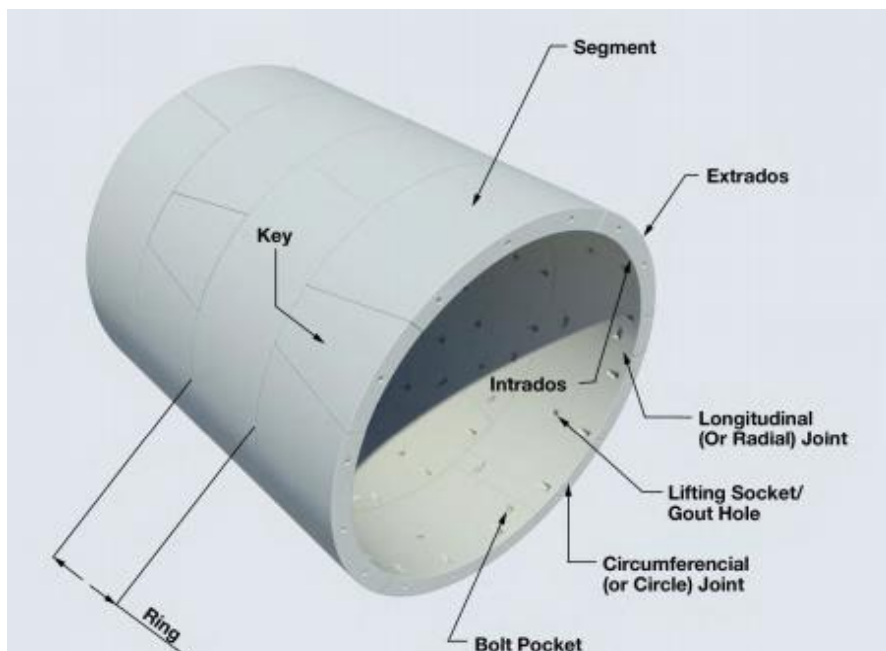


Figure 3.12. Lining definitions (Hurt & Hart, 2011)

The number of segments forming the ring changes according to the tunnel diameter. One ring consists of four to nine segments and one key segment that is the last segment to be inserted in a ring. The key segments have tapered sides to simplify sliding into ring and the segments adjacent to the key are called as counter segments (Çimentepe, 2010).

Determining the dimensions of segments is quite important in order to obtain efficient solutions. In particular, the dimensions of segments are selected to be as large as possible regarding to use the minimum number per ring. In fact, the main purpose is to accelerate the advance of Tunnel Boring Machine. However, the available space for transportation and storage of segments, the maximum possible extension of the jacks and lifting capacity of erector are also important factors for determining the dimensions of the segments (Luttikhokt, 2007). According to Thewes study (as cited in Çimentepe, 2010), based on the results of wide experiences, ranges for the dimensions of a segmental lining are illustrated in Table 3.1.

Table 3.1. *Ranges for the dimensions of segmental linings, from Thewes (2008) (as cited in Çimentepe, 2010)*

Ring Size	Segment Thickness	Segment Width	Segment Numbers per Ring
Small Diameter Rings (2 to 5m)	15 to 25cm	75 to 150cm	4 to 5 segments, 1 key
Medium Diameter Rings (5 to 8m)	20 to 40cm	125 to 200cm	5 to 6 segments, 1 key
Large Diameter Rings (D>8m)	30 to 75 cm	150 to 225cm	6 to 9 segments, 1 key

The shape of segments shows differences depending on the project. Segments are normally formed in either a rectangular, rhomboidal, trapezoidal or hexagonal arrangement (see Figure 3.11). The rectangular and trapezoidal shapes are the most commonly used in the design practice in particular for largest ring diameters with the tendency to use hexagonal segments for smaller ones (Fabozzi, 2017). It is necessary to understand the assembly process of the ring inside the tail of the shield in order to choose the type of segment. The assembly process involving the construction of the ring starts from the first segment, and finishes up with the key segment, whose

presence is always foreseen and is placed at the opposite side of the ring that has the counter segment (Çimentepe, 2010).

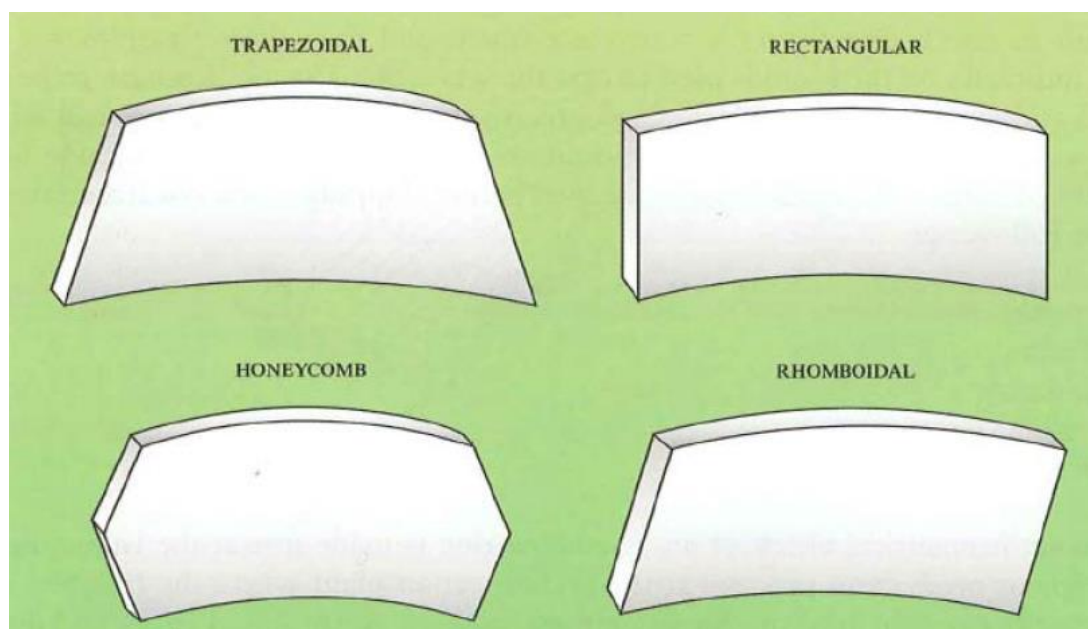


Figure 3.13. Segment types (Guglielmetti et al., 2007)

3.2.1.1. Joint Details

The proportion of joints in the tunnel tube is relatively high due to the segmental building of the individual rings and the ring-wise production of the lining. As previously mentioned, these are the longitudinal joints between the segments and the circumferential joints between the adjacent rings (Maidl et al., 2008).

3.2.1.1.1. Longitudinal Joints

The main functions of longitudinal joints are that they transfer axial forces, bending moment due to eccentric axial forces, and shear forces from external or internal loads, by reducing the forces acting on the adjacent segments. Today, two different types of method are used in tunnelling. The most common one is performed by the contact of the contact surfaces, however in some cases also by the bolting of the longitudinal segment joints (Maidl et al., 2008). As it is seen in Figure 3.12, the contact surfaces of two adjacent segments in the same ring can be flat, convex or convex-concave.

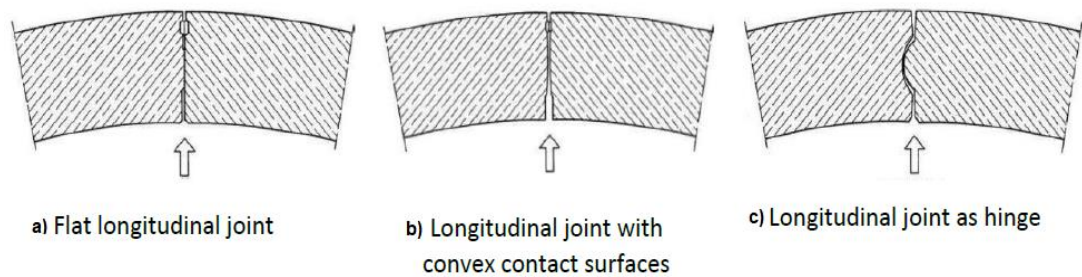


Figure 3.14. Longitudinal joints with a) two flat surfaces, b) two convex surfaces, c) convex-concave surfaces (Maidl et al., 2008)

With longitudinal joints having flat surfaces according to Figure 3.12a, the free rotation of the segments is hindered by the geometry. In this way, in addition to the axial compression load, bending moments can also be transferred, which reduces the bending loading on the segment (Maidl et al., 2008).

Convex surface contact is usually preferred in the case of high axial compressive forces and for a high value of joint rotation. However, this joint system is not very stable during ring installation since there is no sufficient compressive force and no resistance to rotation. Therefore, it is necessary to add bolting joints to avoid segment collapse (Maidl et al., 2008; Fabozzi, 2017).

Convex-concave contact surfaces have a high rotational capacity and they provide a better stability in terms of ring assembly. However, in this type of joint, the edges of the concave side of the joint are particularly at risk when sufficient reinforcements are not provided at this location (Fabozzi, 2017).

As mentioned above, the contact surface between the segments is generally designed by a concrete-concrete surface, however, in some cases, the contact surface can be made of packers material to distribute the loads in the joints. In general, plastic or bituminous materials are used for the production of packers and bolts are made of steel. As it is seen in Figure 3.13, they can straight, curved or inclined shape. In this type of connections, pockets and grooves into which the bolts are inserted, are necessary for collocations of segments (Fabozzi, 2017).

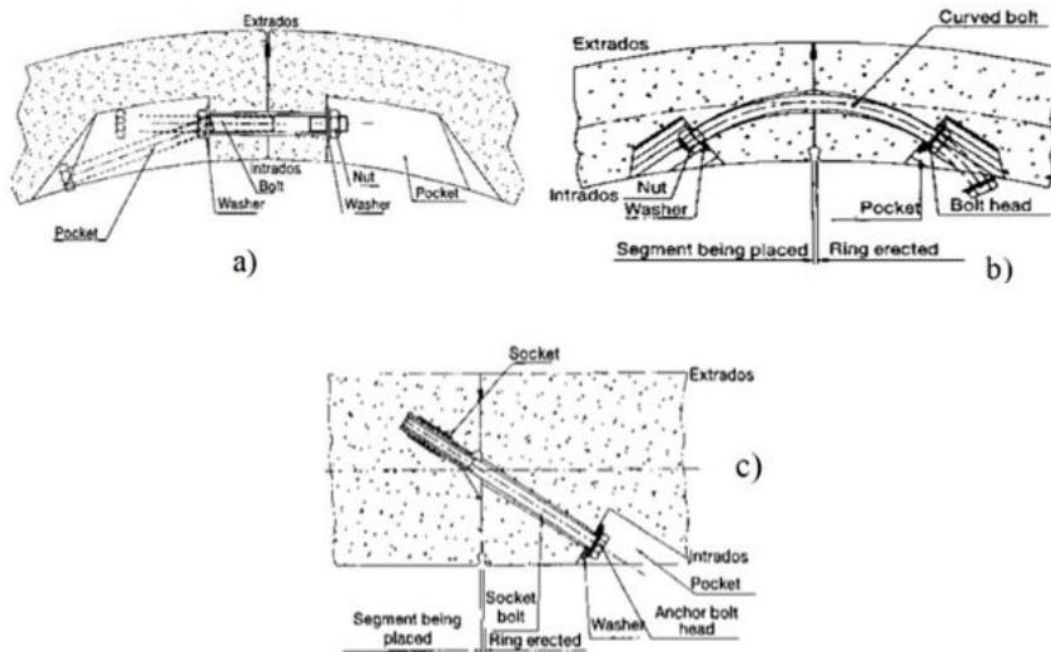


Figure 3.15. Longitudinal joints with a) straight bolt, b) curved bolt, c) inclined bolt, from AFTES 1999 (as cited in Fabozzi, 2017)

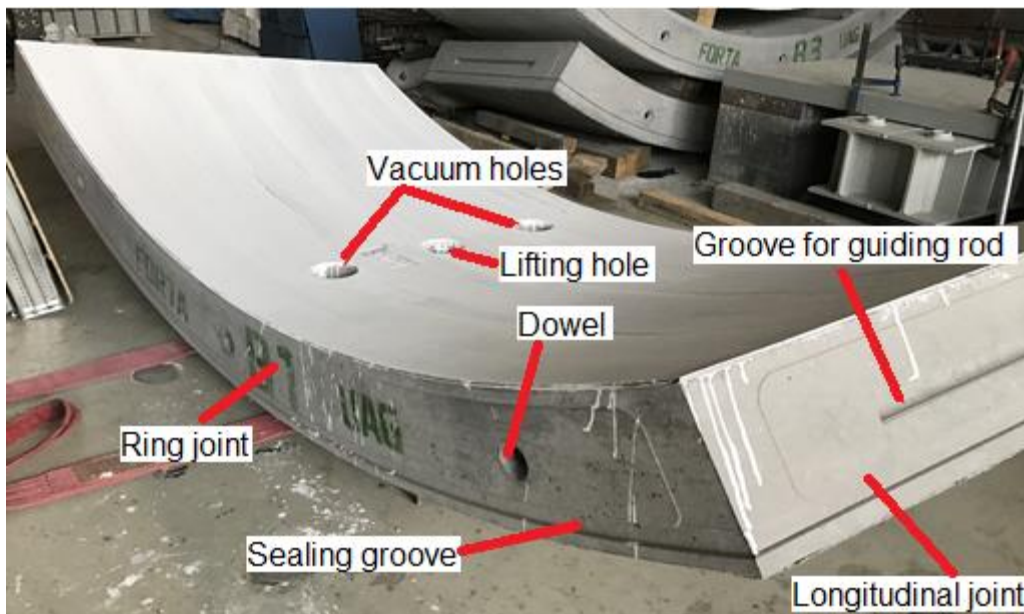


Figure 3.16. Detailing of precast tunnel segment

Apart from that, as it is seen in Figure 3.14, guiding rods are used in longitudinal joints in order to obtain a precise installation of the ring.

3.2.1.1.2. Circumferential (or Ring) Joints

The contact surface between adjacent rings is referred to as circumferential (or ring) joints. These surfaces of segments are subjected to thrust forces applied by TBM during excavation and transferred through the segment to the next ring joint. Therefore, proper design of ring joints is very important to prevent possible cracking on these surfaces. The ring joints are usually flat or convex-concave form. Bolts can be used in circumferential joints as for longitudinal ones. However, in general, contacts between rings are established by concrete-to-concrete contact or by means of the thickness of packing materials. Dowels and sockets systems can be used in the ring joints in order to prevent large deformations of a tunnel. Today, different configurations for dowels are available. To make placement of the segments easier, small and non-constructive type of dowels can be used (see Figure 3.15a). They usually do not provide a mechanical effort or any coupling transferring mechanism. In other words, they do not prevent large deformation. In some cases, structural dowels are used in order to prevent failure of lining by resisting the shear force on the contact surface. On the other hand, pin and socket systems (see Figure 3.15b) or permanent bolts provide a coupling effect at the point location. (Luttikhokt, 2007; Fabozzi, 2017).

Additionally, kaubit is usually used as a packing material to avoid any damage of concrete when the two surfaces touch. These packing materials also increase the concrete durability since concrete-to-concrete contacts have an unsmooth surface that causes local peak stresses. Therefore, packing material is applied to prevent this possible occurring local stress. As it is seen in the Figure 3.16, in most cases, kaubit is placed between the two concrete surfaces. These packing materials introduce axial, radial and tangential forces into the next ring. As it can be seen in the Figure 3.16, these contact areas are placed in line with the thrust shoes of hydraulic cylinders in order to get a good transition of applied thrust forces into the adjacent rings (Luttikhokt, 2007).

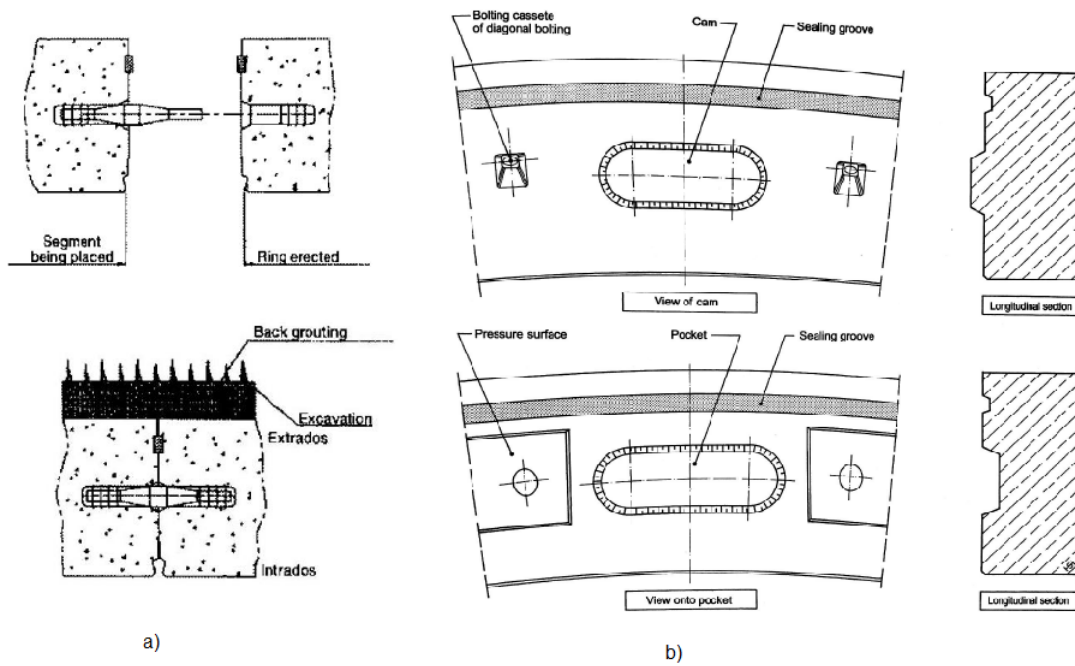


Figure 3.17. a) Joints with dowels, from AFTES (1999) (as cited in Fabozzi, 2017), b) joints with pin and socket system (Maild et al., 2008)



Figure 3.18. Tunnel segments with kaubit used as a packing material (Luttikhokt, 2007)

3.2.1.2. Waterproofing System

Tunnel linings have to be waterproof and guarantee the functionality of structure during the entire life period. Waterproofing of segmental lining for single layer

construction is generally provided by two ways to prevent possible infiltration of water in tunnel.

The first precaution for leakage is use of sealing elements (or gaskets) positioned in special grooves placed on each side of all segments close to the outer surface of segments (see Figure 3.14). Water tightness is provided by the compression of these elements, therefore, they should be always under compression. Determining the groove type and size of the gap is very important to obtain safe systems. Within this framework, the behavior of gasket under the maximum and minimum pressure should be known in the presence of the maximum gap and offset values. However, in case of joint rotation, the gaskets can undergo de-compression due to sagging or hogging moment. And this de-compression effect on the gaskets could influence their water tightness function (Fabozzi, 2017).

The second waterproofing system of lining comes from the filling material (grout) used to fill the annular gap between the segments and the ground (see Figure 3.4). This filling provides an appropriate bedding for the segmental tunnel lining. The gap filling is a very sensitive operation playing an important role in minimizing the surface settlements. This application protects the tunnel against water coming from outside and also decreases the permeability of surrounding soils (Fabozzi, 2017).

Apart from these, there are some important factors that should be taken into consideration during construction in order to obtain effective waterproof lining. According to research conducted by Guglielmetti et al. (2007), these factors are; 1) an optimal quality of the concrete and of the segment, resulting from high level strength of the concrete used together with an accurate prefabrication process, 2) precaution taken while moving the individual segments to avoid the formation of cracks, 3) proper assembly of ring, aligning the segments, and avoiding any possible damage, 4) filling the annular gap with suitable material.

CHAPTER 4

TEST SPECIMENS AND MATERIALS

The Istanbul Mediciyekoy – Mahmutbey Metro Project consist of the construction of a twin tunnel of total length approximately 23 km, which has been designed to be excavated both by TBM and New Austrian Tunnelling Method (NATM). The alignment starts at Mediciyekoy station and runs westwards till Mahmutbey station. The tunnel stretch between Km 15+509 (YeniMahalle station) and Km 22+359 (Mahmutbey station) excavated by TBM and lined with precast segmental lining rings (see Figure 4.1). Along with this alignment stretch, the tunnel runs below an urban area with an overburden ranging from 10.2 to 42.8 m.

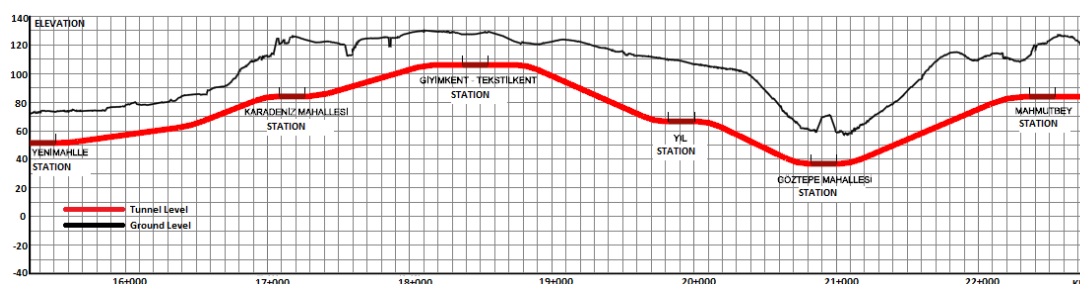


Figure 4.1. Longitudinal profile corresponding to the Line 1 tube of metro project, taken from related project report prepared by Yuksel Project International

Mediciyekoy – Mahmutbey Metro Project is located within the European side of Istanbul city. Main geology of Istanbul area is composed of Palaeozoic and Mesozoic bedrock covered by sediments from Tertiary period and intruded locally by andesite and diabase Dykes.

According to the available geological and geotechnical information, the TBM tunnel stretch object of this project (from Yenimahalle Station to Mahmutbey Station) was excavated both in rock (sandstone, mudstone and claystone with different weathering grades) and soil (clay and sand) conditions. The tunnel geological profile is shown in Figure 4.2.

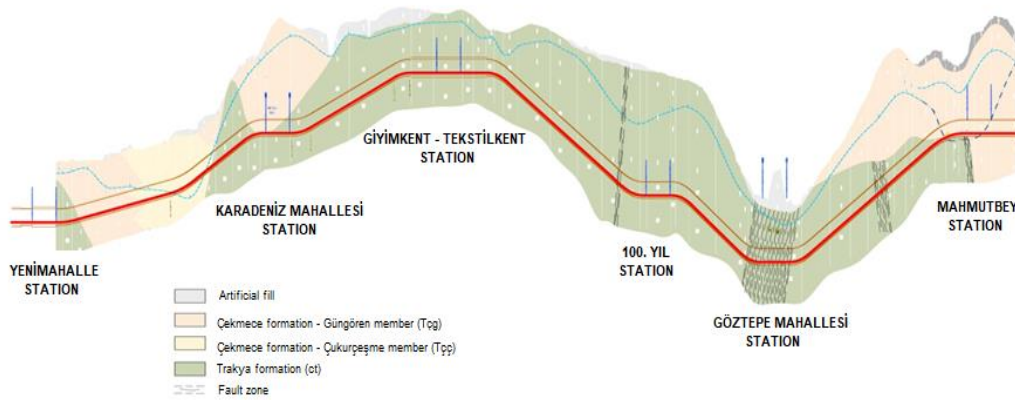


Figure 4.2. Geological profile between Yenimahalle and Mahmutbey stations

The initial stretch of TBM tunnel alignment, from Yenimahalle station to Karadeniz Mahallesi station, runs at shallow depth (10 to 20 meters) predominantly within grey clay and clayey sand; at chainage 16+150 a gradual passage at tunnel level from sandy-silty clay to sand silty sands are formed towards Karadeniz Mahallesi station. Approximately at chainage 16+700, there is a transition to rock conditions represented by the moderately weathered sandstone belonging to Trakya formation; upon the initial 1 km long TBM tunnel stretch, the overburden increases to higher values (up to 42.8 m that is the maximum overburden along the captioned stretch) and the tunnel alignment, after having run entirely within Trakya mudstone-claystone for a 300 m long stretch, has to face mixed ground conditions given by the simultaneous presence at tunnel face of rock and soil material (in this case sandstone-siltstone and silty-sandy clay). Upon Karadeniz Mahallesi station, the alignment runs for about 5 km along Trakya formation (Carboniferous period aged) consisting predominantly in poor-fair sandstone belonging to a Rock Mass Rating (RMR*) class IV-III (Total RMR values range between 30 and 60) and characterized by a weathering grade W1 to W3. Along this tunnel stretch (from chainage 17+290 to 22+080), several faults have been detected (they are indicated in Table 3-1); along the fault zones, Trakya sandstone-mudstone is very weathered (weathering grade W4) and shows very poor geomechanical quality (soil-like behavior). Along this stretch, the overburden ranges between 20 and 40 meters, with exception for a 400 m long stretch around

chainage 18+775 along which the minimum overburden of the entire TBM alignment (10.2 meters) is found. Approximately the final 200 meters of the alignment run within an alternation of grey clay and silty sand with a mean overburden ranging between 20 and 35 meters. The main geological formations expected at tunnel level along the captioned alignment stretch are summarized in Table 4.1 with corresponding geotechnical parameters.

*RMR: The Rock Mass rating value consists of the summation of the six parameters' rating; Uniaxial compressive strength of rock material, Rock Quality Designation, Spacing of discontinuities, Condition of discontinuities, Groundwater conditions and Orientation of discontinuities. This system is used for the classification of rock. According to Bieniawski (1989), there are five class available according to total rating; Class-I (100-81, Very good rock), Class- II (80-61, Good rock), Class- III (60-41, Faird rock), Class- IV (40-21, Poor rock), Class- V (<21, Very poor rock).

Table 4.1. *General geological description between Yenimahalle and Mahmutbey stations*

Stretch	From [KM]	To [KM]	Geology at tunnel face	γ [kN/m ³]	c [kPa]	ϕ [°]	Em [Mpa]	ν [-]
Yenimahalle - Karadeniz Mahallesi stations	15+510	15+595	Sandstone and mudstone	26	150	36	1750	0,30
	15+595	15+665	Mudstone and sandstone	24/25	60	26	520	0,32
	15+665	16+105	Clay, silty clay and sandy clay	19,5/21	150	0	30	0,32
	16+105	16+695	Sand and Silty sand	18,5/19,5	5	32	30	0,32
	16+695	16+975	Mudstone and sandstone	26	110	33	1260	0,30
	16+975	17+085	Clay, silty clay and sandy clay	19,5/21	150	0	30	0,32
Karadeniz Mahallesi - Gıyımkent – Tekstilkent stations	17+265	17+375	Sandstone	26	110	33	1260	0,30
	17+375	18+370	Sandstone, claystone and mudstone	26	150	36	1750	0,30

Giyimkent – Tekstilkent - 100. Yil stations	18+550	19+595	Sandstone, claystone and mudstone	26	150	36	1750	0,30
	19+595	19+755	Sandstone, mudstone and fault (km 19+750)	26	110	33	1260	0,30
				23	0,1	32	50	0,32
19+755	19+945	Sandstone and mudstone	26	150	36	1750	0,30	
100. Yil - Gröztepe Malleis stations	19+945	20+695	Sandstone and mudstone	26	150	36	1750	0,28
	20+125	20+821	Fault zone	23	0.1	32	50	0,32
Gröztepe Mahallesi - Mahmutbey stations	20+821	21+035	Fault zone	23	0,1	32	50	0,32
	21+000	21+595	Mudstone, claystone and sandstone	26	150	36	1750	0,28
	21+595	21+755	Sandstone and mudstone and fault (km 21+680)	25	75	30	780	0,30
				23	0,1	32	50	0,32
	21+755	22+055	Mudstone and sandstone	24/25	60	26	520	0,32
	22+055	22+175	Sandstone, hard clay and clayey sand	24/25	60	26	520	0,32
				21/22	10	32	40	0,32
22+175	22+358	Hard clay and clayey sand	21/22	10	32	40	0,32	

The geometry of the constructed segmental lining ring is shown in Figure 4.3. It presents an inner diameter of 5.7 m, a segments thickness of 30 cm and a mean length of 1.4 m. According to tender specifications, the ring type is universal, composed of six segments: 4 rhomboidal and two trapezoidal segments (key and counter-key); the key segment angle is 22.50°.

Rhomboidal segments: B, C, E and F

Trapezoidal segments: A (key) and D (invert)

Three-dimensional view of the segmental lining is also shown in Figure 4 .4

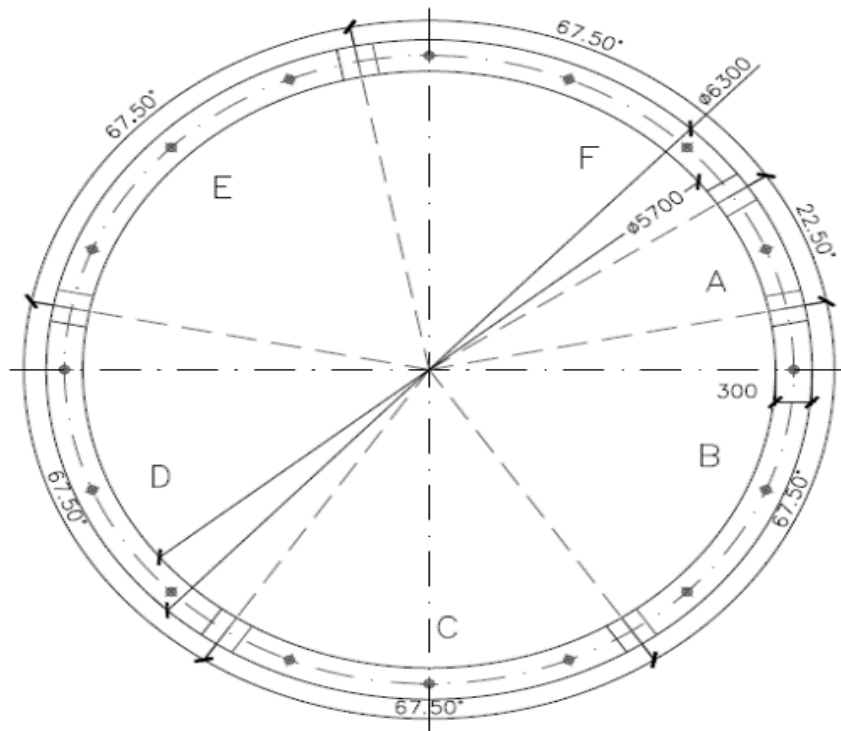


Figure 4.3. Segmental lining ring geometry (units mm)

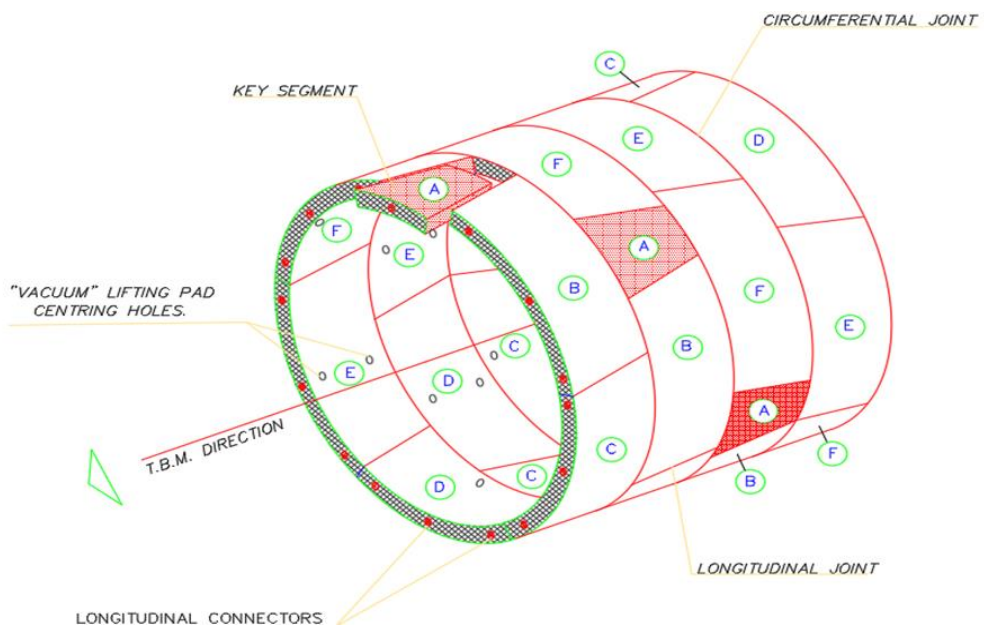


Figure 4.4. 3D view of the segmental lining

According to specification, this tunnel geometry is categorized by medium size tunnel since the diameter of the ring is between 5 m and 8 m. Detailed information about segments and tunnel features are tabulated in Table 4-2.

Table 4.2. Segmental lining ring – general features

Total tunnel length approximately	23 km
Overburden (min-max)	10.2 m - 42.8 m
Lining type	Segmental
Ring type	Universal type
Boring diameter	6.6 m
Internal diameter D_i	5.7 m
External diameter	6.3 m
Number of segments	4 segments +1 counter key segment + 1 key segment
Thickness h	0.3 m
Tunnel aspect ratio (D_i/h)	19
Segment length/width	3.534 m/ 1.4 m
Average segment aspect ratio	11.78
Ring taper	+/- 85mm
Available erecting positions	16
Eurocode-2 concrete class	C40/50
Connections between rings (circumferential joint)	Type Biblock 84-46-274
Water tightness	Sealing gaskets, 1 row on each joint (longitudinal and circumferential)

4.1. Test Specimens

4.1.1. Specimen Geometry

In this thesis, one of the full-scale precast tunnel segments belonging to Mecidiyeköy - Mahmutbey metro project was chosen for the experimental study. Considering the difficulties of the ring experiments, segment C was chosen in the experimental program. The reason is that they are located on the bottom during storage phase and exposed to high forces. Detailed information about segment C is given in Figures 4.5 - 4.11.

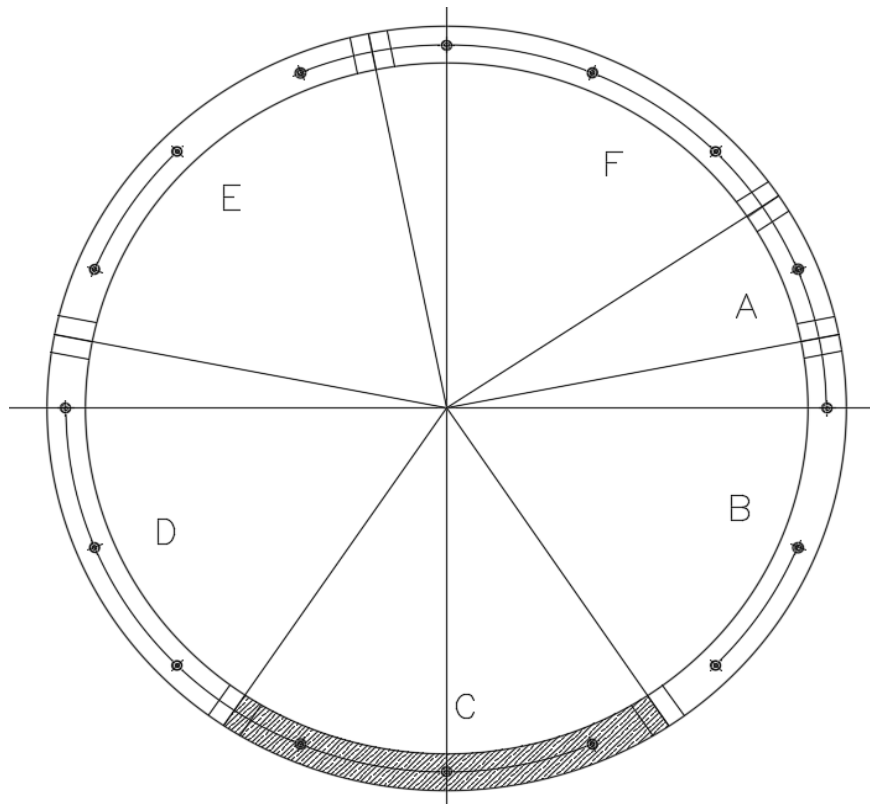


Figure 4.5. 4.5 Segment C

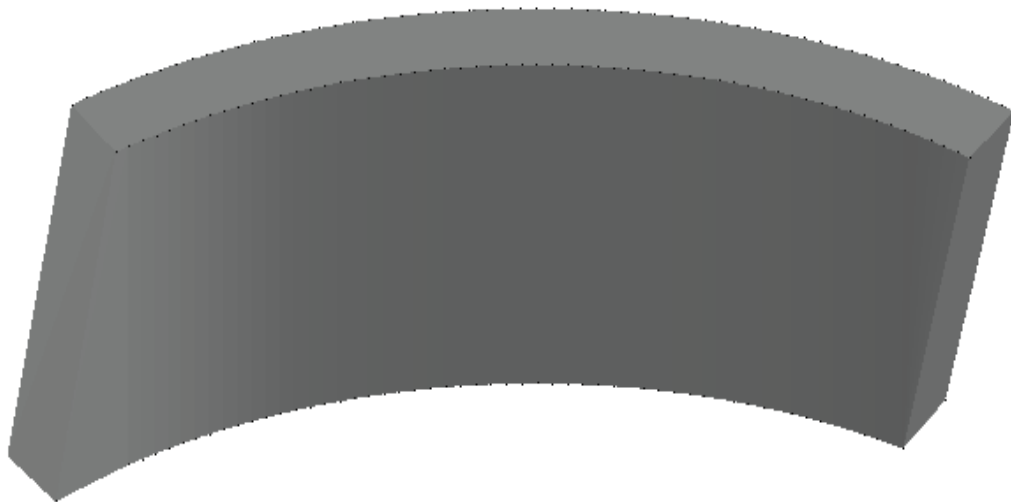


Figure 4.6. 3D view of segment C

Segment C geometry details are shown in Figures 4.7 - 4.11

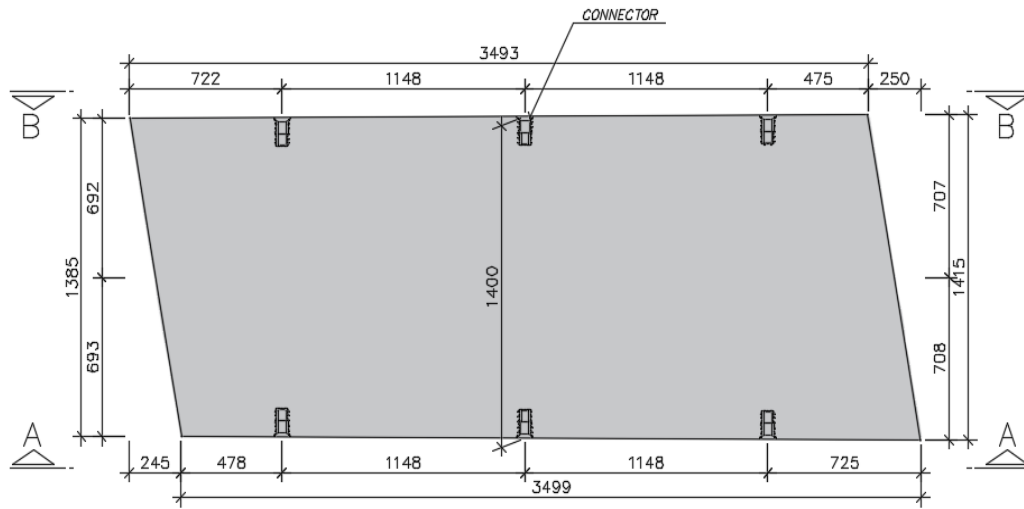


Figure 4.7. Outer view (units mm & not to scale)

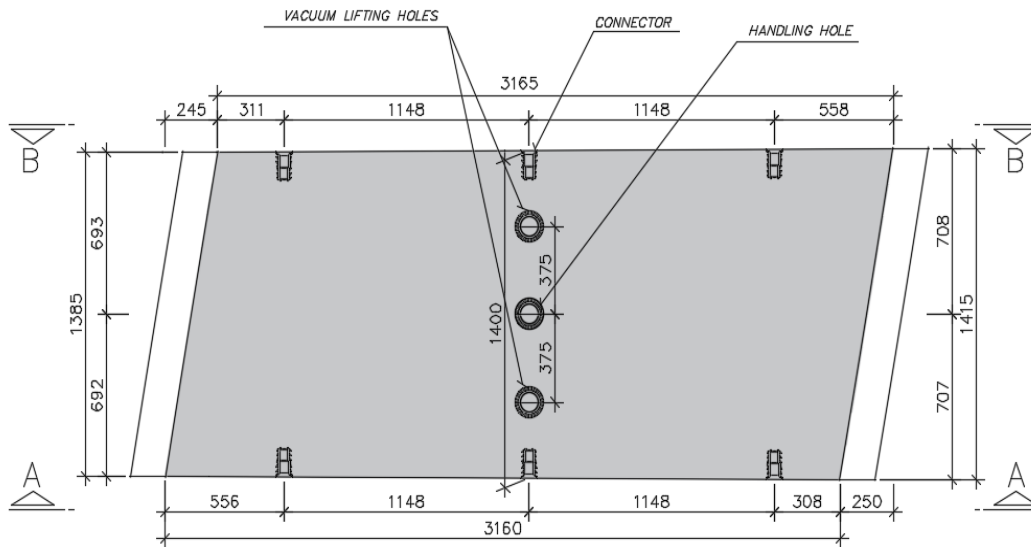


Figure 4.8. Inner view (units mm & not to scale)

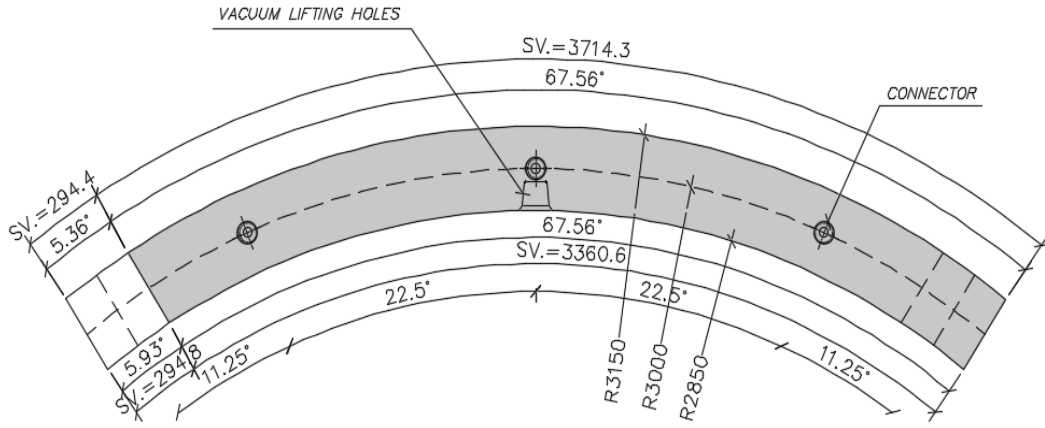


Figure 4.9. Section A-A (units mm & not to scale)

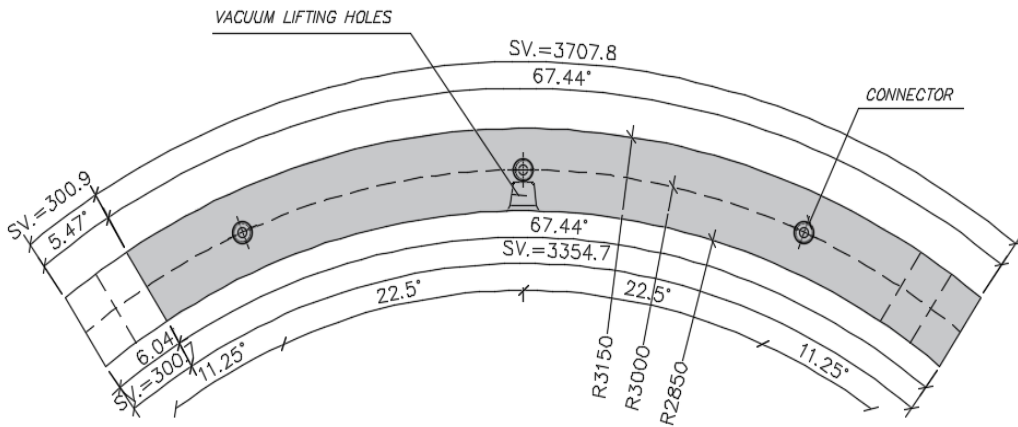


Figure 4.10. Section B-B (units mm & not to scale)

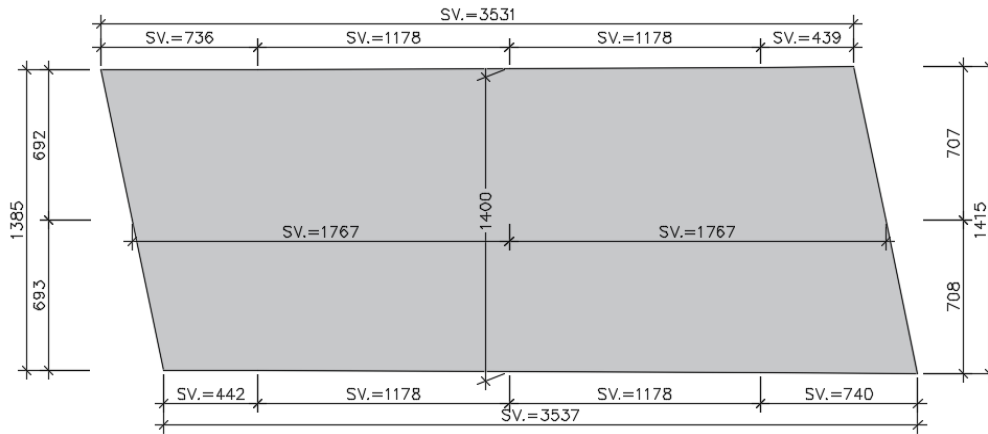


Figure 4.11. Central deployment (units mm & not to scale)

4.1.2. Reinforcement Details

Four different reinforcement solutions were carried out both in flexural test and point load test. In fact, one of them is reference sample which is currently used, and others designed as an alternative solution. These are;

- A. Typical conventional reinforcement (RC segments)
- B. Combination of polypropylene fibers and traditional reinforcing bars, also known as a classical hybrid solution (RC + PFRC segments)
- C. Combination of polypropylene fibers and glass fiber reinforced polymer reinforcing bars, hybrid solution (GFRP + PFRC segments)
- D. Polypropylene (PP) fibers only (PFRC segments)

Four specimens from each type were produced. However, fifteen precast tunnel segments were tested. Since the bending test results of type A segments were applicable and nearly similar, it was not required to carry out an extra experiment.

Table 4.3. Segment designations, concrete and reinforcement details

Type	Segment designation	Concrete	Reinforcement types	Specimen of tunnel
A	RC	PC	Conventional reinforcement	Segment C
B	RC+PFRC	PFRC	Classical hybrid solution	Segment C
C	GFRP+PFRC	PFRC	Hybrid solution	Segment C
D	PFRC	PFRC	Polypropylene fibers only	Segment C

4.1.2.1. Type A - RC Sample

Type A was consisted of traditional reinforcement and Figure 4.12 summarizes the reinforcement details of RC segments, which were used as reference samples. This reinforcement solution, which is characterized by a total steel content equal to 160.24 kg. This value can be considered as 108.3 kg/m³.



Figure 4.12. Reinforcement details of RC segments

- Longitudinal reinforcement or curved rebars: 8 ϕ 10 in poses 1&3 and 4 ϕ 12 in poses 2&4 for flexure
(longitudinal reinforcement ratio under flexure (ρ_s) is 0.32%)
- Shear reinforcement; stirrups ϕ 10 with 2 legs in pose 5
- Local tie for splitting stresses: tie ϕ 8 with 1 leg in pose 8
- Curved bar for spalling stresses: 4 ϕ 12 in poses 6&7

Pose details are explained in Figure 4.13

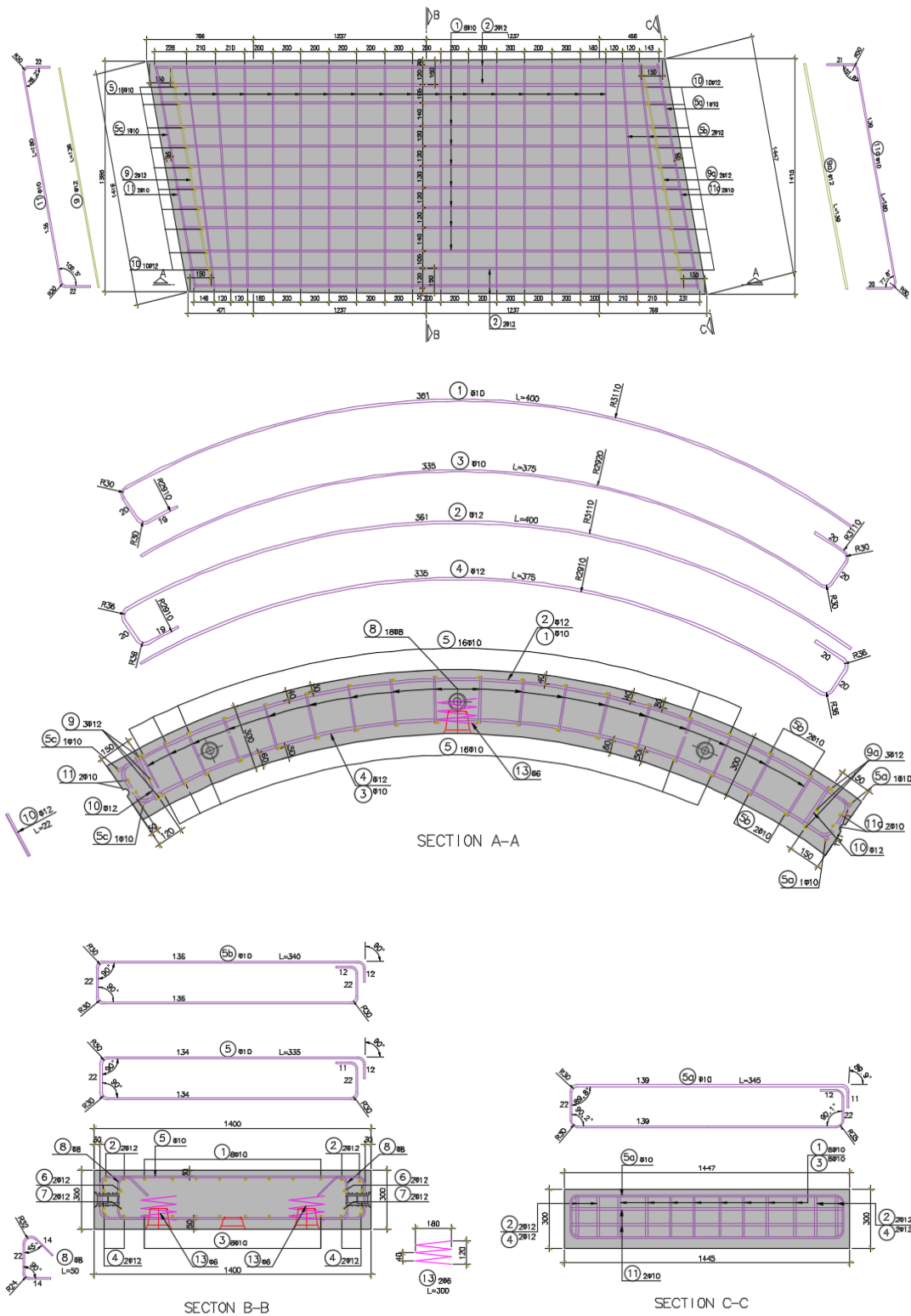


Figure 4.13. Reinforcement details of RC segments (units mm, not to scale)

4.1.2.2. Type B - RC+PFRC Sample

Type B comprises of both traditional reinforcements and polypropylene fibers. Figure 4.14 summarizes the reinforcement details of RC+PFRC segments, which were used as a hybrid sample. This reinforcement solution, which is characterized by a total steel and PP fiber content equal to 42.1 kg/m^3 , 4 kg/m^3 ($V_f = 0.44 \%$) respectively.



Figure 4.14. Reinforcement details of RC + PFRC segments

- Longitudinal reinforcement or curved rebars: $4\phi 12$ in poses 1&2 for flexure and partially helping of PP fibers for spalling stresses (longitudinal reinforcement ratio under flexure (ρ_s) is 0.13%)
- Shear reinforcement: stirrups $\phi 8$ with 2 legs in pose 6
- Local stirrups for splitting stresses: stirrups $\phi 8$ with 2 legs in pose 6

Pose details are explained in Figure 4.15. Polypropylene fiber reinforcement generally considered to resist splitting and shear stresses for tunnel segments, also to obtain better control of spalling stresses (Conforti et al., 2017). Compared to the type A, the traditional steel reinforcement content of this hybrid solution was reduced by 61% by using macro-synthetic fibers. This classical hybrid solution is based on a combination of fibers and steel reinforcing bars recommended by Plizzari and Tiberti (2007). In addition to this proposal, as mentioned before experimental programs on precast

tunnel segments carried out by De la Fuente et al. (2012) and Conforti et al. (2017) represent competitive solutions and show significant examples of hybrid cases.

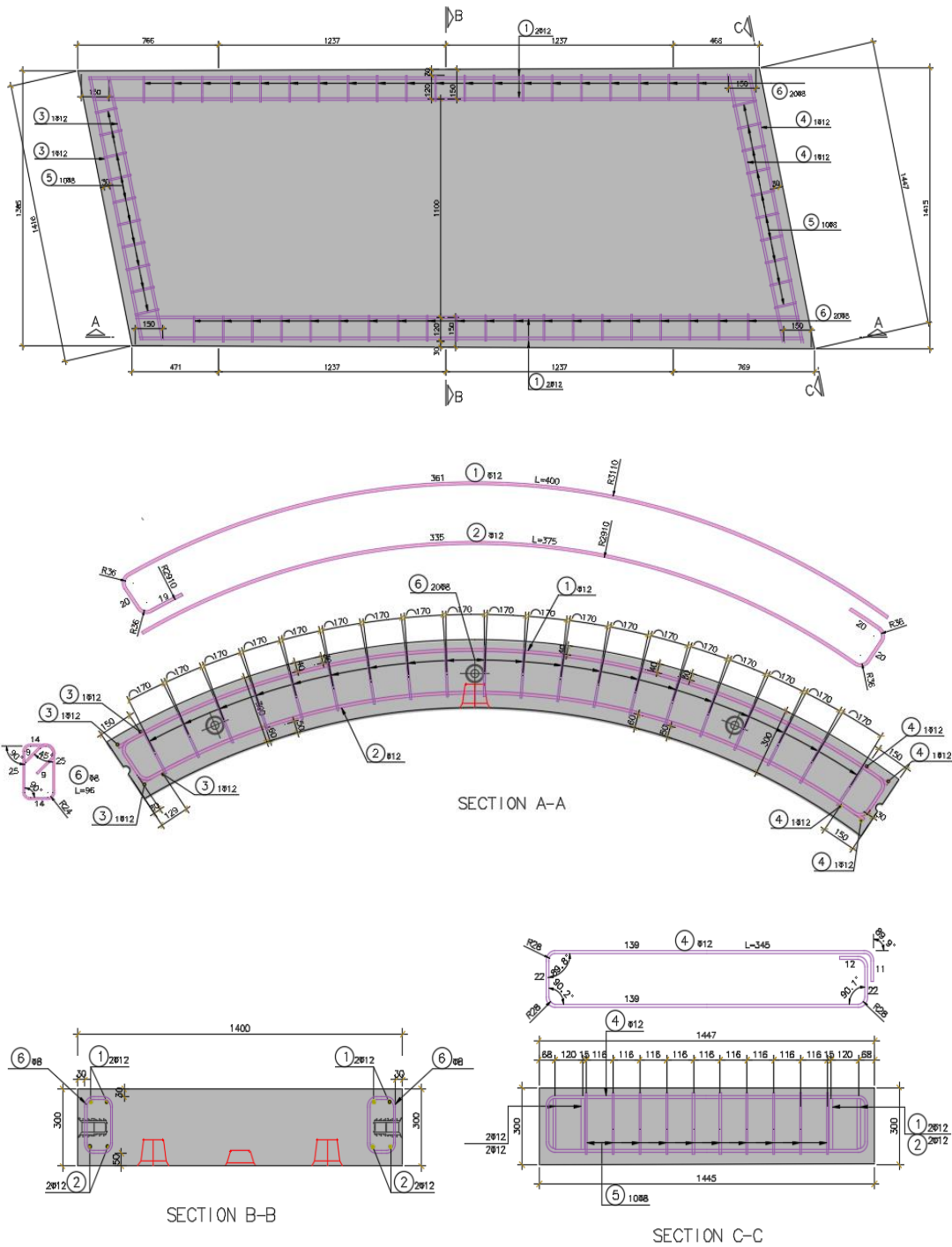


Figure 4.15. Reinforcement details of RC + PFRC segments (units mm, not to scale)

For the B4 specimens, the total number of stirrups ($\phi 8$ with 2 legs in pose 6) in the curved side was preferred fifteen instead of twenty.

4.1.2.3. Type C - GFRP + PFRC Sample

Type C consisted of both glass fiber reinforced polymer (GFRP) rebars and polypropylene fibers. Figure 4.16 summarizes the reinforcement details of GFRP + PFRC segments, which were used as an alternative hybrid sample. This reinforcement solution, which is characterized by a combination of PP fiber which is equal to 4 kg/m^3 ($V_f = 0.44 \%$) with 28.20 meters $\phi 8$ rebar and 44.70 meters $\phi 10$ rebar.

- Longitudinal reinforcement or curved rebars: $4\phi 10$ in poses 1&2 for flexure and partially helping of PP fibers for spalling stresses
- Local stirrups for splitting stresses: stirrups $\phi 8$ with 2 legs in pose 6
- Since shear capacity of glass fiber reinforced polymer bars is very low compared to conventional reinforcement, polypropylene fibers are considered to resist shear stresses in precast tunnel segment.

Pose details are explained in Figure 4.17.



Figure 4.16. Reinforcement details of GFRP + PFRC segments

Previous experimental studies carried by Caratelli et al. (2016, 2017) showed that using glass fiber reinforced polymer (GFRP) reinforcing bars in precast tunnel segments is possible as an innovative solution. Although the cost of GFRP rebars is

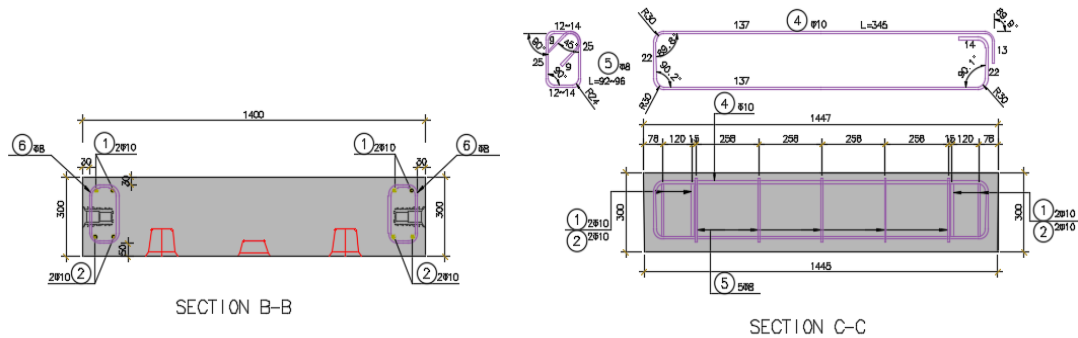


Figure 4.17. Reinforcement details of GFRP + PFRC segments (units mm, not to scale)

4.1.2.4. Type D - PFRC Sample

Type D was reinforced only by 6 kg/m^3 ($V_f = 0.66 \%$) macro-synthetic polypropylene fibers, considering a solution only by using fibers for the flexural, shear, spalling, and splitting stresses. Although the amount of fibers selected is lower compared to similar experimental programs carried out by Tiberti et al. (2015) and Conforti et al. (2016, 2017) and ITA report n.16 (2016) suggestion, which ranges from 8 to 10 kg/m^3 dosage for macro-synthetic fibers, it was thought to be a guide for determining of quantity for the future works. Moreover, the fibers quantity and type were determined on the basis of the preliminary design of FRCs segments. Concrete mix design details were designated by considering the applications of previous slabs casting, which the fiber manufacturer was responsible. The other reason why 6 kg/m^3 MSF were chosen in the mix design is that comparison cost analysis with the RC segment type was made. In most of the fiber applications in Turkey, structures contain between 2 and 6 kg/m^3 macro-synthetic fibers. Since the workability of concrete is getting harder with the increasing fiber quantity, some special admixtures are needed in concrete to easy the casting process. These admixtures cause the increasing of the total cost of the concrete, considering the fiber cost, as well.

However, material tests results, which are explained in the following pages, indicated that the fiber amount adopted did not show significant post-cracking residual

strengths. Preferred concrete matrix did not meet the criteria of fib Model Code 2010 for both structural applications and using only polypropylene fibers as minimum shear reinforcement. It should be noticed that the number of beam samples that were taken during the production of segments is quite low to obtain the accurate information on FRCs. Full-scale experimental test results take placed in the next chapter, therefore, these data would be more accurate and reliable for the evaluation of the structural performance exactly and obtaining more information about PRFC segments.



Figure 4.18. Reinforcement details of PFRC segments

4.2. Material Properties

In this part, properties of materials which were used in the production of specimens were discussed and summarized in tables. Related specifications have been followed properly in order to define the characteristics and structural properties of materials.

4.2.1. Concrete Properties

Table 4-4 represents the mix proportions of concrete for the production of precast tunnel segments, namely PC and PFRC. The first mix design is commonly used for tunnel segments with conventional reinforcement. The second, as already mentioned,

was used for both RC + PFRC and GFRP + PFRC hybrid segments without any difference of fiber amount. The last one represents the mix design which corresponds to the macro-synthetic fibers only. All the mix designs were provided from the ready-mixed concrete plant at the precast manufacturing yard that produced four concrete batches. In this experimental program, the C40/50 concrete class was chosen to produce specimens according to Eurocode 2 (2004). With reference to this code, the target mean cylindrical compressive strength which is generally adopted in practice at 28 days was of nearly 48 MPa ($f_{cm} = f_{ck} + 8\text{MPa}$). The specimens were casted by precast steel moulds belonging to type C segments within a day and same environmental conditions and consolidated by means of the vibration system. All concrete mixes showed a sufficient workability with no considerable reduction of their flowability from the beginning to the end of the casting process. All specimens were cured in the steam-curing chamber approximately 5.5 hours before demolding. The main criteria is that before realizing the segments demoulding operation, a concrete with a compressive strength of $f_{ck} = 15\text{ MPa}$, which has to be reached, has been considered in the verifications. Within this framework, laboratory tests were carried out by the manufacturer to determinate the minimum curing time necessary to achieve this strength. Moreover, for the sake of safety, the one casted sample from each batches was tested after 5.5 hours for measuring the early strength and all of them satisfied the minimum compressive strength. Then all specimens stored at the precast manufacturing yard up to testing (age of 28–90 days). In this way, the same environmental conditions were ensured for real precast tunnel segments of metro project although, in some projects, this duration can last up to a year. When concrete was reached its full characteristic strength $f_{ck} = 40\text{MPa}$, four different types of specimens, totally sixteen precast tunnel segments, were stored four of them together. In all four concrete batches six cubes (150 mm side dimensions) were cast for measuring the compressive strength at ninety days, while three cylindrical samples (100 x 200 mm) were prepared to measure the compressive strength at both seven and twenty-eight days according to EN 12390-3 (2009). In addition to this samples, totally

nine small beams (150 x 150 x 550 mm), three samples for each mix designs which consist of macro-synthetic fibers, were prepared for the evaluation of PFRC residual flexural tensile strengths according to EN 14651 (2005).

At it is seen in Table 4-4, the water-cement ratio of fiber reinforced concreted are same, but when the cement content are compared, type D is higher than type B and C. The reason is that more water is used in the mix design to increase the workability of type D samples. Type A concrete mix designs are commonly used for the production of ordinary precast tunnel segments.

Table 4.4. *Concrete mix designs of specimens*

Sample type	A	B and C	D
Concrete designation	PC	PFRC	PFRC
Cement type	CEM I*	CEM I*	CEM I*
Cement content [kg/m ³]	365	374	385
Water [L/m ³]	152	142	146
W/C Ratio	0.42	0.38	0.38
Admixture [kg/m ³]	3.33 (adva 575)	3.23 (grc)	3.71 (grc)
Crushed sand [kg/m ³]	361	361	358
Aggregate 5-12 [kg/m ³]	498	498	494
Aggregate 12-19 [kg/m ³]	413	395	392
Aggregate 19-25 [kg/m ³]	585	604	599
Fiber content [kg/m ³]	-	4	6
Fibers V _f (%)	-	0.44	0.66

*According to EN 197-1, CEM I type of cement is a Portland cement with a maximum of 5% other materials.

All cubes, cylinders and small beams were cured under the same environmental conditions and kept in the curing storage pool. The Table 4-5 report the mean cubic compressive strength ($f_{cm,cube}$) at 90 days and the other tables illustrate the mean cylindrical compressive concrete strength (f_{cm}) at 7 and 28 days respectively.

Table 4.5. The cubic compressive strength at 90 days

Specimens 150 x 150 x 150 mm	A	B (4 kg/m ³)	C (4 kg/m ³)	D (6 kg/m ³)
1	63.65	62.74	63.27	68.20
2	61.83	61.45	63.65	70.44
3	65.70	60.39	63.61	70.49
4	56.33	59.75	65.15	66.88
5	64.73	57.09	64.18	67.79
6	63.20	59.51	64.69	69.96
Average (MPa) $f_{cm,cube}$	62.57	60.15	64.09	68.96

Table 4.6. The cylindrical compressive strength at 7 days

Specimens 100 x 200 mm	A	B (4 kg/m ³)	C (4 kg/m ³)	D (6 kg/m ³)
1	41.2	41.3	41.4	47.6
2	41.3	41.0	42.2	47.1
3	41.6	42.3	43.3	48.6
Average (MPa) $f_{cm,7}$	41.3	41.5	42.3	47.7

Table 4.7. The cylindrical compressive strength at 28 days

Specimens 100 x 200 mm	A	B (4 kg/m ³)	C (4 kg/m ³)	D (6 kg/m ³)
1	47.5	48.7	50.3	55.6
2	51.3	49.5	49.5	55.1
3	50.8	46.6	50.4	54.8
Average (MPa) $f_{cm,28}$	49.9	48.3	50.1	55.2
$f_{cm,90}=0.83f_{cm,cube}$	51.93	49.92	53.2	57.24

According to Eurocode the mean cylindrical compressive concrete strength (f_{cm}) was also assumed as 83% of the cubic one ($f_{cm} = 0.83f_{cm,cube}$) and results were tabulated in

Table 4-7 , and when the mean cylindrical compressive concrete strength (f_{cm}) at 28 days taken into consideration, all samples showed higher strength than 48 MPa.

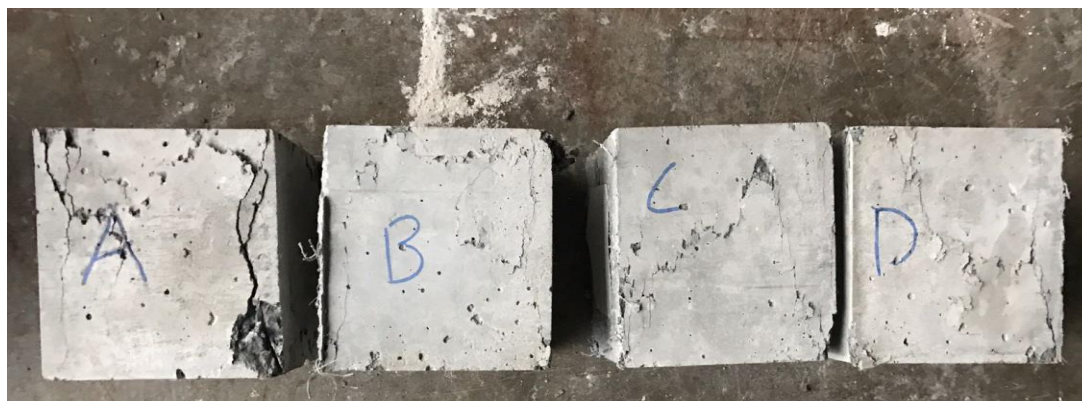


Figure 4.19. Examples of cracked samples after the test

It has been observed that higher fiber reinforcements content used in concrete samples increase the compressive strength of concrete. In addition, as can be seen from the Figure 4.19, the fibers in the concrete also provide a decreasing crack opening of the specimens during fracture.

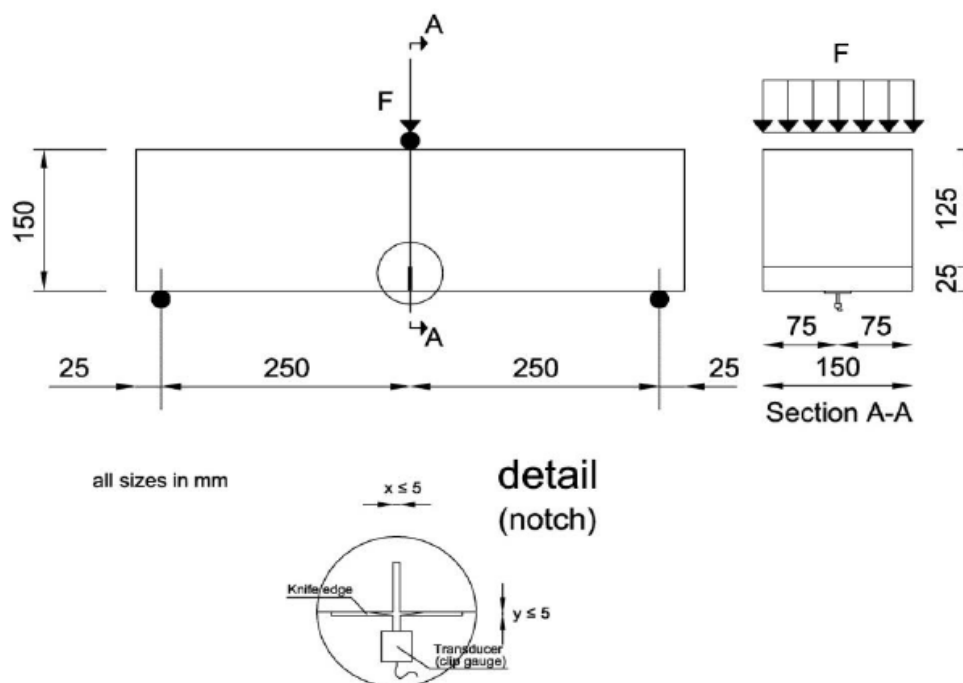


Figure 4.20. Dimensions of 3-point bending test on a notched beam (EN 14651, 2005)

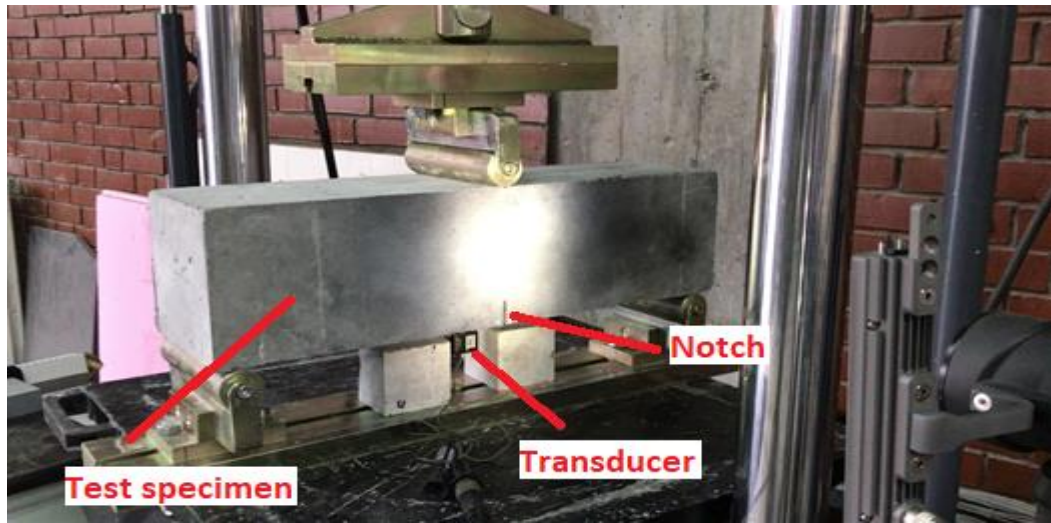


Figure 4.21. Test specimen and experimental set-up

Moreover, fib Model Code 2010, which is commonly used by designers, was used to classify and obtain more information about FRC in the view of this information. In order to characterize the fiber reinforced concrete used for the production of test specimens and EN 14651 test standard was applied to obtain design values. Figure 4.20 shows the dimensions of test specimens and notch details. Also, the general view of the test set-up, which is adopted for determining the load versus crack mouth opening displacement (CMOD) curves, are shown in the Figure 4.21. CMOD values were measured by means of transducer. As previously mentioned, the tensile and fracture behavior of fiber reinforced concrete were characterized through bending tests on three 150x150x550 mm notched beam specimens for each sample, according to the EN 14651 (2005). The limit of proportionality f_L and the residual flexure tensile strengths (f_{R1} , f_{R2} , f_{R3} , f_{R4} , corresponding to CMOD values of 0.5, 1.5, 2.5 and 3.5 mm, respectively), as defined in EN 14651, were determined by applying the following equations:

$$f_L = \frac{3F_L l}{2bh_{sp}^2} \quad (1)$$

$$f_{R,j} = \frac{3F_{j,l}}{2bh_{sp}^2} \quad (2)$$

Where;

$l = 500 \text{ mm}$,

$b = 150$,

$h_{sp} = 125 \text{ mm}$,

F_L = is the load at the limit of proportionality

F_j = is the load corresponding with $\text{CMOD} = \text{CMOD}_j$.

Figure 4.22 was taken from EN 14651 in order to display how to obtain test results and represents criteria such as CMOD values, corresponding load levels and load at the limit of proportionality.

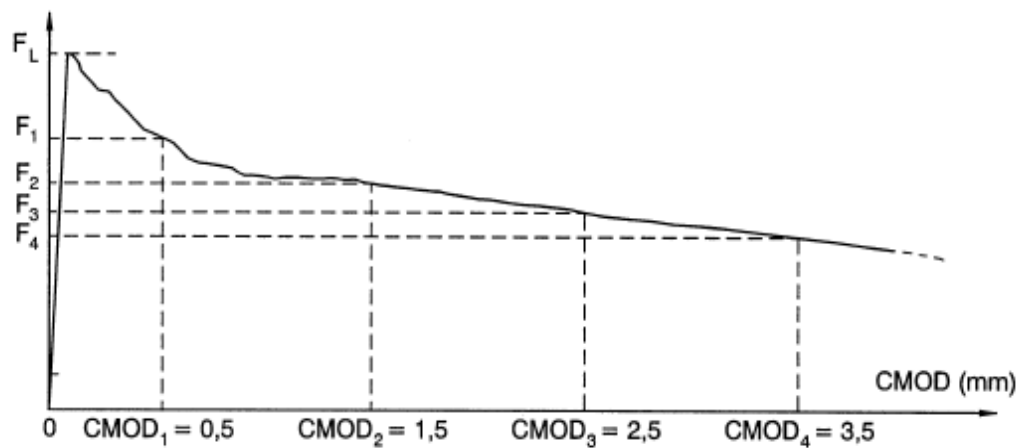


Figure 4.22. Example of load versus CMOD diagram (EN 14651, 2005)

Within these frameworks, the load versus mid-span deflection graph are shown in the Figure 4.23. In addition to this, the diagrams of the nominal stress versus the crack mouth opening displacements (CMOD) are plotted in Figure 4.24. It should be noticed that CMOD_4 value (3.5 mm crack width) at the one of the RC + PFRC sample and all GFRP + PFRC samples could not be measured due to technical problems.

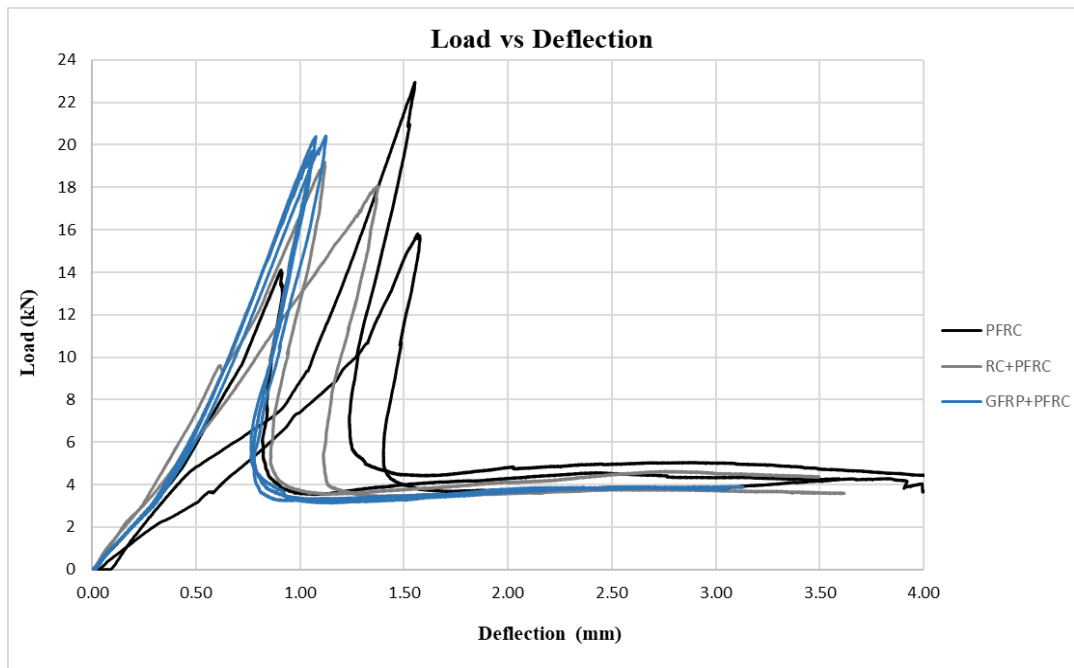


Figure 4.23. Experimental results of bending tests in terms of load versus vertical deflection

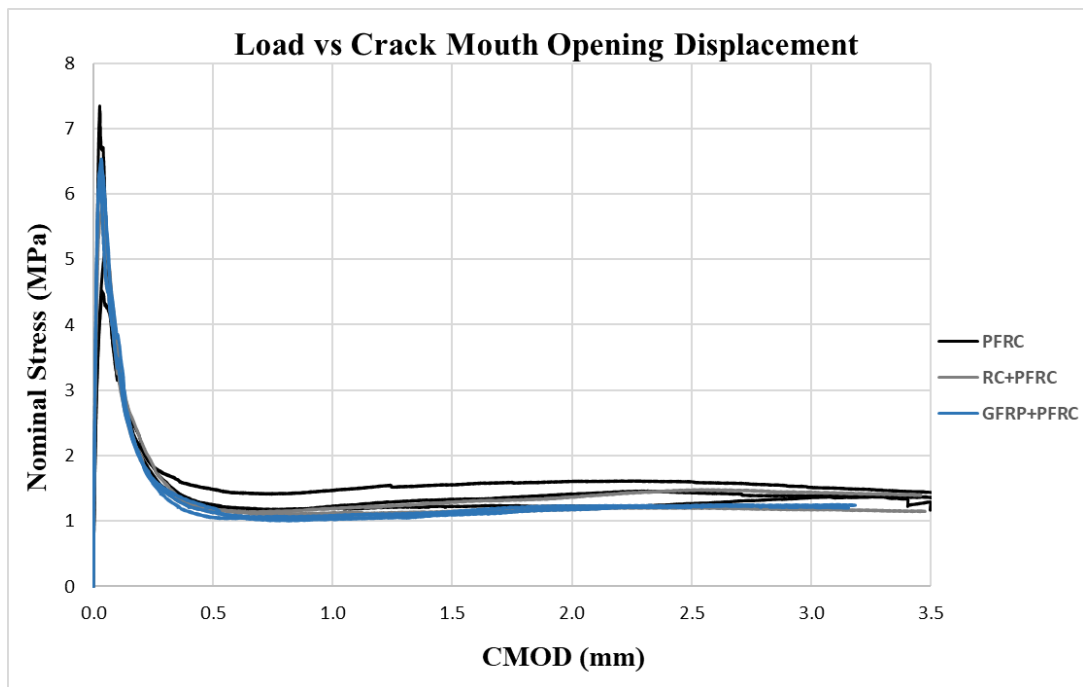


Figure 4.24. Nominal stress vs. CMOD curve

Furthermore, energy absorption capacity can be obtained from the load versus displacement graphs. According to Figure 4.23, the area under the graphs of PFRC specimens is higher than the others, therefore, energy absorption capacity is higher. Another important point in Figure 4.23 is that after the first crack occurs in the samples, applied load level decreased sharply and then displacement values increased with approximately the same load level. According to ITA report n.16 (2016), this is typical flexural softening behavior of fiber reinforced concrete under bending. In general, uniaxial test is preferred to directly evaluate the post-cracking tensile behavior of fiber reinforced concrete, however, this test is quite difficult to carry out. Therefore, bending tests, such as EN 14651, are usually suggested by design recommendations in order to analyze the flexural response of cementitious composites after cracking (ITAtch report n.7, 2016). Previous study performed by Kooiman (2000) stated that flexural softening or hardening behavior occurs after reaching the initial crack depending upon concrete matrix, amount and type of fiber reinforcement. Experimental result of bending test according to EN 14651 indicated that all fiber reinforced concrete samples displayed flexural softening behavior since there was no considerable increase in load after the first crack (see Figure 4.24). Apart from that during tests, multiple cracking was not observed on the FRC samples. Moreover, simplified stress-strain relationships for both softening and hardening FRC are shown in the Figure 4.25.

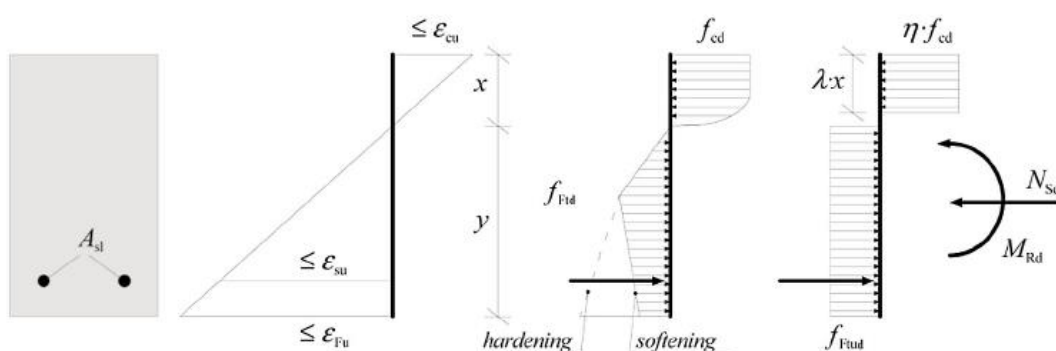


Figure 4.25. Simplified stress-strain relationships (fib Model Code 2010, 2012)

The values of the limit of proportionality f_L and the residual flexure tensile strengths are summarized with the mean values in Table 4-8. It can be observed that 6 kg/m³ PP fibers has not provided significant structural performances both at serviceability limit states (f_{R3m} of about 1.44 MPa) and ultimate limit states (f_{R1m} of about 1.32 MPa) since the results are considerably lower than expected. According to ITAtech report n.7 (2016), after the 28 days, the typical minimum performance levels for tunnel segmental linings under the bending effect are $f_{R1k} > 2.2$ MPa and $f_{R3k} > 1.8$ MPa in terms of residual tensile strength. As it is seen the Table 4-8, this fiber content does not satisfy the minimum criteria. In a similar manner, samples that contain 4 kg/m³ ($V_f=0.44\%$) fibers displayed also lower residual flexural tensile strength. However, as previously mentioned these results may not reflect the exact situation since the number of the specimen is quite low and there is some technical problem occurred during EN 14651 test. Additionally, as discussed in chapter 2, softening and hardening behaviors of fiber reinforced samples shows differences depending on the sample size and test method (fib Model Code 2000, 2012).

Characteristic values are obtained by considering the following formula that is given in the ITAtech report n.7 (2016) and the results were tabulated in Table 4-8.

$$f_{fctk} = f_{fctm} * (1 - k_n * V_x) \quad (3)$$

Where;

f_{fctk} : characteristic FRC flexural tensile strength,

f_{fctm} : mean FRC flexural tensile strength,

V_x : coefficient of variation, equal to the ratio of standard deviation of the mean,

k_n : is a statistical coefficient.

For the three number of samples, statistical factor (k_n) is equal to 0.95 for known V_x (Normal distribution and 95% reliable estimation the mean value was assumed).

The RC + PFRC samples can be classified as 1c according to Model Code 2010. In fact, the characteristic value of f_{R1k} represents the first value of classification and shown as a number (the first number of f_{R1k}). For RC + PFRC samples, this value was determined to 1.14 MPa. Then, the second values are found by the ratio between f_{R3k} and f_{R1k} and it is represented by a letter. This ratio for the RC + PFRC samples is equal to 1.02. According to Model Code 2010, this represents the class c because it is inside the range between the 0.9 and 1.1, which is the limit for the class c. After the same procedure was applied, the classification of GFRP + PFRC and PFRC samples were found 1d and 1c, respectively.

Since brittleness should be avoided in structural members, fiber reinforcement can substitute (even partially) the conventional reinforcing bars or steel mesh at the ultimate limit state, if both the relationships ($f_{R1k}/f_{Lk} > 0.4$ and $f_{R3k}/f_{R1k} > 0.5$) are fulfilled according to fib Model Code 2010, (2012). As a result of experiments, the following ratios are obtained: $f_{R1k}/f_{Lk} = 0.2$ and $f_{R3k}/f_{R1k} = 1.02$ MPa for RC+ PFRC; $f_{R1k}/f_{Lk} = 0.17$ and $f_{R3k}/f_{R1k} = 1.15$ MPa for GFRP+ PFRC; $f_{R1k}/f_{Lk} = 0.28$ and $f_{R3k}/f_{R1k} = 1.1$ MPa for PFRC. The obtained fracture properties of FRC samples indicated that they do not fulfil the requirements of the fib Model Code 2010 for use in structural elements. Moreover, this test results also showed that the quantity of fibers that used for the production of precast tunnel segments was very low in term of structural performance. Both RC + PFRC and GFRP + PFRC segment concretes showed a very similar post-cracking behavior under the flexure. PRFC samples results revealed slightly higher compared to others, although the fibers content 1.5 times higher.

Furthermore, according to equation 7.7-14 of Model Code 2010, the minimum amount of conventional shear reinforcement (stirrups) is not needed if the characteristic value of ultimate tensile strength (considering with $w_u=1.5$ mm) for fiber reinforced concrete is higher than the following limit (4).

$$f_{Ftuk} \geq 0.08\sqrt{f_{ck}} \quad (4)$$

In order to calculate the f_{Ftuk} value, equations 5.6-5 and 5.6-6 of Model Code 2010, (2012) were used.

$$f_{Fts} = 0.45f_{R1} \quad (5)$$

$$f_{Ftuk} = f_{Fts} - \frac{wu}{CMOD3}(f_{Fts} - 0.5f_{R3} + 0.2 f_{R1}) \geq 0 \quad (6)$$

In general, f_{ck} values is taken as 40 MPa for C40/50 class concrete. Thus, based on the equation (4), the f_{Ftuk} value should be equal or greater to 0.506 MPa. According to formula (6), the characteristic value of ultimate tensile strength is calculated as 0.454 MPa for PFRC. Consequently, results of PFRC samples did not satisfy the requirement of above the equation, which allows to use only fibers as minimum shear reinforcement in the precast tunnel segments. However, it should not be overlooked that the number of test specimen significantly affect the results due to higher standard deviation. Therefore, to obtain more accurate values higher number of small beam should be tested. ITAtech report n.7 (2016) recommends the minimum 12 tests required for verification of the variation coefficient. Nonetheless, shear stress was assumed that it would not be critical for PFRC segments since shear capacity of specimens significantly higher than design values due to higher cross sectional area of tunnel segments.

Table 4.8. Residual tensile strengths of test specimens and compressive strength of concrete

Specimen Type	A (RC)	B (RC+PFRC)	C (GFPR+PFRC)	D (PFRC)
$f_{cm,cube}$ [MPa]	62.57	60.15	64.09	68.96
$f_{cm,cylinder}$ [MPa]	49.9	48.3	50.1	55.2
Beam 1		5.79	6.54	7.35
Beam 2		6.14	6.31	5.06
Beam 3		6.31	6.53	4.52
V_x		0.04	0.02	0.27
$f_{L,m}$ [MPa]	-	6.08	6.46	5.64
$f_{L,k}$ [MPa]		5.83	6.34	4.22
Beam 1		1.18	1.06	1.49
Beam 2		1.18	1.14	1.25
Beam 3		1.13	1.20	1.21
V_x		0.03	0.06	0.12
$f_{R,1m}$ [MPa]	-	1.16	1.13	1.32
$f_{R,1k}$ [MPa]		1.14	1.07	1.17
Beam 1		1.15	1.10	1.56
Beam 2		1.29	1.14	1.22
Beam 3		1.14	1.14	1.34
V_x		0.07	0.02	0.13
$f_{R,2m}$ [MPa]	-	1.19	1.13	1.37
$f_{R,2k}$ [MPa]		1.11	1.10	1.21
Beam 1		1.20	1.23	1.60
Beam 2		1.48	1.24	1.27
Beam 3		1.23	1.23	1.44
V_x		0.12	0.01	0.12
$f_{R,3m}$ [MPa]	-	1.30	1.23	1.44
$f_{R,3k}$ [MPa]		1.16	1.23	1.28
Beam 1		1.15	-	1.44
Beam 2		1.40	-	1.28
Beam 3		-	-	1.36
V_x		0.14	-	0.06
$f_{R,4m}$ [MPa]	-	1.26	-	1.36
$f_{R,4k}$ [MPa]		1.11	-	1.28

4.2.2. Reinforcements Properties

In this study, three different reinforcement types were used for the specimens production and the detailed information about these materials are given in this section.

4.2.2.1. Conventional Steel Rebars

In this experimental study, three different steel deformed reinforcements with diameters ($\phi 8$, $\phi 10$ and $\phi 12$) were used as both transverse and longitudinal reinforcement in the production of precast tunnel segments. Since the rebars properties could not measure by means of experimental way, used S420 class steel reinforcement properties have been considered by TS-708-2010 “Steel Bars for Concrete” specification. According to related specification, minimum yielding and ultimate tensile strength of these steel reinforcement should be 420 MPa and 500 MPa, respectively and it is thought that they satisfy the minimum criteria of the specification.

4.2.2.2. Polypropylene Fibers

Table 4-9 summarizes the main macro-synthetic fiber characteristics which were taken from related company’s catalogue that prepared according to EN 14889-2 (2006).

Table 4.9. *Polypropylene fiber properties*

Type:	Polypropylene
Brand	Forta-ferro
Length (mm):	54
Diameter ϕ (mm):	0.677
Aspect ratio l/ϕ :	79.76
Tensile strength (MPa):	550-750
Elastic modulus (MPa)	5750
Density (kg/m^3)	910
Number of fiber per kg (approximate)	220000

4.2.2.3. Glass Fiber Reinforced Polymer Rebars

In the experimental program, glass fiber reinforced polymer rebars were used only for the production of C type of specimens and preferred ribbed surface types were used. Figure 4.26 shows the examples view of experimental set-up and anchorage length of rebars.

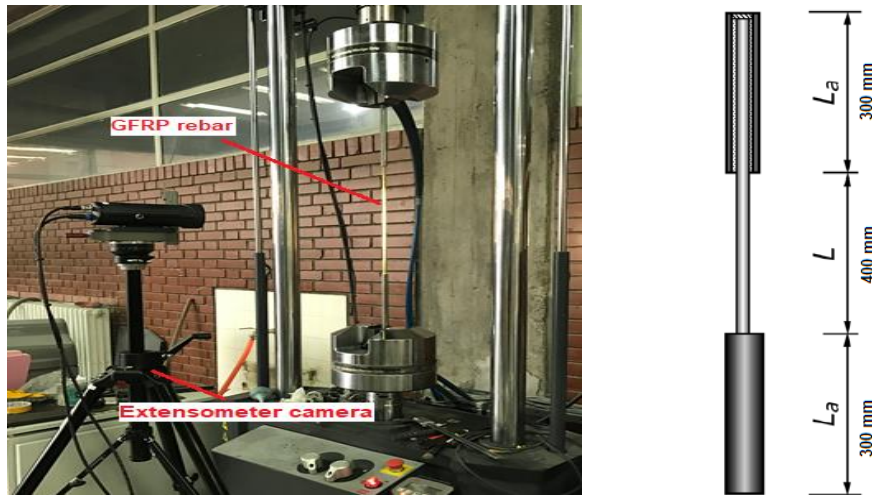


Figure 4.26. Enter the Figure Caption here

Table 4-10 summarizes the main glass fiber reinforced polymer rebar characteristics which were taken from related company's catalogue that prepared according to ISO 10406-1 (2008). The first four values were taken by experimental results which were carried by Darendililer (2017), and the others were taken from Turkish Standards Institute's report.

Table 4.10. *Properties of Glass Fiber Reinforced Polymer Rebars.*

Diameter Φ (mm)	8	10
Nominal diameter (mm)	7.4	9.2
Nominal cross-sectional area (mm ²)	43	67.1
Elastic modulus (GPa)	50.2	51.7
Ultimate strength (MPa)	997	895
Coefficient of thermal expansion (Longitudinal direction, 1/°C)	2.2×10^{-7}	2.2×10^{-7}
Rupture strain (%)	4.50	6.40
Shear strength (Transverse direction, MPa)	222	248

CHAPTER 5

FULL-SCALE EXPERIMENTAL TESTS

5.1. Flexural Test

The main purpose of this test is measuring and comparing the flexural bearing capacity of specimens that consist of different type of materials. Segments are subjected to flexure during demolding, transportation and storage. The purpose of flexure test is to show whether the segments satisfy the demand or not. Design moment for the production and transient phase of Mecidiyeköy - Mahmutbey metro project is 44.25 kN.m. It is related to storage phase, considering that each ring can be stacked in one pile according to the configurations shown in Figure A.1. The dead load of each segment is about 37.11 kN and key segments weight is nearly 12.37 kN. In order to perform a safe side analysis, the distance between two bearing timbers was taken 2.3 m and an accidental eccentricity ($e = 0.30\text{m}$) concerning the supports at the base of the pile was considered. In this situation, the higher bending moment occurs at the bottom segment. Detailed information about design values take places in appendix A

In this experiment, crack width opening due to flexure and mid-span deflections of the segment were measured to evaluate the specimen's capacities. In order to properly determine the maximum bending moment capacity of specimens, allowable serviceability limit state of crack width was taken into consideration. The allowable SLS crack width limit shows differences between the specifications and guidelines. For instance, this limit value is 0.3 mm for the ACI 224.1R (2007) and EN 1992-1-1 (2004) however, it is 0.2 mm for fib Model Code 2010 (2012) and DAUB (2013). In this experimental program project's crack with limit was considered to 0.3 mm which is based on EN 1992-1-1 (2004). 0.3 mm crack width is also the permissible limit for Mecidiyeköy - Mahmutbey Metro line.

5.1.1. Test Set-up and Instrumentation of Flexural Test

To determine the flexural bearing capacity of specimens, test set-up was designed by considering the exact dimensions of precast tunnel segments. In the literature, two different test methods are available to measure bending capacity of specimens. These are mainly known as three point and four-point bending test. Four-point bending tests are most commonly preferred for testing nonhomogeneous materials since in between the loads, the moment is constant and the shear is zero, thus a pure flexure region is obtained. However, in four-point tests, measuring cracks width and observation of crack patterns are difficult because the peak moment occurs in a huge region, where between the load. In contrast to the four-point bending test, the stress concentration of a three-point test is small and concentrated under the center of the loading point. In this way, the maximum moment is obtained at the mid-span of specimens. Moreover, a three-point test is easier to perform than a four-point test for full-scale precast tunnel segments. Therefore, in accordance with the previous experimental tests which were carried out by Caratelli et al. (2012), Abbas et al. (2014), Meda et al. (2016) and Conforti et al. (2017), three-point bending test was adopted for evaluation of the flexural behavior of precast tunnel segments (see Figure 5.1).

In this test, the load was applied to the segments to the outer face by two loading steel plates (200x200 mm) on the mid-span. In addition, since the outer surface of segments have curved shape, the same sizes of rubber layers having a 20 mm thickness were placed below the steel plates to obtain full contact with the surface. Apart from that, a larger rubber layer with a thickness of 10 mm was located at the bottom of layers and one teflon layer was placed between two rubbers to decrease friction effect (see figure 5.4). The above-mentioned load was applied to the system by means of a hydraulic jack with a loading capacity of 500 kN and applying load level was measured by a load cell during experimental process. Figure 5.1 shows the flexural loading system. Two roller supports were placed continuously on the entire segment width, providing that 2.6 m net span length between these supports. After the first experiment attempt, two additional roller supports were also adapted to both sides of the rigid steel frame

in order to prevent sliding of the frame. In this way, more stable loading system was obtained.



Figure 5.1. Test set-up and flexural loading system

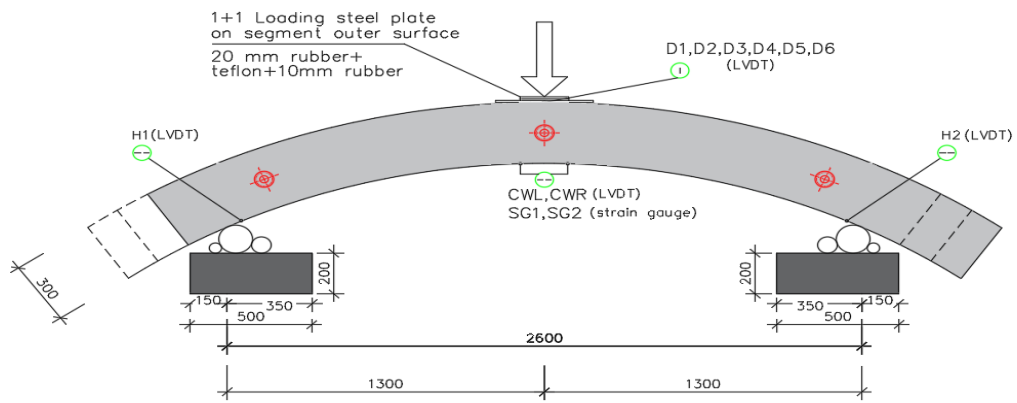
During this test Strain gauges and Linear Variable Differential Transformers (LVDTs) were installed to the specimens in order to measure flexural crack opening width and mid-span deflections. Two LVDTs (CW.L and CW.R) and two strain gauges (SG.L and SG.R) were placed on the segment's inner surface to measure crack opening width due to flexure. Since the maximum flexural moment occurs at the mid-span of specimen due to three-point bending test system and the weakest section of the segments is in the middle zone because of the holes, measuring devices were installed to this region. In almost all segments, the first crack was observed along the weakest section. 6 LVDTs were placed outer surface of specimens to evaluate the mid-span deflection of segments. Deflections were measured by identifying vertical displacement of segments during the test.

The average value was obtained from the four LVDTs which were located in the middle (D3, D4, D5 and D6), while the others measured left and right side deflections of the mid-span (D1 and D2 respectively). Figure 5.2 describes the direction of the test specimen. In addition to vertical displacement, horizontal displacements were measured by means of two LVDTs which are located at two longer corners of segments (H1 and H2). The location of instruments on segments and support locations are shown in figure 5.3.

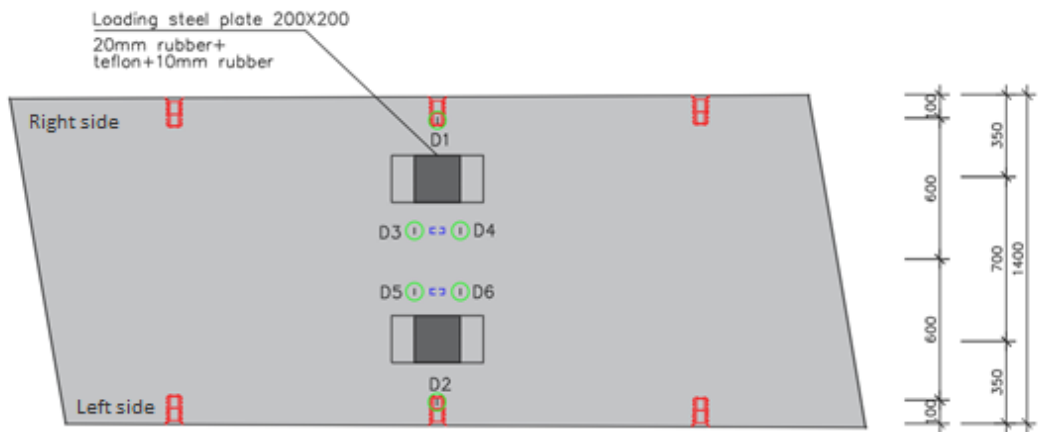


Figure 5.2. Side description of test set-up

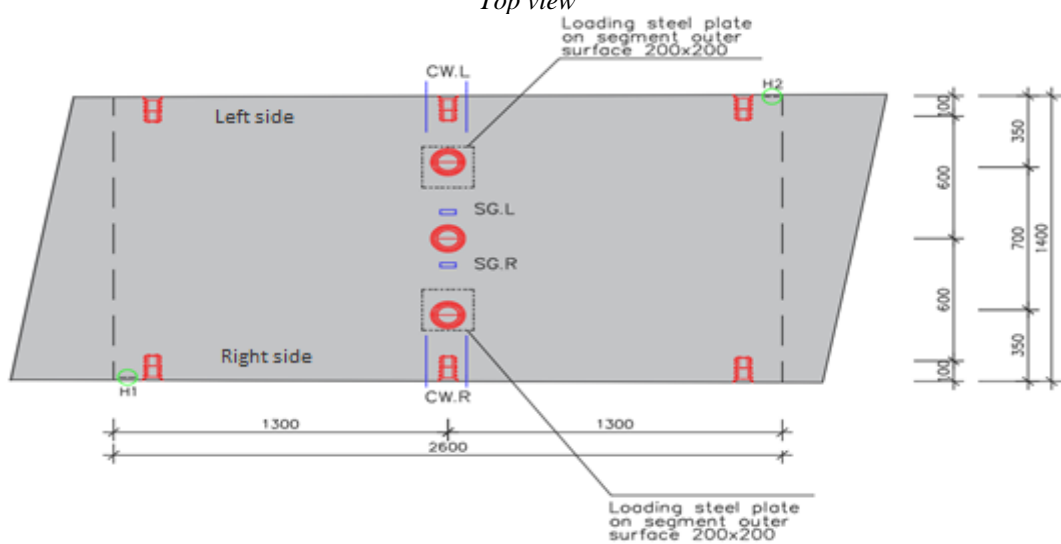
In addition, all instrumentations were controlled before the experiment starts. From Figure 5.3 to Figure 5.8 the instrumentations details and general view of the flexural test are illustrated. First experiments showed that strain gauges cannot give any data at higher crack width. Since they are a very sensitive device, they generally break at a small crack width. For this reason, extra two LVTDs were installed instead of strain gauges in the experiments of B3, C2 and C4 specimens in order to collect more values about flexural crack opening width. As it is seen in Figure 5.8, new LVTDs were placed on the same alignment of the strain gauges.



Frontal view



Top view



Bottom view

Figure 5.3. Instrumentation details of flexural test (units mm, not to scale).



Figure 5.4. Vertical and horizontal LVDTs



Figure 5.5. Left side of the flexural test set-up

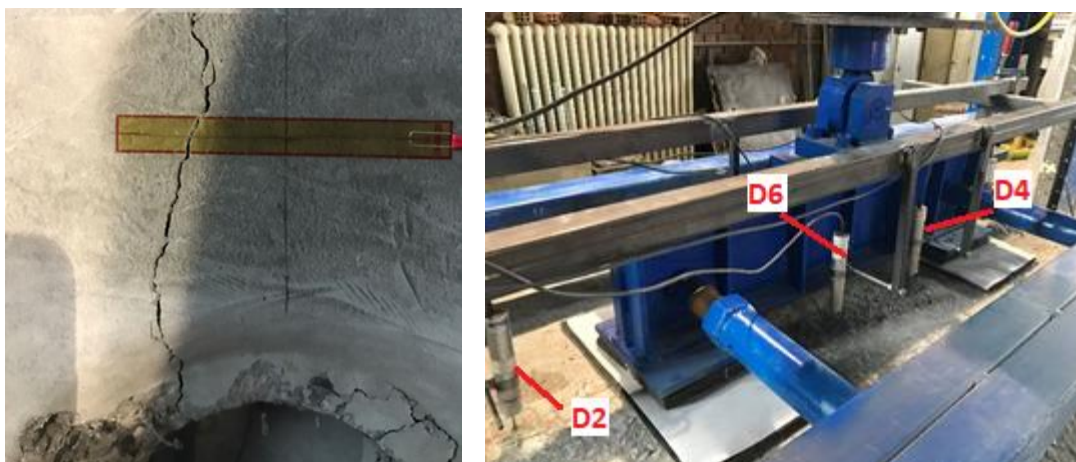


Figure 5.6. Broken strain gauge and vertical LVDTs

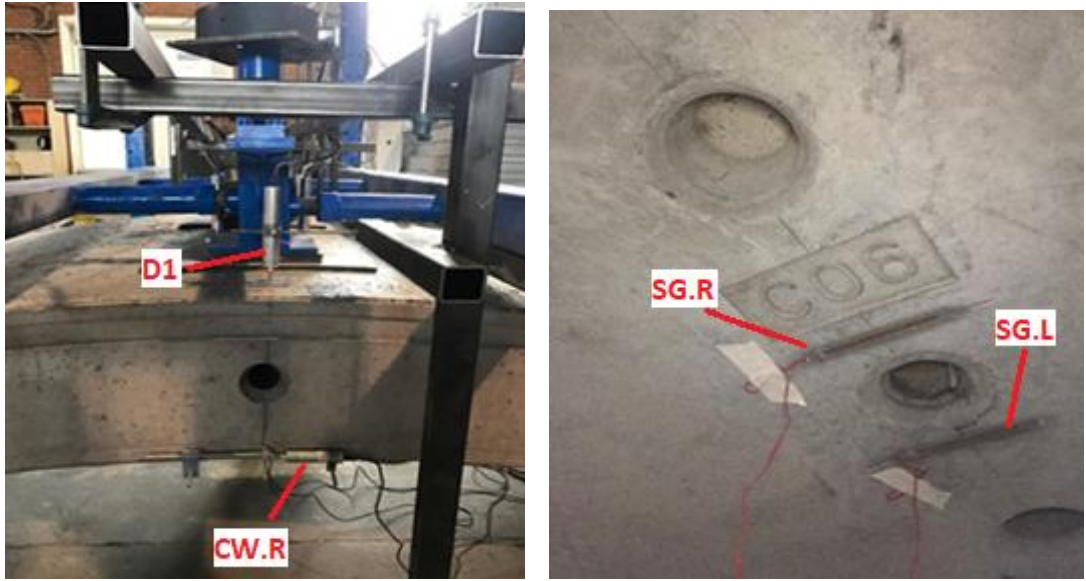


Figure 5.7. Right side and bottom view of the flexural test



Figure 5.8. View of located 2 LVDTs instead of strain gauges

5.1.2. Experimental Results of Flexural Test

In these experiments, load has not been applied with displacement-controlled due to the unsatisfying of the used hydraulic jack. In addition, there is not any information related to loading rate for this full-scale test which was adopted as three point bending. For these reasons, although it was paid attention to applying load rate as close as possible during experiments, loading rate showed slight differences between specimens. Figure 5.9 illustrates the applied load versus time graph of full-scale flexural test.

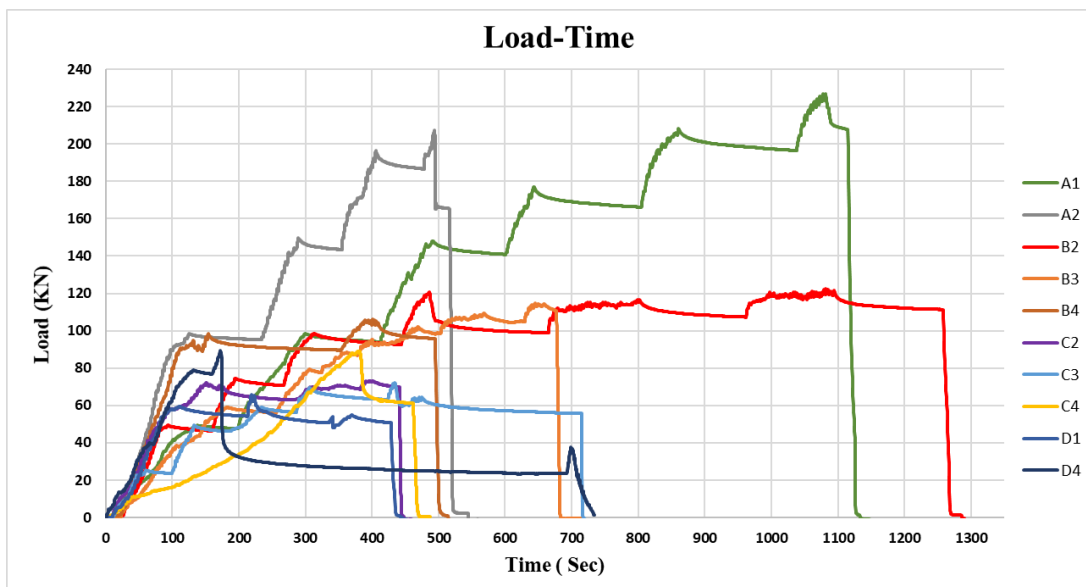


Figure 5.9. Load versus time graph of flexural tests

As it was previously mentioned, totally 6 LVDTs were used in order to measure vertical displacements of tunnel segments. Figure 5.10 shows the mid-span deflections of the segments obtained by average of four LVDTs in the middle, while figure 5.11 illustrate same curves up to 2 mm deflection limit. The values from other LVDTs which were located the left and right side of the mid-span was given in Appendix C. In addition, Table 5-1 displays the load level corresponding to 2 mm vertical displacement that was measured by the four LVDTs in the middle of mid-span. Since all LVDTs measured almost the same displacements values i.e., not torsion was observed, therefore only central LVDTs were considered.

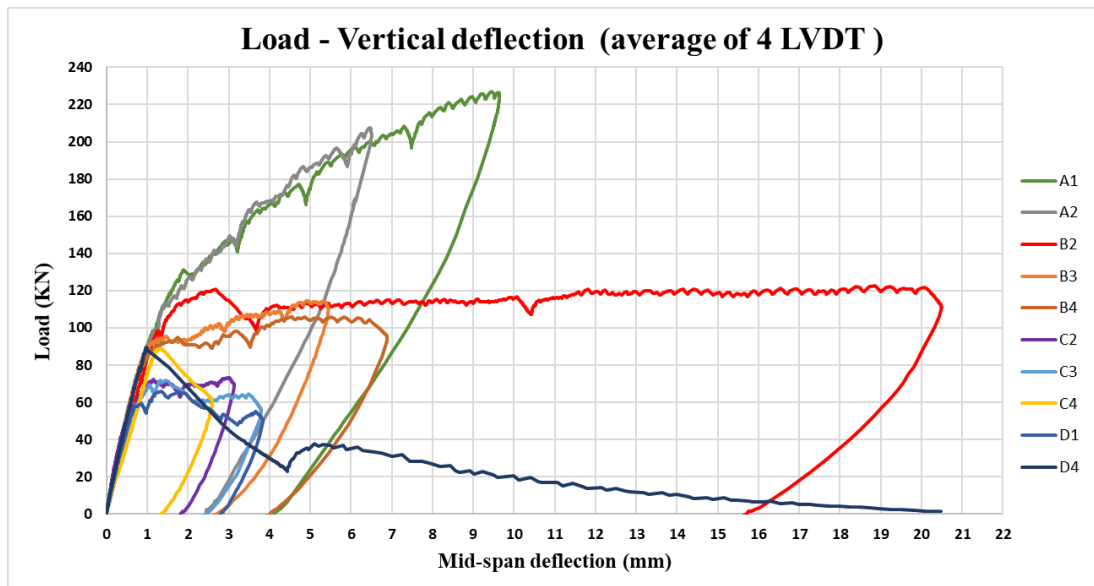


Figure 5.10. Load versus mid-span displacement curves

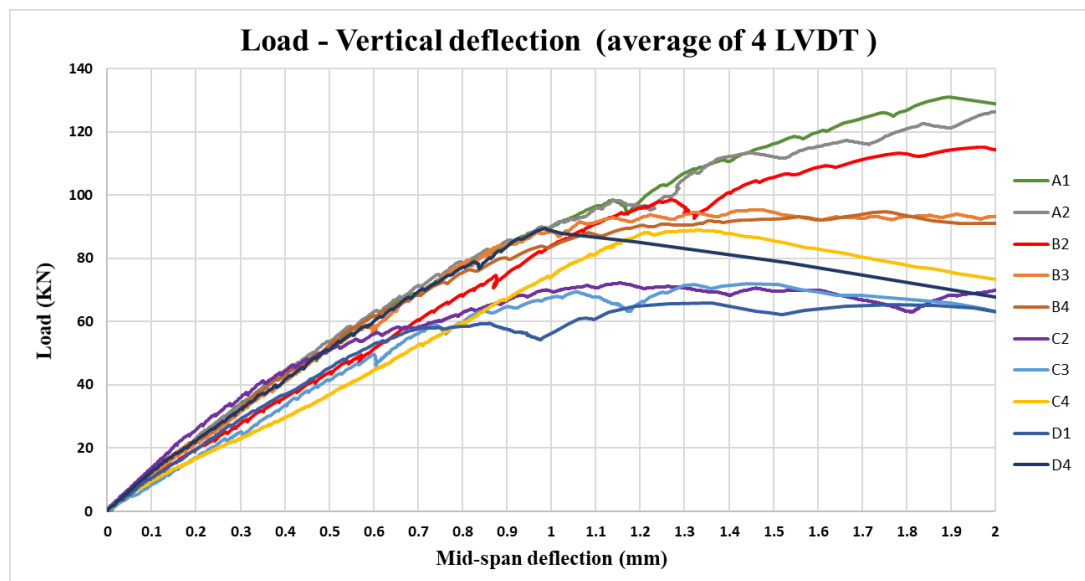


Figure 5.11. Load versus mid-span displacement curves up to 2 mm

Table 5.1. Force corresponding to 2 mm vertical deflection

Specimen number	RC		RC + PFRC			GFRP + PFRC			PFRC	
	A1	A2	B2	B3	B4	C2	C3	C4	D1	D4
Load (kN)	128.83	126.50	114.25	93.90	90.96	69.63	63.01	73.55	63.01	67.98

In the flexural test, an occurring moment on the segment was calculated by according to equation (7).

$$M = 8.6325 \text{ kN.m} + 0.65xP \text{ kN.m} \quad (7)$$

The first value is related to self-weight of the segment and the second one is the effect of applied load. Within this formula, the load corresponding to the design moment of 44.25 kN.m is calculated as approximately 55 kN.

As it is seen from Figure 5.11, although, the vertical displacements seem to nearly the same for different specimens at the low load level, the stiffness values of specimens show huge differences. Nonetheless, for all the segment types mid-span deflection value is lower than 1 mm at the 55 kN load level that constitutes design moment of the metro project for the construction phase. On the contrary, deflection values change significantly between the specimens depending on the reinforcement type at the high load level. It can be clearly seen that RC and RC + PFRC segments are stiffer than others. Compared to load level at 2 mm deflection, RC segments are nearly twice as much stiff as than PFRC and GFPR + PFRC. Moreover, when energy absorption capacity that up to 2 mm deflections are taken into consideration, segments with steel reinforcement shows higher capacity than other types.

Before the evaluation of flexural cracking results it should be noted that during the experiments of RC segments steel apparatus between the hydraulic jack and load cell was bent at high load level due to large stresses. However, this situation did not affect the results significantly since the critical data that is related to serviceability limit state had already been obtained. In addition to this, flexural crack width at the left side could not be measured for the C3 because of the crack pattern. As it is seen in Figure 5.14, crack occurred in the area where width measurement is not possible by LVDT (CW.R). For this reason, in Figures 5.12 and 5.13, for the C3 segment average value of the flexural crack width was obtained only by LVDT which was located at the right side. During flexural test, D4 specimen was loaded up to failure, and at the end of test period segment was broken into two pieces due to the lack of any reinforcements (see

Figure 5.14). For the others, load was applied with the consideration of SLS crack width. Although reaching failure load level was important for the determination of failure mode of segments, it could not be applied because of the safety reasons for both devices and humans. Nonetheless, the main purpose of test is measuring bearing capacity of different types within the serviceability limits. Apart from that during test of B2 huge crack occurred in different region where cracking could not be measured by LVDTs, after the first crack has occurred in the weakest section. This situation had an effect on the measuring values, especially for the cracking width. However, results are acceptable for the comparison because this occurred after the SLS cracking width. Therefore, vertical deflection of B2 and D4 segments is higher than others as reflected in the figures. Flexural cracking was measured to some extent for these specimens, as a result, permanent cracking values could not be determined after unloading situation (see Figure 5.12).

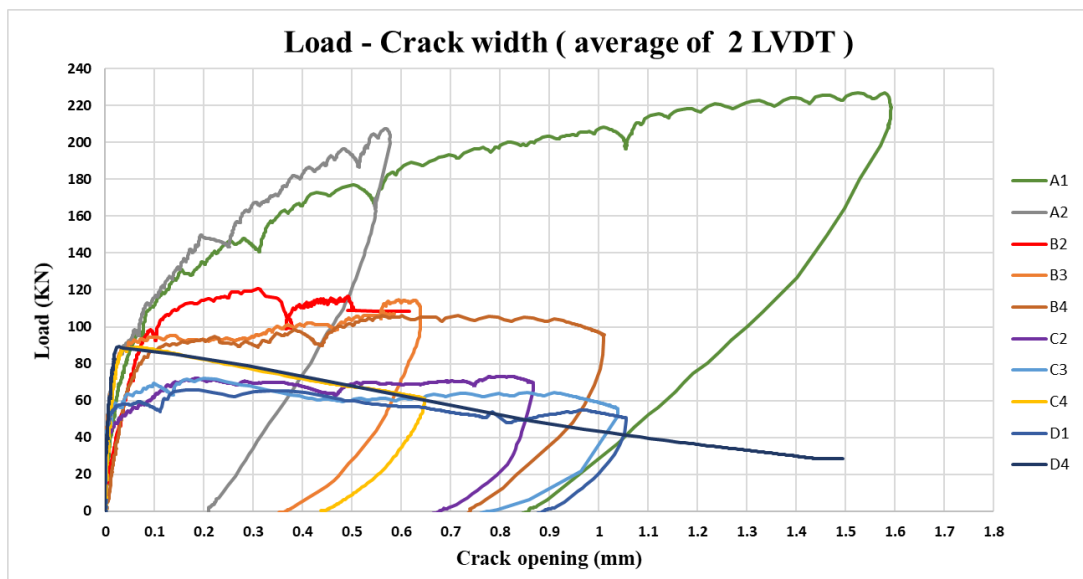


Figure 5.12. Load versus flexural crack width

Figure 5.12 shows load versus flexural cracking opening relationship, which were obtained by average values of 2 LVDTs that located on the left and right side of the segments, for all specimens. Table 5-2 illustrates the first flexural crack width which was measured by strain gauges and corresponding load level. Results of the

experiment based on first cracking values indicate that all segment types satisfy the minimum bearing capacity for Mecidiyeköy - Mahmutbey metro project. In the flexural test, as previously mentioned occurring moment on the segment was calculated according to the equation (7). The first cracking width of segments is very small compared to serviceability limit value. In addition, load versus cracking values up to allowable SLS crack width limit are shown in the figure 5.13 to evaluate the capacity easily. It should be noted that after first structural cracking, experimental bearing capacity of segments which was obtained at the serviceability limit also satisfies minimum criteria of the construction phase of the project. Moreover, Table 5-3 summarizes the load level of test specimens at the 0.3 mm cracking width which is defined as serviceability limit and corresponding moments and mid-span displacement values, while Table 5-4 illustrates the maximum load level of specimens that reached during experiments and corresponding moment and deflection values.

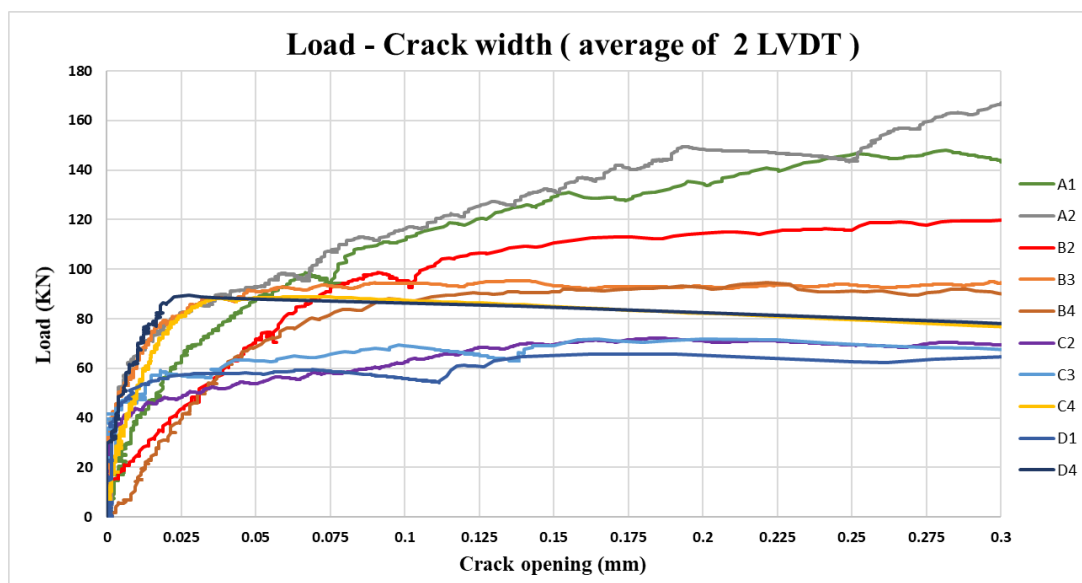


Figure 5.13. Load versus flexural crack width up to 0.3 mm

Table 5.2. First cracking width vs. corresponding loads, moments and deflection

Specimen types	RC		RC + PFRC		GFRP + PFRC	PFRC	
	A1	A2	B2	B4	C3	D1	D4
Load (kN)	77.23	85.20	69.87	68.16	67.79	58.60	85.93
First crack width (mm)	0.072	0.082	0.040	0.040	0.069	0.072	0.041
Moment (KN.m)	58.83	64.01	54.05	52.94	52.70	46.72	64.49
Mid-span deflection (mm)	0.80	0.90	0.74	0.70	1.00	0.80	0.93

The moment capacity of RC segments that were designed for metro project is quite higher than the design moment of the construction phases. Therefore, RC segments showed more durable and stiff behavior as expected due to the high value of longitudinal reinforcement. It should be noted that moment at serviceability cracking limit significantly greater than the design bending moment which is equal to 44.25 kN.m. The segment also showed a significant ductility with a gradual increase of bearing capacity up to serviceability limit. Ductility was determined by the ratio of deflection value that corresponding to occurred first structural cracking to deflection value at the serviceability crack width limit (0.3mm). For both RC specimens, the ductility ratio is approximately 4.0. The first cracking of RC specimens (A1 and A2) occurred at about 77 and 85 kN load levels, respectively. Corresponding moment values of these loads are nearly 59 and 64 kN.m. Bearing capacity of these segments at the serviceability limit measured as 1.74 and 1.83 times greater than the first cracking values. Moreover, the maximum bearing capacity of these segments measured at the maximum force resulted 2.66 and 2.24 times greater than the first cracking values. Apart from that, considered the final situation of the tunnel, these experimental results indicate that RC segments had stable post-cracking response under flexure, which is important for workers since this enables them to escape in case of exceptional events (ITA Report n. 16, 2016).

Table 5.3. Load and the corresponding moment at allowable SLS crack width limit (0.3 mm).

Specimen type	RC		RC + PFRC			GFRP + PFRC			PFRC	
	A1	A2	B2	B3	B4	C2	C3	C4	D1	D4
Load (kN)	143.91	166.60	119.89	95.51	90.47	69.50	68.16	76.61	64.72	78.70
Moment (kN.m)	102.17	116.92	86.56	70.71	67.44	53.81	52.94	58.43	50.70	59.79
Deflection (mm)	3.19	3.66	2.58	2.10	2.55	1.50	1.70	1.86	1.66	1.53

RC + PFRC hybrid segments that the combination of PP fibers with conventional reinforcements, showed also durable and stiff behavior under the flexure. The positive effect of macro-synthetic fibers was observed in RC + PFRC segments, especially in terms of deflections. Although a longitudinal reinforcement ratio was 40.6% smaller than RC ones, deflection values at the serviceability limit are much less. Moreover, bearing capacity of segments satisfy the design criteria of production and transient stages for both the first structural cracking occurred and the serviceability limit state. The first cracking of RC + PFRC specimens (B2 and B4) occurred at about 54 and 53 kN load levels, respectively. Bearing capacity of these segments at the serviceability limit resulted in 1.6 and 1.27 times greater than the first cracking values. It should be noticed that number of stirrups in segments affects the bending capacity after cracking occurred. For this reason, it has been observed that the experimental bending capacity of B4 specimen was lower than the other RC + PFRC segments because of less number of stirrups. As far as the maximum bearing capacity is considered, it can be observed that there was no significant increase in bending capacity after serviceability limit. In fact, RC + PFRC segments exhibited a hardening behavior under flexure after first cracking of concrete occurred, with multiple cracking (see Figure 5.15). Post-cracking stiffness of RC + PFRC segments has changed significantly, it showed high resistance up to a certain crack width. However, after cracking width reached the serviceability limit, the resistance level decreased dramatically (always remaining greater than cracking load) up to unloading time. When load levels between maximum and serviceability limit compared, it is seen that there is a slight increase in the specimens.

The ratio between these for the B2, B3 and B4 specimens are 1.01, 1.20 and 1.17 respectively. Based on the flexural test results RC + PFRC segment also showed a significant ductility. For the B2 and B4 specimens ductility ratio is nearly 3.49 and 3.64, respectively. These values are very close to RC segments although existence of conventional reinforcement's quantity is less.

Table 5.4. *Maximum load and the corresponding crack width and moment*

Specimen type	RC		RC + PFRC			GFRP + PFRC			PFRC	
	A1	A2	B2	B3	B4	C2	C3	C4	D1	D4
Maximum load (kN)	227.02	207.41	120.74	114.62	106.03	73.18	71.96	88.87	65.83	89.49
Crack width (mm)	1.525	0.569	0.312	0.628	0.716	0.742	0.200	0.065	0.162	0.049
Moment (KN.m)	156.20	143.45	87.11	83.14	77.55	56.20	55.41	66.40	51.42	66.80

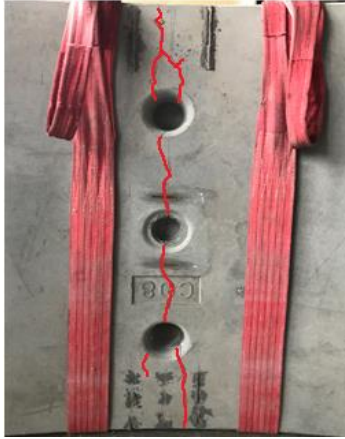
When another hybrid solution, GFPR + PFRC segments which consist of the combination of PP fibers with glass fiber reinforced polymer rebars, is taken into consideration, it was seen that the experimental results of this solution are below the expected design. Even though the bearing capacity of these segments satisfied the design bending moment criteria in both cases, they showed lower ductility under the flexure compared to previous specimens. The behavior of hybrid segments (GFRP + PFRC) is remarkably different from segments contains traditional reinforcement. The first recordable crack for C3 specimen was detected by strain gauge at a load level of 68 kN. Thereafter, the stiffness increased slightly up to 72 kN because of the stress transmitting along the cracks providing by fiber reinforcement. At this stage, specimen has reached the maximum bearing capacity that was calculated nearly 55 kN.m according to formula (7) and with 0.2 mm crack width. Afterwards, a softening branch was developed, and the resistance started dropping in a stable way and the critical crack continued to open. When the critical crack width reached the serviceability limit, 53 kN.m bending moment was measured on the segment. Similarly, during the experiment of C4 specimen, the same structural behavior was observed, but C2

specimen showed more ductile and stiff behavior compared to others. It reached the maximum load level that is nearly 73 kN after the serviceability limit, 0.3 mm. The crack with corresponding to maximum load is 0.71 mm and it is approximately 2.4 times higher than serviceability limit.

As far as the PFRC segments are concerned, it can be observed that similar scenario happened with the GFRP + PFRC specimens. PFRC segments exhibited a softening behavior under flexure due to the low quantity of PP fibers in the specimen. The first cracking of PFRC specimens (D1 and D4) occurred at about 59 and 89 kN load levels, respectively. Following this stage, the specimens reached maximum load levels at a crack width very close to the initial structural cracking values. According to these results, although the bearing capacity of PFRC segments fulfil the minimum requirement of design bending moment the ductility of the specimens was very low. Besides these, it was seen that the ratio between maximum loads and the loads at which first crack is formed showed, is very close each other and resulted in 1.12 and 1.04 respectively. PP fibers led to a partial increase of ductility after first structural cracking, and ductility ratios of the specimens are nearly 2.1 and 1.7. These results are very low compared to RC and RC + PFRC segments. In addition, the results demonstrated that RC + PFRC segments have a low energy absorption capacity.

Figure 5.14 shows final crack patterns which occurred on the inner surface of precast tunnel segments due to flexure. It should be considered that, maximum cracking widths cannot be seen in the figure since cracking width closes to some extent after unloading. Therefore, these pictures indicate the occurred permanent cracking pattern of segments. Similarly, Figure 5.15 demonstrates the crack localization on the side view of specimens and the multiple cracking that occurred in RC and RC + PFRC segments. It can be noted that multiple cracking occurred at the specimens that showed hardening behavior under the flexure, on the contrary single critical cracks occurred at the segments that exhibit a softening behavior (GFRP+PFRC and PFRC segments). Furthermore, as it is seen in the figure 5.14, almost the all specimens' cracking pattern

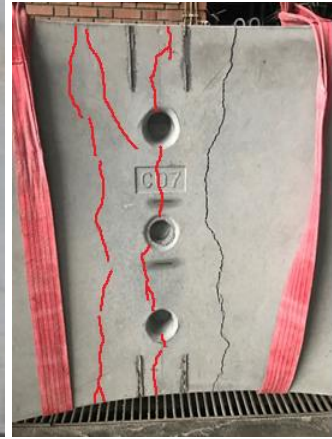
pass through the critical section that is the weakest region of segment due to existing of vacuum and longitudinal connectors holes.



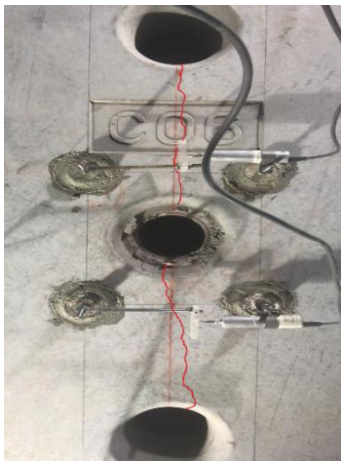
(A1)



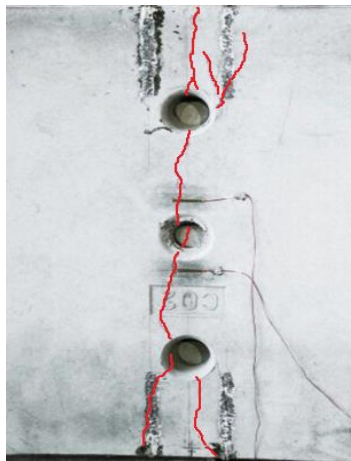
(A2)



(B2)



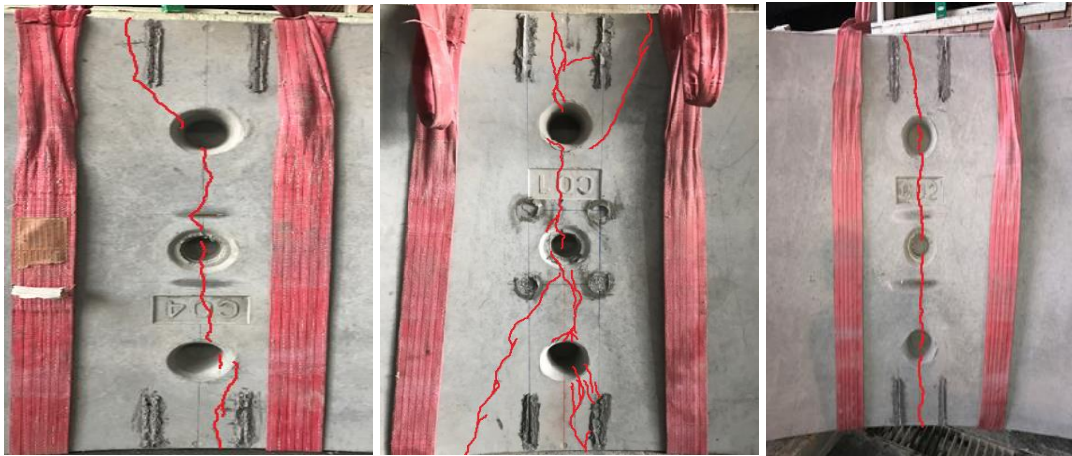
(B3)



(B4)



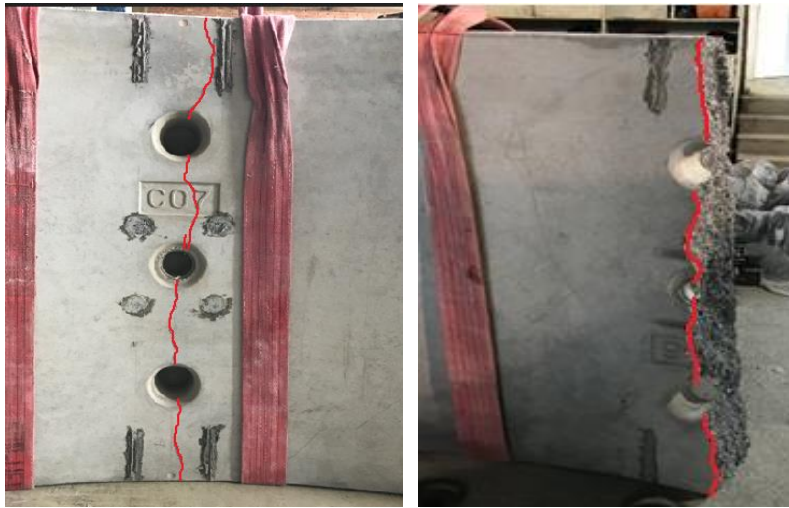
(C2)



(C3)

(C4)

(D1)



(D3)

(D4)

Figure 5.14. Final crack pattern of specimens (bottom view)



(A1)



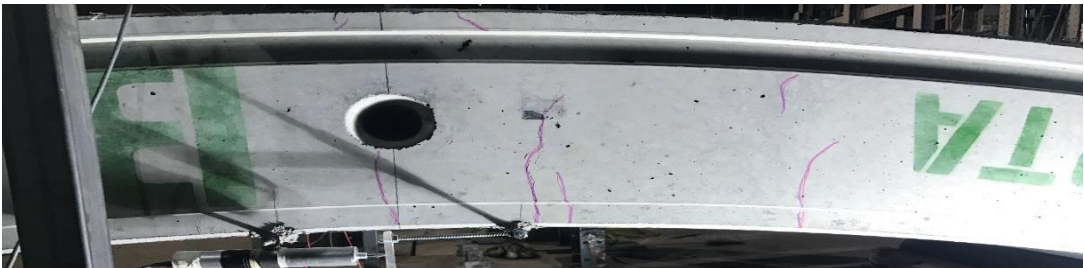
(A2)



(B2)



(B3)



(B4)



(C2)



(C3)



(C4)



(D1)



(D3)



(D4)

Figure 5.15. Final crack pattern of specimens (side view)

5.1.3. Creep tests

The main purpose of these studies is to obtain more information about the structural behavior of PFRC and GFRP + PFRC specimens and evaluate the ductility. Within this framework, cyclic loads were applied to the segments and related data were recorded by LVDTs located same region as previous flexural tests.

5.1.3.1. Cyclic Loading for PFRC specimen

As mentioned before, PFRC segments displayed less ductile behavior under the flexure and had reached maximum load levels before the cracking width arrives in serviceability limit. In addition to that in flexure tests, the loads applied in a short period by means of a hydraulic jack. This situation causes some obstacle for evaluation of the structural performance of segments exactly under the flexure. Since most of the time storage phase of the precast tunnel segments take about one year, structural verification of these segments under permanent load is needed. Therefore, 55 kN load level that create the design bending moment of production and transient stages of the project, was applied on the D3 specimen for evaluation.

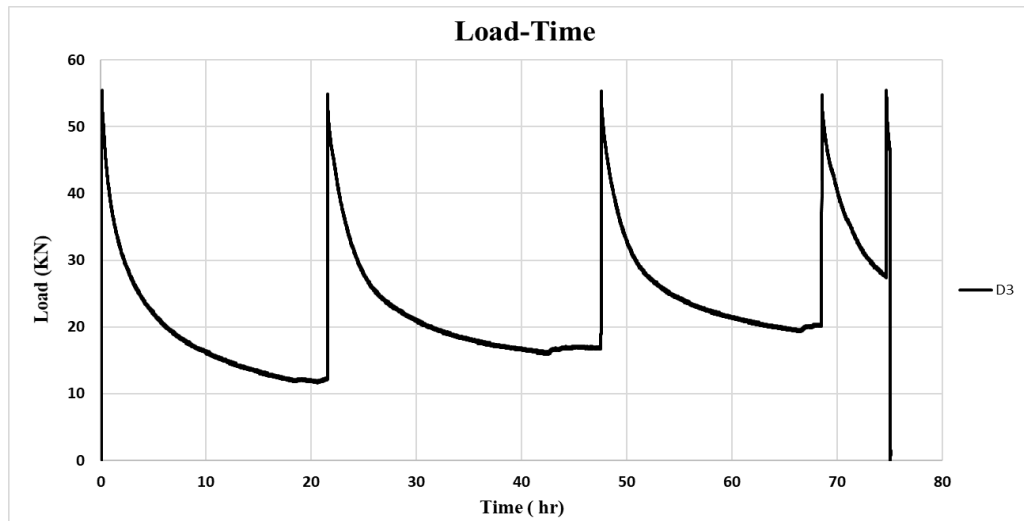


Figure 5.16. Load versus time graph of D3 specimen

When the load level reached 55 kN the valves have been closed to prevent decreases of load level and keep the pressure constant. However, as it is seen in Figure 5.16, applied load level decreased as the time passed. It is estimated that this decline is caused by the deflections of specimens. Another reason might be the leakage in hydraulic jack. For this reason, when the load level decreased, and it remained almost constant at a certain level, the load increased again up to 55 kN. This implementation was repeated five times until the flexural cracking width arrived in serviceability limit. In this way, specimen was subjected to cyclic load.

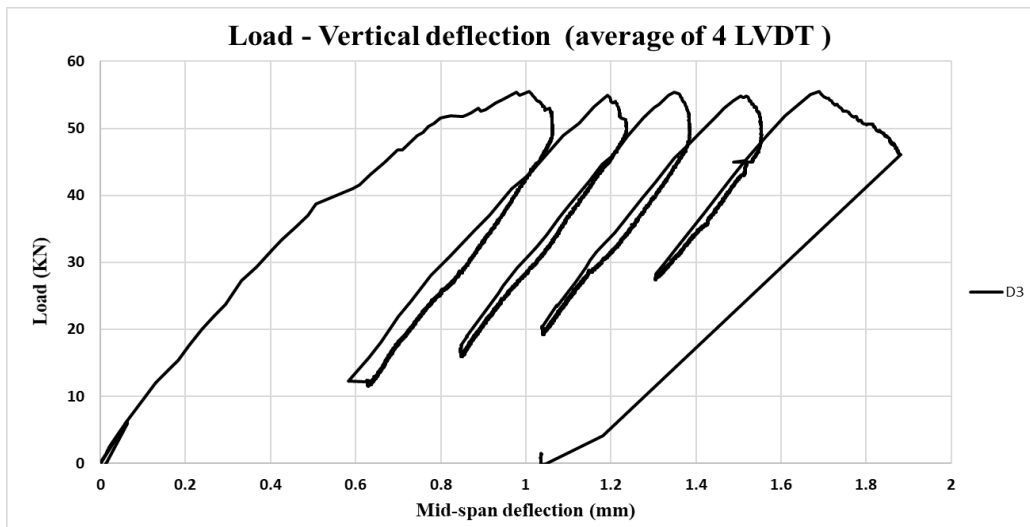


Figure 5.17. Load vs. mid-span displacement curve

Figure 5.17 shows the load versus vertical mid-span displacement curve that is obtained by average of four LVDTs. For the first cycle deflection was recorded just above the 1 mm and it came back to nearly 0.6 mm at the end of first decreasing. For the others, differences between final and initial deflection values are approximately 0.2 mm. In other words, energy absorption capacity of the first cycle is higher than the other that capacities are almost same. It should be noted that each time stabilization load level increased to some extent compared to previous cyclic (see Figure 5.16).

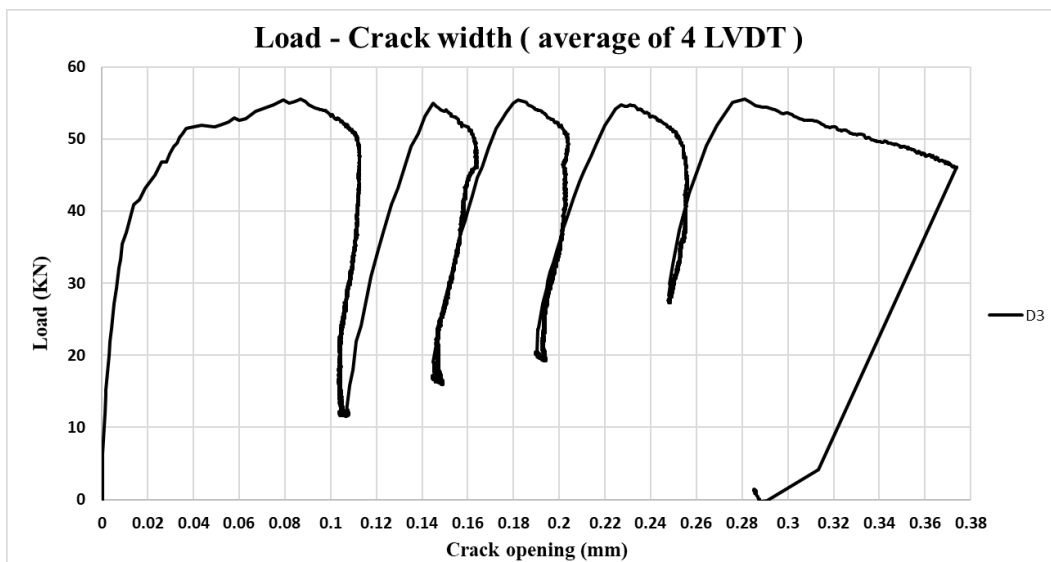


Figure 5.18. Load vs. flexural crack width of D3 specimen

Figure 5.18 shows load versus flexural cracking opening, which were obtained by average values of 4 LVDTs that located on the middle, left and right side of the specimen. As it is seen in the figure, after first loading flexural cracking width reached around the 0.1 mm, and cracking width arrived in serviceability limit at the end of the fifth loading. Load versus horizontal displacement curves of D3 specimen were given in the following figures. Figure 5.19 was obtained by LVTD located on right side, while figure 5.20 obtained by LVDT on the left side of segment. In the flexure test of FPRC segment, single crack occurred around the mid-span portion of segment and then it continued to opening up to failure, without any other cracking were observed. This is a typical pure concrete behavior. According to ITA report n.16 (2016) this phenomenon is explained as “Fiber reinforced concretes typically used in tunnel linings present a post-cracking softening behavior, which means that generally, they tend to localize cracking phenomena occurring in a certain region in a single crack”.

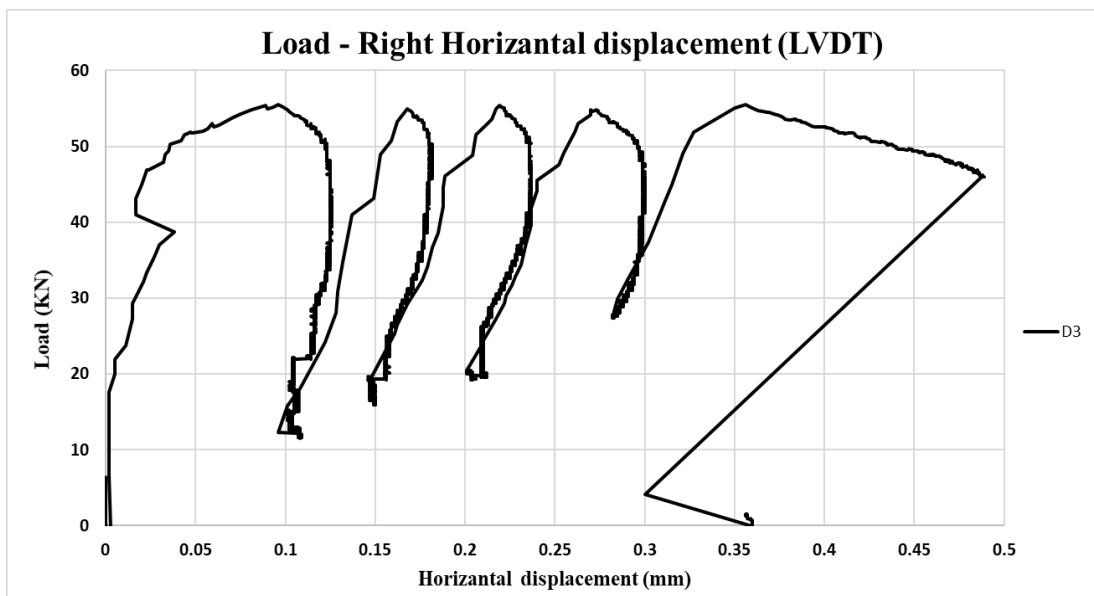


Figure 5.19. Load vs. horizontal displacement curve of D3 specimen-right

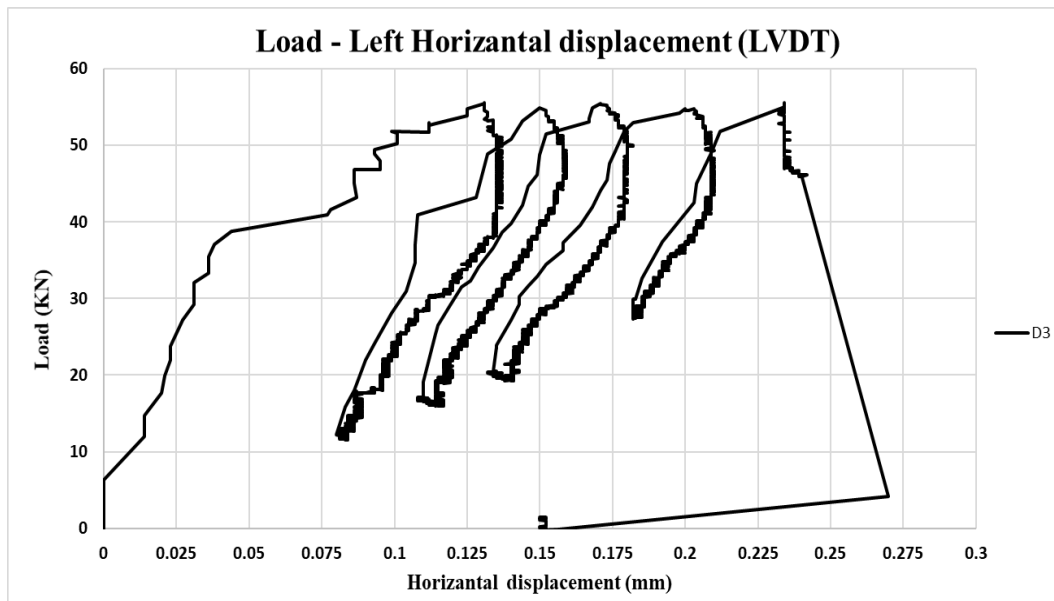


Figure 5.20. Load vs. horizontal displacement curve of D3 specimen-left

5.1.3.2. Cycling Loading for GFRP+ PFRC specimen

Similarly, a hybrid solution, which is the combination of glass fiber reinforced polymer rebars with PP fibers, displays a low ductile behavior and had reached maximum load levels before the cracking width arrive in serviceability limit except the C2 specimen. It is estimated that having lower bearing capacity is caused by the bond problem between GFRP bars and concrete. Although curvilinear GFRP bars should be used in production, straight GFRP bars came to the site and used in specimen by trying to bend them. Since the experimental results of these segments were lower than as expected design values, drilling core sample was taken from a tested specimen. It was thought that some cracks can occur on the surface of GFRP because the GFRP bars are too brittle materials and have a low shear capacity. However, it is seen that there was no damage on the rebar and specimens acted as an only fiber reinforced concrete. In addition, after first structural cracking the resistance started dropping in a stable way and the critical crack continued to open and no more cracks developed. This situation indicates that there is a bonding problem between GFRP bars and FRC. Shortly GFRP+ PFRC segments exhibited a softening behavior under flexure after first cracking of concrete occurred.

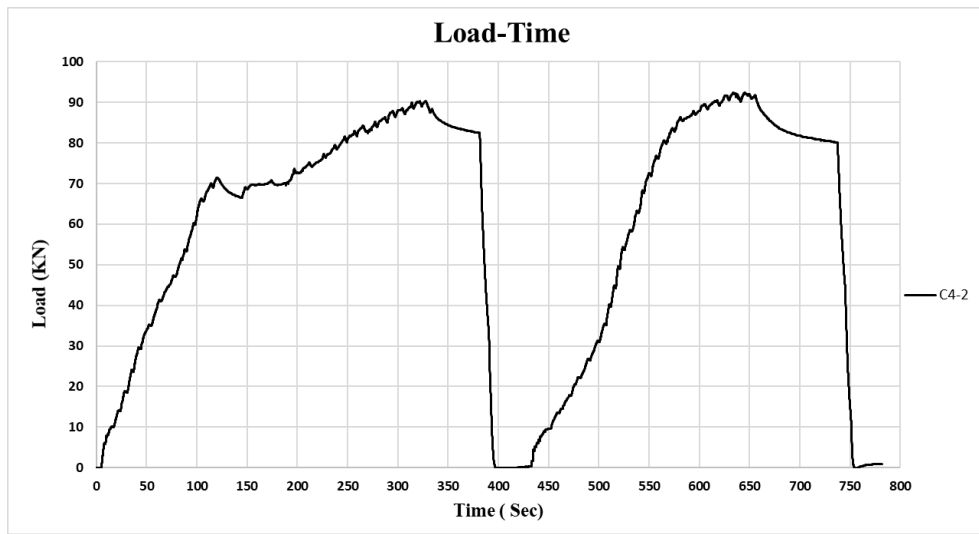


Figure 5.21. Load vs. time graph of C4 specimen

As mentioned before, loads were not applied up to specimens' failure level in these experiments, flexural tests were stopped after crack width reaches the SLS limit. Thus, to obtain more information about structural behavior of specimen, specimen C4 was subjected to the loading pattern shown in Figure 5.21. Contrary to previous experiments, results of this experiment were very different. It exhibited hardening behavior under the flexure and multiple cracking observed on the specimen. Final cracking patterns of C4 specimens were shown in Figures 5.23 and 5.24. Moreover, load versus vertical displacement curve of mid-span is given in Figure 5.22.

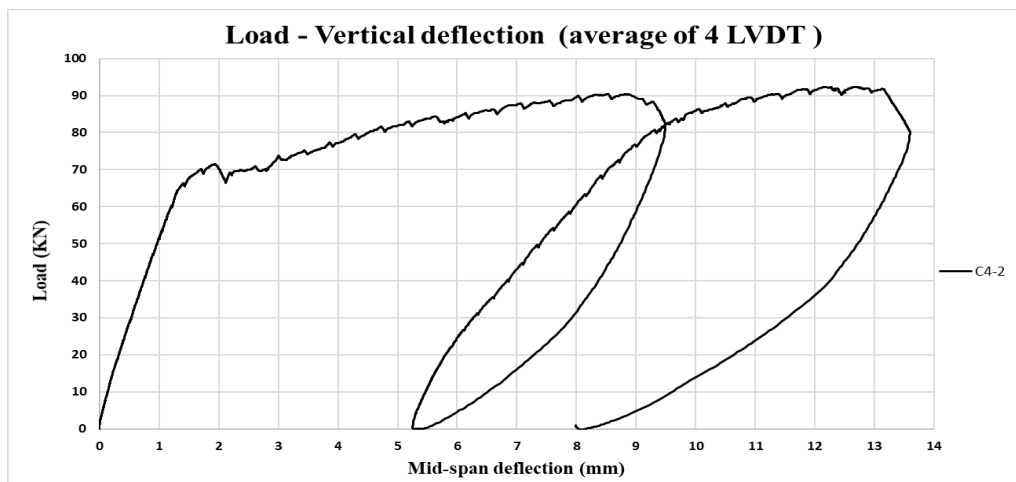


Figure 5.22. Load vs. mid-span deflection curve of C4 specimen



Figure 5.23. Final crack pattern of C4 specimen (right side)

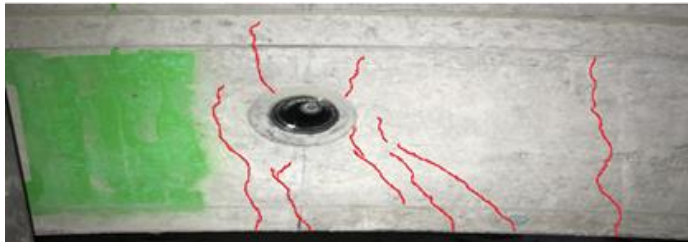


Figure 5.24. Final crack pattern of C4 specimen (left side)

5.2. Point Load Test

The main purpose of this test is to evaluate the structural performance of precast tunnel segments subjected to the Tunnel Boring Machine (TBM) actions during the excavation process. TBM is pushed itself forward by thrust jacks which are acting on the last placed lining ring. Even though the applying forces on the tunnel lining, which is induced by TBM thrust, is a temporary loading condition for construction stages, this causes serious stresses on precast tunnel segments. Therefore, it must be properly considered since this may be the most critical condition for the segment design (Meda et al 2016). For that reason, point load tests were conducted to the namely designed segments. As it is seen in Figure 5.25, in the excavation process and in this test, two important local tensile stresses which arise during the TBM jacks thrust effect in precast tunnel segments were observed. The application of the high concentrated TBM thrust load on relatively small surfaces causes splitting stresses or bursting stresses on a plane perpendicular to the direction of the applied thrust. The other one is known as spalling stresses that they appear in the unloaded zone between the TBM rams in the circumferential direction. Similarly, in this test allowable serviceability limit state for

the occurred cracking width was considered to evaluate the structural performance of specimens. In addition, vertical displacements of segments and cracking pattern was also considered.

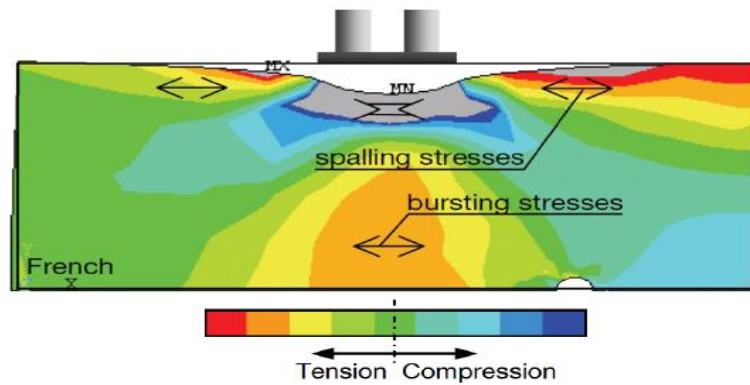


Figure 5.25. Local tensile stresses due to applied high concentrated load (Bakhshi, 2015)

5.2.1. Test Set-up and Instrumentation of Point Load Test

In Mecidiyeköy - Mahmutbey metro project, Terratec S-42 which is an earth pressure balanced (EPB) type of tunnel boring machine has been used for the construction of tunnel. Therefore, in this experiment, loading systems were adapted to reflect the actual TBM thrust loading in order to evaluate the structural performance of precast tunnel segments better. During the excavation, totally sixteen jacks apply load to the tunnel lining, and they have a 22.5 degree distance between each of them due to tunnel geometry. In other words, three jacks are located in every segment except for key segment (A), that loaded through only one jack because of the being small. Table 5-5 summarizes the general features of Terratec S-42 machine and according to these information, TBM jack configurations on the segment C was simulated in Figure 5.26. In order to perform full-scale test simulating the actual condition, a suitable testing system has been designed and constructed regarding to both actual pad configuration on the segment C and geometry used by the Terratec S-42.

Table 5.5. Features of TBM

Manufacturer	Terratec S-42
TBM type	EPB
Exceptional thrust force	40000kN
Number of jacks	16
Maximum jack force	2500kN
Shoes dimensions [cm]	(71-82)w x 34h

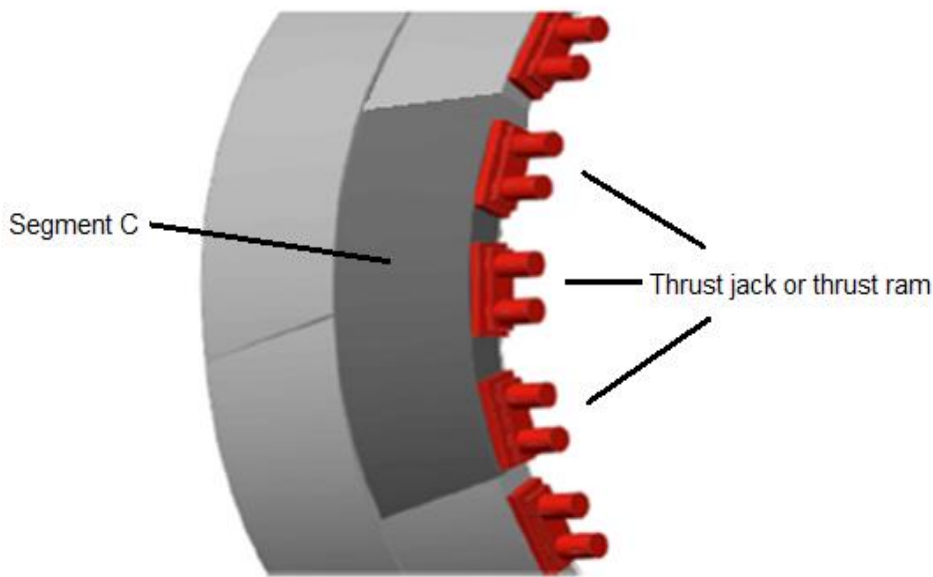


Figure 5.26. TBM jack configurations (adopted from Meda, 2016)

Within this framework, a rigid steel system, which close ring frame made with HEB 300 steel beams and 52 mm diameter stem bars (see Figure 5.27), were designed for equal load distribution of 3 pads. As it is seen in Figure 5.27, steel beams were strengthened with stiffener and they were welded side by side. In this experiment, irregularities that can occur during the segment placement in the ring, has not considered. Therefore, tunnel segments were placed on a stiff steel base that having a continuous support. In the adopted configuration of Terratec S-42 on the Mecidiyeköy - Mahmutbey metro project, it is able to apply 2500 kN load on a single pad in exceptional cases i.e., it is its maximum capacity. Since three pads are placed on

segment C, the maximum total load capacity is equal to 7500 kN. In the view of these information, six hydraulic jacks that having a load capacity of 1500 kN each were inserted in the closing rigid ring frame. These hydraulic jacks were located between steel pads and frame (see Figure 5.29). In the experimental set-up, two hydraulic jacks were acted on every steel pads, which were produced exactly the same dimensions as the real one. The locations of pads on the segment surface and dimensions of pads are demonstrated in Figure 5.28. In addition below the steel pads rubber layer was used in order to provide full contact between precast segment and steel plate. Applied loads on the specimens were measured by means of pressure transducers (transmitters) that were located at the every hydraulic jacks and main distribution at output of hydraulic pump. Totally seven digital pressure transducers have been used in the system and all the data were continuously recorded by an acquiring digital system and transmitted to a computer during experiments. Moreover, check valves have been used to maintain a constant value of the oil pressure in the circuits. However, this is not able to prevent decreasing applied load level to some extent. Aforementioned information are shown in the figure 5.31.

In order to measure cracking width due to local tensile stresses that caused by high compression load, linear variable differential transformers (LVDTs) were placed on the specimen surfaces. Two LVDTs (H1-T, H2-T) were located on the top sides of segment between loading pads to record the spalling crack width. Similarly, another two LVDTs (H1-I, H2-I) were located on the inner surface of segment between loading pads. One LVDT (H3-I) was also placed under the middle loading pad near the vacuum hole to measure splitting crack width.

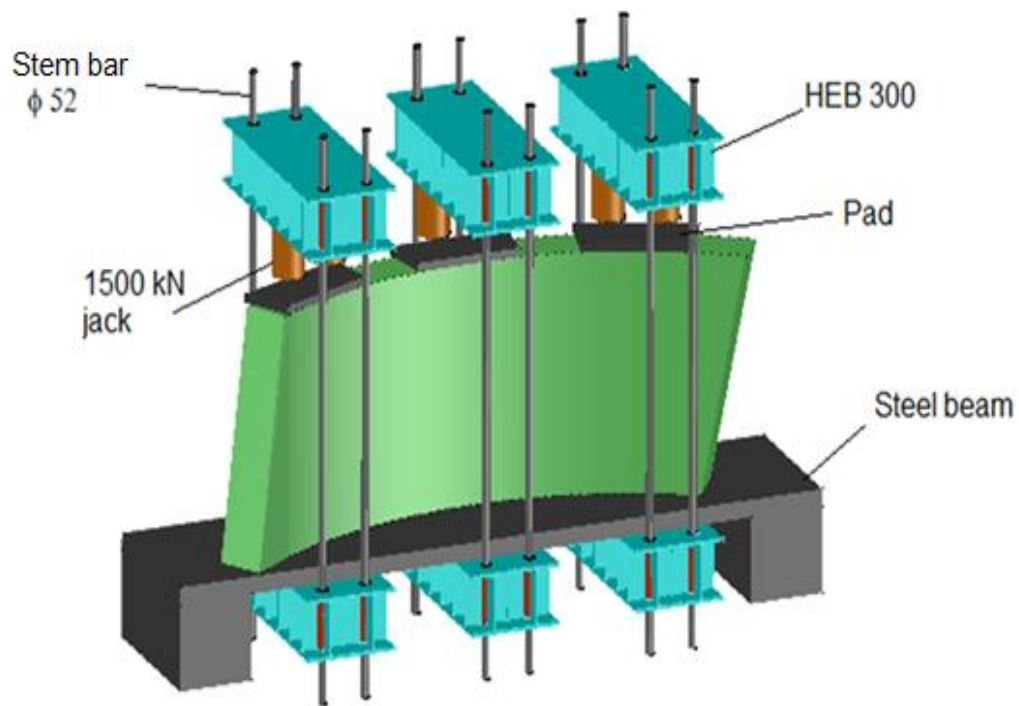
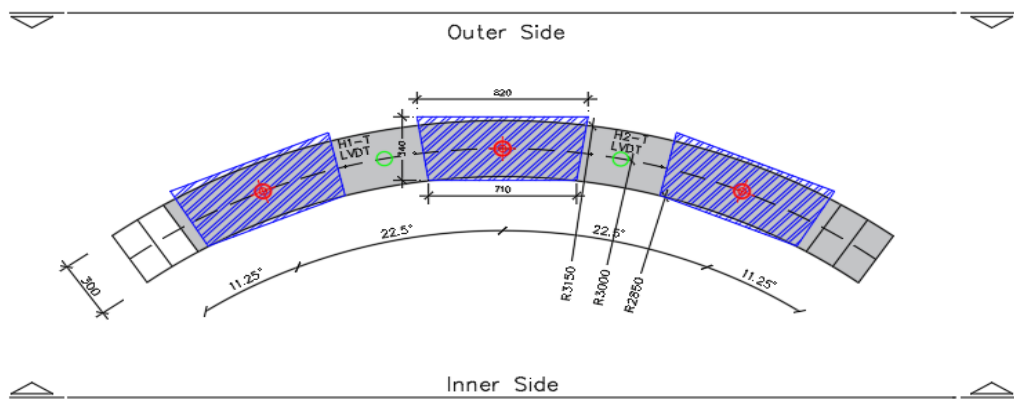
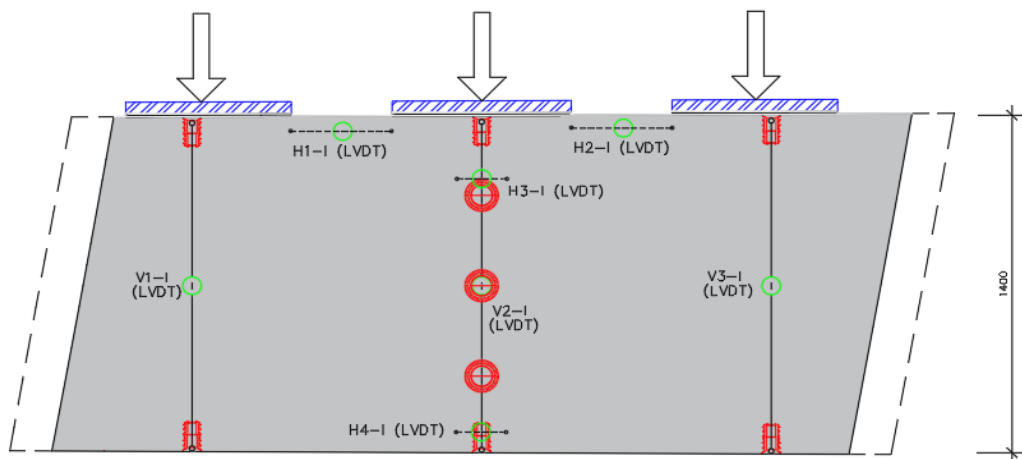


Figure 5.27. Point load testing system

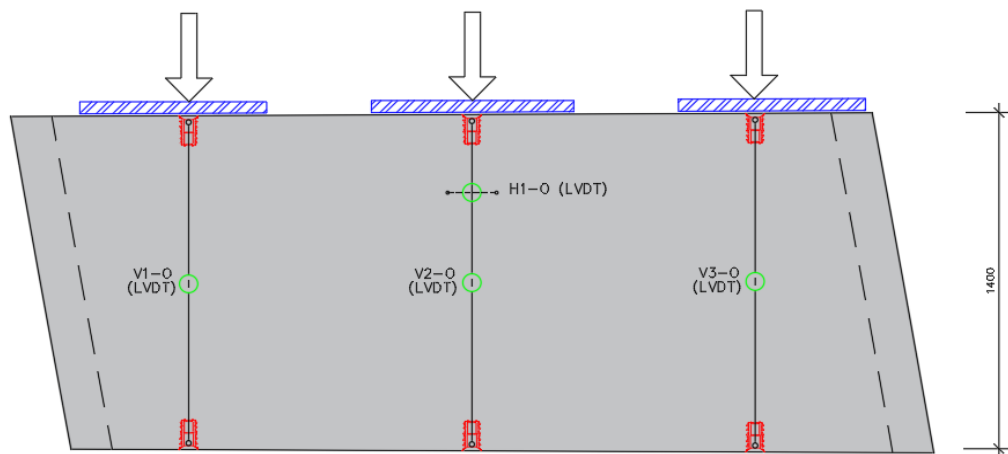
Moreover, two LVDTs (H4-I, H1-O) were inserted at predicted regions where cracking may be occurred. Apart from that, totally six LVDTs (V1-I, V2-I, V3-I, V1-O, V2-O, V3-O) were placed on both outer and inner surface of segments to measure the vertical shortening of specimens under the loading plates. The locations of instruments on segments and details of full-scale point load test are shown in Figures 5.28 to 5.33.



Top view of specimen



Inner surface view of specimen



Outer surface view of specimen

Figure 5.28. Instrumentation details of point load test (units mm, not to scale).

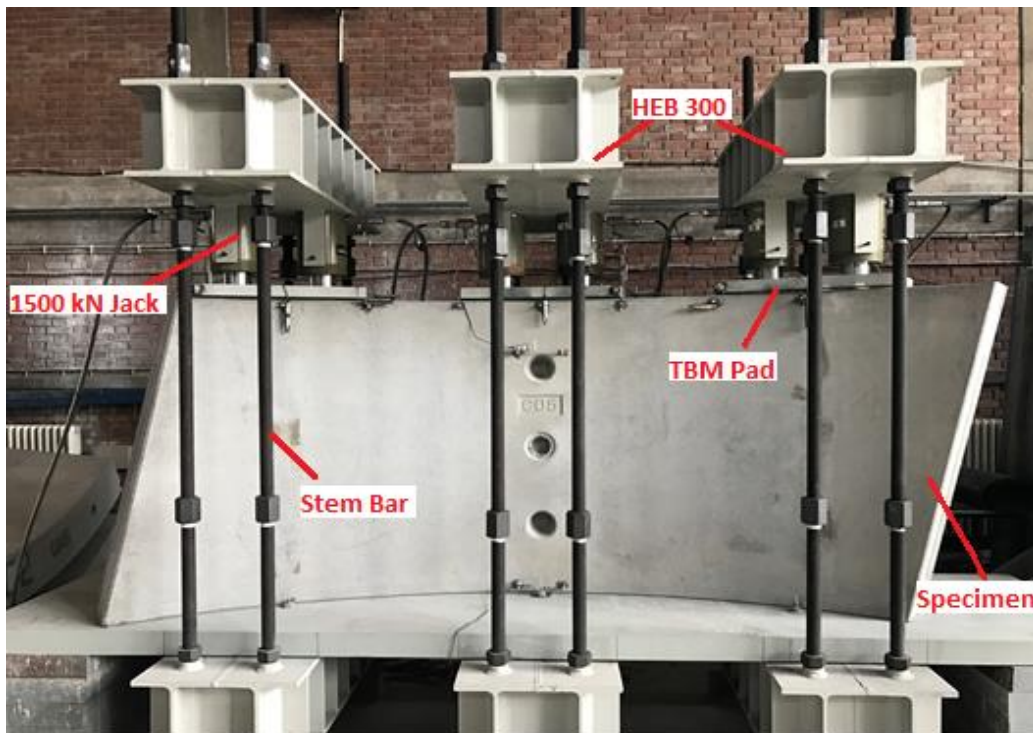


Figure 5.29. Point load test set-up and loading systems



Figure 5.30. Outer surface of test specimen



Figure 5.31. Point load test set-up and instrumentation details (1)



Figure 5.32. Point load test set-up and instrumentation details (2)



Figure 5.33. Point load test set-up and instrumentation details (3)

5.2.2. Experimental Results of Point Load Test

In this experiment, loads were applied by means of hydraulic pump without any displacement control. Similar to previous experiment, although it was paid attention to applying load rate as close as possible in each experiments, loading rate showed slightly differences between specimens. Figure 5.34 illustrates the total applied load by six hydraulic jacks versus time graph of full-scale point load test. As it is seen in Figure 5.34, loads were applied higher than maximum TBM thrust force for all specimens. In other words, the applied load level is more than 2500 kN for all pads.

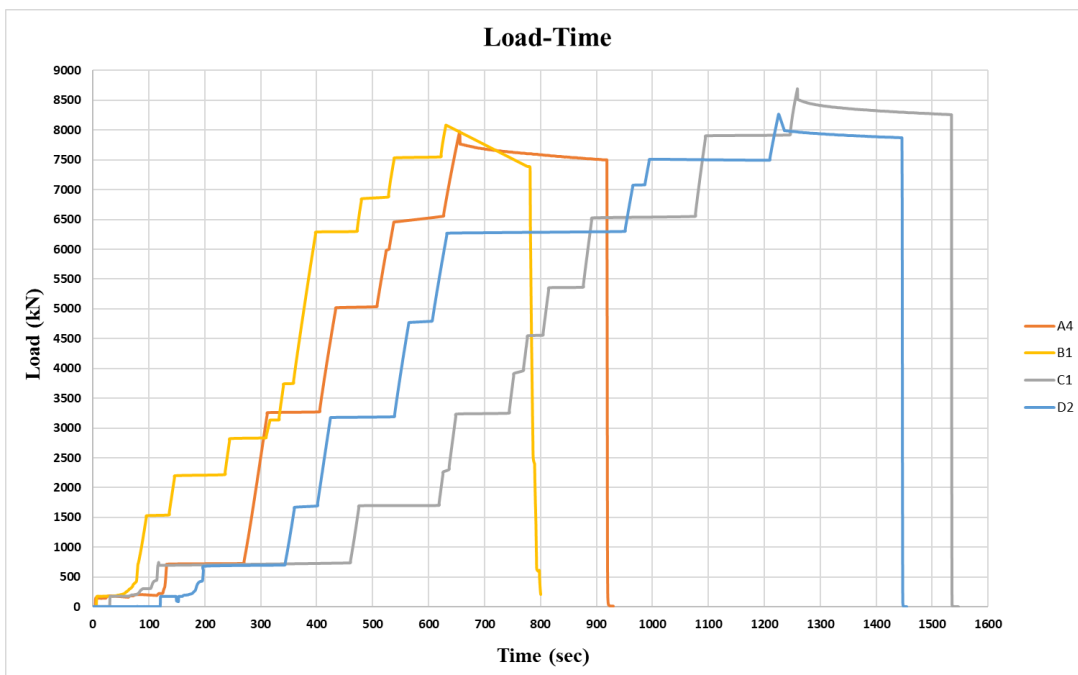


Figure 5.34. Load vs. time graph of point load tests

As it was previously mentioned, a total of 4 LVDTs were inserted on tunnel segments' surfaces to measure crack opening due to spalling stresses. Figure 5.35 shows the applied load level versus spalling cracking opening values, which they were obtained from H1-I, in terms of mm. In a similar manner, measured spalling cracking width values from H1-T are shown in Figure 5.36.

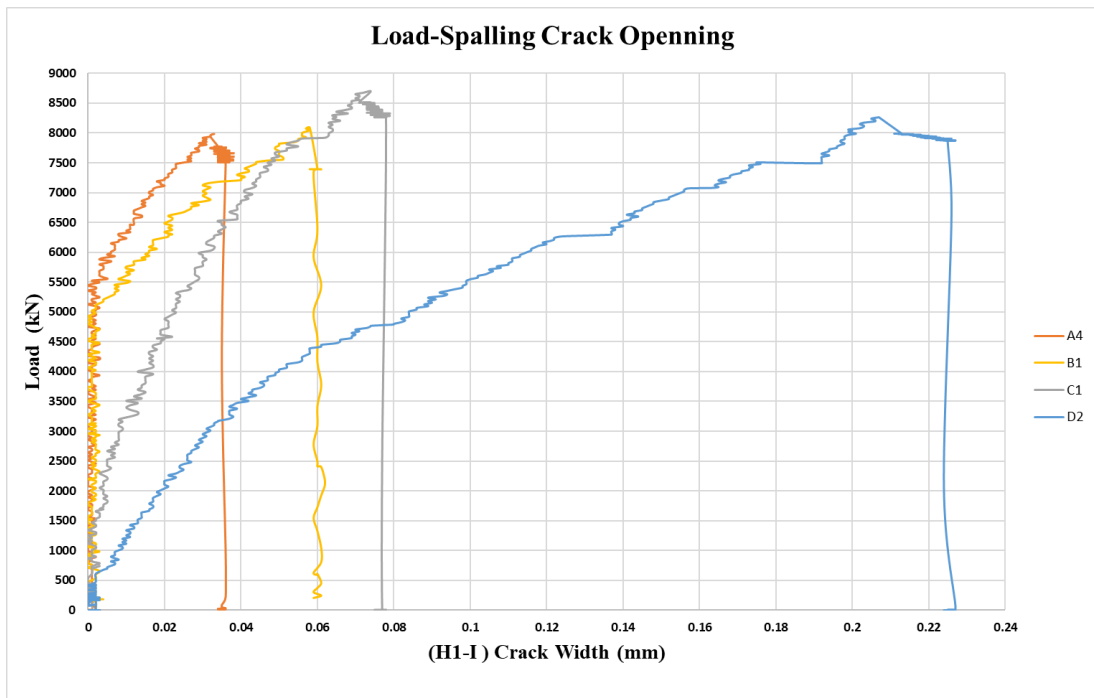


Figure 5.35. Load vs. spalling cracking width (H1-I)

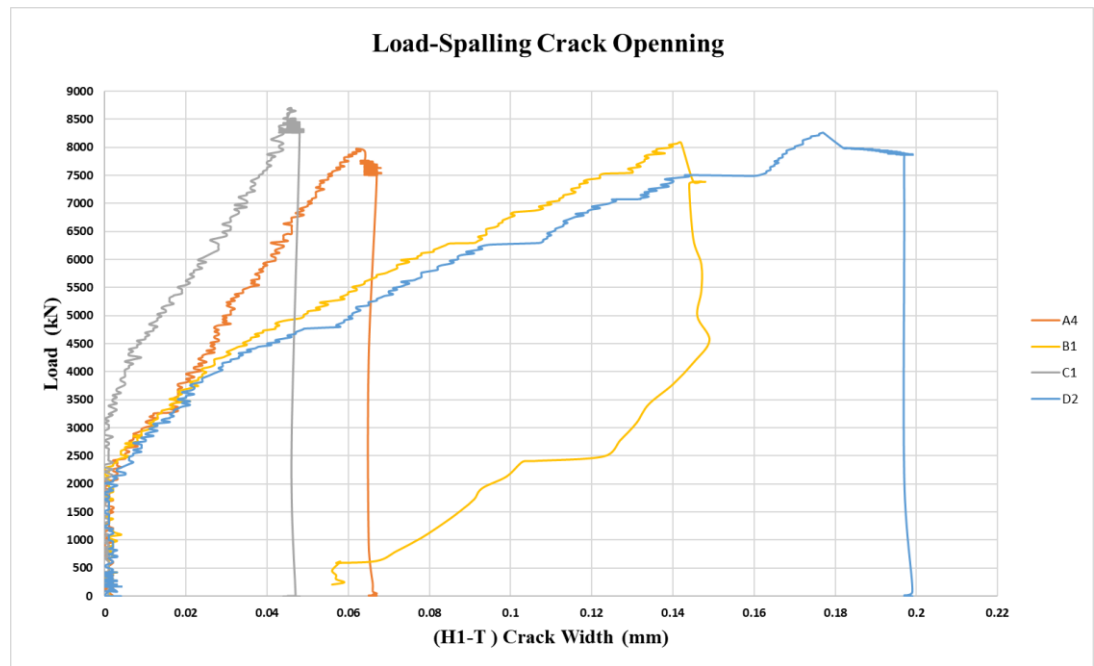


Figure 5.36. Load vs. spalling cracking width (H1-T)

These graphs indicate that all types of segments satisfy the serviceability crack limit under the maximum thrust forces. Even though results show a slightly differences between the top and inner surface, all the crack widths are less than 0.3 mm. However, it should be noted that PFRC segment has a lower resistance to spalling stresses compared to other types of segments. As it is seen, the cracking values at the highest load level are around the 0.2 mm for PFRC segment. The reason for that there is no any reinforcement rebar in the corresponding regions where the local stresses are high. Also it may be caused by the low amount of fiber content present in the PFRC segments ($V_f = 0.66\%$). In addition to PFRC, RC + PFRC segments also displayed lower durability against to thrust forces. Spalling cracking width was nearly 0.14 mm under the maximum thrust (see figure 5.36). For RC and GFRP + PFRC segments cracking widths were lower than 0.08 mm. Moreover, when the first concrete cracking values of segments are concerned, graphs display a different trend. According to Figure 5.36, first crack on the top surface of all segments has occurred almost at the same load level except for GFRP + PFRC segment, the first crack occurs at a load level higher than others. While the inner surface is considered, load level of single pad corresponding to occurred first cracking for RC and RC + PFRC segments were nearly 1700 kN and 1830 kN, respectively. Nonetheless, the values for both PFRC and GFRP + PFRC were considerably lower (see figure 5.35). Apart from that, after completing the test permanent crack width could not be recorded properly due to fast unloading of the specimen. It can be clearly seen that crack in the RC + PFRC segment closed to some extent when the load level decreased, as expected, since its unloading time took a long time compared the others. As a result of this situation, elastic deformation of concrete could not determine appropriately.

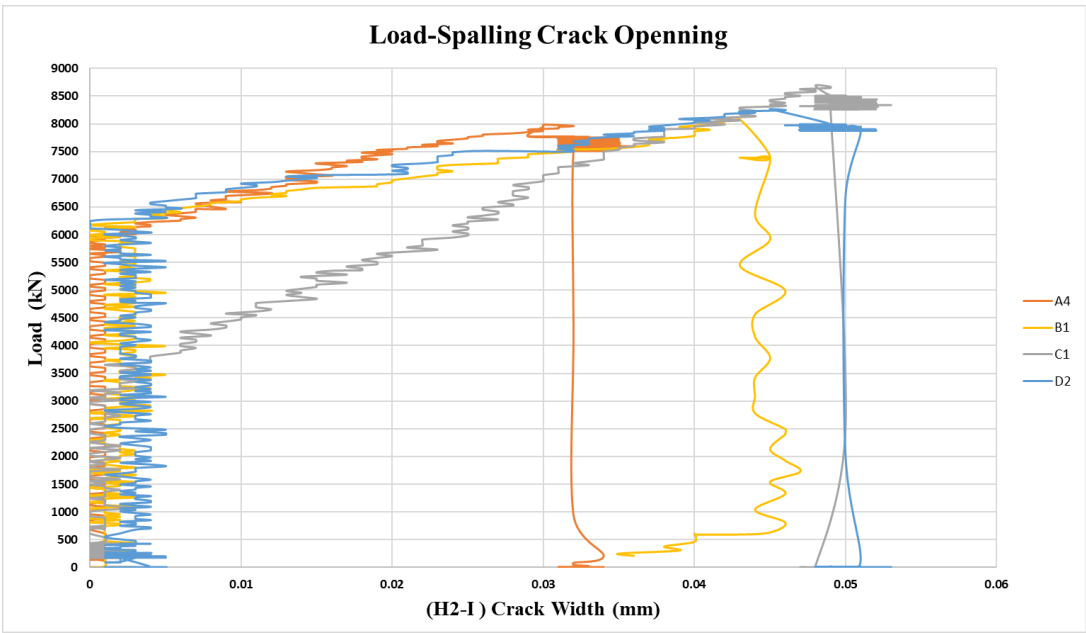


Figure 5.37. Load vs. spalling cracking width (H2-I)

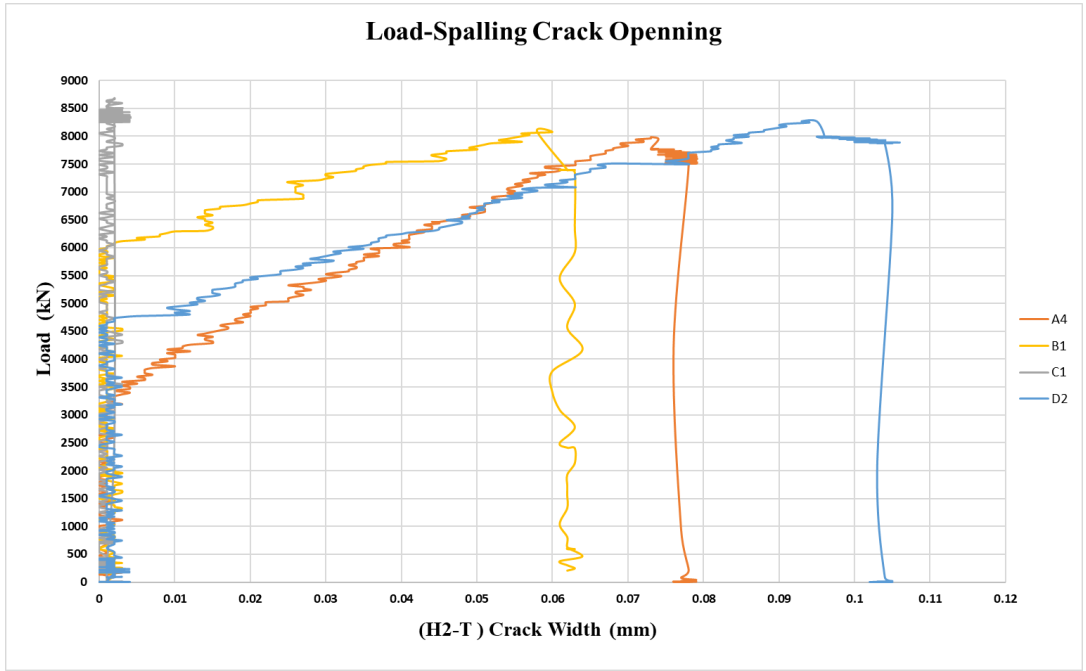


Figure 5.38. Load vs. spalling cracking width (H2-T)

Figure 5.37 shows the applied load level versus spalling cracking width on the inner surface while cracking width that occurred on the top surface of specimens are shown in Figure 5.38. As it is seen, cracking results, which were measured by H2-I and H2-T, display huge differences compared to previous ones. In other words, cracking values are considerably smaller than the recorded by H1-I and H1-T. The situation may be caused by having a rhomboidal geometry of precast tunnel segments. Furthermore, it should be noticed that H2-T were not able to measure cracking values on the top surface of the C1 specimen. However, there was no any permanent crack observed at this region after the point load test completed.

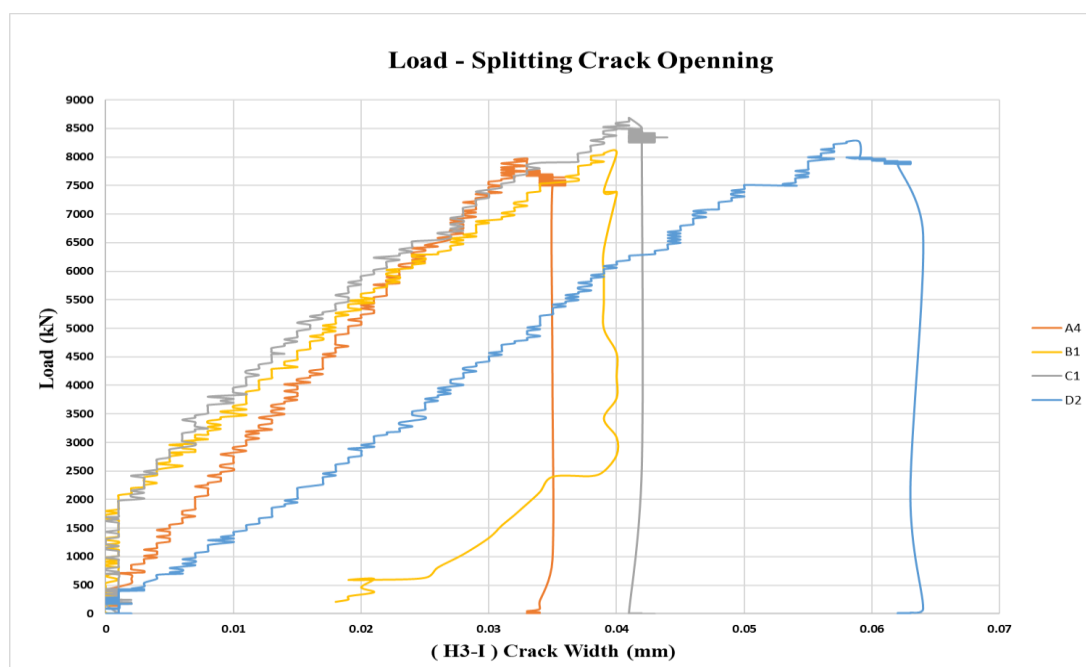


Figure 5.39. Load vs. splitting cracking width (H3-I)

As it was mentioned earlier, one LVDT was used during point load test to measure the splitting cracking. Since the presence of the vacuum hole at mid portion of segments, it was predicted that this region is the weakest section for the splitting stresses. Figure 5.39 shows the applied load versus splitting or bursting cracking curve measured by LVDT (H3-I) that was located below the middle loading shoe. According to this graph, all type of segments showed a durable behavior under the maximum thrust force.

Considering the allowable serviceability limit state, splitting cracking values of segments are very insignificant and they are smaller than 0.07 mm width.

The results of point load tests in terms of thrust load versus vertical displacement are shown in Figures 5.40 to 5.42. These results indicate that shortening values of mid portion are smaller than the others that measured by LVDTs located near the corners. As previously mentioned, elastic and plastic deformations of segments could not be measured, however, these results are applicable to evaluate the vertical displacements values under the maximum thrust force. Final values consist of the summations of plastic and elastic displacements, except for RC + PFRC segments. The reason for that, RC + PFRC segment shows some elastic displacement during the unloading period. The main inference from these graphs presence of fibers in concrete affects the vertical shortening values. Since fibers increase the compression capacity of concrete, the shortening values of RC segments are higher compared to others. Furthermore, it should be considered that there were some rotations occurred on the segments during the tests since the outer and inner results display differences (see Appendix B). Apart from that, high displacement results at the low load levels may be caused by the deflections of rubbers that were located under the loading shoes or between the steel beams. Therefore, results measured by LVDTs are not exactly correct because of corresponding references points of LVDTs.

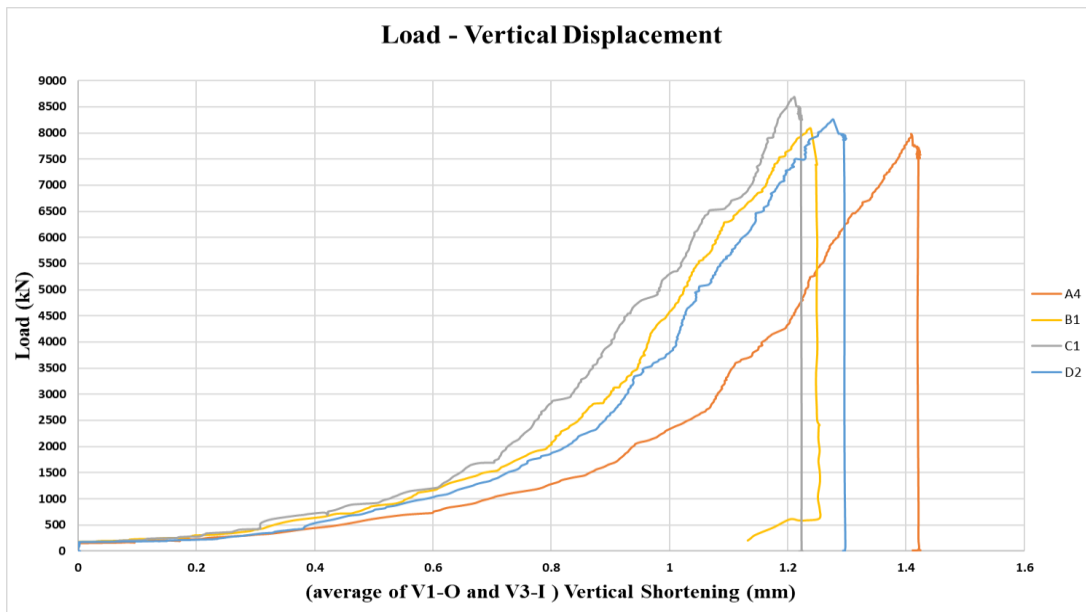


Figure 5.40. Load vs. average of vertical displacement curve (V1-O and V3-I)

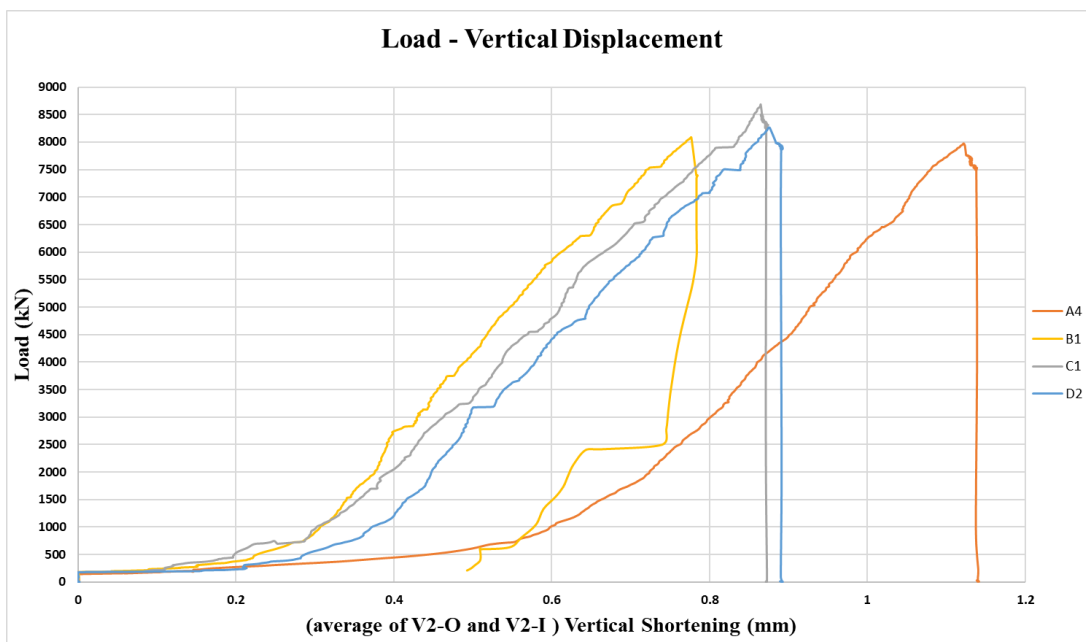


Figure 5.41. Load vs. average of vertical displacement curve (V2-O and V2-I)

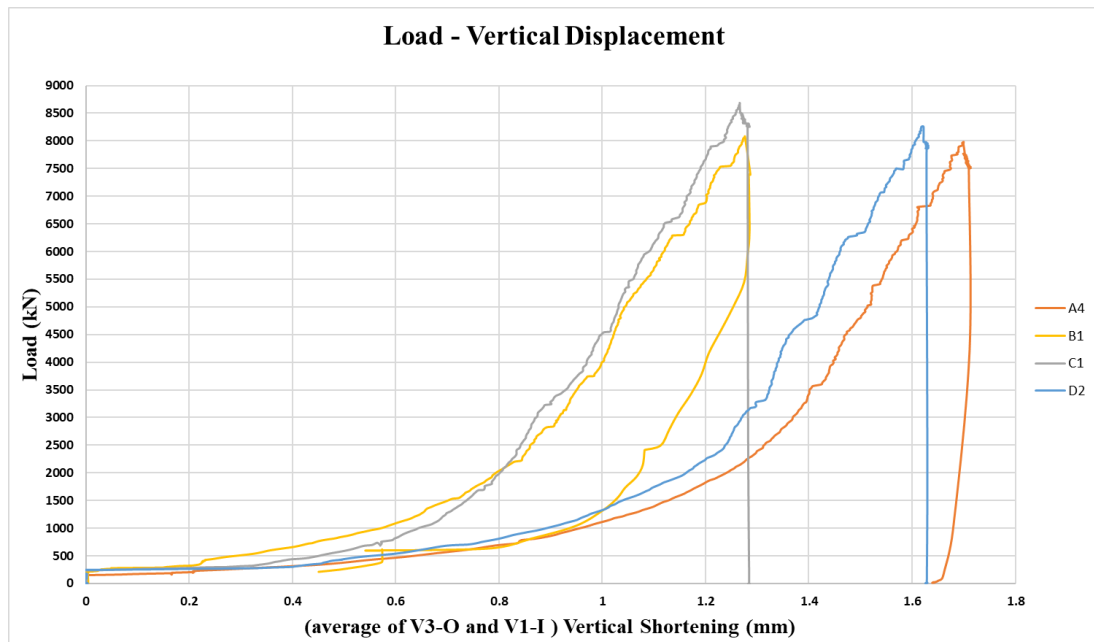


Figure 5.42. Load vs. average of vertical displacement curve (V3-O and V1-I)

Considering the results of PRFC segment, first cracks have occurred between the loading pads. Thereafter, with the increasing load, cracking depth has extended along the segment width. Figure 5.43 illustrates the crack pattern and crack depth of PFRC segment (D2) after the point load test carried out. Furthermore, marked colors on the segment surface represent the occurred cracks during experiment, and corresponding load levels are shown in Figure 5.43. These marked cracks also known as spalling cracks, which generally occurs between the loading areas due to thrust forces. As it is seen in Figure 5.43, no cracks were observed in this test, caused by splitting or bursting stresses. In other words, no multiple cracking was observed during test. It can also be noticed that the absence of reinforcement rebar in the segment led to higher values of spalling cracks compared to others. In addition to this, the low amount of PP fibers in the concrete ($V_f = 0.66\%$) causes to having low post-cracking tensile strength. Hence, around 830 ton load, the maximum spalling crack was measured as 0.22 mm at a depth equal to 371 mm. However, it should not be overlooked that the capacity of PFRC segment is sufficient for the allowable SLS limit.

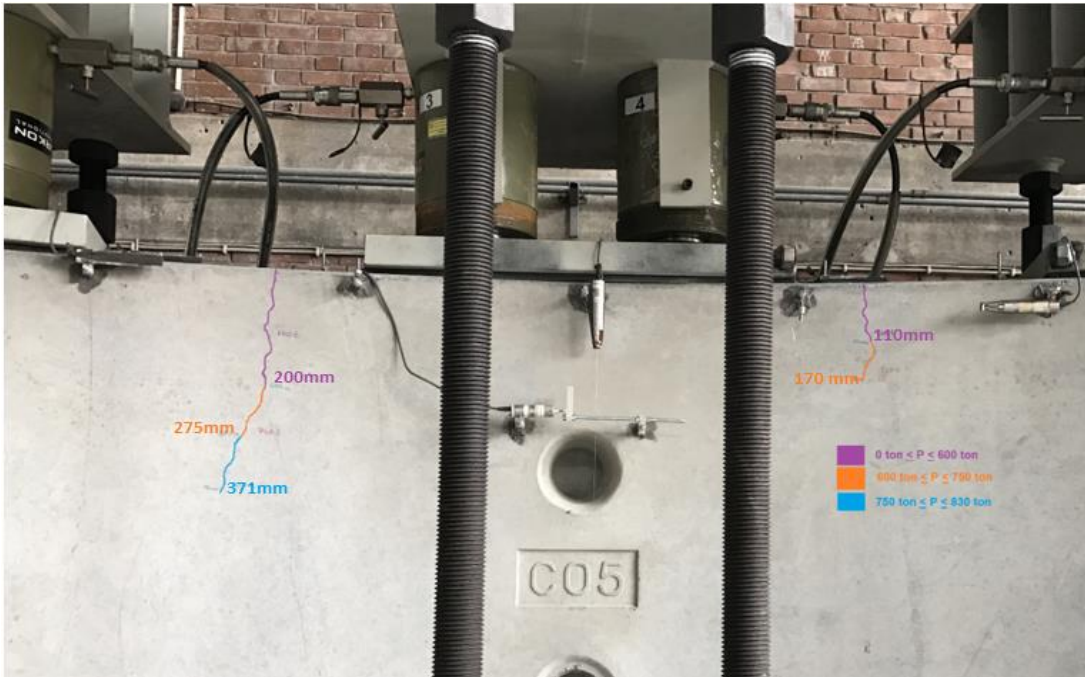


Figure 5.43. Crack pattern and crack depth of PFRC specimen

As far as the RC+ PFRC segment is concerned, it can be observed that hybrid solution that is comprised of the combination of PP fibers ($V_f = 0.44\%$) and conventional reinforcement rebars, has displayed well sufficient behavior under maximum thrust effect. Compared to the PFRC segment, both the cracking width and depth values are significantly smaller. Based on the experimental results maximum spalling crack width was recorded on the segment's top surface approximately 0.14 mm, and according to experimental observation maximum crack depth was measured as 140 mm. Similar to PFRC, any cracks, which are caused by splitting or bursting stresses, were not observed in this segment. These results demonstrated that PP fibers have a huge ability for controlling the circumferential splitting cracks. In addition, it should be noted that the presence of PP fibers in the concrete mixture increases the post-cracking tensile properties noticeably. Consequently, results of this experiment showed that PP increased the segment's capacity against both spalling and splitting stresses. Crack pattern and depth of the RC + PFRC specimen (B1) are displayed in the Figure 5.44. In this experiment, maximum load level of total system reached nearly 800 ton.

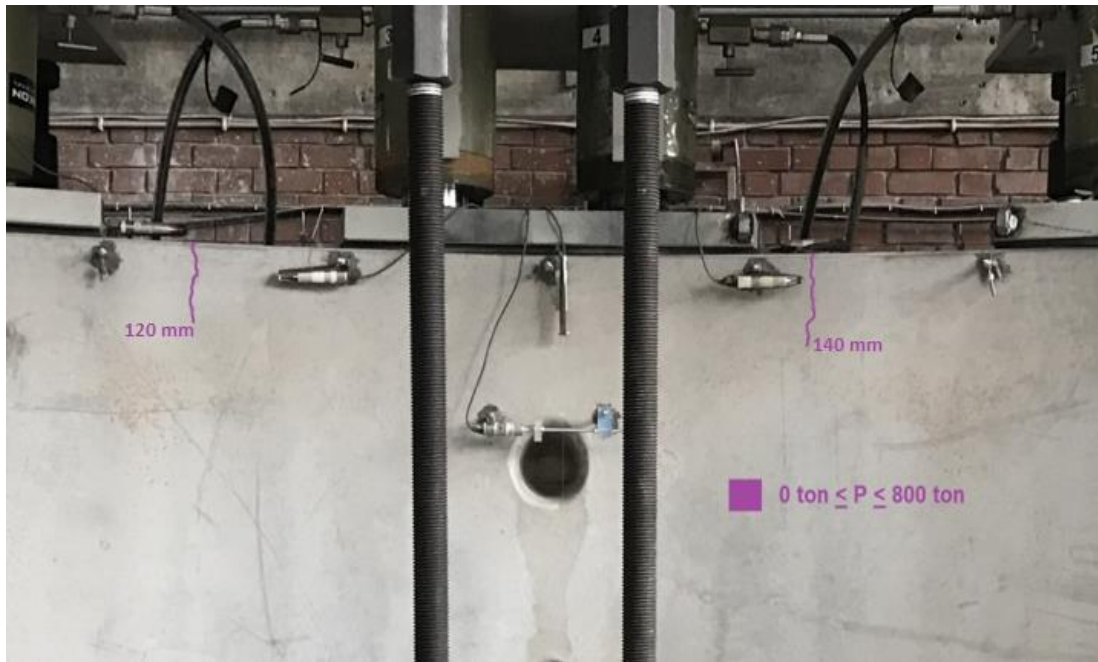


Figure 5.44. Crack pattern and crack depth of RC + PFRC specimen

RC segment, which is the reference sample, displayed a significantly durable behavior under the thrust action. After the point load test, occurred cracks were marked red colour on the inner surface of the specimen (A4), and both the final crack pattern and depths are shown in Figure 5.45. Compared to other types, splitting or bursting stresses caused by cracking were observed easily on the RC segment. The main reason is that the presence of conventional rebars allowed a noticeable crack opening control. As previously mentioned, fibers in the concrete mixture enhance the post-cracking behavior of concrete, especially in combination with reinforcement rebars (ITA report n.16, 2016). Although more cracks were observed on the segment surface, cracking widths were measured to a small extent than the others. This is because a high amount of steel rebars in the segment led to preventing of occurring larger cracks. Apart from that, contrary to expectation, crack has emerged on the mid region that near the base level of the test system (see Figure 5.45). Based on the results maximum spalling crack width was recorded as approximately 0.08 mm on the segment's top surface. Maximum spalling and splitting cracking depth were measured 213 mm and 230 mm, respectively.

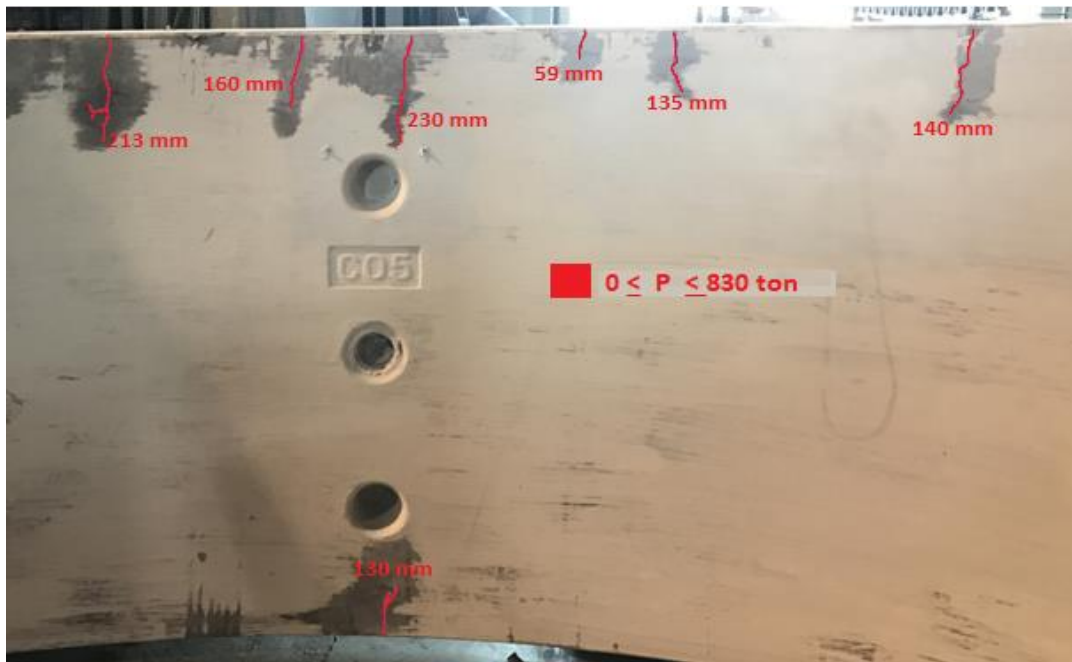


Figure 5.45. Crack pattern and crack depth of RC specimen



Figure 5.46. Final view of GFRP + PFRC specimen

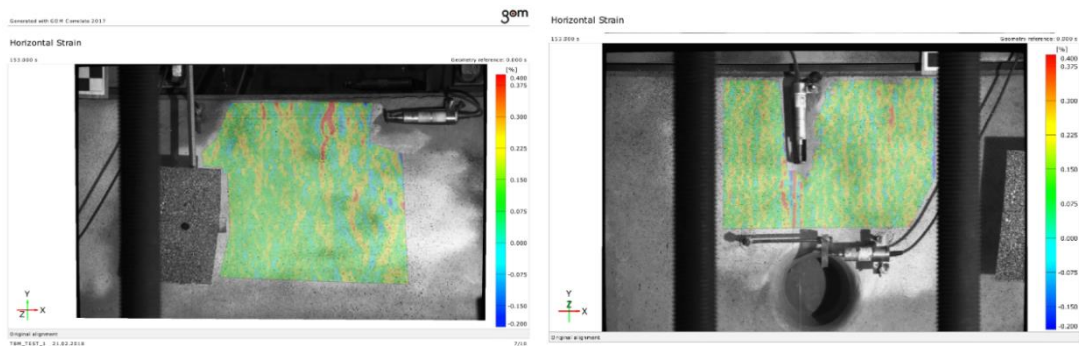


Figure 5.47. Horizontal strain values at the spalling and splitting region

Another hybrid solution, which is comprised of the combination of glass fiber reinforced polymer (GFRP) rebars and PP fibers, showed also well sufficient performance under the applied maximum thrust forces. In this experiment, in addition to the LVDTs, a special technique was used to measure strain values. Two cameras were adapted to record data during the experiment and then these data were transferred to programs to visualize strain values on the segment surface (see Figure 5.47). Based on the experimental results maximum spalling crack width was recorded by LVDTs on the segment's inner surface approximately 0.08 mm. However, as it is seen in Figure 5.46, there was no crack observed after the test, although, applied load level pretty much higher than the others. The reason for this is the presence of GFRP in the segment which provides a higher tensile strength with respect to traditionally reinforced segments.

CHAPTER 6

CONCLUSIONS

6.1. Summary

The main purpose of this research was to evaluate the structural applicability of using macro-synthetic fibers in precast tunnel segments by means of an experimental program on full-scale specimens. Within this framework totally fifteen full-scale precast tunnel segments of Mecidiyeköy - Mahmutbey metro tunnel characterized by three different alternative reinforcement cases and conventional reinforcement case were studied both under the flexure and point load test. The four different reinforcement solutions analyzed were; typical conventional steel reinforcement that is commonly adopted in practice (reference specimens, RC); combination of polypropylene fibers and conventional reinforcement (classical hybrid solution, RC + PFRC segments); combination of polypropylene and glass fiber reinforced polymer rebars (hybrid solution, GFRP + PFRC segments); polypropylene fibers only (PFRC samples). Macro-synthetic polypropylene fibers with a volume fraction of 0.44% (4 kg/m³) were adopted in hybrid cases, GFPP + PFRC and RC + PFRC segments, on the other hand, the volume fraction of 0.66% (6 kg/m³) was used for PFRC samples.

6.2. Conclusion

Based on this experimental research, the following conclusions can be drawn:

- Precast tunnel segments of metro project can be reinforced either by combination of glass fiber reinforced polymer rebars and polypropylene fibers (hybrid solution) or by a combination of conventional reinforcement and polypropylene fibers (classical hybrid solution). However, it should be noted that the conventional reinforcement case (RC) guarantees a better structural performance when compared with the use of low volume fraction of fibers. If

the aim is to improve the structural performance in addition to crack control, higher volume fractions should be preferred.

- Although PFRC specimens (6 kg/m³ polypropylene fibers) satisfy the serviceability limit state of the metro project in terms of crack width, this quantity of polypropylene fibers cannot significantly enhance both the bearing capacity and the ductility of precast tunnel segments under flexure. They showed low ductile behavior and post-cracking softening behavior under the flexure. In fact, the singular flexural crack that was characterized by higher values of the crack opening was observed in PFRC segments compared to other solutions;
- However, polypropylene fibers can considerably increase both the bearing capacity and the ductility of precast tunnel segments under flexure in case of hybrid solutions; GFRP + PFRC and RC + PFRC. In fact, performed flexural test results of RC + PFRC solutions showed that the structure was able to develop a significant multiple cracking and exhibited not only a significant strength but also an adequate ductility, while GFRP+PFRC showed a lower ductile behavior compared to classical hybrid case because of the brittleness of the GFRP rebars;
- Under point load test, PP fibers both in case of PFRC and hybrid solutions (RC + PFRC and GFRP + PFRC) satisfied the required structural performance at design TBM thrust load. The GFRP + PFRC (hybrid solution) exhibited a suitable behavior and guaranteed a better cracking control ability compared to other solutions. In all specimens, the maximum crack widths, even under high load level, were always lower than the allowable limit;
- On the point of view of the structural behavior under the point load test, polypropylene fibers can be used as splitting and spalling reinforcement of

precast tunnel segments of metro project. Concerning the splitting reinforcement, polypropylene fibers remarkably enhanced the splitting stress capacity of structure. Under TBM thrust loads splitting cracks were occurred only in conventional reinforcement case (RC). In addition, considered to the spalling reinforcement, results of PFRC specimen showed that PP fibers provide high resistance of structure against to spalling stress.

Full-scale test results revealed that both the macro-synthetic polypropylene fibers and glass fiber reinforced polymer rebars could be an attractive innovative reinforcement solution for precast tunnel segments in case of using a suitable quantity that satisfy the requirements of codes. PFRC and GFRP + PFRC segments enable to fully exploit the advantages of macro-synthetic fibers in terms of corrosion resistance in presence of an aggressive surrounding environment, while the combination of PP fibers with conventional steel reinforcement as a classical hybrid solution result in enhancing structural performance that could be particularly effective in presence of aggressive conditions.

6.3. Future studies

In spite of the achievements that were reported previously, some issues regarding the topics presented in this master thesis still remain. For this reason, suggestions for future research are taken place in this section.

Even though the experimental results of alternative reinforcement solutions satisfy the design values of Mecidiyeköy - Mahmutbey metro project in terms of serviceability limit state, more studies should focus on the optimization of the quantity of both fibers and reinforcements in precast tunnel segments in order to obtain more economic and durable solutions. In particular, finding suitable fiber quantity and concrete mix design is significantly important to satisfy the minimum requirement of fib Model Code 2010 for fiber reinforced concrete segments, enhance the ductility of segments and obtain the post-cracking hardening behavior.

Comprehensive studies on hybrid solutions that combination of the glass fiber reinforced polymer rebars and macro-synthetic fibers could be performed to evaluate the structural applicability in terms of ductility requirements and to increase the bending capacity of segments. Furthermore, it would be interesting to investigate the effect of using the curvilinear shapes of GFRP rebars in the production of tunnel segments.

More full-scale experimental tests with considerable amounts of fibers are needed in order to determine whether fibers can entirely substitute ordinary reinforcement or not. If the macro-synthetic fibers are to entirely replace ordinary reinforcement, more experiments on strain hardening materials should be considered.

Another important point is that carrying out many full-scale flexural tests is necessary to go deeper on topic related to bending capacity of hybrid solutions. In addition to serviceability limit state analysis, performing an in-depth analysis to evaluate the ultimate bearing capacity of alternative solutions of precast tunnel segments would be important to understand the general structural behavior of segments. This is significantly crucial for the safety of tunnel lining under the extreme or unexpected conditions.

Although the experimental studies provide comprehensive information about mechanical behavior of precast tunnel segments numerical studies such as complex model analysis considered smeared cracking in other words, a model that capable of capturing the crack formation process could be used to analyze the alternative reinforcement solutions. Since full-scale experimental studies are difficult to perform, take a long time and expensive process, numerical model may be verified by means of these experimental results and are used in further analysis. For that reason, more information related to design values of metro project were given in Appendix A.

REFERENCES

- Abbas, S., Soliman, A. M., & Nehdi, M. L. (2014). Experimental study on settlement and punching behavior of full-scale RC and SFRC precast tunnel lining segments. *Engineering Structures*, 72, 1–10. doi:10.1016/j.engstruct.2014.04.024
- Abid, A., & Franzén, K. (2011). *Design of Fibre Reinforced Concrete Beams and Slabs*. (Master's thesis, Chalmers University of Technology, Göteborg, Sweden). Retrieved from <http://publications.lib.chalmers.se/records/fulltext/146607.pdf>
- ACI Committee 224. (2007). Control of Cracking in Concrete Structures. ACI 224.1R. American Concrete Institute.
- ACI Committee 440. (2015). Guide for the Design and Construction of Structural Concrete Reinforced with FRP Bars. ACI 440.1R-15. American Concrete Institute
- ACI Committee 544. (2016). Report on Design and Construction of Fiber Reinforced Precast Concrete Tunnel Segments. ACI 544.7R-16. American Concrete Institute.
- Ahmadi, M. H., Mortazavi, A., Davarpanah, S. M., & zarei, H. (2016). A Numerical Investigation of Segmental Lining Joints Interactions in Tunnels-Qomrud Water Conveyance Tunnel. *Civil Engineering Journal*, 2(7), 334–347.
- Arnau, O., & Molins, C. (2011). Experimental and analytical study of the structural response of segmental tunnel linings based on an in situ loading test. Part 2: Numerical simulation. *Tunnelling and Underground Space Technology*, 26(6), 778–788. doi:10.1016/j.tust.2011.04.005
- Arnau, O., & Molins, C. (2015). Theoretical and numerical analysis of the three-dimensional response of segmental tunnel linings subjected to localized loads. *Tunnelling and Underground Space Technology*, 49, 384-399. doi:10.1016/j.tust.2015.05.012

- Bakhshi, M., & Nasri, V. (2015). Design of segmental tunnel linings for serviceability limit states. In: ITA/AITES World Tunnel Congress 2015 and 41st General Assembly, May 22–28, 2015. Lacroma Valamar Congress Center, Dubrovnik, Croatia.
- Bakhshi, M., & Nasri, V. (2016). Design of fiber-reinforced tunnel segmental lining according to new ACI report. Proceedings, Annual Conference - Canadian Society for Civil Engineering, 3(November), 18–20.
- Beno, J., & Hilar, M. (2013). Steel fibre reinforced concrete for tunnel lining-verification by extensive laboratory testing and numerical modelling. *Acta Polytechnica* 53(4):329–337.
- Bentur, A., & Mindess, S. (2007). *Fibre reinforced cementitious composites* (2nd ed.). London: Taylor & Francis.
- Bieniawski, Z. T. (1989). Engineering rock mass classifications: *A complete manual for engineers and geologists in mining, civil, and petroleum engineering*. Wiley.
- Britannica, T. E. (2011, May 11). Tunneling shield. Retrieved from <https://www.britannica.com/technology/tunneling-shield>
- Caratelli, A., Meda, A., Rinaldi, Z., & Romualdi, P. (2011). Structural behavior of precast tunnel segments in fiber reinforced concrete. *Tunnelling and Underground Space Technology*, 26(2), 284–291. doi:10.1016/j.tust.2010.10.003
- Caratelli, A., Meda, A., & Rinaldi, Z. (2012). Design according to MC2010 of a fibre-reinforced concrete tunnel in Monte Lirio, Panama. *Structural Concrete*, 13(3), 166–173. doi:10.1002/suco.201100034
- Caratelli, A., Meda, A., Rinaldi, Z., & Spagnuolo, S. (2016). Precast tunnel segments with GFRP reinforcement. *Tunnelling and Underground Space Technology*, 60, 10–20. doi:10.1016/j.tust.2016.07.011

- Caratelli, A., Meda, A., Rinaldi, Z., Spagnuolo, S., & Maddaluno, G. (2017). Optimization of GFRP reinforcement in precast segments for metro tunnel lining. *Composite Structures*, 181, 336–346. doi:10.1016/j.compstruct.2017.08.083
- Cignitti, F., Sorge, R., Meda, A., Nerilli, F., & Rinaldi, Z. (2012). Numerical analysis of precast tunnel segmental lining supported by full-scale experimental tests. *Geotechnical Aspects of Underground Construction in Soft Ground - Proceedings of the 7th International Symposium on Geotechnical Aspects of Underground Construction in Soft Ground*, 481–487.
- CNR DT 204/2006. (2006). Guidelines for the Design, Construction and Production Control of Fibre Reinforced Concrete Structures, Italian National Research Council - CNR.
- CNR DT 203/2006. (2006). Guidelines for the Design and Construction of Concrete Structures Reinforced with Fiber-Reinforced Polymer Bars, Italian National Research Council - CNR.
- Cominoli, L., Failla, C., & Plizzari, G. A. (2007). Steel and synthetic fibres for enhancing concrete toughness and shrinkage behavior. *Sustainable Construction Materials and Technologies*, 231–240.
- Conforti, A., Tiberti, G., & Plizzari, G. A. (2016). Combined effect of high concentrated loads exerted by TBM hydraulic jacks. *Magazine of Concrete Research*, 68(21), 1122–1132. doi.org/10.1680/jmacr.15.00430
- Conforti, A., Tiberti, G., Plizzari, G. A., Caratelli, A., & Meda, A. (2017). Precast tunnel segments reinforced by macro-synthetic fibers. *Tunnelling and Underground Space Technology*, 63, 1–11. doi:10.1016/j.tust.2016.12.005
- Çimentepe, A.G. (2010). *Evaluation of structural analysis method used for the design of TBM segmental linings* (Master thesis, Middle East Technical University, Ankara, Turkey).

- Darendeliler, H. (2017). *Cam elyaf takviyeli 8 mm, 10 mm, 12 mm çaplı nervürlü kompozit inşaat çubuklarının çekme deneyleri ile elastik modülüsünün tespiti* (Rep.). Ankara, Turkey: Middle East Technical University.
- DAUB (German Tunneling Committee). (2013). Recommendations for the design, production and installation of segmental rings. Working group “Lining Segment Design”, English version, 46.
- De la Fuente, A., Pujadas, P., Blanco, A., & Aguado, A. (2012). Experiences in Barcelona with the use of fibres in segmental linings. *Tunnelling and Underground Space Technology*, 27(1), 60–71. doi:10.1016/j.tust.2011.07.001
- Deutscher Ausschuss für Stahlbeton (DAfStb) Guideline. (2012). German committee for reinforced concrete, steel fibre reinforced concrete; design and construction, specification, performance, production and conformity, execution of structures, draft. November 2012, pp. 48.
- Di Carlo, F. D., Meda, A., & Rinaldi, Z. (2016). Design procedure for precast fibre-reinforced concrete segments in tunnel lining construction. *Structural Concrete*, 17(5), 747-759. doi:10.1002/suco.201500194
- Di Prisco, M., Colombo, M., & Dozio, D. (2013). Fibre-reinforced concrete in fib Model Code 2010: Principles, models and test validation. *Structural Concrete*, 14(4), 342–361. doi:10.1002/suco.201300021
- EN 14651. (2005). Test method for metallic fibred concrete - Measuring the flexural tensile strength (limit of proportionality (LOP), residual). European Standard.
- EN 1992-1 1. (2004). Design of concrete structures - Part 1–1: General rules and rules for buildings. European Standard.
- EN 12390-3. (2009). Testing hardened concrete Part 3: Compressive strength of test specimens. European Standard.

- EN 14889-2. (2006). Fibers for concrete. Polymer fibres. Definitions, specifications and conformity. European Standard.
- EN 197-1. (2011). Cement. Part 1: Composition, specifications and conformity criteria for common cements. European Standard.
- Fabozzi, S. (2017). *Behavior of segmental tunnel lining under static and dynamic loads* (Doctoral thesis, University of Naples Federico II, Naples, Italy).
- Falkner, H., Huang, Z., Teutsch, M. (1995). Comparative study of plain and steel fiber reinforced concrete ground slabs. *Concrete International* 17 (1), 45–51.
- fib Bulletins 65-66. (2012). *Model code 2010: Final draft*. Lausanne, Switzerland: International Federation for Structural Concrete (fib)
- fib Bulletin 40. (2007). *FRP reinforcement in RC structures: Technical report*. Lausanne, Switzerland: International Federation for Structural Concrete (fib)
- Gong, C., Ding, W., Mosalam, K. M., Günay, S., & Soga, K. (2017). Comparison of the structural behavior of reinforced concrete and steel fiber reinforced concrete tunnel segmental joints. *Tunnelling and Underground Space Technology*, 68(May), 38–57. doi.org/10.1016/j.tust.2017.05.010
- Guglielmetti, V., Grasso, P., Mahtab, A., & Xu, S. (2007). *Mechanized tunnelling in urban areas: Design methodology and construction control*. Boca Raton, FL: Taylor & Francis.
- Hurt, J., & Hart, J. (2011). *Concrete for underground structures guidelines for design and construction* (R. J. Goodfellow, Ed.). Englewood: Society for Mining, Metallurgy, and Exploration.
- Hemphill, G. B. (2013). *Practical tunnel construction*. Hoboken: John Wiley.

Istanbul Metropolitan Municipality (2017). *Metro İstanbul Faliyet Raporu 2017*.

ISO 10406-1 (2008). Fibre-reinforced polymer (FRP) reinforcement of concrete – Test methods – Part 1: FRP bars and grids. International Standard.

ITA report n. 16 (2016). Twenty years of FRC tunnel segments practice: lessons learnt and proposed design principles. April 2016, pp. 71, ISBN 978-2-970-1013-5-2.

ITATech report n. 7 (2016) Guidance for precast fibre reinforced concrete segments – vol. 1: design aspects. April 2016, pp. 47, ISBN 978-2-970-1013-2-1.

ITA Working Group-2 (2000). Guidelines for the design of shield tunnel lining. *Tunneling and Underground Space Technology*, 15(3), 303–331.

ITA Working Group-14 (2000). Recommendations and Guidelines for Tunnel Boring Machines (TBMs). www.ita-aitec.org

Jansson, A. (2008). *Fibres in reinforced concrete structures – analysis, experiments and design*. (Thesis for Licentiate, Chalmers University of Technology, Sweden) Retrieved from <http://publications.lib.chalmers.se/records/fulltext/68889.pdf>

Jose, S., Stephan, S.J., & Gettu, R. (2015, December). *Study of the post-cracking behavior of steel and polymer fibre reinforced concretes*. Paper presented at the 2nd R N Raikar Memorial Biennial International Conferences & ‘Banthia – Basheer International Symposium. Mumbai, India.

Kanstad, T., & Døssland, Å. L. (2004). Testing and Modelling of Steel fibre Reinforced Concrete Beams Designed for Moment Failure. *Fracture Mechanics of Concrete Structures*, 2, 1171–1178.

Kooiman, A.G. (2000). *Modelling steel fibre reinforced concrete for structural design*. (Doctoral thesis, Delft University of Technology, Delft, Netherlands).

- Liao, L., de la Fuente, A., Cavalaro, S., & Aguado, A. (2015). Design of FRC tunnel segments considering the ductility requirements of the Model Code 2010. *Tunnelling and Underground Space Technology*, 47, 200–210. doi:10.1016/j.tust.2015.01.006
- Liao, L., de la Fuente, A., Cavalaro, S., & Aguado, A. (2016). Design procedure and experimental study on fibre reinforced concrete segmental rings for vertical shafts. *Materials and Design*, 92, 590–601. doi:10.1016/j.matdes.2015.12.061
- Liao, L. (2015). *Structural design and characterisation of FRC precast segments* (Doctoral thesis, Universitat Politècnica de Catalunya, Barcelona, Spain).
- Löfgren, I. (2005). *Fibre Reinforced Concrete for Industrial Construction – a fracture mechanics approach to material testing and structural analysis*. (Doctoral Thesis, Chalmers University of Technology, Göteborg, Sweden). Retrieved from <http://publications.lib.chalmers.se/records/fulltext/8627/8627.pdf>
- Luttikholt, A. (2007). *Ultimate Limit State Analysis of a Segmented Tunnel Lining*. (Master thesis, Delft University of Technology, Delft, Netherlands). Retrieved from http://homepage.tudelft.nl/p3r3s/MSc_projects/reportLuttikholt.pdf
- Maidl, B., Herrenknecht, M., & Anheuser, L. (1996). *Mechanised shield tunnelling*. Berlin: Ernst & Sohn.
- Maidl, B., Schmid, L., Ritz, W., & Herrenknecht, M. (2008). *Hardrock tunnel boring machines*. Berlin: Ernst & Sohn.
- Meng, G., Gao, B., Zhou, J., Cao, G., & Zhang, Q. (2016). Experimental investigation of the mechanical behavior of the steel fiber reinforced concrete tunnel segment. *Construction and Building Materials*, 126, 98–107. doi:10.1016/j.conbuildmat.2016.09.028
- Meda, A., Rinaldi, Z., Caratelli, A., & Cignitti, F. (2016). Experimental investigation on precast tunnel segments under TBM thrust action. *Engineering Structures*, 119, 174–185. doi:10.1016/j.engstruct.2016.03.049

- Molins, C., & Arnau, O. (2011). Experimental and analytical study of the structural response of segmental tunnel linings based on an in situ loading test.. Part 1: Test configuration and execution. *Tunnelling and Underground Space Technology*, 26(6), 764–777. doi:10.1016/j.tust.2011.05.002
- Möller, S. C. (2006). *Tunnel induced settlements and structural forces in linings* (Doctoral thesis, Universitat Stuttgart, Stuttgart, Germany). Retrieved from http://www.unistuttgart.de/igs/content/publications/IGS_Dissertationen/Doctoral_Thesis_Sven_Moeller.pdf
- Naaman, A. E. (2003). Engineered Steel Fibers with Optimal Properties for Reinforcement of Cement Composites. *Journal of Advanced Concrete Technology*, 1(3), 241-252. doi:10.3151/jact.1.241
- Nedreliid, H. (2015). *Structural FRC – Design Approach and Experimental Results*. SINTEF Building and Infrastructure, COIN project report 66.
- Nehdi, M. L., Abbas, S., & Soliman, A. M. (2015). Exploratory study of ultra-high performance fiber reinforced concrete tunnel lining segments with varying steel fiber lengths and dosages. *Engineering Structures*, 101, 733-742. doi:10.1016/j.engstruct.2015.07.012
- Plizzari, G.A., Tiberti, G. (2007). Structural behavior of SFRC tunnel segments. In: Proceedings of the 6th International Conference on Fracture Mechanics of Concrete and Concrete Structures (FraMCoS), vol. 3, 1577–1584, ISBN 978-0-415-44066-0.
- RILEM TC 162-TDF (2003): Test and design methods for steel fibre reinforced concrete, σ - ϵ design method. *Materials and Structures*, 36, 560-567.
- Spagnuolo, S., Meda, A., Rinaldi, Z., & Nanni, A. (2017). Precast Concrete Tunnel Segments with GFRP Reinforcement. *Journal of Composites for Construction*, 21(5), 04017020. doi:10.1061/(asce)cc.1943-5614.0000803

- Tiberti, G., Conforti, A., & Plizzari, G.A. (2015). Precast segments under TBM hydraulic jacks: experimental investigation on the local splitting behavior. *Tunnelling and Underground Space Technology*, 50, 438–450. doi:10.1016/j.tust.2015.08.013.
- Tiberti, G., Plizzari, G.A., & Chiriotti, E. (2018, May). *Structural use of fibre reinforced concrete in precast segments*. Retrieved from https://www.ethz.ch/content/dam/ethz/special-interest/baug/igt/tunneling-dam/kolloquien/2018/31_Tiberti_ITA-WG2%20Tiberti%20Lessons%20from%2020%20years%20of%20application%20Zurich.pdf
- Yan, Z., Shen, Y., Zhu, H., Li, X., & Lu, Y. (2015). Experimental investigation of reinforced concrete and hybrid Fiber reinforced concrete shield tunnel segments subjected to elevated temperature. *Fire Safety Journal*, 71, 86-99. doi:10.1016/j.firesaf.2014.11.009
- Yan, Z., Shen, Y., Zhu, H., & Lu, Y. (2016). Experimental study of tunnel segmental joints subjected to elevated temperature. *Tunnelling and Underground Space Technology*, 53, 46–60.

APPENDICES

A. THE DESIGN VALUES OF MECİDİYEKÖY-MAHMUTBEY METRO PROJECT

General information about Mecidiyeköy-Mahmutbey metro project was given in chapter 4 and the construction method of segmental tunnel lining was explained deeply in chapter 3. Therefore, this part only shows the design values of this metro project and demonstrates the assumptions for safe side analysis. Most of the values were determined by the Yuksel Project International Company that is the consultant of this project and the others adopted from related specifications. These values were taken into consideration on the preliminary design part of the test specimens. Design values were demonstrated according to related load cases that explained in the ACI 544.7R-16 specification.

A.1 Production and Transient Load Cases

A.1.1 Segment Demoulding

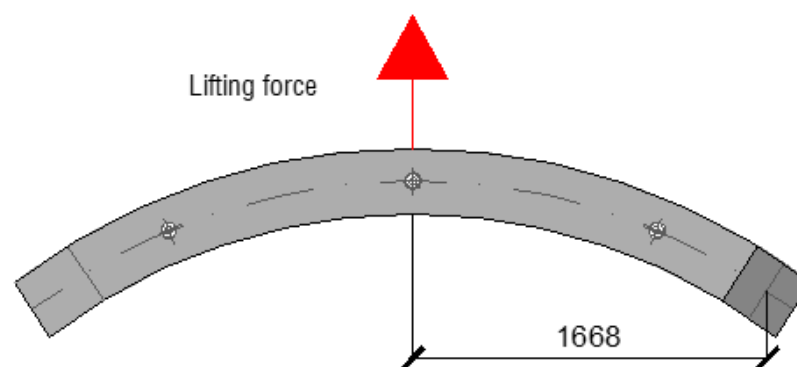


Figure A.1. Statical scheme of the demoulding phases (units mm)

The main load acting in the segment demoulding phase was the segment self-weight which is almost 37.11 kN. As it can be seen from Figure A.1 only one lifting point, placed in the middle of the segment was considered in the analysis. The assumed static condition leads to a safe side analysis, since in reality segment handling is always performed through a vacuum systems which minimize any bending moment and shear

force which might develop in the segment section. In this project amplification factor was taken 1.35 and dynamic factor also was taken 1.5. According to these criteria design values for flexure and shear were calculated as 31.31 kN.m and 37.57 kN respectively.

A.1.2 Segment Storage

The storage configuration refers to the completely hardened stage of segments which obtained target compressive strength of concrete at 28 days. Each ring can be stacked in one pile according to the configuration shown in Figure A.2. Due to segments self-weight and occurring of higher shear force which develops in the bottom segment of the pile, the supports which located at the bottom segments of the pile must be positioned carefully otherwise, it can cause cracks in the bottom segments. Therefore, in order to perform a safe side analysis, accidental eccentricity ($e = 0.30\text{m}$) was considered at the supports at the base of the pile. In this situation, the higher bending moment and shear forces occur in the bottom segments. For this phase, the amplification factor and the dynamic factor was taken 1.35, 1.0 respectively. According to these criteria design values for flexure and shear were calculated as 44.253 kN.m and 128.085 kN. Detailed information and assumptions were tabulated in Tables A-1 to A-3

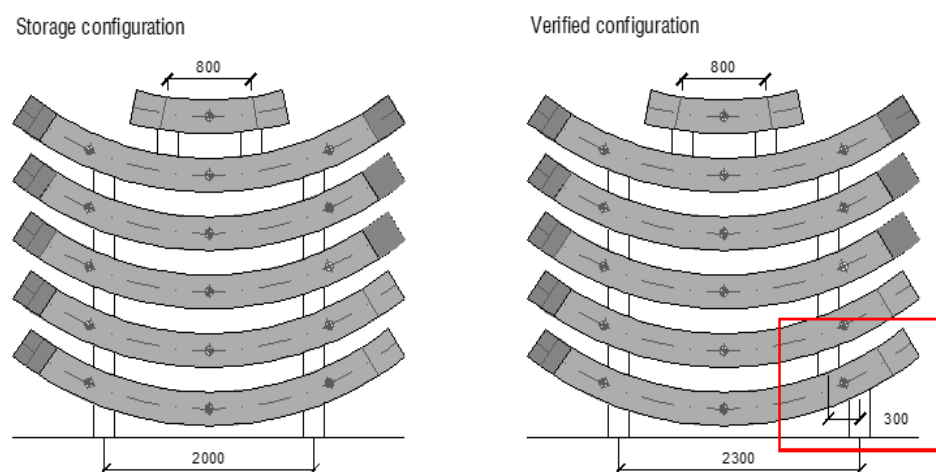


Figure A.2. Storage configuration of entire ring segments (units mm)

Table A.1. *Storage configuration detail*

Number of segments (without key segment)	5
Key segment on top of pile	1
Optimum free distance	0.69 m
Optimum distance between supports	1.95 m
L: Considered distance between supports	2.00 m
as: Free length	0.67 m
Lk: Distance between supports of key segment	0.80 m
D: Total horizontal length	3.33 m
Lt: Distance between supports at the base of the pile	2.6 m
e: Eccentricity between supports	0.3 m
ab: Free base length	0.37 m

Table A.2. *Forces action on the storage systems*

Fk: Self weight of key segment/2	6.185 kN
F: Self weight of upper segments/2	80.405 kN
R: Reaction	98.960 kN
W: Self weight per meter	11.133 kN

Table A.3. *Calculations' results and design values of storage phase*

Upper segment acting forces	
M-	-2.474 kN.m
M+	6.803 kN.m
V1	7.422 kN
V2	17.318 kN
Lower segment acting forces	
M-	-0.749 kN.m
M+	32.780 kN.m
V1	4.082 kN
V2	94.878 kN
Mk (static):	32.780 kN.m
Vk (static):	94.878 kN
Mk (dynamic):	32.780 kN.m
Vk (dynamic):	94.878 kN
Md:	44.253 kN.m
Vd:	128.085 kN

A.1.3 Segment Transportation

The segments of one ring shall be transported in two piles, the first pile of three segments and the second pile with the remaining two segments plus the keystone. In this case, an eccentricity of 0.3 m is considered for the supports at the piles bottom. As for the demoulding phase, the dynamic factor was 1.5 and the amplification factor was taken 1.35. The followings calculations refer to the left configuration, pile formed by three segments, which was the most demanding situation shown in Figure A.3. The results of design values and details about the transportation configuration of segments are summarized in Tables A-4 to A-6.

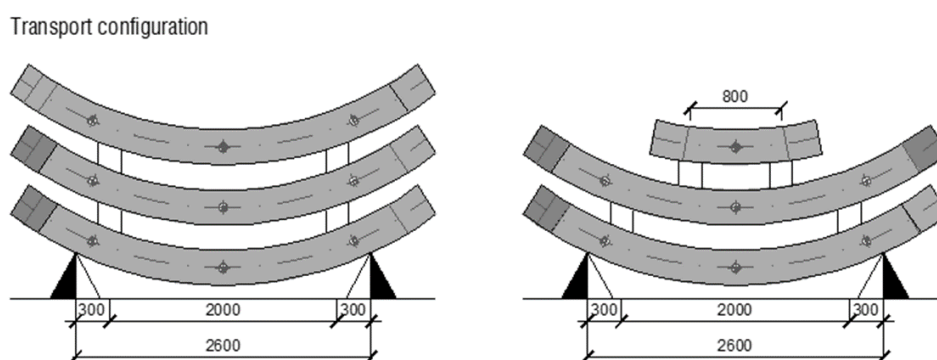


Figure A.3. Static condition in the transporting phase (units mm)

Table A.4. Transportation configuration detail

Number of segments (without key segment)	3
Key segment on top of pile	no
Optimum free distance	0.69 m
Optimum distance between supports	1.95 m
L: Considered distance between supports	2.00 m
as: Free length	0.67 m
Lk: Distance between supports of key segment	0.80 m
D: Total horizontal length	3.33 m
Lt: Distance between supports at the base of the pile	2.6 m
e: Eccentricity between supports	0.3 m
ab: Free base length	0.37 m

Table A.5. Forces action on the transportation phases

Fk: Self weight of key segment/2	0.000 kN
F: Self weight of upper segments/2	37.110 kN
R: Reaction	55.665 kN
W: Self weight per meter	11.133 kN

Table A.6. Calculations' results and design values of transportation phase

Upper segment acting forces	
M-	-2.474 kN.m
M+	3.092 kN.m
V1	7.422 kN
V2	11.133 kN
Lower segment acting forces	
M-	-0.749 kN.m
M+	19.792 kN.m
V1	4.082 kN
V2	51.583 kN
Mk (static):	19.792 kN.m
Vk (static):	51.583 kN
Mk (dynamic):	29.687 kN.m
Vk (dynamic):	77.374 kN
Md:	40.078 kN.m
Vd:	104.455 kN

A.1.4 Segment Handling

Segment handling stage is the same as demoulding phases, however, the only difference is that when the segment stripping concrete segment strength was about 15 MPa and it is more critical for the design. Therefore, in this part, no calculation has been shown since all procedures are same with demoulding. Table A-7 summarizes the design values of production and transient load cases.

Table A.7. Design values of production and transient load cases

	Md (kN.m)	Vd (kN)	Concrete Strength
Demoulding	31.31	37.57	15 MPa
Storage	44.25	128.08	40 MPa
Transportation	40.08	104.46	40 Mpa
Handling	31.31	37.57	40 Mpa

A.2 Construction Load Cases

A.2.1 Tunnel Boring Machine Thrust Jack Force

The verification has been performed considering the maximum TBM exceptional thrust value of 40000kN. Due to having sixteen jack, the design value of thrust force is calculated as $N_d = 40000/16 = 2500\text{kN}$.

The maximum eccentricity was assumed to be 20mm to remain safe side. The considered geometrical conditions at segment/thrust shoe interface are shown in Figure A.5. Also, other design considerations are shown in Figures A.4, A.6 and A.7.

Design checks:

1. Compressive stresses

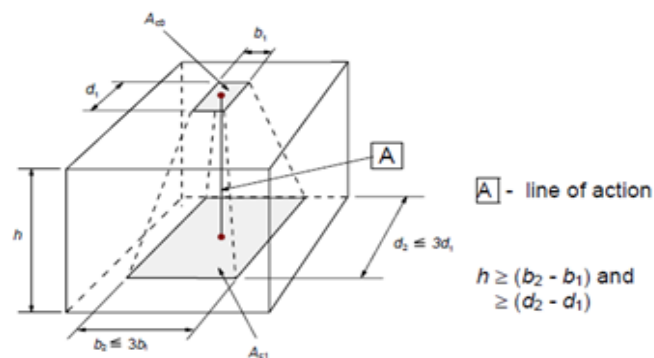


Figure A.4. Load distribution for the partially loaded area (Eurocode-2)

The maximum compression force verification performed, according to the “EN 1992-1-1: 2004: Design of Reinforced Concrete Structures”, considering the following formula:

$$FR_{du} = A_{c0}f_{cd} \sqrt{A_{c1}/A_{c0}} \leq 3.0f_{cd}A_{c0};$$

In this project, both amplification factor and dynamic factor for the TBM thrust forces were taken 1.0.

2. Bursting or Splitting tensile stresses

In order to analyze this action for determining the design values both the empirical formulas, according to DAUB, ACI or other specification, and FEA were used.

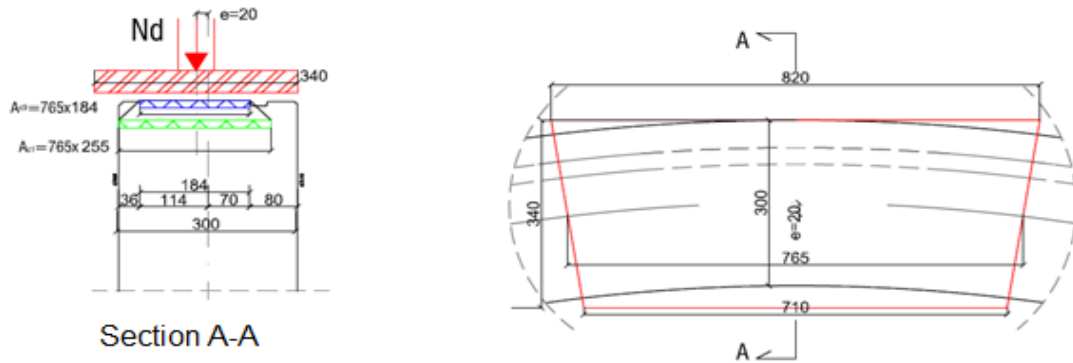


Figure A.5. Static condition to evaluate the bursting effect in segments perpendicular plane

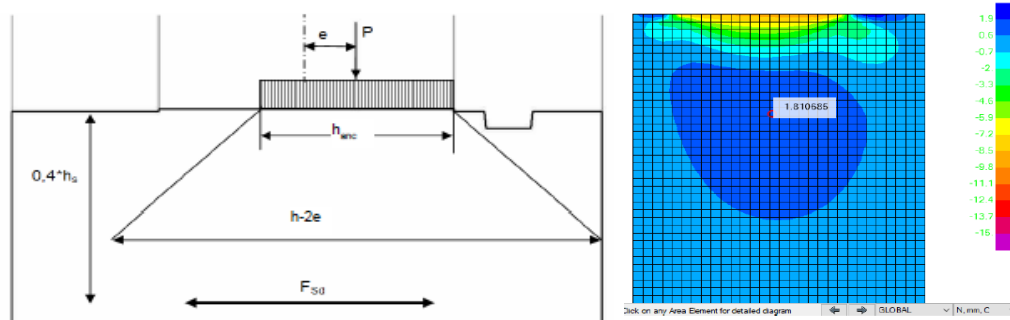


Figure A.6. Empirical method and FEA method for the evaluation of splitting

According to DAUB, the empirical formula for the calculate the bursting force and effect;

$$T_{burst} = 0.25 P_{pu} \left(1 - \frac{h_{anc}}{h - 2e_{anc}} \right); d_{burst} = 0.4(h - 2e_{anc})$$

3. Spalling tensile stresses

For the evaluation of spalling stresses on the precast tunnel segments, under the effect of TBM thrust force, FEA methods were used.

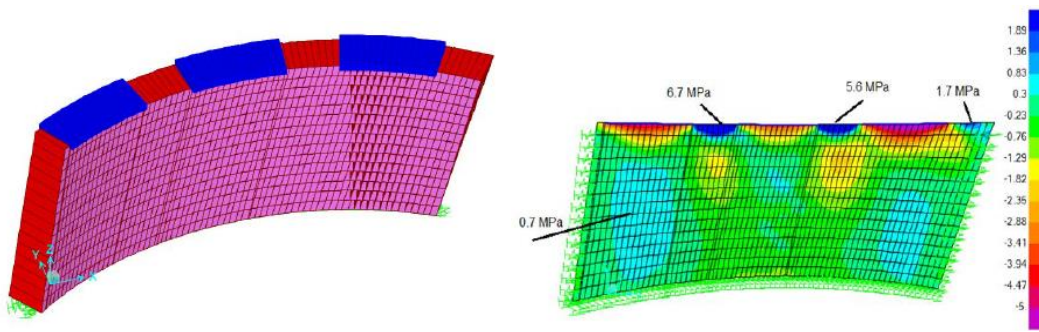


Figure A.7. Finite Element Analysis model and results of segment C

A.3 Final Service Load Cases

Final service stage is represented by the long-term interaction of the tunnel, which the segmental lining ring is already installed, with the ground, groundwater pressure and surcharges loads. In this part, the main hypotheses considered for the segmental lining structural verification against final loads were described according to the ITA guideline. The sectional forces acting in the TBM segmental lining were computed in relation to long-term load conditions, for which ground loads and water loads derived from available geological information were considered.

- Permanent Loads

SW: load due to lining self-weight

G: ground load acting on tunnel lining

W: groundwater load acting on the tunnel lining

BL: building surcharge at the surface (considered only for critical section 4)

- Variable Loads

TL: traffic surcharge at the surface

SG: load due to the effect of the annular void grout injections

- Exceptional Loads

EQ: seismic (earthquake) load of the Maximum Design Earthquake (MDE) on tunnel lining

In this phase, three different load combinations were considered according to the segmental lining design manual which was prepared for Mecidiyeköy-Mahmutbey metro project. These are expressed below;

Combination A = 1,35 (SW+G+W+BL) +1.5 TL

Combination B = 1,35 (SW+G+W+BL) +1.5 (TL +SG)

Combination C = 1,00 (SW+G+W+BL) +1.0 TL + 1.0 EQ

Considering the actual geometrical and geological conditions of the alignment stretch from Yeminhalle to Mahmutbey stations, five critical sections have been selected for lining structural verifications against permanent loads. The criteria for their selection and their main characteristics are shown in Table A-8.

Table A.8. *Critical sections were considered in the TBM tunnel segmental lining*

Critical Section	Criteria	PK	OB at tunnel crown [m]	Water table height at tunnel crown [m]	The distance between tubes axes [m]	Geologic description
S1	Minimum Overburden in soil+ Minimum GWL	16+153	13.7	-3.4	24.87	Sand and silty clay
S2	Maximum overburden in Soil-Rock	17+075	28	22.8	32	Silty clay and weathered sandstone

S3	Minimum overburden close to high rise building	18+775	10.2	8	14	Fresh sandstone, claystone and mudstone
S4	Maximum Overburden in Fault Zone + Maximum GWL	21+750	42.3	23.45	14	Weathered sandstone and detected fault zone
S5	Maximum Overburden	21+800	42.8	24.5	14	Weathered sandstone and mudstone

Critical sections model and mesh refinement at the Plaxis software are shown in Figures A.8 to A.12.

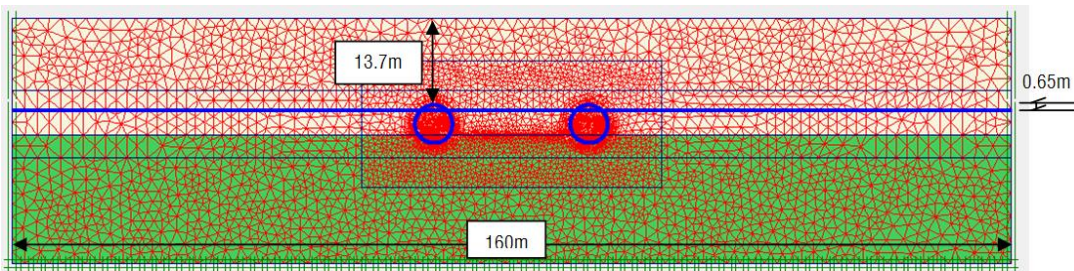


Figure A.8. Section 1 geometry

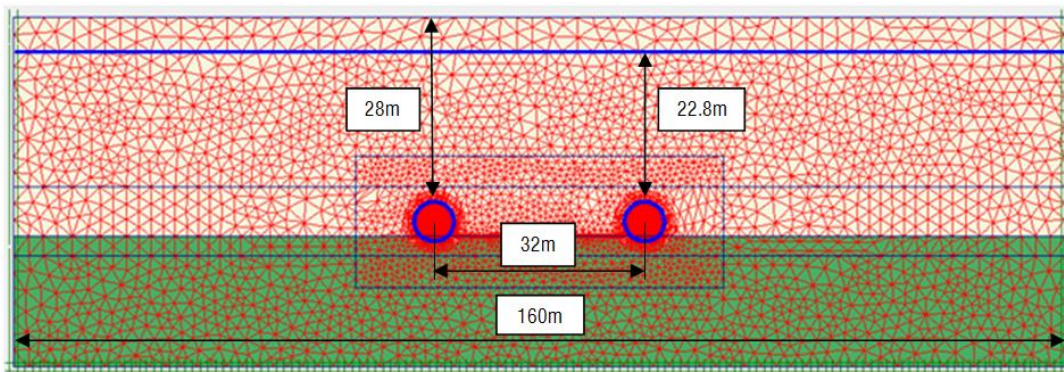


Figure A.9. Section 2 geometry

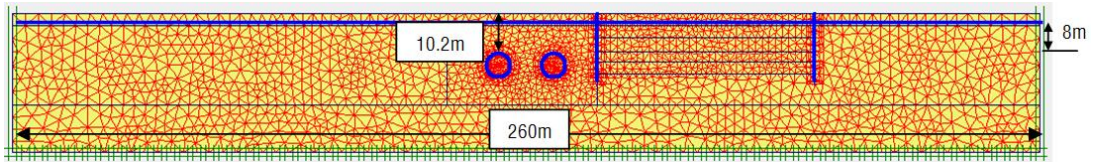


Figure A.10. Section 3 geometry

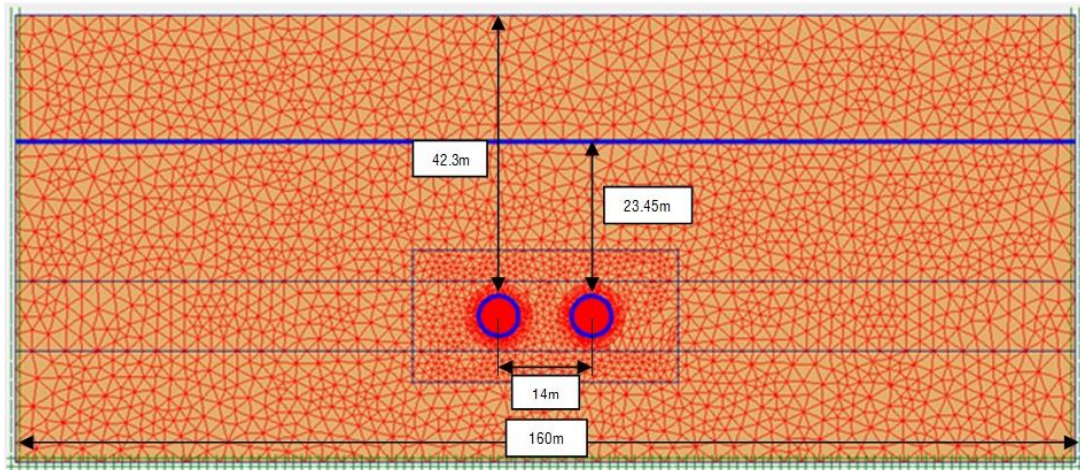


Figure A.11. Section 4 geometry

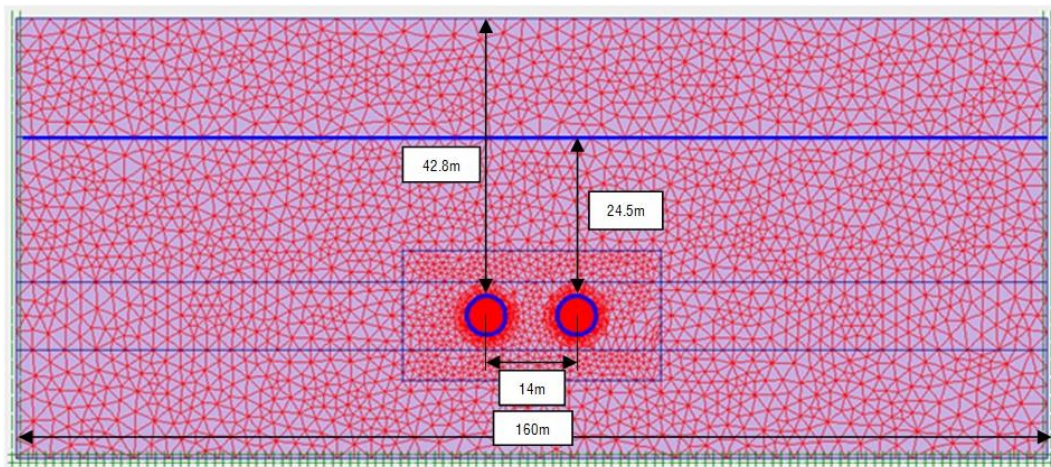


Figure A.12. Section 5 geometry

A.3.1 Earth Pressure, Groundwater, Surcharge and Seismic Loads

The design values of the final service phase, which is based on load combinations and Plaxis models of critical sections, were summarized in Tables A-9 to A-10.

Table A.9. Design values of full section segments- Combination A and B

Section & Combination Tunnel		Design Loads			Section & Combination Tunnel		Design Loads		
		Nd (kN)	Md (kNm)	Vd (kN)			Nd (kN)	Md (kNm)	Vd (kN)
S1 A L	max	-540.33	56.79	29.1	S1 B L	max	-712.51	130.77	90.29
	min	-787.01	-59.03	-33.47		min	-957.14	-94.2	-95.47
S2 A L	max	-2079.96	92.18	74.58	S2 B L	max	-2283.9	236.47	159.94
	min	-2640.64	-115.72	-76.61		min	-2970.91	-205.84	-177.65
S3 A L	max	-361.55	3	3.04	S3 B L	max	-504.56	10.9	18.37
	min	-621.33	-6.5	-4.17		min	-783.03	-8.87	-18.69
S4 A L	max	-3052.55	154.97	145.89	S4 B L	max	-3283.39	230.6	165.12
	min	-4231.6	-208.85	-136.45		min	-4489.37	-243.45	-162.31
S5 A L	max	-2701.05	24.06	18.65	S5 B L	max	-2790.26	30.26	40.34
	min	-3371.41	-30.97	-19.8		min	-3561.54	-34.54	-40.94
S1 A R	max	-513.06	49.06	26.59	S1 B R	max	-705.2	127.23	93.63
	min	-727.65	-43.59	-26.44		min	-908.72	-91.45	-91.06
S2 A R	max	-1986.5	77.54	63.52	S2 B R	max	-2212.55	235.48	175.08
	min	-2517.28	-98.93	-63.55		min	-2870.75	-194.98	-166.38
S3 A R	max	-241.01	2.55	3.3	S3 B R	max	-389.34	12.76	23.91
	min	-463.03	-4.62	-3.09		min	-636.46	-10.65	-10.48
S4 A R	max	-2935.49	127.47	115.19	S4 B R	max	-3178.6	205.32	167.8
	min	-4000.79	-176.43	-116.43		min	-4266.72	-213.61	-152.38
S5 A R	max	-1764.13	19.99	16.39	S5 B R	max	-2074.64	53.99	58.8
	min	-2036.8	-17.53	-19.92		min	-2360.92	-40.08	-63.64

Table A.10. Design values of full section segments- Combination C

Section & Combination Tunnel		Design Loads			Section & Combination Tunnel		Design Loads		
		Nd (kN)	Md (kNm)	Vd (kN)			Nd (kN)	Md (kNm)	Vd (kN)
S1 C L	max	-518.05	73.92	41.89	S1 C R	max	-515.81	73.79	40.72
	min	-868.27	-94.33	-48.85		min	-870.65	-94.86	-53.5
S4 C L	max	-2269.47	99.17	89.45	S4 C R	max	-2242.46	97.54	78.72
	min	-3162.36	-143.11	-55.95		min	-3144.33	-140.13	-57.57
S5 C L	max	-2319.5	143.05	106.88	S5 C R	max	-2359.93	116.89	90.89
	min	-3591.51	-160.98	-193.4		min	-3380.23	-145.52	-149.97

A.3.2 Longitudinal Joint Bursting Load

The radial joint is the contact between segments of the same ring and allows the forces transmission due to ground loads. Design values of longitudinal joint bursting load were summarized in Tables A-12 to A-13.

Table A.11. Design forces on radial joint segments – Combination A&B

Section & Combination Tunnel		$N_{d,max}$	e_{max}	e_{min}
S1 A L	Nd (kN)	-787.01	-697.03	-783.30
	e (cm)	-3.65	4.15	-3.84
S1 B L	Nd (kN)	-957.14	-712.51	-911.03
	e (cm)	-4.84	9.34	-5.23
S2 A L	Nd (kN)	-2640.64	-2278.99	-2577.01
	e (cm)	-2.03	2.06	-2.29
S2 B L	Nd (kN)	-2970.90	-2578.67	-2909.81
	e (cm)	-3.10	4.67	-3.60
S3 A L	Nd (kN)	-621.33	-399.16	-618.76
	e (cm)	-0.50	0.38	-0.53
S3 B L	Nd (kN)	-783.03	-551.23	-644.71
	e (cm)	-0.58	1.01	-0.62
S4 A L	Nd (kN)	-4231.60	-3081.87	-4103.16
	e (cm)	-2.51	2.55	-2.54
S4 B L	Nd (kN)	-4489.37	-3299.32	-4356.59
	e (cm)	-2.66	3.56	-2.84
S5 A L	Nd (kN)	-3371.40	-2774.81	-2856.25
	e (cm)	-0.29	0.44	-0.53
S5 B L	Nd (kN)	-3561.54	-2896.27	-3076.63
	e (cm)	-0.24	0.53	-0.57
S1 A R	Nd (kN)	-727.65	-654.33	-718.30
	e (cm)	-2.93	3.82	-3.09
S1 B R	Nd (kN)	-908.72	-705.20	-888.96
	e (cm)	-4.49	9.19	-5.23
S2 A R	Nd (kN)	-2517.28	-2194.74	-2487.50
	e (cm)	-1.82	1.80	-2.02
S2 B R	Nd (kN)	-2870.75	-2533.89	-2845.28
	e (cm)	-3.10	4.73	-3.49
S3 A R	Nd (kN)	-463.03	-297.92	-446.75
	e (cm)	-0.48	0.43	-0.53
S3 B R	Nd (kN)	-636.47	-468.20	-583.45
	e (cm)	-0.53	1.39	-0.93
S4 A R	Nd (kN)	-4000.79	-2935.49	-3979.53
	e (cm)	-2.05	2.21	-2.26
S4 B R	Nd (kN)	-4266.72	-3224.32	-4253.18
	e (cm)	-2.25	3.23	-2.55
S5 A R	Nd (kN)	-2036.80	-1765.43	-1909.86
	e (cm)	-0.41	0.58	-0.46
S5 B R	Nd (kN)	-2360.92	-2245.42	-2310.57
	e (cm)	-0.41	1.22	-0.88

Table A.12. *Design forces on radial joints – Combination C*

Section & Combination Tunnel		$N_{d,max}$	e_{max}	e_{min}
S1 C L	Nd (kN)	-868.27	-522.50	-777.40
	e (cm)	-4.50	7.19	-6.18
S4 C L	Nd (kN)	-3162.36	-2292.54	-3142.12
	e (cm)	-2.19	2.17	-2.32
S5 C L	Nd (kN)	-3591.51	-2879.54	-3581.11
	e (cm)	-2.18	2.52	2.29
S1 C R	Nd (kN)	-870.65	-521.18	-771.62
	e (cm)	-4.33	7.19	-6.26
S4 C R	Nd (kN)	-3144.33	-2279.22	-3074.09
	e (cm)	-2.24	2.18	-2.32
S5 C R	Nd (kN)	-3380.23	-2671.48	-3340.87
	e (cm)	-1.01	2.22	-2.22

B. FULL-SCALE TEST RESULTS

B.1 Flexural Test Results

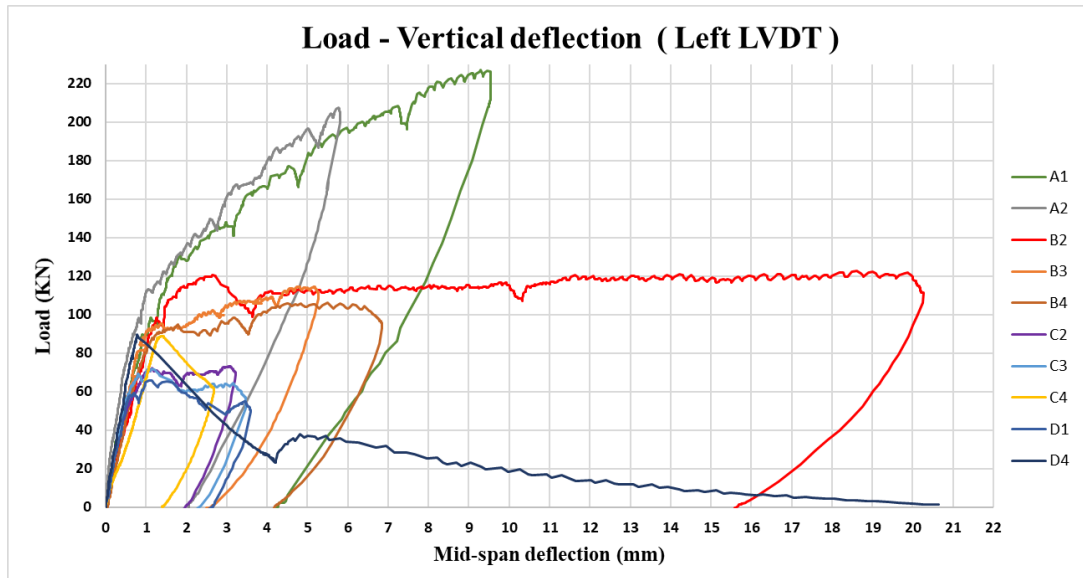


Figure B.1 Load versus vertical displacement curves obtained by left LVDT

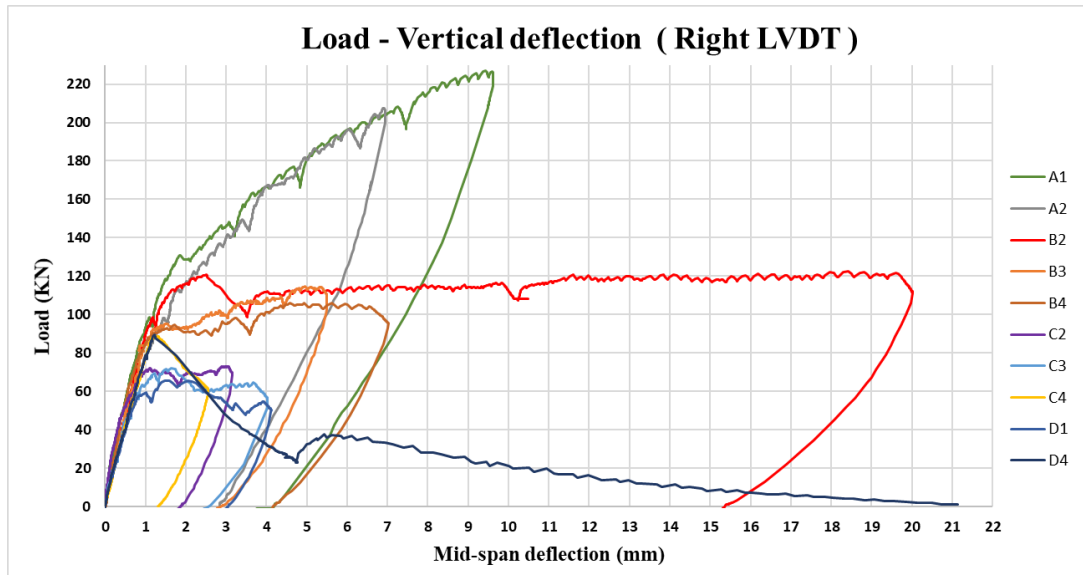


Figure B.2. Load versus vertical displacement curves obtained by right LVDT

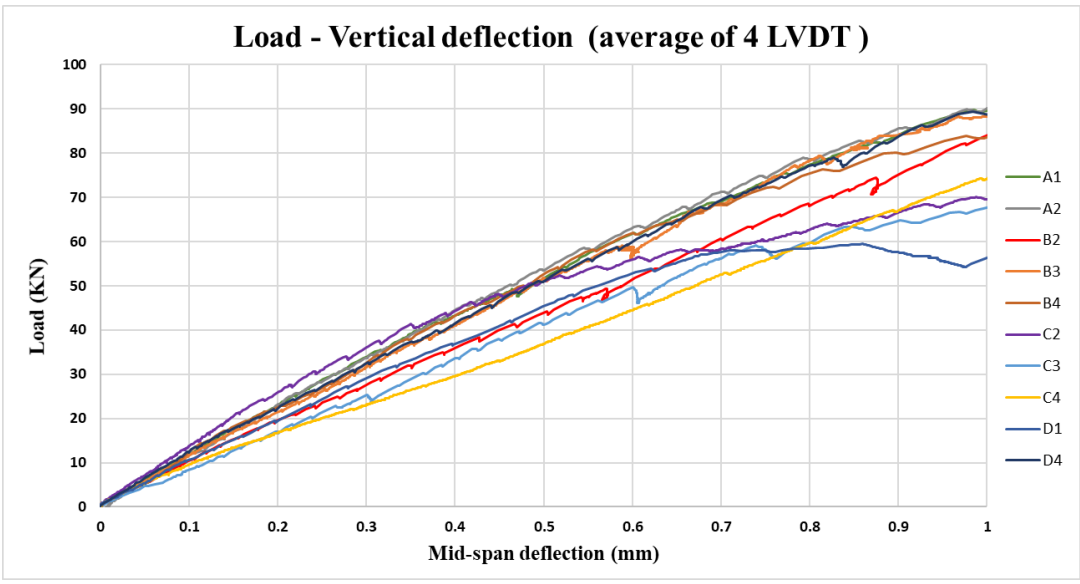


Figure B.3. Load versus vertical displacement curves obtained by average of 4 LVDTs.

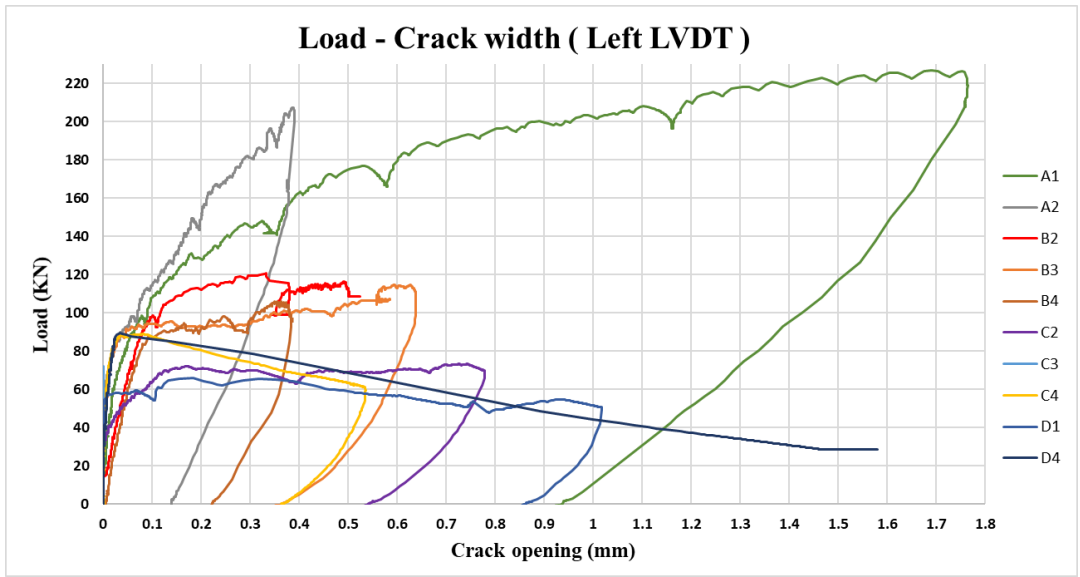


Figure B.4. Load versus flexural crack width graph measured by left LVDT.

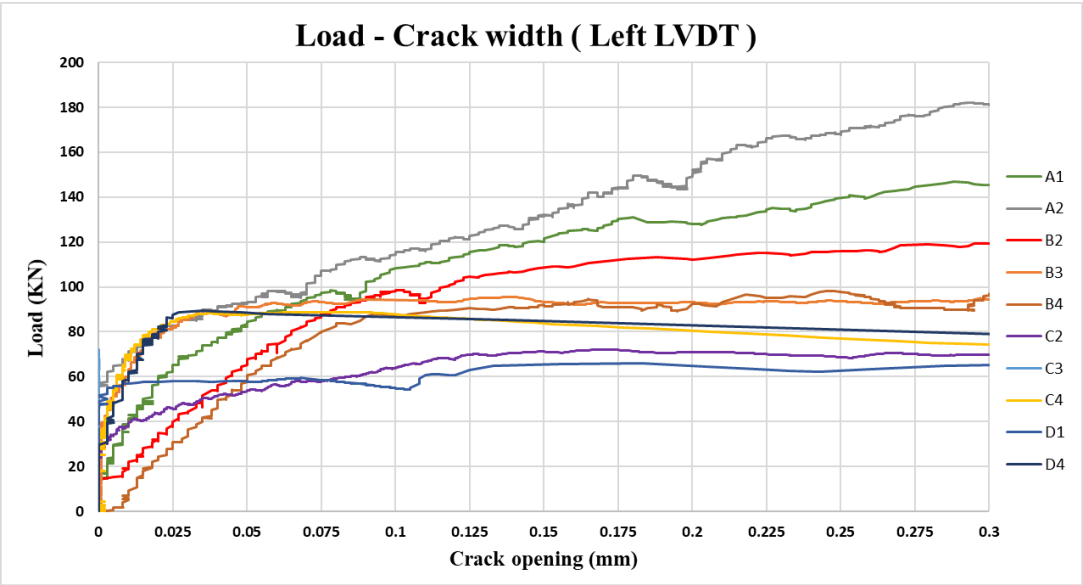


Figure B.5. Load versus flexural crack width graph measured by left LVDT, up to 0.3 mm.

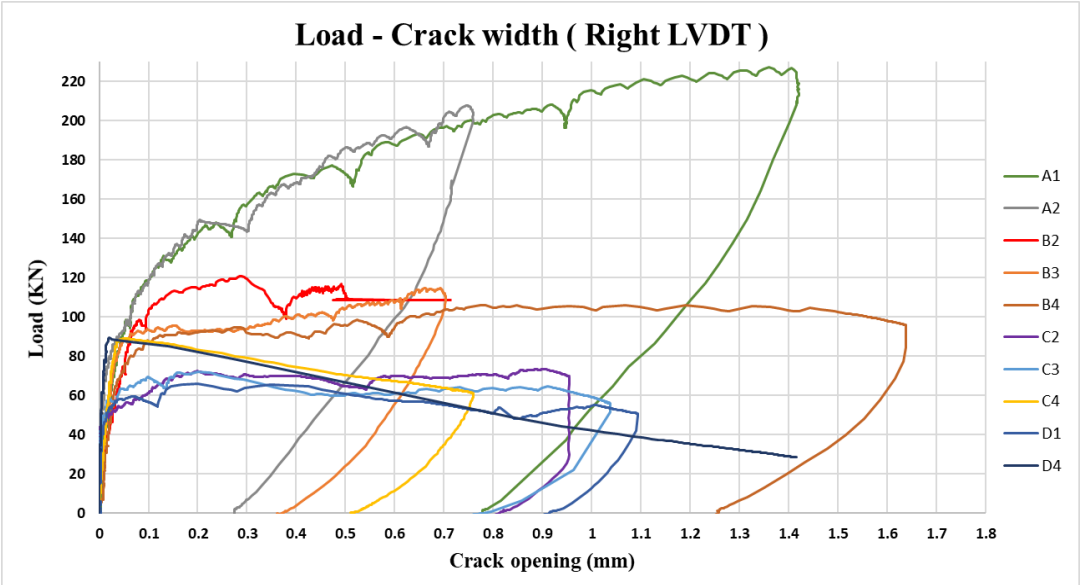


Figure B.6. Load versus flexural crack width graph measured by right LVDT.

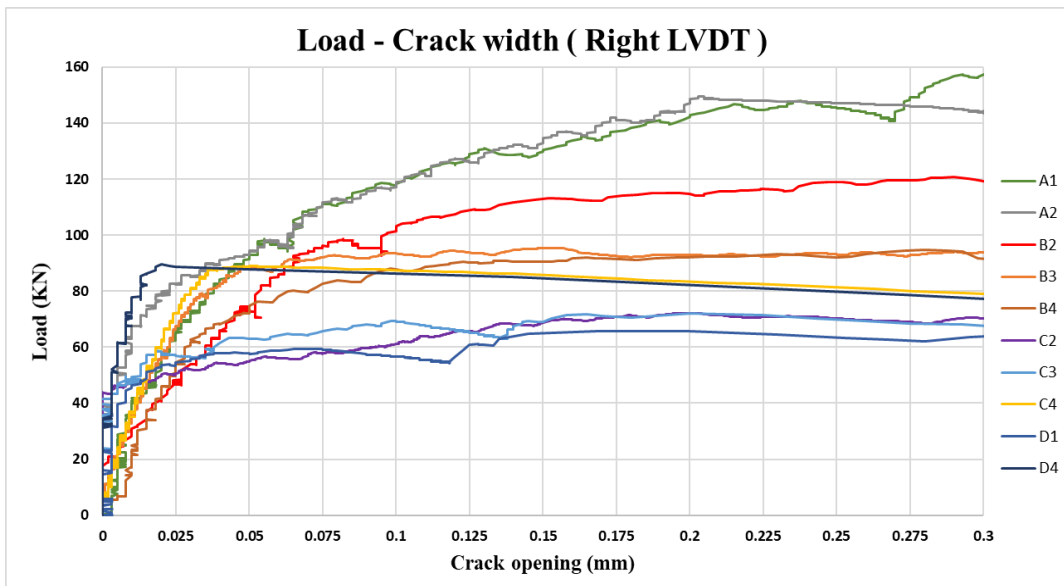


Figure B.7. Load versus flexural crack width graph measured by right LVDT, up to 0.3 mm.

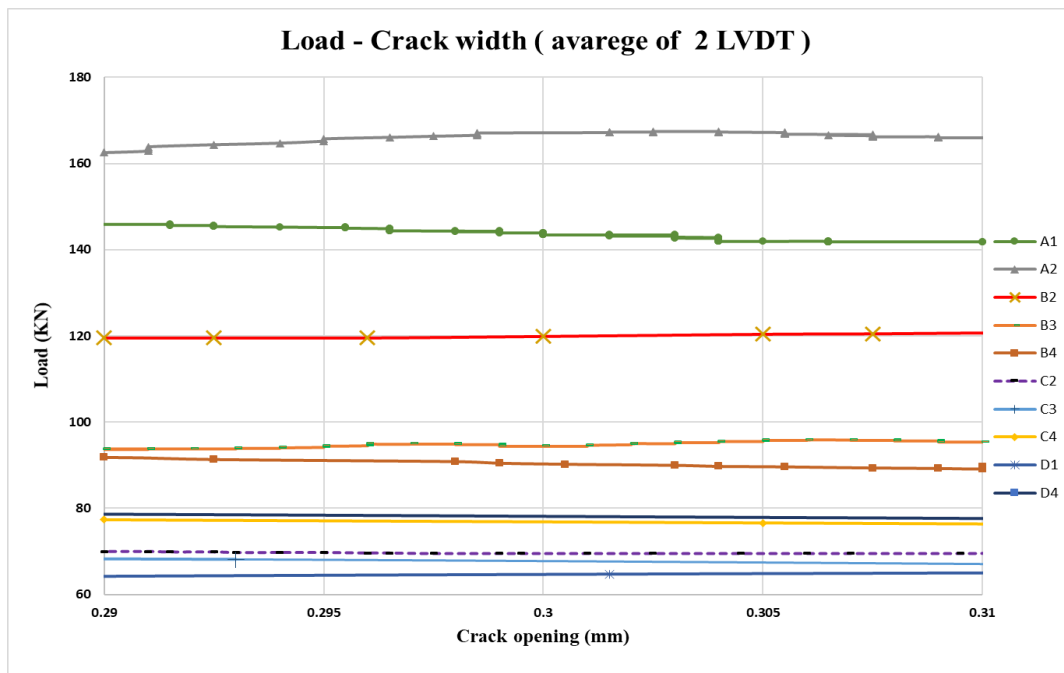


Figure B.8. Load versus flexural crack opening width curves obtained average of 2 LVDTs, around the SLS limit.

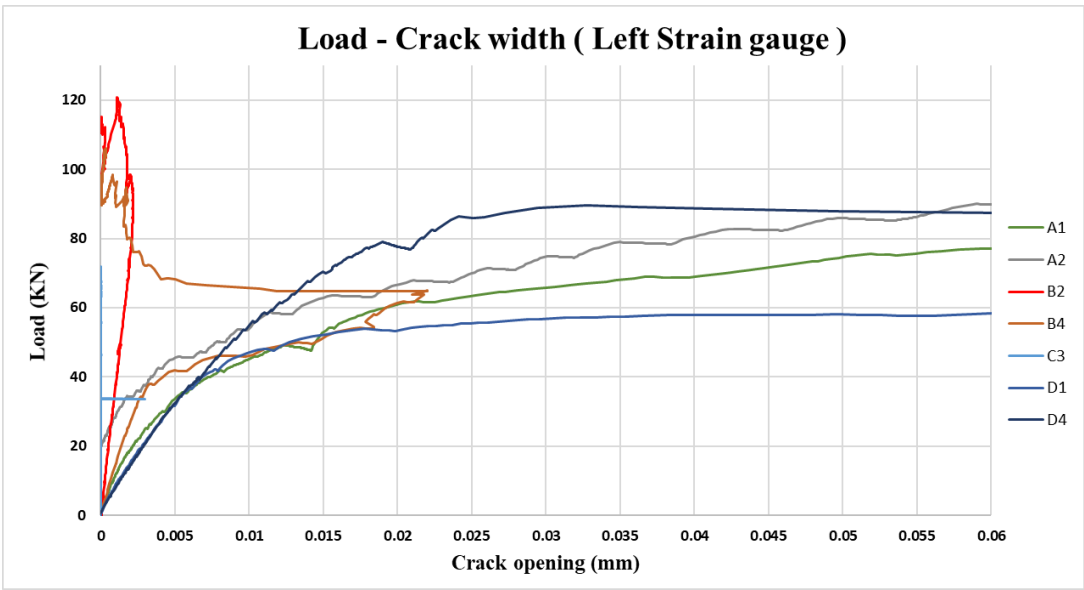


Figure B.9. Load versus flexural crack width curves measured from the left strain gauge.

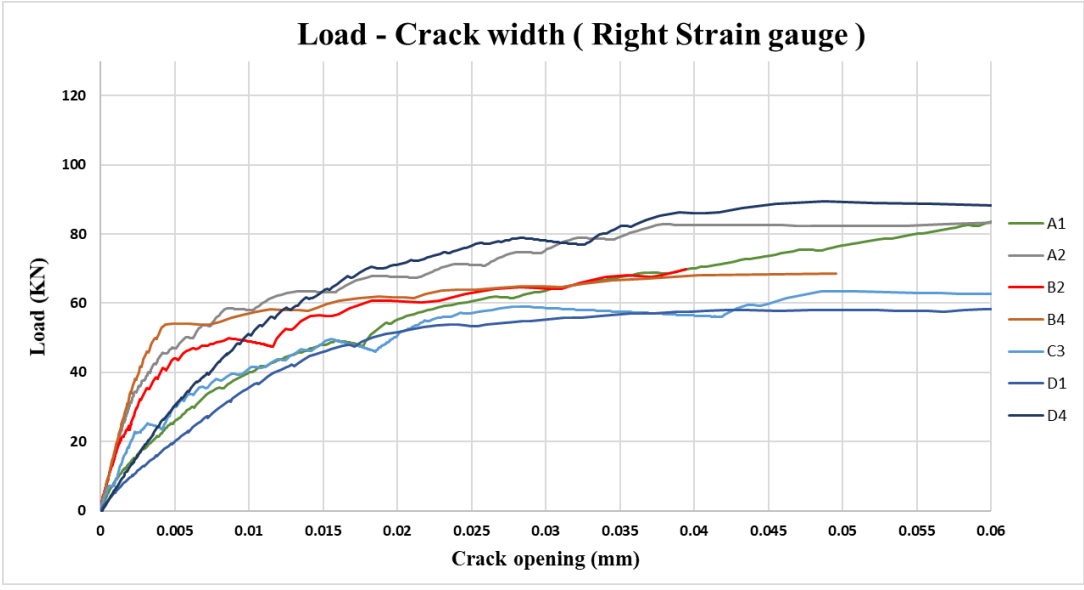


Figure B.10. Load versus flexural crack width curves measured from the right strain gauge.

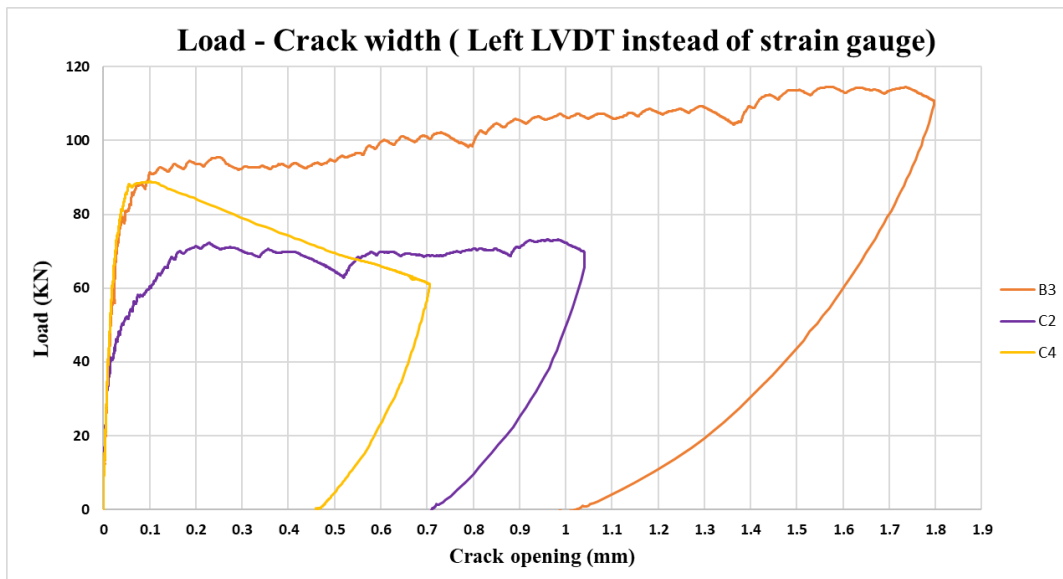


Figure B.11. Load versus flexural crack width curves measured by left LVDT located at the strain gauge position.

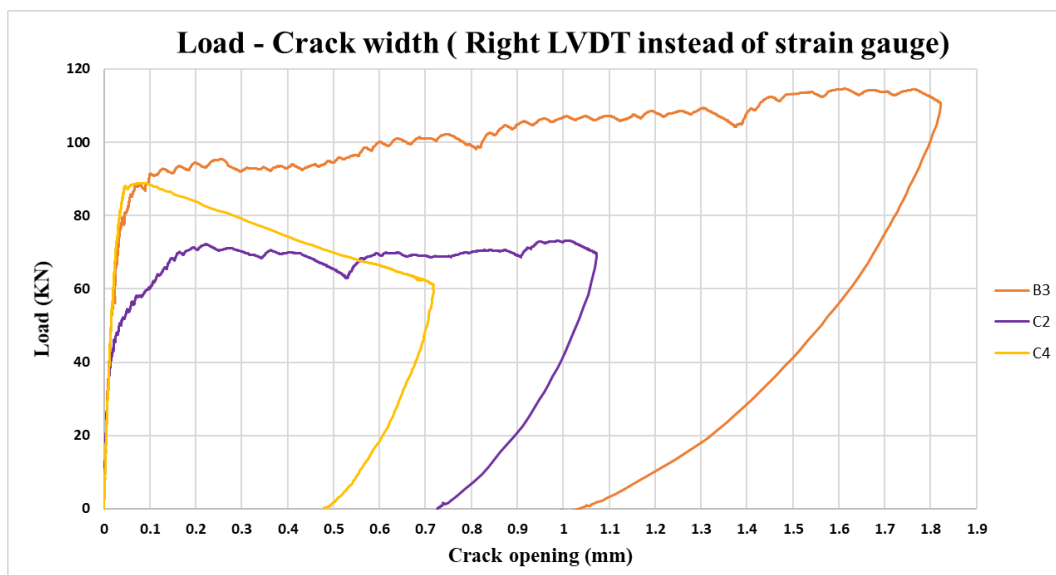


Figure B.12. Load versus flexural crack width curves measured by right LVDT located at the strain gauge position.

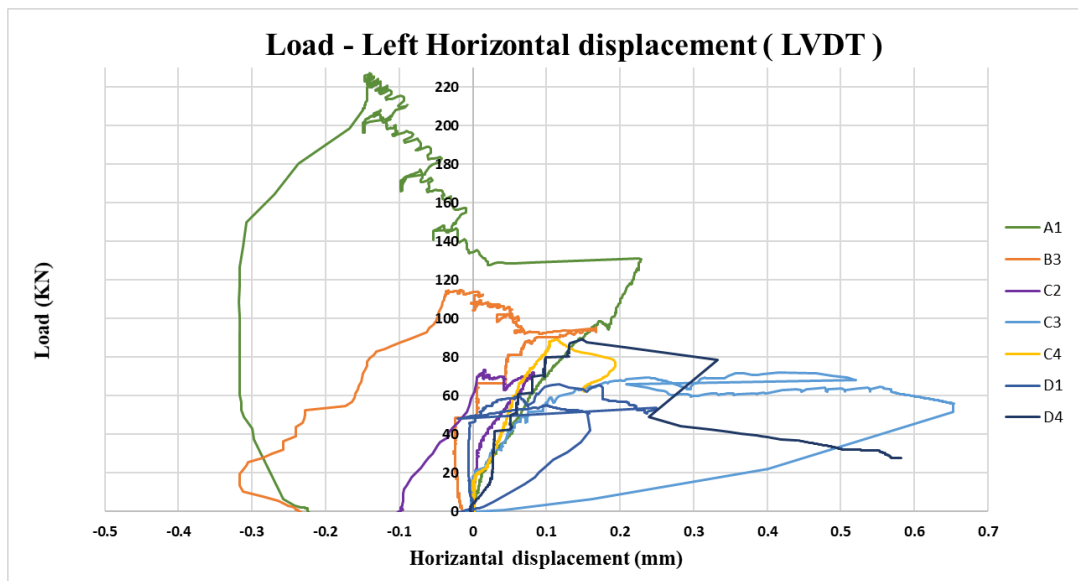


Figure B.13. Load versus horizontal displacement curves obtained from left LVDT

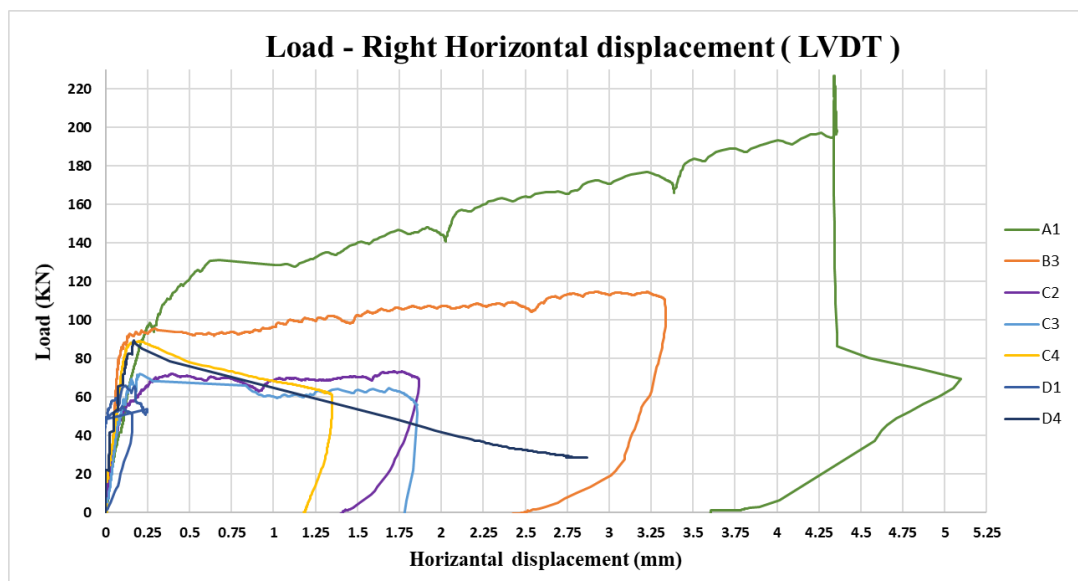


Figure B.14. Load versus horizontal displacement curves obtained from right LVDT

B.2 Creep Test Results

B.2.1 Cycling Loading for PFRC specimen

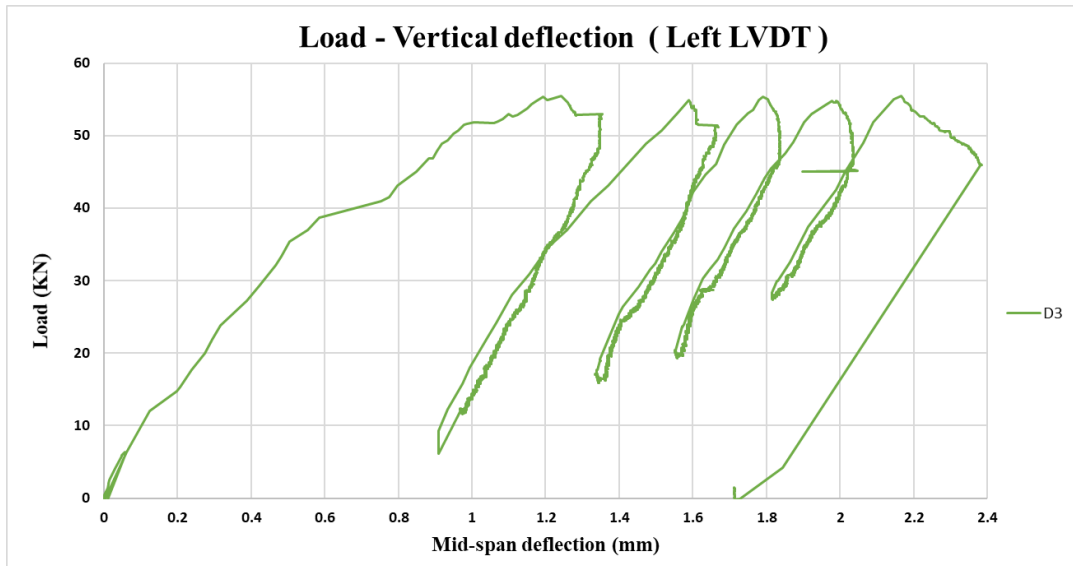


Figure B.15. Load versus vertical displacement curve obtained from left LVDT

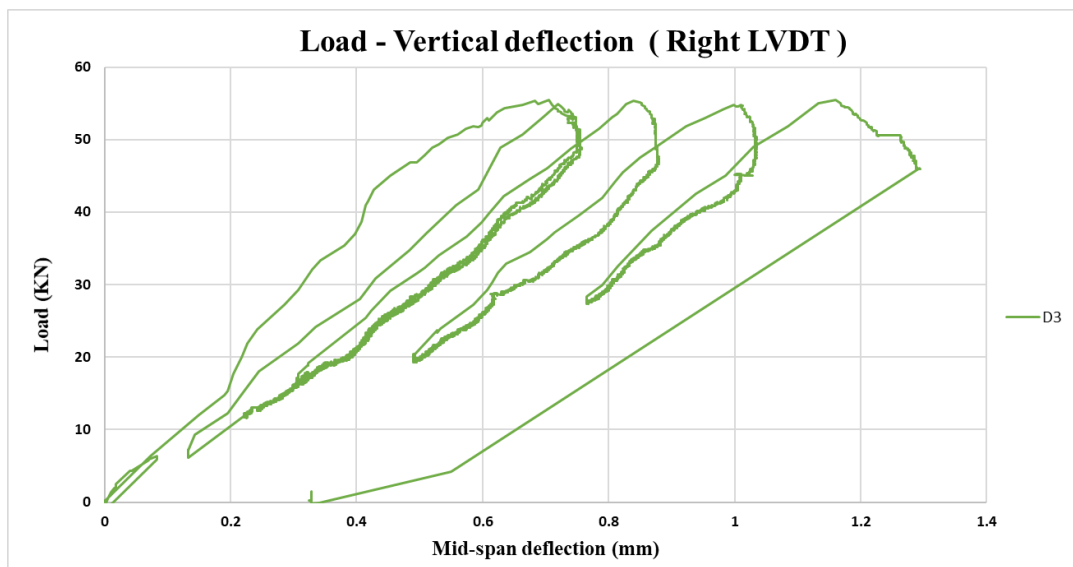


Figure B.16. Load versus vertical displacement curve obtained from right LVDT

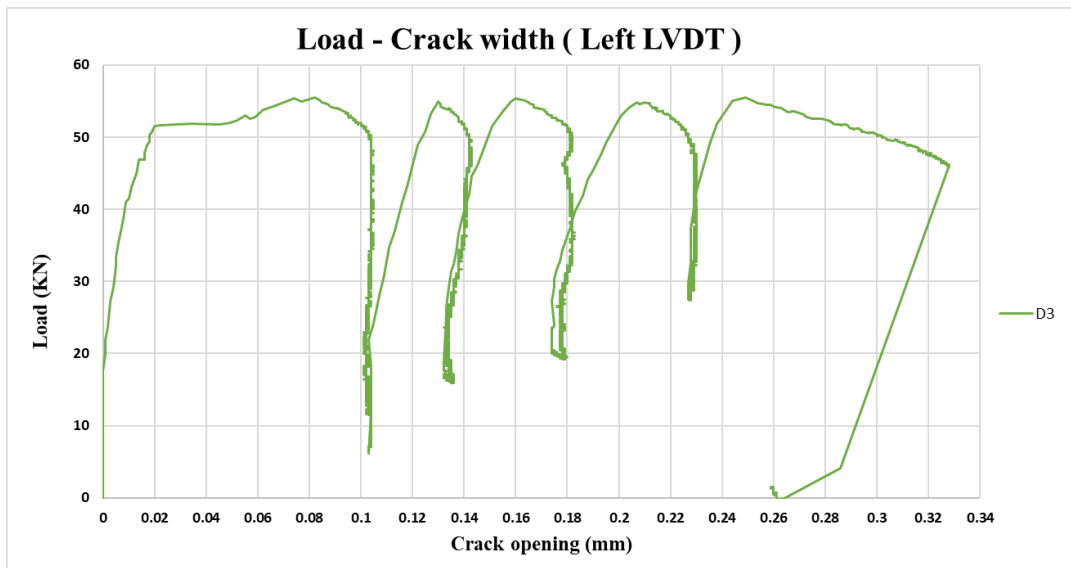


Figure B.17. Load versus flexural crack width curve measured by left LVDT

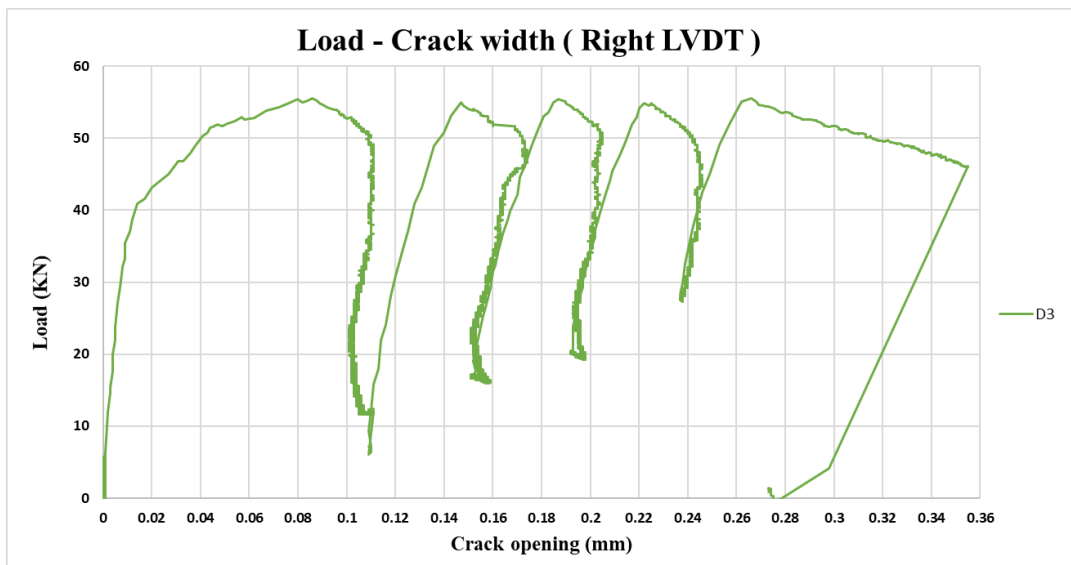


Figure B.18. Load versus flexural crack width curve measured by right LVDT

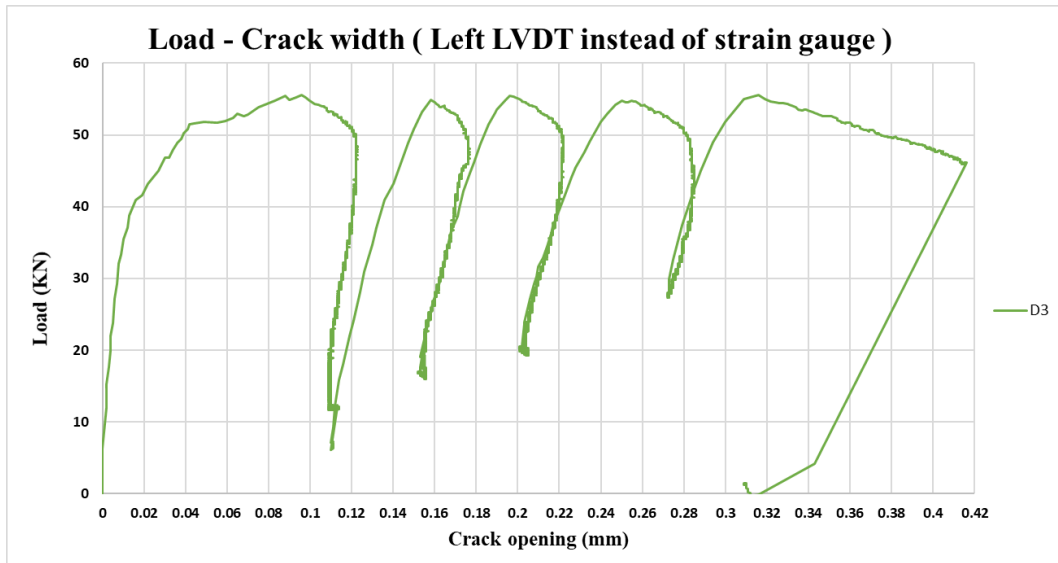


Figure B.19. Load versus flexural crack width curves measured by left LVDT located at the strain gauge position.

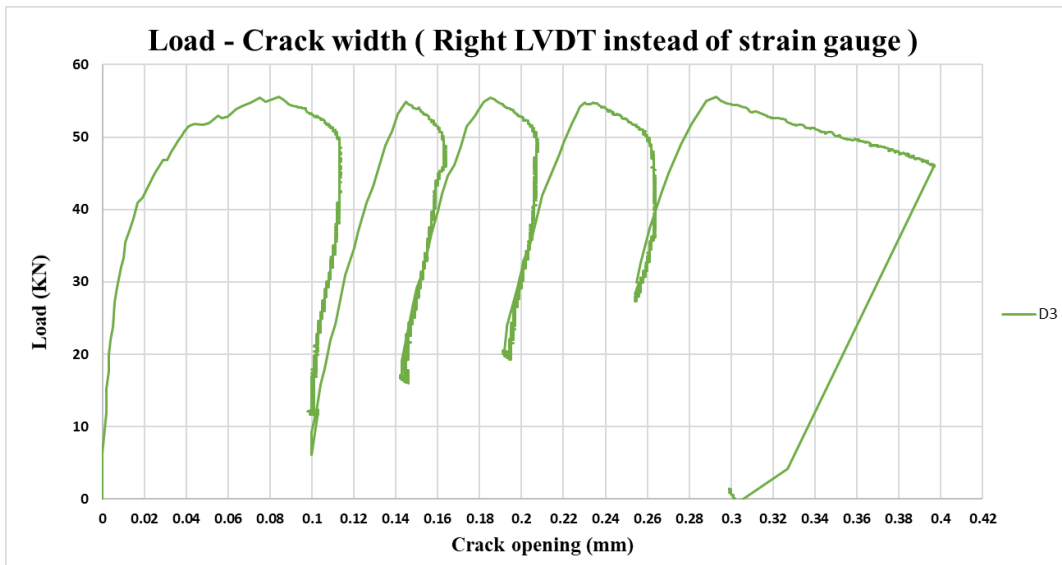


Figure B.20. Load versus flexural crack width curves measured by right LVDT located at the strain gauge position.

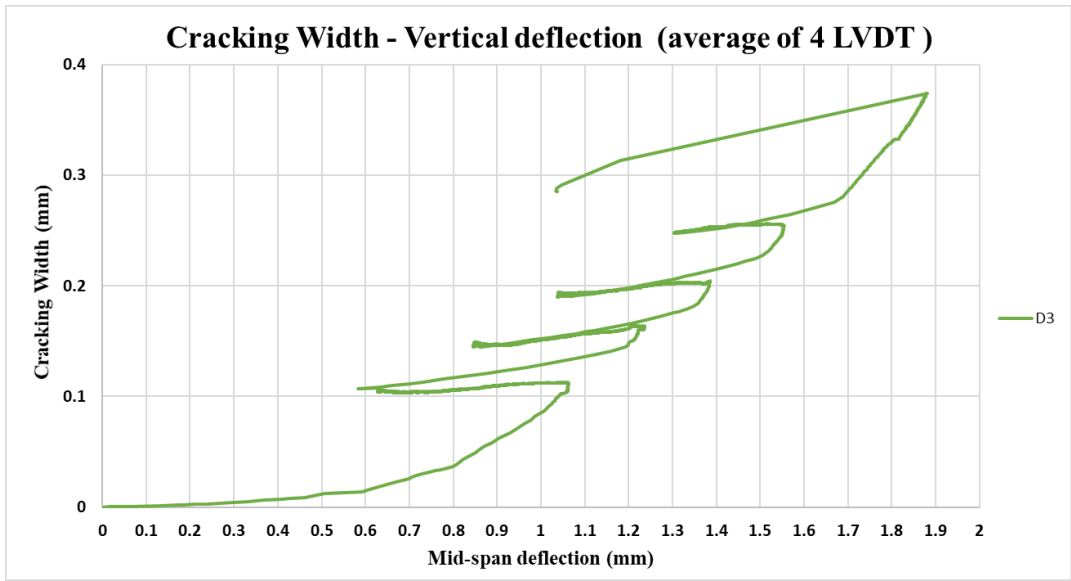


Figure B.21. Cracking width versus vertical displacement curve

B.2.2 Cycling Loading for GFRP + PFRC specimen

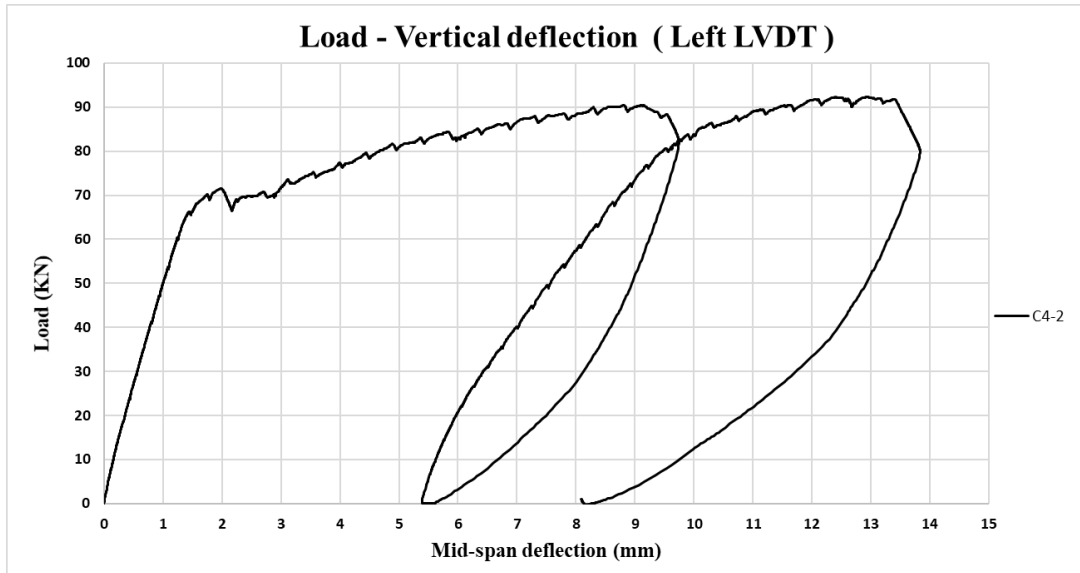


Figure B.22. Load versus vertical displacement curve obtained from left LVDT

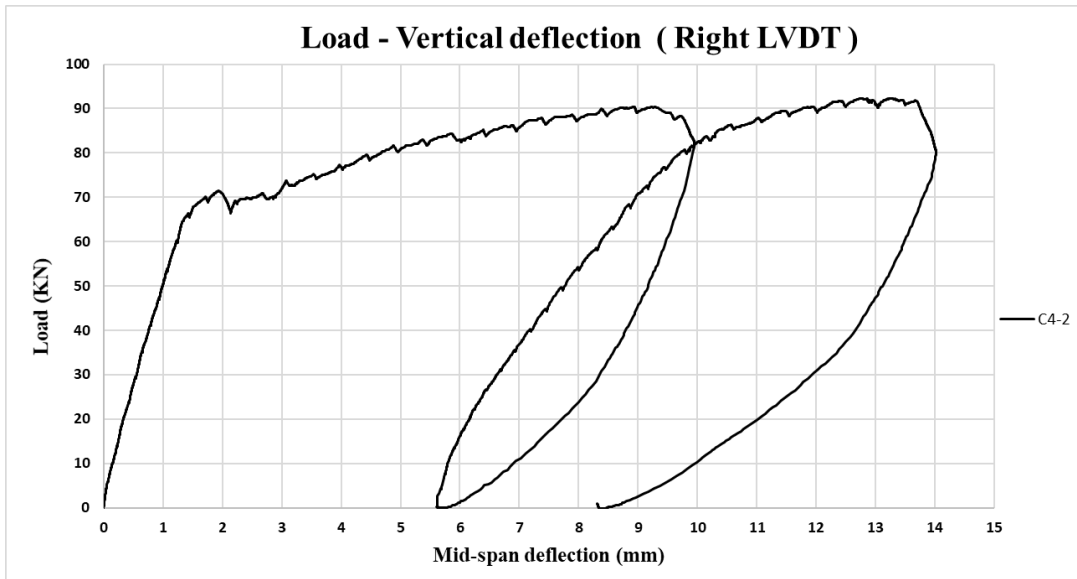


Figure B.23. Load versus vertical displacement curve obtained from right LVDT

B.3 Point Load Test Results

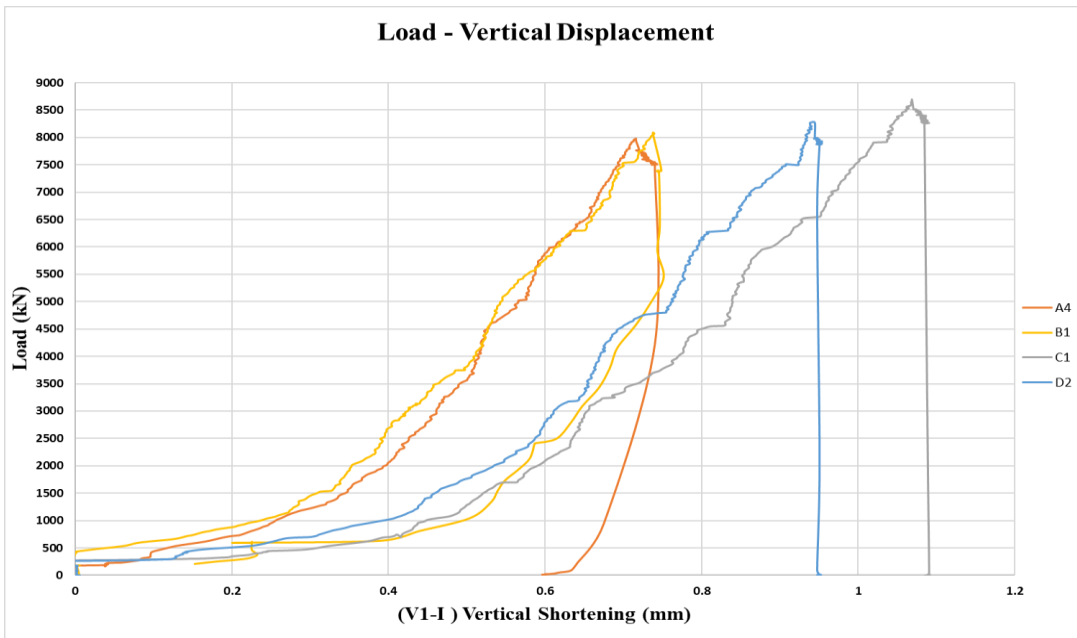


Figure B.24. Load versus vertical displacement curves (V1-I)

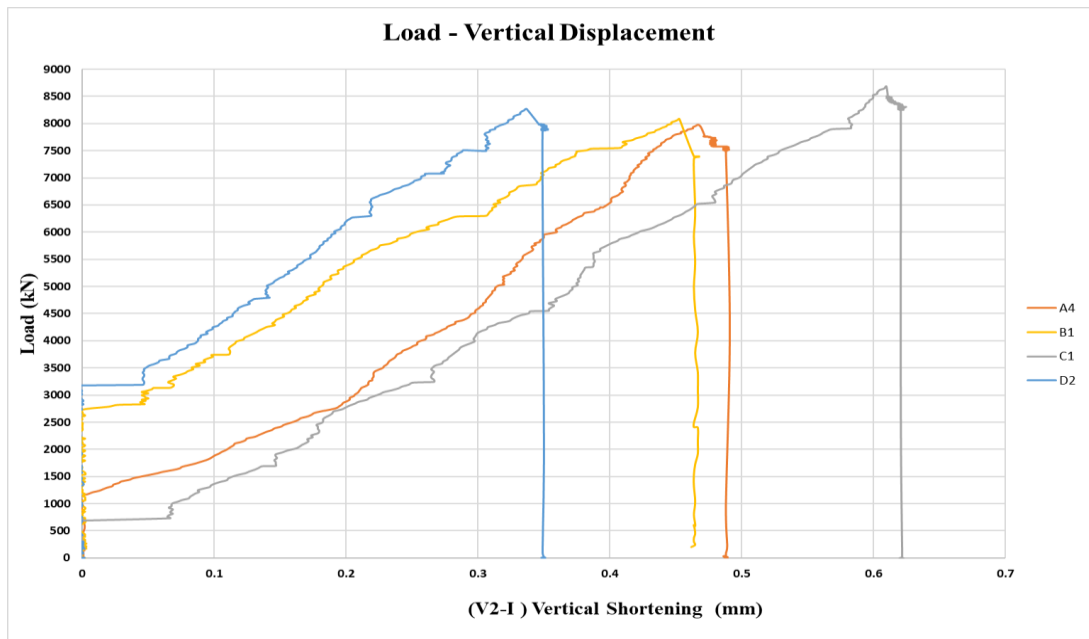


Figure B.25. Load versus vertical displacement curves (V2-I)

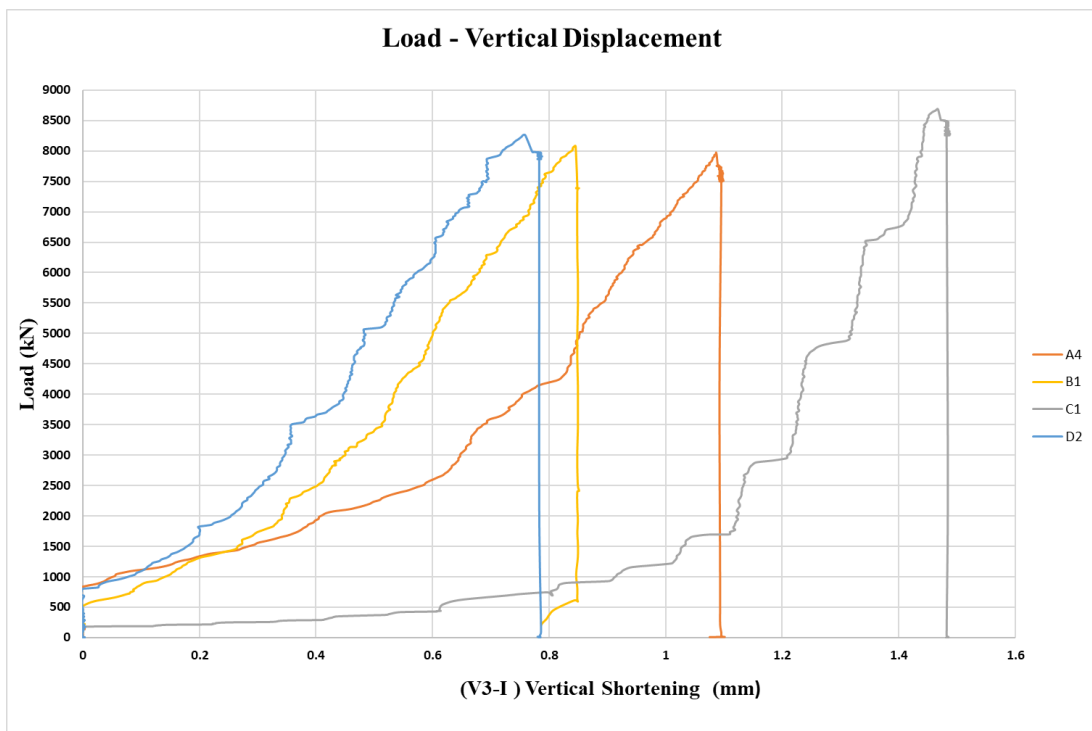


Figure B.26. Load versus vertical displacement curves (V3-I)

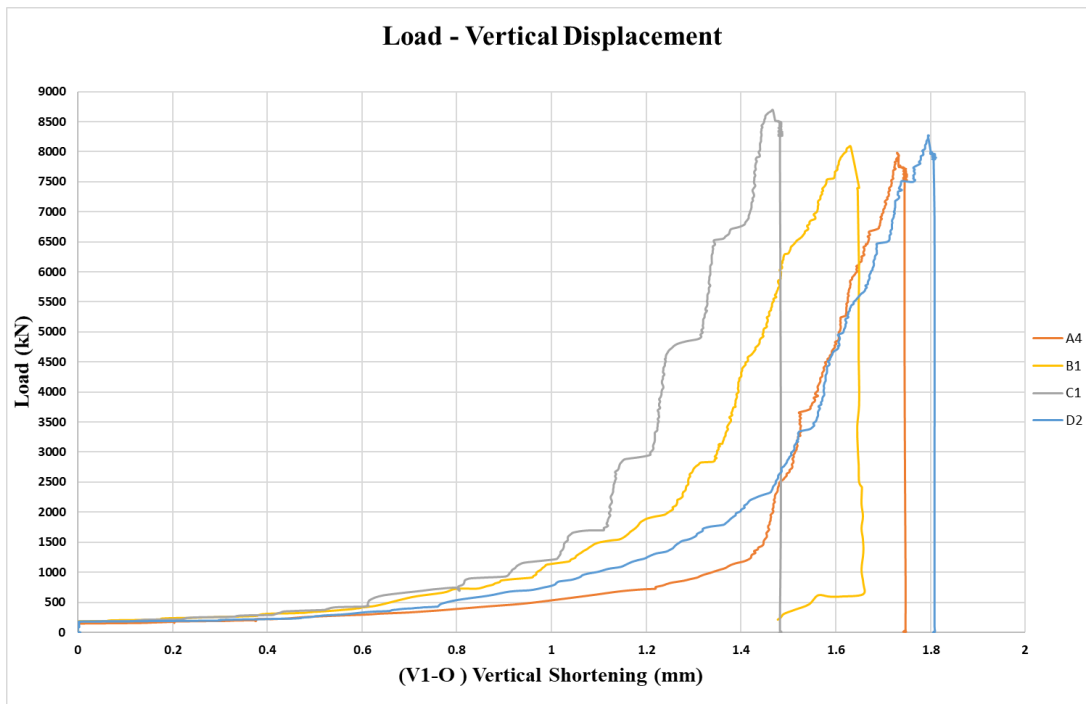


Figure B.27. Load versus vertical displacement curves (V1-O)

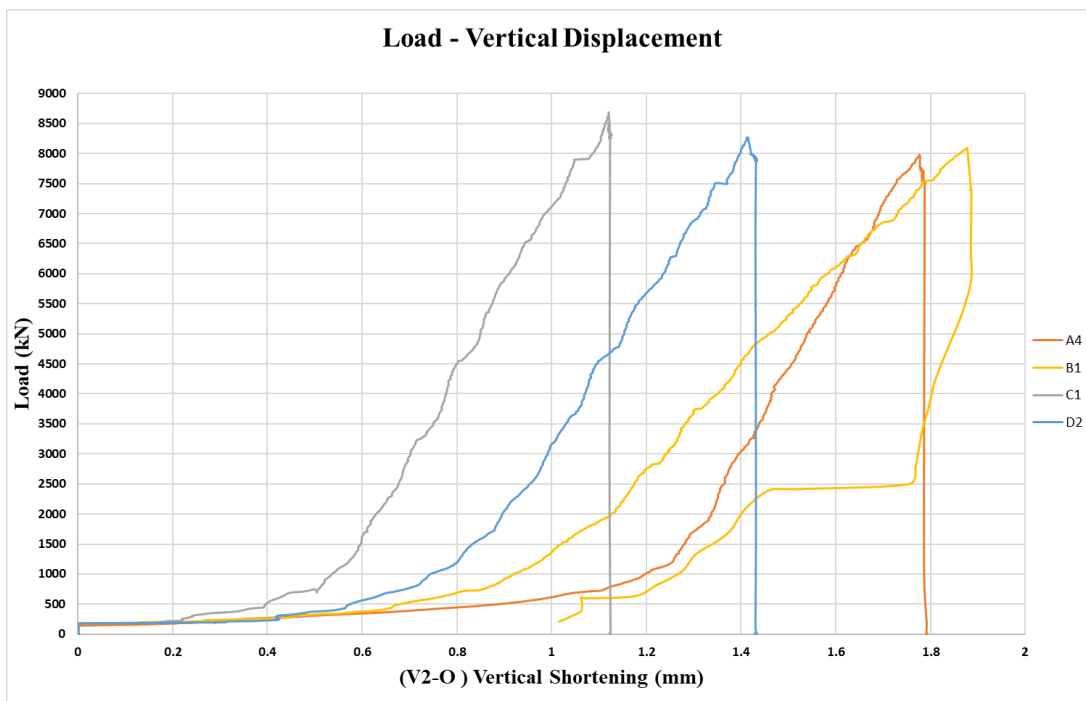


Figure B.28. Load versus vertical displacement curves (V2-O)

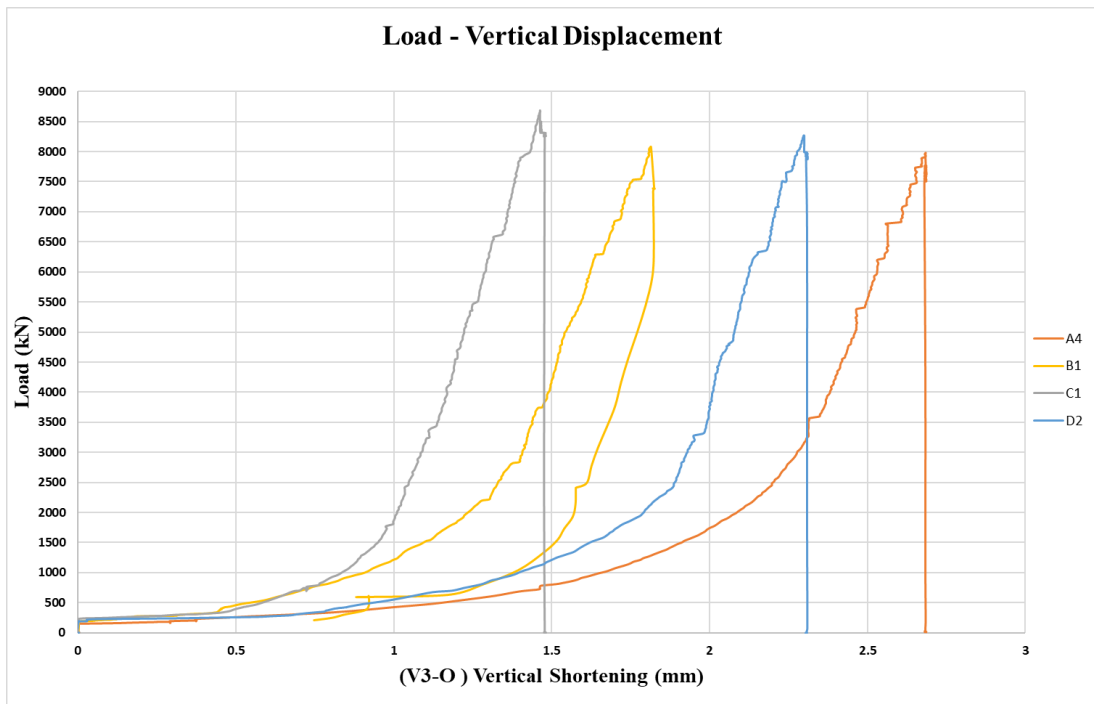


Figure B.29. Load versus vertical displacement curves (V3-O)